INELASTIC COLUMN BEHAVIOUR -

ITS APPLICATION TO COMPOSITE COLUMNS IN BIAXIAL BENDING AND STIFFENED PLATES IN COMPRESSION

A Thesis submitted for the degree of
Doctor of Philosophy
in the Faculty of Engineering of the
University of London

by

Kuldeep Singh Virdi, B.Sc., B.Tech., M.E.

Imperial College of Science and Technology

London

November, 1973

To my parents

ABSTRACT

This thesis describes the development of an inelastic column analysis for isolated pin-ended columns having an axial load and biaxial end moments. The column cross-section may be comprised of any combination of materials with known uniaxial stress-strain relationships. The analysis has been developed primarily for composite steel concrete columns but is, nevertheless, equally applicable to bare steel columns, reinforced concrete columns, concrete encased steel stanchions, or concrete-filled steel tubular columns. Two different methods of solution are presented. One is a general method based on the calculation of the actual deflected shape of the column and is applicable to columns loaded with any combination of end eccentricities. The other is a simpler method based on an assumed deflected shape of the column and is restricted in its application to cases with symmetrical biaxial bending. It is shown, however, that the loss in accuracy obtained with the simple method is less than about 6% compared with the more exact method for the range of problems to which it is applicable. In both methods torsional effects are ignored, a limitation which should not restrict their application to most practical cases.

Experiments on nine full-scale concrete encased steel columns loaded biaxially in symmetrical bending are reported and used to check the accuracy of the two methods of analysis. The columns tested cover the practical range of column slenderness and it is believed they represent the first such tests reported to date. The discrepancy between the observed and calculated strengths remains within an average of 5% with a standard deviation of 10%. The theory developed has been sub-

sequently used to check the accuracy of a previously proposed biaxial interaction formula currently being included in the draft specifications for composite buildings and bridges. In all cases, the results obtained by the formula have been found to be conservative. In the case of unsymmetrical bending, the strength obtained by using the design formulas may be underestimated by as much as 25 - 43%. However, in view of its simplicity and its consistent conservativeness, it is recommended that this interaction formula may be retained for design purposes for the immediate future. The analysis developed within this thesis can be used at a later stage to develop a more suitable design approach.

To illustrate the flexibility of the theory in its application to various types of cross-sections, attention in the final part of this thesis is turned to the problem of the strength of stiffened steel plates in compression. The theory is used to examine various factors influencing the strength of such plates. Among these factors are initial deformations in the panel, residual stresses due to welding, initial eccentricity of loading, and local plate buckling. It is shown that these factors can combine to lower the strength of practical stiffened plates by up to 50% of that based on idealised column theory. The results are also used to suggest how a column approach can be adopted for the design of stiffened compression flanges in box girders. Such an approach has the advantage of being simple with an acceptable degree of accuracy for design when it is compared with the results predicted by the inelastic column theory developed within this thesis.

ACKNOWLEDGEMENTS

The investigation reported in this thesis was carried out under the supervision and constant guidance of Dr. P.J. Dowling, to whom the author is deeply grateful for his encouragement and valuable advice throughout the duration of the work, and under the general direction of Professor S.R. Sparkes, Professor of Engineering Structures.

The author is deeply grateful to Dr. J.C. Chapman, Director, Constructional Steel Research and Development Organisation, who was responsible for initiating the work on biaxial bending of composite columns at Imperial College, and provided helpful suggestions from time to time during the course of this study.

The author is indebted to the Highway Engineering Computer Branch of the Department of the Environment for their financial support and sponsorship of the analytical aspects of the investigation. In particular, thanks are due to Mr. F. Boeuf of HECB, DoE for his interest in the project. The tests described in the thesis were carried out as a project jointly sponsored by the Constructional Industry Research and Information Association and the British Constructional Steelwork Association.

Thanks are due to Mr. M.J. Zand, a former colleague, and to the staff members of the Engineering Structures Laboratories, Imperial College, for their help in carrying out the tests; to Mrs. M. Frieze for her typing and to Mr. J. Cima for the drawings.

Finally, the author wishes to record his gratitude to Dr. P. Krishna, Reader in Civil Engineering, University of Roorkee, India, who was instrumental in arranging the author's stay at Imperial College for the purpose of this research.

CONTENTS

CONTENTS Contd. Page

CONTENTS Contd. Page

CONTENTS Contd.

CONTENTS Contd. Page

CHAPTER 1

INTRODUCTION

1.0 GENERAL INTRODUCTION

Research on the buckling strength of compression elements in engineering structures has progressed considerably since Euler[1], more than two hundred years ago, first treated the problem of an isolated column as one of instability rather than one of stable equilibrium with flexural stresses. The interest in the stability of compression elements has now diversified from straight columns to plate and shell elements and further to the stability of complete structures. Yet several aspects of the stability of an isolated column remain to be fully understood. A large amount of experimental and theoretical investigation is being carried out even at this stage primarily with the objective of obtaining simple yet reliable design rules for such elements. The voluminous work recently carried out to establish the so-called European Column curves for structural steel sections can be cited as one outstanding example. The experimental and theoretical studies on stiffened plates in compression triggered off by the recent collapse of three box girder bridges within a short space of time, is another. As a result of the work carried out by Beer and Schulz[2] for the projected European code the designer can now predict the strength of axially loaded pin-ended metal columns with a certain degree of confidence. On the other hand the study of stiffened plates in compression, is relatively still in its infancy. As a simple approach, the experience gained in the study of the ultimate strength of columns is being extended to

the more complex problem of stiffened plates in compression. This thesis reflects this trend in that while it started out as an investigation of one of the remaining aspects of the strength of pin-ended columns, namely that of biaxial bending of composite columns, the general theory so developed was subsequently used to investigate some of the fundamental parameters governing the behaviour of stiffened plates in compression. These seemingly different albeit very important problems represent only two of the many which may be studied with the theory developed within this thesis.

1.1 REVIEW OF COLUMN RESEARCH

The problem of instability of compression elements is concerned with the investigation of conditions under which the structure ceases to be in a stable equilibrium between external forces and internal stress resultants. An added complication stems from the fact that the response of the structure is in general controlled by the material stress-strain relationship. Euler's formula[3] predicted the strength of slender columns very closely, but was soon found to be inadequate for shorter columns. The mathematical soundness of Euler's formula was confirmed by Lagrange[4], but it was found that the margin with which the formula overestimated the strength of short columns increased with diminishing slenderness. That this failure of the formula was due to the material elastic limit being attained before the theoretical stress required for buckling, was not recognised until 1845 when Lamarle[5] pointed out the lower limit of slenderness for the Euler formula to be valid. In 1889, Considére[6] and Engesser[7] presented, independently of each other, generalised forms of Euler's formula based on a variable modulus of

elasticity, and covering the entire range of slenderness ratios. Much experimental and theoretical work on axially as well as eccentrically loaded columns followed. It was only in 1947 that Shanley[8] finally established that the tangent modulus load represented the maximum load under which an initially straight column will necessarily remain straight. In other words it represented the lower bound for the buckling load of such columns. Most practical columns, however, lack initial straightness and may have other imperfections as well. Notable amongst these are the locked-in residual stresses. Also, a practical column seldom has a perfectly concentric axial load. All these imperfections have a detrimental effect on the strength of the column. Ostenfeld[9], in 1898, made an attempt to derive design formulae for centrally and eccentrically loaded columns. His method was based on the first yield criterion. The first to consider the determination of the buckling load of eccentrically loaded columns as an instability problem was Kármán[10] who, in 1910, gave a general and exact theory for the determination of the ultimate load of such columns loaded beyond the material elastic limit. Kármán's theory was related to uniaxial eccentricities only and bending was assumed to be in the plane of the applied eccentricities. The importance of Kármán's work lies in the fact that it has formed the basis of considerable research, including this thesis, on numerous aspects of column behaviour. Ros[11] and Brunner gave a simplified theory assuming the deflected shape of the column in the form of a sine wave but based their computations upon the actual stress-strain diagram. A simple solution to Kármán's equations was given by Westergaard and Osgood[12] who assumed the deflected shape of the column to be part of a cosine wave. The errors introduced by this assumption were found to be within practical acceptable limits. Ježek[13]

employed a bilinear stress-strain curve for steel and showed that the results gave acceptable agreement with those obtained from real stress-strain curves.

Apart from imperfections, several other problems related to the stability of columns have been identified, for example lateral stability, lateral torsional stability and local stability of thin-walled cross-sections. Following the works of Timoshenko[14], Bleich[15], Winter[16], and others, Goodier[17] presented a solution of the problem of the stability of bars of thin-walled open sections under compression, bending and twisting. Goodier's solution is applicable to elastic systems only. Although several solutions have been given for inelastic columns with uniaxially eccentric loads, few solutions are available for the general problem of an inelastic column under biaxially eccentric loading with or without torsion. Klöppel and Winkelmann[18] based their solution on polynomial expressions for the lateral displacements and satisfied equilibrium at a sufficient number of points to obtain the coefficients of the power series assumed. The first general solution may be said to have been given by Birnstiel and Michalos[19] based on a successive trial and correction procedure. The procedure was improved by Birnstiel, Harstead and Leu[20] in that a systematic procedure for the correction of successive trial values was suggested. The results obtained showed a good agreement with experiments carried out by Harstead[21]. The solution given by Sharma and Gaylord[22] was obtained by assuming the deflected shape in the form of a sine wave for deflections along both the bending planes as well as for the twist of the section. Their approximation has been shown to be satisfactory.

The effect of restraints from connecting beams on biaxially loaded columns was first studied by Milner[23]. Milner's approach differs from others' in that Milner has constant end moments for increasing axial loads while most other studies assume moments increasing in the same proportion as the axial load. Being a non-linear problem, the two loading paths inevitably produce different results. Restrained columns have also been studied by Baker, Horne and Heyman[24] and recently by Wood[25]. Considerable work still needs to be done on the strength of a column forming part of a framework as also on the inelastic stability of structural frames as a whole.

Much of the work on columns has been concerned with bare steel columns. Many steel columns in buildings are encased in concrete for fire protection. Some columns consist of steel tubes filled with concrete, particularly those used in buildings situated in earthquake zones. The introduction of concrete having material properties substantially different from steel makes an exact analysis including composite action very difficult. The strength of encased columns has, until very recently, been estimated on the basis of empirical rules. It is now well established that consideration of composite action in composite structures leads to more competitive designs.

The investigation of the ultimate strength of encased columns in particular, and composite columns in general, has understandably lagged behind that for bare steel sections. While the strength of composite columns with uniaxial bending and compression has been studied in some depth by Basu[26,27,28] and others, little work has so far been reported on biaxial bending of composite columns with or without end restraints. Basu and Sommerville[28] did extend Bresler's formula[29] for short

reinforced concrete columns in biaxial bending and compression to slender composite columns, but no theoretical or experimental support was given. Need was therefore felt to devise an analytical method to predict the behaviour of composite columns in biaxial bending up to and possibly beyond collapse. This was the original, and remained the main, objective of this thesis. Experimental verification was sought for the limited case of symmetrical end eccentricities at the two ends. The theoretical and experimental evidence so obtained was also aimed at examining the accuracy of the existing design method due to Basu and Sommerville, when applied to composite columns in biaxial bending.

Columns are, of course, only parts of structural frames. Considerable research has been carried out on the behaviour of composite beams and slabs. The work of Yam[30] at Imperial College may be cited as one of the many advanced studies on the subject. The ultimate aim of research on composite structures has been to obtain methods of design and analysis for frameworks composed of composite elements - beams, slabs, and columns. The present study may therefore be regarded as a preliminary step taken before the more complex problem of the inelastic behaviour of composite space-frames is tackled.

1.2 HISTORICAL NOTE ON RESEARCH ON COMPOSITE COLUMNS

Tests carried out by Burr[31] in 1912 demonstrated that the surrounding concrete added appreciably to the strength of an encased stanchion. Most building codes, however, ignored the strengthening effect of concrete, even though several tests[32,33,34,35] reported between 1912-1936 substantiated Burr's findings. These tests showed that for columns with low slenderness the load bearing capacity of the axially loaded composite column was safely predicted by summing the

individual strengths of steel cross-section and the effective concrete cross-section. The British Code for structural steel in buildings[36] as revised in 1948 stipulated that an allowance could be made for the contribution of concrete, provided the increase in load carrying capacity thereby did not exceed 50% of the capacity of the bare steel column. In 1956 Faber proposed design formulae[37], applicable to encased stanchions, which gave load factors varying from 2.26 to 3.74 for the columns tested by him. It was shown, in the discussion[38] to the same paper that the ACI Code 318 - 1956 formula[39] gave load factors varying from 2.18 to 3.64 for the same columns. The work of Faber was followed by that of Rizk[40], Jones[41], and Stevens[42]. Tests at the Building Research Establishment reported by Stevens, were performed on axially as well as eccentrically loaded specimens. On the basis of these tests, Stevens suggested formulas for the design of encased columns and compared them with the existing BS449[36] formulas. In the revised BS449, 1959, the strength of a composite column was limited to an increase of 100% over the load bearing capacity of the bare steel column.

No attempt had so far been reported to obtain the failure load of a composite column by rigorous analytical procedures. Bondale[43] extended the Kármán procedure for obtaining the inelastic buckling load of metal columns to concrete encased steel columns loaded eccentrically about one axis. He also showed the applicability of the tangent-modulus approach for obtaining the failure load of axially loaded encased sections. The good agreement observed between this approach and test results on columns in symmetrical bending showed that his fundamental assumption that the two materials acted compositely was substantially valid. Bondale further showed that the columns designed by existing

design rules had load factors against collapse varying from 2.4 to 5.0 for failure about the minor axis. An "approximate" method was also proposed by Basu[26], in which the deflected shape of the column was assumed to be part of a cosine wave. Subsequently, Basu and Hill[27] suggested a procedure to compute numerically the "exact" collapse load of composite columns with unequal end eccentricities, under uniaxial bending and compression. The results of numerical experiments using the "approximate" method were used by Basu and Sommerville[28] in formulating a comprehensive ultimate load design method for both concrete encased steel sections and concrete-filled steel tubes. Expressions presented by Roderick and Rogers[44] based on trilinear concrete stress-strain curve, and bilinear steel stress-strain curve, can also be used in calculating the collapse load of encased columns.

Rectangular or circular steel tubes filled with concrete have attracted the attention of investigators in recent years. Klöppel and Goder[47] considered the buckling of axially loaded tubular sections. Rectangular and circular steel tubes filled with concrete were considered by Furlong[45,46] who suggested empirical formulae for approximate design. With the construction of Almondsbury interchange[48], work was carried out at Imperial College to study such sections. Neogi, Sen and Chapman[49, 50] confirmed that the procedures mentioned above for encased sections could be applied to these sections also, except in the case of axially loaded concrete-filled tubular sections of low slenderness, in which case the ultimate loads calculated will be conservative. The high column strength obtained in this latter case is due to the containment of the concrete by the surrounding steel shell when the filled tube is uniformly compressed, as the triaxially stressed concrete exhibits a much greater strength than

that of uncontained concrete. The enhancement of strength diminishes for increasing slenderness of the column, as also for increasing eccentricity of the load.

An analytical procedure for computing the strength of such columns was proposed by Neogi[51]. He based his method on the previous work of Richart, Brandtzaeg and Brown[52] on stocky spirally reinforced concrete columns. A more exact procedure was suggested by Sen[53], wherein the effect of lateral stresses was incorporated in the expression for the increased longitudinal stress in concrete, which in turn was used for computing the failure load of the column. Knowles and Park[54] suggested a criterion to determine whether triaxial effects would in a given case be significant or not. Guiax and Janss[55] have recently proposed improved methods of calculating the triaxial effects in concentrically loaded circular tubes filled with concrete.

Any analytical procedure for computing the buckling load of an eccentrically loaded composite column would require the determination of the moment-thrust-curvature relationship. Roderick and Rogers[41] made an attempt to do this with the aid of linearised stress-strain relationships both for concrete and steel. However, the numerical integration procedures adopted by Basu[26], Neogi[51] and Sen[53] have the advantage of being general and more exact to the extent that the accuracy depends only on the fineness with which the cross-section is subdivided. The procedure facilitates the adoption of any stress-strain curve, polynomial or multilinear, making it possible to trace the stress-strain history of each element with a desired degree of accuracy. This approach has been extended by Gesund[56] and Brettle and Taylor[57] for column sections in biaxial bending by subdividing the section between parallel lines in two

orthogonal directions. It is presumed that such computations will be attempted only where a digital computer is available. The numerical integration procedures also lend themselves to simple modifications for studying the effects of initial imperfections, unequal end eccentricities at top and bottom, long term loading, residual stresses in steel, and shrinkage of concrete.

Most of the investigations so far have been confined to axial compression with or without uniaxial bending. In practice, columns rarely have a purely axial load, and are very frequently subjected to bending about two axes. Three-dimensional space structures are normally treated as an array of parallel two-dimensional planar structures with all the loads applied in the same plane. The columns in such frames are usually designed to resist bending moments in the plane of the frame. While columns designed in the past in this manner have proved satisfactory, this does not represent the true loading condition in a space structure. In an actual structure, the columns are frequently subjected to bending moments acting in two orthogonal directions in addition to the axial load. Even when the moments are primarily in one plane the presence of geometrical imperfections may induce moments in the perpendicular plane. As observed, earlier solutions for the biaxial bending and compression of composite columns have been attempted only in a few instances. Sharples[58] obtained a solution for the lateral instability of composite columns with eccentric loading about the major axis based on a successive trial and correction procedure. Although essentially a uniaxial bending approach this method can be applied approximately to cases where small moments are introduced about minor axis. Roderick[59] has mentioned an approximate solution to the biaxial bending problem assuming that the deflections are confined to the plane of

bending. Such an assumption has the limitations in that it is very complicated to compute moment-thrust-curvature relations for an axis other than the principal axes of the section. Also, a lack of symmetry in the section would lead to considerable errors due to neglecting components of moments in a plane perpendicular to the bending axis. A simple interaction formula for design which relates the biaxial strength of composite columns to the uniaxial strengths in the major and minor axis directions was suggested by Basu and Sommerville[28] without any experimental or theoretical backing.

1.3 SUMMARY OF PREVIOUS WORK ON COMPOSITE COLUMNS AND ITS RELATIONSHIP TO THIS THESIS

From the review of literature mentioned in the preceding sections it may be observed that no comprehensive theoretical approach on composite columns in biaxial bending has so far been attempted. Nor is there any related experimental work available. Substantial work has, however, been done on the problem of bare steel columns under general conditions of end loading, including biaxial bending. The problem of composite columns in uniaxial bending has also received comprehensive treatment in the work of Basu and others[26,27,28]. The formulations of Harstead, Birnstiel and Leu[20] and Milner[23] for the relatively exact solution of bare steel columns in biaxial bending and that of Sharma and Gaylord[22] for an approximate solution of the same problem have all proved satisfactory. For this reason, the formulation of the problem of composite columns in biaxial bending was parallel to that of the three works on bare steel columns mentioned above with the simplification that twisting forces and deflections are ignored in view of the large torsional

rigidity of composite column cross-sections. The procedure for computing the basic moment-thrust-curvature relationship is an extension of Basu's[26] approach for composite columns in uniaxial bending. Two solutions to the problem have been given, one based on the determination of the exact shape of the deflected column, and the other based on an assumed deflected shape. Both solutions are based on an iterative technique similar to the Newton-Raphson iteration formula and are believed to be the first such application. The computerised methods of analysis have been used to evaluate the applicability of the design rules due to Basu and Sommerville[28] as applied to composite columns under general biaxial end eccentricities.

1.4 STIFFENED PLATES IN COMPRESSION

Stiffened panel construction has been widely used in steel box girder bridges in recent times. It has been used for ship and aircraft plating for even longer. Following the collapse of the three steel box girder bridges in Milford Haven, Melbourne and Koblenz, much experimental and theoretical work has been undertaken to study various stability problems associated with stiffened panels in compression. A committee of enquiry was set up in Britain to examine the existing design rules and to put forward recommendations[60] for the design of stiffened panels under compression among other components of steel box girders.

An elastic solution to the problem of stiffened plates was given by Timoshenko[61] in 1921 based on energy principles. Exact solutions were later given by Loshkin[62] and Barbré[63] for the elastic critical buckling of such plates. However, the ultimate load of a thin plate and stiffener combination may be considerably above the load for local

buckling of the plate[64]. The problem of finding the ultimate load is of course very distinct from that of finding the buckling load. Little is known about the inelastic behaviour of such plate elements, or for that matter, of the effect of residual stresses due to welding and of initial lack of imperfections on the ultimate strength of such panels. The distribution of residual stresses in welded plates, and their effect on the ultimate strength has been discussed by Dwight, Chin and Ratcliffe[65], Ratcliffe[66], and by Nishino, Ueda and Tall[67]. Further experimental and theoretical work has been done by Vojta and Ostapenko[68] and by Dwight and Moxham[69,70,71]. Related work on box girder models has been carried out by Dowling, Chatterjee, Frieze and Moolani at Imperial College[72].

On the basis of experimental evidence, Lundquist[73] obtained good results by including an effective portion of the sheet into the cross-section of the stiffener. The effective width concept has also been advocated by Kármán, Sechler and Donnell[74] among others, but this approach has been criticised by Dwight and Moxham[69].

Stiffened compression panels are essentially anisotropic plate elements. An exact solution of the problem is likely to be very tedious. However, in many practical cases the rigidity of a stiffened panel in the direction of longitudinal stiffeners is far greater than that in the transverse direction. The post-buckling behaviour of such a panel in such a case approaches that of a strut consisting of an individual stiffener together with an associated width of the plate, i.e. there is no appreciable overall post-buckling reserve. This approach has been adopted here to study the effect of residual stresses due to welding and the effect of initial lack of straightness on the strength of stiffened compression panels.

The computer programs developed for the study of composite columns in biaxial bending were general enough to analyse a wide variety of cross-sections including reinforced concrete columns, concrete encased steel stanchions, concrete-filled steel tubes, and bare metal sections, all of arbitrary shape. A ready application was found for stiffened plates in compression using the approach outlined above.

Another factor influencing the strength of stiffened plates in compression is the local buckling of the plate element spanning between the stiffeners. A semi-empirical approach was suggested by Vojta and Ostapenko[68] using an average stress-strain curve, defining the local behaviour of the plate, in place of the material stress-strain relationship. Mittleman[75], who employed the author's computer programs for his study, and later Dwight, Little and Rogers[76], used the same approach with different curves defining the behaviour of plate elements subjected to local buckling. The curves selected in this thesis are based on Ratcliffe's experiments[66]. The relative merits of various curves are discussed in detail in Section 7.4.

1.5 SUMMARY OF PREVIOUS WORK ON STIFFENED PANELS AND ITS RELATIONSHIP TO THIS THESIS

It is clear that an exact solution to the problem of stiffened plates in compression with the objective of finding their ultimate loads is difficult to obtain. For panels having a large number of closely spaced stiffeners, the inelastic behaviour of the plate may be approximated by that of a strut consisting of an individual stiffener and an associated width of the plate. This approach has been adopted here using a width of the plate equal to the stiffener spacing. The effect of residual stresses due to welding and of initial lack of straightness

has been studied over the full practical range of slenderness ratios. The results obtained have been presented in a form suitable for use in the design of stiffened plates. A semi-empirical approach towards including the effect of local plate buckling in similar design curves is also indicated.

1.6 SCOPE AND LAYOUT OF THE THESIS

The general objective of this thesis, as mentioned in the opening section, was to obtain an analytical method for the determination of the collapse load of composite columns under biaxial bending. The study was limited to pin-ended columns. However, the entire range of combinations of end eccentricities was covered. An approximate solution using deflected shape in the form of part of a cosine wave was first obtained for columns with symmetrical eccentricities at the two ends. Tests on 9 columns in this category are reported, and the results used to check the applicability of the approximate solution. The existing design method due to Basu and Sommerville is scrutinised in the light of more exact analytical results for various cases of biaxial bending. Application of the computer programs to a parametric study on stiffened plates in compression is also reported.

The experimental investigation on 9 composite columns is first described in some detail in Chapter 2. Sufficient data were collected to examine some of the fundamental assumptions made in the theoretical calculations. The next three chapters contain the theoretical aspects of the problem of composite columns in biaxial bending.

Chapter 3 deals with the development of a procedure to compute the moment-thrust-curvature characteristics of a composite column cross-section under biaxial moments and thrust. The moment-thrust-curvature relationships are relevant to any computations, approximate or exact, of the failure loads of composite columns of finite length. Hence they have been assigned a separate chapter.

Chapter 4 presents an approximate method for the determination of the ultimate load of composite columns under biaxial bending with symmetrical eccentricities at the two ends using the part-cosine wave assumption for each of the two deflection components.

In Chapter 5 a method has been developed to determine the exact deflected shape of a column under generalised biaxial bending. This is used as a basis for the determination of the failure load of such columns.

All the numerical experiments on composite columns have been grouped in Chapter 6. First, the accuracy of the procedure for moment-thrust-curvature is established. Next, the validity of the computer program is examined in the light of comparisons with the existing solutions for uniaxial bending for encased columns as well as filled tubes. Verification of the results for biaxial bending is carried out by comparing computed results with the experimental results on columns with symmetrical end eccentricities. Also examined in this section is the effect of making the part-cosine wave assumption. The following section examines in detail the design method due to Basu and Sommerville as applied to columns in biaxial bending.

Chapter 7 describes the results obtained from a study of the effects of residual stresses and of lack of initial straightness on the strength of stiffened plates in compression. An approximate method for estimating the effect of local plate buckling on the stiffened plate strength is also indicated.

The conclusions drawn from the theoretical and experimental studies described in the thesis have been grouped together in the final chapter.

CHAPTER 2

TESTS

2.0 GENERAL

Tests were carried out on nine pin-ended concrete encased steel H-sections of varying lengths which were subjected to compressive loads applied at varying biaxial eccentricities, different in the two planes of bending but symmetrical at the two ends. Apart from testing the columns for the ultimate load, their load-deflection and load-strain responses were also monitored.

2.1 CHOICE OF SCALE

The tests were carried out on full-scale specimens. One of the considerations was that it is difficult to obtain concrete of comparable properties in reduced scale models. In addition, it is not easy to simulate imperfections in the steel section, viz. the initial lack of straightness and the presence of residual stresses, in scaled down models. In particular, the effects of scale on interaction between steel and concrete components are not clear.

2.2 DETAILS OF CROSS-SECTION

For convenience, the smallest practical column H-section viz. 6 in x 6 in @ 15.7 lb, was selected for the column core. A 2 in cover, the minimum required by code regulations, resulted in the overall dimensions of 10 in x 10 in for the composite column. Concrete was effectively tied around with transverse binders (3/16 in diameter) at a spacing of 6 in centres. These were held in place by four longitudinal

bars of 1/2 in diameter at the four corners, situated at half the depth of the cover.

2.3 PARAMETERS INVESTIGATED

The two parameters that were systematically varied within the test programme were the slenderness of the column and the eccentricity of applied load. Three specimens, each of three different lengths - 6 ft, 12 ft and 24 ft were cast. These lengths were chosen to give values of slenderness ratios at the extreme ends and centre of the practical range. Specimens of the same length were tested under three sets of biaxial eccentricities. The three eccentricities of load used with each column were all confined to the same plane. The small eccentricity was well within the cross-section, the medium one on the perimeter, and the large one outside the cross-section. Table 1 lists the lengths and eccentricities of all nine specimens.

2.4 PARAMETERS NOT INVESTIGATED

Several other parameters, for example, material strengths, concrete cover, unequal end eccentricities at the two ends, and concrete contribution parameter, would require investigation for a comprehensive experimental verification of various design cases. However, these parameters were not studied systematically in this test programme because of the limited funds available for the project.

2.5 MANUFACTURE OF SPECIMENS

The specimens were cast with two steel end plates, 10 in x 10 in x $1\frac{1}{2}$ in thick, already welded to the main steel sections. The end plates were provided with tapped holes by which they were fixed to the rig plates.

Figure 1 shows the specimen with details of the end plates. At the time of casting, access holes were provided at four places on the mid-section to facilitate fixing of strain gauges on the H-section. The casting was done with the columns in the vertical position. Sufficient space was left between end plates and concrete for subsequent filling with a dry mix mortar. This ensured that the concrete shrinkage did not result in separation between end plates and concrete.

2.6 MATERIAL PROPERTIES

A concrete strength of 4,500 lbf/in^2 was specified. This was to be obtained using a 1:2:4 mix with a water cement ratio of 0.55. All specimens were manufactured from the same lot of materials (sand, aggregate, cement, H-section and reinforcing bars), and similar casting and curing procedures were adopted. The period of curing was 28 days. Standard 6 in cubes were taken from all batches of concrete. Tests on the cubes supplied by the manufacturers of the columns, Taylor Woodrow Anglian Ltd., indicated that the concrete strength actually obtained was much higher than the specified value. The cubes were tested at the time of testing of the corresponding test specimens. The results of compression tests on all the cubes are listed in Table 2.

Several tests on coupons cut from the H-section were also carried out to determine the yield stress of steel. Some of the coupons were taken from the web, others from the flanges. The yield strengths and the ultimate strengths obtained in these tests are given in Table 3. Tensile tests were done on the steel bars used as the longitudinal reinforcement, and the results obtained appear in Table 4.

Six stub columns of length 30 in cut from the main steel section were tested with axial loads to study the effect of residual stresses and local buckling of the flanges on the behaviour of the bare steel section. These specimens were prepared and tested in accordance with the procedures laid down in the Column Research Council's Guide to the Design Criteria for Metal Compression Members[77]. A notable feature of these tests was that the stub columns failed by inelastic buckling of the flanges followed by the buckling of the webs. The flange width to thickness ratio for the section was 22.3. Thus the exclusion of this section from the list of available universal column sections which may be used in plastic design of bare steel columns as suggested by Horne[78], is confirmed experimentally. No such restriction applies of course when the column is encased in concrete as the surrounding concrete prevents premature local buckling of the flanges prior to failure of the whole cross-section. Another specimen was tested after cutting 1 in off the flanges on all four tips thus reducing the flange width to thickness ratio to 14.9. This column failed by overall yielding. The average failure stress over the cross-sectional area obtained was higher than for the first five specimens and was only 5% less than that obtained by coupon tests. The results obtained from these tests are grouped in Table 5.

In view of the results given in Tables 3-5 an average yield strength of 20.375 tonf/in^2 was assumed for steel in the H-section, and the corresponding yield strain was taken as 0.00155. The strength of concrete as obtained from cubes differs substantially from that obtained in actual beam/column specimens. It is common practice to employ a reduction factor of 0.85 in conjunction with a variability factor of 0.80 in the case of laboratory specimens. This results in an overall reduction

factor of 2/3, a value commonly used for laboratory results. However, to assess the concrete strength as obtained in the specimens, some short column tests were carried out on 36 in long composite sections sawn off from the undamaged lengths of the original test columns after the latter had been loaded to failure. Results obtained are listed in Table 6. It may be observed that the average strength obtained is less than the average cube strength by a factor 0.6415, which is very near to the factor 2/3 mentioned above.

2.7 INSTRUMENTATION

Four electrical resistance strain gauges were positioned, one at each of the four flange tips of the section at mid-span, to pick up the strain distribution across the section. The gauges were placed through the access holes provided at the time of casting. Figure 2 shows the strain gauges before the access holes were filled with concrete. To ensure satisfactory working of the gauges it was necessary to prevent them coming into contact with moisture. The following procedure was adopted.

(1) The tip of the flange was ground to a smooth finish;

(2) The adhesive resin was applied on to the ground tip of the flange, and the strain gauge was then stuck in position;

(3) The surrounding concrete was dried by focussing a light on it for a period of four hours;

(4) The strain gauge circuit was tested using a Peekel instrument;

(5) An insulating sleeve was placed over the gauge;

(6) A 1/8 in layer of Prepot sealing mixture was poured into the hole and allowed to set overnight;

(7) The strain gauge circuit was tested once again;

(8) The remainder of the hole was filled with a fast curing cement mix.

The strain gauges used were of 10 mm length with a gauge factor of 2.06. The strain measuring circuit included dummy strain gauges fixed to an unstressed steel specimen embedded in concrete for temprature compensation.

Concrete strains were measured using demountable mechanical gauges between Demec points. The Demec points were fixed on to the side of the column at selected points by means of a quick-hardening resin. Two gauge lengths were used, 4 in and 8 in. The positions of gauges for the three lengths of test specimen are shown in Fig. 3.

The deflections of the specimens under load were measured using dial gauges and vernier scales. These gauges and scales were supported on a rig running parallel to the column. The deflection rig was isolated from the loading rig, so that the observed deflections were absolute. Deflections were measured at mid-span, quarter-span, and end-points. For the long columns, they were also measured at 1/8th span points. The end stations were intended primarily to detect any slip or rigid body rotation of the test specimens. At each station along the length, three or four gauges/scales were fixed to measure the average horizontal and the vertical deflections. A close-up view of one such station is shown in Fig. 4. The dial gauges used in measuring deflections had an accuracy of 0.001 in and a travel of $2\frac{1}{2}$ in, although in some cases gauges with an accuracy of $\pm$ .0001 in and a travel of $1\frac{1}{2}$ in were used. The respective figures for the vernier scales were 0.001 in and 6 in. The vernier scales

were employed mainly in the case of long columns, as the expected deflections were large.

The faces of all columns were painted white to assist in the detection of tensile cracks in the concrete. At each stage of loading, the developing cracks were marked with dark lines. In the case of long columns, particular cracks nearest to the mid-span were monitored and the growth of the crack width measured with the aid of a microscope.

2.8 LOADING RIG

The columns were tested in a horizontal position. The main reason for testing them in such a position was that a vertical loading rig to test the 24 ft columns was not available and would have had to be specially designed. Apart from considerations of cost it was considered that the recording of measurements would have been very time-consuming and inconvenient in the vertical position. By testing horizontally the need for a large frame was eliminated, the monitoring of various gauge readings was simplified, and it became possible to keep the entire column length under observation throughout the duration of the test.

Testing columns horizontally required some mechanism for counter-balancing the dead weight of the column. This was effected by supporting the columns at various points along the length. The arrangement of the rig for 6 ft, 12 ft and 24 columns is shown in Fig. 5, indicating the points where the column was supported. In each case the supporting rig was carried on load maintaining jacks, so that the dead weight effect did not become significant even after the column had deflected under applied longitudinal load. The maximum dead weight strain induced in the columns supported as shown in Fig. 5, was found experimentally to be less than 10 microstrain.

The longitudinal load was applied by means of a hydraulic jack. The jack was reacted off heavy concrete blocks which were prestressed to the strong floor to prevent slip. The columns were placed with the jacks at one end and a further set of concrete reaction blocks at the other. Ball and socket type bearings were used at each column end to simulate pin-ended conditions. The rig plates, which were each bolted to a column end-plate on one side, had a spherical socket machined on the other side. The nominal diameter of the ball and of the socket was $3\frac{1}{4}$ in. The bearings were greased to minimise friction. Figure 6 shows a typical rig arrangement with a 24 ft column in position.

To prevent rigid body rotation of the column, one of the two end-plates was supported off the strong floor by a special pin-ended steel strut. The loading was controlled by an Amsler Load Control Cabinet. Two similar cabinets were used for the self-weight supporting mechanism.

2.9 TEST PROCEDURE

Before recording any observations, it was imperative to ensure that the specimen was adequately "bedded-in". For this purpose small loads were applied, and then removed, a few times. During the test, loads of increasing magnitudes were applied, and strains and deflections recorded. After reaching the ultimate load, an attempt was made to obtain the descending branch of the load-deflection curve in the case of some of the specimens. The complete test consisted of three phases in each case.

(1) Initially, the load was applied in increments of about 10% of the estimated failure load for each column. For the first few steps, after each increment of load, the specimen was unloaded to zero load. The observations for strains and deflections after each unloading were

compared with those at the first zero. The process of unloading was continued while the two zeros showed negligible difference. The load at which the deflections after unloading differed from the initial deflections was recorded as the elastic limit load (or the load corresponding to the limit state of unserviceability). The process of unloading was discontinued beyond this stage.

(2) The loads were then increased by increments, and deflections and strains recorded. As the growth of deflection with load indicated an increasing degree of non-linearity, the increment of load was successfully reduced. During this stage, steady deflections were obtained after a short time, while the load maintained a constant value. The time interval needed to obtain a steady deflection reading tended to increase with successively higher values of load, beginning initially with almost instantaneous equilibrium. When the load reached about 80-85% of the failure load value, the interval became as much as 3-5 minutes. Beyond this stage, therefore, the testing procedure was slightly modified.

(3) The observations were recorded, not for increasing loads, but for increasing deflections during the final phase. After the last equilibrium state, the load was increased slightly and the column allowed to deflect progressively. However, when the new increment in deflection was roughly the same as the previous one, the valve on the cabinet regulating the flow of oil to the jacks was closed. In the early stages of this third phase, it was observed that the column sustained successively smaller increments of load. A stage was finally reached when the load was decreased from the previous value in order to maintain equilibrium at the higher deflection. This reversal in trend corresponds to the peak load or the failure load. The observations for load-deflection relation-

ship were carried on further along the descending branch until it was considered that no further useful information could be obtained from the test.

The time taken for recording observations at each load level varied from about 10 minutes in the early stages to about 15 minutes in the later stages. The total time required for each test varied from about 4 to 6 hours.

2.10 TEST RESULTS

2.10.0 Mechanism of Failure

The failure in all cases followed an almost parallel course. The first stage always corresponding to yielding in the compression tip of the H-section. The strain in the steel flange at the opposite corner (tensile zone) was next to reach yield. A continuous deterioration in column stiffness was observed. Final collapse was accompanied by spalling of concrete in the compression zone. This immediately resulted in the buckling between ties of the longitudinal reinforcement bar at the compression corner, reducing the column to a mechanism. An attempt was made to monitor the falling branch of the load-deflection curve in the case of long columns 'H' and 'I'. However, the zone beyond the peak of the load-deflection curve is difficult to trace as the column exhibits a negative stiffness at this stage. A summary of test results is given in Table 7.

2.10.1 Short Columns

2.10.1.1 Load-Deflection Curves:

Figure 7 shows the load-deflection curves as recorded for the three short columns. Both vertical and horizontal deflections are shown. The vertical and horizontal deflections tend to be of the same order, mainly because of the particular combination of end-eccentricities chosen. The broken lines in the curves are intended to indicate deflections near collapse which were not monitored. The curves indicate typical load-deflection characteristics with gradual loss of stiffness, and large plateaux near the respective peaks.

2.10.1.2 Load-Strain Curves:

Figure 8 shows the variation of strains with increasing loads. For each column, two curves are given - one for the point in the steel section stressed to the maximum in compression, and the other for the diagonally opposite point stressed to the maximum in tension. The non-linearity exhibited by strains is of the same nature as that exhibited by deflections. In all cases the compression tip indicates earlier yielding. As the biaxial eccentricity of the load is increased from column A to column C the difference in magnitude between the compressive and tensile strains reduces, indicating the increasing predominance of flexural strains.

2.10.1.3 Internal Strain Distribution:

Since strain measurements were made at the four corners of the H-section, sufficient information is available to examine the validity of one of the major assumptions made in current analytical procedures -

viz. plane sections remain plane after loading. Figure 9 shows the strain distribution across the section for three load levels for column 'B'. In drawing these strain distributions, the strains at three points (including the two extreme values) were used in locating the neutral axis, and the value of strain at the fourth point was measured and compared with the recorded value. It may be seen that at very low load level (10 tons) there is a very small error in the strain values. At an intermediate level the error increases, and at the last load level before collapse (60 tons) the error is significant. The extreme values of strain for this last case are however beyond yield strain and so the measurements are more subject to error. Nonetheless the experimental strain distribution may be seen to be reasonably linear in distribution.

In the same strain distribution figures, the strains measured in concrete are also shown (in broken lines). The measured concrete strains conform closely to the linear strain distribution and further confirm the validity of the assumption that plane sections remain plane. It is only near collapse load that there occurs a significant variation (still less than 10%) in the strain and it must not be overlooked that by now the deflections are no longer infinitesimal, and hence some deviation from plane strain distribution is only to be expected.

2.10.1.4 Interaction Between Steel and Concrete:

An important corollary to the observations is the fact that the strains are continuous from steel to concrete. This corroborates the fundamental assumption made in analytical procedures for the calculation of failure loads, viz. the strains in steel and concrete at their interface are compatible.

2.10.1.5 Crushing Strain of Concrete:

Another interesting observation may be made here. The strain in concrete at the load level of 60 tons is about 0.0032 (recorded strain). The extrapolated value at the corner would be approximately 0.0035. As the column collapsed at the next load level (65 tons) with spalling of concrete at this corner, the strain just before crushing of concrete would be around 0.0040, which is the commonly observed value of failure strain even in direct compression tests.

2.10.1.6 Variation in Neutral Axis Position:

The three strain distributions also indicate the shift in the position and direction of neutral axis at various load levels. No consistent pattern can be discerned because at each load level the orientation of the neutral axis is governed by several factors; for example, the relative stress levels in concrete and steel, the degree and extent of yielding in the cross-section, etc.. The neutral axis, however, remains generally at an angle of 35° - 45° with the horizontal.

2.10.2 Medium Columns

2.10.2.1 Load-Deflection Curves:

The load-deflection curves for the three medium length columns are shown in Fig. 10. The curves follow the same general pattern described for short columns. The magnitude of deflections is much larger - these columns were twice as long as the short columns. In the case of column F, the falling branch of the load-deflection curve was successfully monitored. It may be observed from Fig. 10, that the peaks for both the load-horizontal deflection curve and load-vertical deflection curve are clearly defined, although the plateau near the top is of considerable

length. Near collapse, the horizontal and vertical deflections were again almost equal, as was the case for short columns. This, of course, was due to the particular ratio of end-eccentricities chosen in these tests.

2.10.2.2 Load-Strain Curves:

Figure 11 shows the load-strain variation for all three medium columns. For each column the strains plotted are for points under maximum tensile strain and maximum compressive strain. As in the case of short columns, the difference between the magnitudes of the two extreme strains tends to narrow down with increasing eccentricity of the applied load. Once again the compression tip reaches yield strain first.

2.10.2.3 Internal Strain Distribution:

Strain distributions across the cross-section for column E are given in Fig. 12. The figures relate to the strains at 20 tons, 40 tons and 52.5 tons. The broadly linear pattern of strain distribution is once again in evidence at all the load levels, though errors are noticeable for points nearer to the neutral axis.

2.10.2.4 Crushing Strain of Concrete:

The maximum concrete strain recorded was about 0.0032 at a load of 55 tons, that would result in a corner strain of about 0.0035 at this load level. Since the column failed at 57.5 tons, a failure strain of 0.0040 might again have been realised.

2.10.3 Long Columns

2.10.3.1 Load-Deflection Curves:

The deflections obtained for the long columns were large - the failure deflection for column I being in excess of 6 in. The comparative

load-deflection response for the three long columns G - I are shown in Fig. 13. The plateau near the top of the load-deflection curves may be seen to be of considerable length, particularly in the case of column I - the column with a combination of the largest length and the largest eccentricities.

2.10.3.2 Load-Strain Curves:

The load versus steel strain characteristics for these columns are given in Fig. 14. The observed behaviour is similar to that for short and medium columns.

2.10.3.3 Internal Strain Distribution:

The cross-sectional strain distributions shown in Fig. 15 clearly indicate the predominance of flexural strains - the relative magnitudes of compressive and tensile strains tend to converge with increasing load. The variation of strains is once again nearly proportional to the distance from the neutral axis, and shows a continuity of strain between steel and concrete.

2.10.4 Comments on Load-Deflection and Load-Strain Curves

It was mentioned in Section 2.9 that a special procedure was adopted for recording load-deflection characteristics after a load of about 80-85% of the failure load had been achieved. Since the loading machine employed had a hydraulic-mechanical loading device, it was necessary to control deflections by adjusting the applied load. In this way, two values of load are recorded corresponding to each deflected position - the instantaneous load and the smaller equilibrium load. The plots in Figs 7-8, 10-11 and 13-14 correspond to the instantaneous value. Figure 16 shows the relative effect the two loads have on the load-

horizontal deflection curves for the three columns for which the falling branch of the load-deflection curves were monitored (columns F, H and I).

As the bending of the columns was mainly along a diagonal, two diagonally opposite tips of the steel flanges were always very close to the neutral axis. Since the position of the neutral axis changes with increasing load, the strains near the neutral axis show transition from tension to compression, or vice versa. This was observed in almost all specimens. The plot in Fig. 17 is for column I. The phenomenon was very distinct in this case because of relative predominance of bending.

Figures 18-19 show the collapse mode of column I. Figure 18 shows a view from the top of the column in the loading rig. Figure 19 is a close-up of the collapsed zone and clearly shows the extent of spalling of concrete and the buckled shape of the longitudinal reinforcement. Figure 20 is another view of the collapsed zone from a different angle. This figure shows the buckled shape of the flange of the H-section.

Column I was cut at a section slightly away from the crushed mid-span section. Figure 21 shows the crushed concrete, and the approximate direction of neutral axis is given by the boundary between the bonded and loosened concrete zones. The bond between steel and concrete in the zone where no spalling has taken place appears to be undisturbed. This corroborates the deduction made from various strain distribution diagrams shown in Figs 9, 12 and 15, viz. there exists a continuity of strain between steel and concrete - a necessary condition for full composite action.

CHAPTER 3

THEORY - MOMENT-THRUST-CURVATURE RELATIONS

3.0 GENERAL

Moment-thrust-curvature relations depend not only on the shape of the section and the distribution of one material with respect to the other, but also on the individual stress-strain behaviour of the composite materials. In addition, the presence of residual stresses, and their distribution over the steel area, alters the moment-thrust-curvature relations. Analytical evaluation of these relations is very involved, if not altogether impossible. The problem becomes acute in the case of biaxial bending. Eventually, one has to employ numerical integration procedures. The numerical method adopted here is similar to the one suggested by Gesund[56]. The method is so general that reinforced concrete sections and bare metal sections can be analysed as well as composite sections be they concrete encased sections or concrete filled steel tubes. The residual stresses in the steel sections can be easily accounted for in obtaining the moment-thrust-curvature relations.

3.1 ASSUMPTIONS

The problem of biaxial bending of composite columns cannot be solved without recourse to certain simplifications and idealisations. The major assumptions, and their justification or otherwise, are given below:

(1) There exists a complete interaction between steel and concrete. In other words, the strains in steel and concrete at their interfaces are assumed compatible.

The rather close agreement obtained between computations based on this assumption and results obtained from experiments by Bondale[43], Neogi[51], Sen[53], and others on columns in uniaxial bending indicates that the assumption is substantially valid.

(2) The stress-strain curves for concrete and steel are assumed to be reversible. This implies that the loading and unloading stress-strain relations are identical.

This assumption deviates from the observed phenomenon of different unloading characteristics for most inelastic materials, compared with the loading characteristics, particularly when the material is strained beyond the proportional limit. However, since most cases of failure, particularly in laboratory conditions, occur due to progressive loading, this assumption is not likely to cause any serious error in the computed results.

(3) The strain distribution across the section is assumed to be linear, varying in proportion to the distance from the neutral axis. In other words, it is assumed that the plane sections before bending remain so even after the application of the loads.

This assumption is valid for cases in which the bending is about an axis of symmetry. In all other cases, the section is subjected to some twisting stresses, which results in the warping, however slight, of the section.

It may be remarked here that the depth of neutral axis depends not only on the shape and composition of the section, and the material properties, but also on the applied loads and biaxial moments.

(4) The stress-strain curves for concrete used for the analysis are based on experimentally observed relations of test-specimen, usually concrete cubes, or cylinders. The stress-strain relationship for concrete as it exists in the column under uniaxial and biaxial bending, differs from this observed relationship. It is common practice to reduce the stress ordinate by multiplying with a reduction factor. This factor has values varying between 0.8 - 0.9. This factor corresponds closely to that relating cylinder strength to cube strength. Also, the concrete strength varies throughout the column and an additional reduction factor on the cube strength is often used to account for this variation.

The stress-strain relation for steel in the column member is assumed to be identical with the stress-strain relation obtained from standard tensile tests on steel specimen.

(5) The tensile strength of concrete, and the effect of strain hardening in steel are ignored, although a slight modification in the computer program will enable consideration of these two factors as well.

3.2 STRESS-STRAIN RELATIONS

3.2.1 Concrete

Concrete is an inelastic material, and because of several factors involved, does not exhibit a consistent stress-strain relationship. There is no unanimity over a single mathematical function defining the concrete behaviour. From time to time, several authors have suggested different formulae. In order to provide flexibility in the use of the computer program described here, provision has been made for adopting one of the following formulae, suggested by different investigators:

(1) A polynomial curve of the third degree, as proposed by Basu[26]. This formula is based on tests conducted at Cambridge University, by Barnard and Johnson[79]. The formula is as follows:

$$\frac{\sigma}{\sigma_u} = C_1 \left(\frac{\varepsilon}{\varepsilon_u}\right) + C_2 \left(\frac{\varepsilon}{\varepsilon_u}\right)^2 + C_3 \left(\frac{\varepsilon}{\varepsilon_u}\right)^3 + C_4 \left(\frac{\varepsilon}{\varepsilon_u}\right)^4 \qquad (1)$$

where σ_u = maximum concrete stress

ε_u = concrete strain corresponding to σ_u.

The coefficients C_i $(i = 1, 2, 3, 4)$ are obtained by fitting data obtained from uniaxial compression of concrete cubes/cylinders. The Cambridge University results gave the following values for these coefficients:

$C_1 = 2.410$ $\qquad$ $C_2 = -1.865$

$C_3 = 0.500$ $\qquad$ $C_4 = -0.045$

This formula has also been adopted by Sen and Chapman[50] in preparing design tables for concrete-filled tubular steel sections in uniaxial bending.

(2) The Desayi-Krishnan Equation[80]. According to Desayi and Krishnan, the concrete stress-strain relation can be given by the formula:

$$\frac{\sigma}{\sigma_u} = \frac{2\left(\frac{\varepsilon}{\varepsilon_u}\right)}{1 + \left(\frac{\varepsilon}{\varepsilon_u}\right)^2} \qquad (2)$$

(3) The Equation adopted by the investigators at New South Wales University. This formula has been adopted by Warner[81] to study the biaxial bending of short reinforced concrete columns. According to the formula,

$$\frac{\sigma}{k_1 \sigma_c} = \gamma\left(\frac{\varepsilon}{\varepsilon_u}\right) + (3 - 2\gamma)\left(\frac{\varepsilon}{\varepsilon_u}\right)^2 + (\gamma - 2)\left(\frac{\varepsilon}{\varepsilon_u}\right)^3$$

$$\text{for} \quad 0 \leqslant \frac{\varepsilon}{\varepsilon_u} \leqslant 1.0 \tag{3a}$$

and,

$$\frac{\sigma}{k_1 \sigma_c} = 1 - \frac{\left(\frac{\varepsilon}{\varepsilon_u}\right) + \left(\frac{\varepsilon}{\varepsilon_u}\right)^2}{1 - 2\left(\frac{\varepsilon_f}{\varepsilon_u}\right) + \left(\frac{\varepsilon_f}{f_u}\right)^2} \tag{3b}$$

$$\text{for} \quad 1.0 \leqslant \frac{\varepsilon}{\varepsilon_u} \leqslant \frac{\varepsilon_f}{f_u}$$

where σ_c = observed, maximum concrete stress

ε_u = concrete strain corresponding to σ_c

ε_f = failure strain, where σ_c, stress in concrete, reduces to zero after failure

k_1 = factor relating member stress with the observed stress for identical strains.

(4) A generalised multilinear curve. The curve is most useful for computational purposes and can be made to fit any theoretical or experimentally observed stress-strain relationship. By choosing the data points at a sufficiently close spacing, reasonable smoothness of the stress-strain curve can be obtained.

Figure 22 shows a comparison between various forms of stress-strain curves for concrete that can be chosen in the computer program.

3.2.2 Steel

A typical stress-strain curve for ordinary structural steel is shown in Fig. 23. For computational purposes, the stress-strain relationship is idealised. It is common practice to adopt an elastic-perfectly plastic (bilinear) curve for steel, ignoring the effect of strain hardening. The computer program can accept the steel stress-strain relation in one of the following two forms:

(1) A multilinear curve:

This option can be used to specify any theoretical or experimentally observed stress-strain relationship, including the bilinear idealisation mentioned above. The trilinear curve adopted by Neogi, Sen and Chapman[49] can also be similarly specified.

(2) Basu's[26] exponential formula:

This formula, adequate mainly for steels with no definite yield point, expresses stresses as an exponential function of strains. Different curves are obtained by altering the value of the parameter β (Fig. 23).

According to this formula

$$\frac{\sigma}{\sigma_y} = \frac{1}{\beta} \log_e \left[\frac{1 + e^{\beta}}{1 + e^{\beta} \left(1 - E_o \frac{\varepsilon}{\sigma_y}\right)} \right] \qquad (4)$$

where σ_y is the yield stress of steel, and

E_o is Young's Modulus for steel at origin.

3.3 RESIDUAL STRESSES

The effect of residual stresses present in rolled steel sections subjected to compressive axial load is to delay, or speed up, the process of yielding in different components depending upon the residual stress in the component being tensile or compressive respectively. The magnitude and distribution of residual stresses across the steel section are highly variable. These residual stresses depend not only on the shape and size of the section, but also on the manufacturing process. The stress patterns also vary because of uneven cooling of different parts of the section after the hot-rolling process. Attempts have been made by various investigators to obtain generalised patterns for the residual stress distribution across the section.

Two patterns of residual stress distribution in steel sections may be considered:

(1) AISC pattern[82]

This is shown in Fig. 24. The peak values depend upon the parameter A_w/A_f where A_w = area of web, and A_f = total area of flanges.

(2) Cambridge pattern[83]

This is shown in Fig. 25. It is claimed[83] that this pattern is generalised, and is valid for all I-shapes.

The residual stress patterns cannot be directly used in considering their effect on the column behaviour. The stress pattern is first converted to the residual strain pattern as it is the residual strain that causes residual stress, and not the other way round. The strains due to the applied loads are then superimposed on the residual strains. The net strains so obtained are then used to determine the net stress in

the section including the effect of residual stresses, using the particular steel stress strain relationship adopted for computations.

3.4 EXPRESSIONS FOR MOMENT-THRUST-CURVATURE RELATIONS

The column cross-section is subdivided into a grid of small size rectangular elements as shown in Fig. 26. The section is assumed to consist of either concrete, steel, or hollow areas. The method is therefore equally applicable to concrete encased steel structures, concrete filled steel tubular columns, reinforced concrete columns or bare steel sections. Irregular steel areas are replaced by rectangular areas, satisfying two conditions:

(a) The substituted area is exactly equal to the area of the equivalent rectangle.

(b) The centroid of the substituted area coincides with that of the equivalent rectangle.

The axes of reference are chosen as indicated in Fig. 26, and it it assumed that point O is always under maximum compression. Thus the value of θ, the inclination of the neutral axis with the y-axis, is to be varied between the limits 0 and $\frac{\pi}{2}$. This helps to reduce the number of cases to be analysed, particularly for those sections which have at least two axes of symmetry. Suitable transformation of axes can be easily made if some other corner of the section undergoes maximum compression. The moment-thrust-curvature relationship, in the case of biaxial bending, consists of a relation between six quantities, viz. axial load P, moment M_x, moment M_y, distance z_n of neutral axis from point O, the curvature ϕ, and angle θ. By assigning all possible values to any three of the variables,

the other three can be found out, at least in principle. One course that can be taken is to assign values to θ, ϕ, and P, and to locate z_n by iteration. Once z_n is determined, M_x and M_y can be easily computed. An alternative approach is to assign values to θ, ϕ, and z_n. In this case no iteration is involved, and P, M_x, and M_y can be directly computed.

With the curvature ϕ and the neutral axis position z_n being specified the strain distribution across the section due to applied loading is determined. This follows directly from the assumption about plane sections listed above. Thus

$$\varepsilon_o = \phi z_n \tag{5}$$

where ε_o is the strain at the origin.

The strain in any element of area Δ_{aij} whose centroid is (x_i, y_j) is given by

$$\varepsilon_{ij} = \varepsilon_o \left(1 - \frac{z_{ij}}{z_n}\right) \tag{6}$$

where z_{ij} is the perpendicular distance of an axis passing through the element, and parallel to the neutral axis, from the origin O.

With this value of strain existing at the element the stress σ_{ij} in the elemental area can be obtained using a stress-strain relationship appropriate to the material of the area. If the elemental area is of steel, the strain should be modified to take into account residual stresses, if any, at this stage.

The elemental force is given by

$$\Delta P_{ij} = \Delta_{aij}\, \sigma_{ij} \tag{7}$$

Summing over all the elements the axial force P for the section is obtained,

$$P = \sum_{i=1}^{n_a} \sum_{j=1}^{n_b} \Delta_{aij}\, \sigma_{ij} \tag{8}$$

where n_a and n_b are the numbers of elements along x and y directions, respectively.

Similarly, the moments about x- and y-axis are obtained,

$$M_x = \sum_{i=1}^{n_a} \sum_{j=1}^{n_b} \Delta_{aij}\, \sigma_{ij}\, y_j \tag{9}$$

and

$$M_y = \sum_{i=1}^{n_a} \sum_{j=1}^{n_b} \Delta_{aij}\, \sigma_{ij}\, x_i \tag{10}$$

If the system of load P and moments M_x and M_y is replaced by a load P acting at eccentricities e_x and e_y with respect to the two coordinate axes, we have

$$e_x = \frac{M_y}{P} \quad \text{and} \quad e_y = \frac{M_x}{P} \tag{11}$$

The axial force P is often non-dimensionalised in terms of the squash load,

$$P_u = \sum_{i=1}^{n_a} \sum_{j=1}^{n_b} \Delta_{aij}\, \alpha_{ij} \tag{12}$$

where $\alpha_{ij} = k_1\sigma_u$ for concrete elements

$= \sigma_y$ for steel elements

$= 0$ for hollow elements.

Equation 12 is usually expressed in a different manner in terms of total areas of steel and concrete as follows

$$P_u = k_1\sigma_u A_c + A_s\sigma_y \tag{13}$$

3.5 COMPUTATION PROCEDURE

Values of θ and ϕ are assumed, and the distance of the neutral axis from the point O is varied between specified limits. For each position of the neutral axis, the strain, stress, and force in each elemental area are computed, taking into account the stress-strain characteristics of concrete or steel as appropriate. Summations over the section are carried out for resultant forces, and for the moments due to the elemental forces about the two axes of reference.

Thus, for different locations of the neutral axis, sets of values of axial force, moment about x-axis and moment about y-axis are obtained. The values obtained are randomly spaced on the P-M_x-M_y system. In order to obtain contours or plots for specific values of P, interpolation is employed. Lagrange's interpolation formula using two points on either side of the specified P value, has been found to be the most suitable for the purpose.

The moment-thrust-curvature relations obtained according to the procedure described above may be used for the determination of the failure loads of columns in biaxial bending either by the approximate method described in the next chapter or by the more exact method described in Chapter 5.

CHAPTER 4

THEORY - FAILURE LOADS WITH PART-COSINE WAVE ASSUMPTION FOR DEFLECTIONS

4.0 GENERAL

A procedure for the computation of moment-thrust-curvature relations for composite columns under biaxial bending and compression was described in the previous chapter. Moment-thrust-curvature relations can be used to generate moment-thrust interaction surfaces for different cross-sections. These surfaces give sufficient information to predict the failure load of short, stocky columns loaded by axial forces and moments. However, the failure of long columns is influenced by their slenderness, and a consideration of their flexural stability under axial loads becomes necessary.

Figure 28 depicts a typical plot of axial load related to the corresponding lateral deflection under equilibrium in uniaxial bending. The curve consists of two branches - one in which the load increases with deflection (ascending branch), and the other in which the load decreases with deflection (descending branch). The curve is usually characterised by a definite peak, which defines the ultimate strength of the eccentrically loaded column. In the case of columns with biaxial bending, the nature of the plot for load versus deflection along either axis remains basically unchanged (Fig. 29). One still obtains a characteristic apex. However, the ratio of deflections along the two axes does not necessarily have a proportionate increase at various load levels. Noting that the failure load is associated with the peak of both the deflection curves,

the following procedure may be adopted for computing the failure load under biaxially eccentric loading.

For successively higher values of the axial load, the displacements along the two axes are obtained corresponding to the equilibrium flexural shape. With increasing load, the rate of change of deflections also increases, until it is found that a given load fails to result in an equilibrium shape. In such an event, equilibrium shapes with increasing deflections are now obtained by reducing the axial load. It is thus possible to compute the failure load as the peak of such a load-deflection relationship in the case of biaxial bending and compression.

4.1 ASSUMPTIONS

These assumptions are in addition to those listed in Section 3.1.

(1) Twisting and warping of the cross-section are negligible, so that the assumption that the plane sections remain plane still holds. While this is reasonable for concrete and composite sections, for most practical bare steel sections it may be non-conservative in a limited number of cases.

(2) Shear stresses are small, so that they have no effect on deflections, or in producing combined yield stress.

(3) Deflections are small, so that curvature could be represented by second derivatives of deflections.

4.2 DETERMINATION OF EQUILIBRIUM SHAPE

Differential equations can be derived for the necessary conditions of equilibrium of the beam column. A direct solution of these equations

for a column with inelastic bending and compression is, in general, not feasible. Recourse has to be taken to a numerical solution. The equations to be solved are now presented.

Under a given load, the column undergoes deflections and there exists a varying curvature all along the length. Deflections of the column are measured with respect to the position of centroidal axis before and after the application of the load. At all sections along the length, the following conditions have to be satisfied:

$$\int_A \sigma dA = P \tag{14}$$

$$\int_A \sigma x dA = M_y \tag{15}$$

$$\int_A \sigma y dA = M_x \tag{16}$$

where σ is the stress over an elemental area dA. The stress distribution is obtained directly from the strain distribution across the section, and the material properties. Thus,

$$\sigma = \sigma(\varepsilon) \tag{17}$$

The strain distribution across the section depends on the location (x, y) of the elemental area dA, as well as the curvature, ϕ, and the direction of neutral axis, θ, for the section. Thus,

$$\varepsilon = \varepsilon(x,y,\phi, \theta) \tag{18}$$

Both θ and ϕ vary along the length of the column and can be conveniently expressed in terms of curvatures along the two principal bending axes. If curvatures along the x and y axes are represented by ϕ_x and ϕ_y, we have,

$$\phi = \sqrt{\phi_x^2 + \phi_y^2} \tag{19}$$

and $$\theta = \tan^{-1} \frac{\phi_y}{\phi_x} \tag{20}$$

Provided that the deflections are small, the curvature ϕ_x and ϕ_y can be related to the deflections u and v (Fig. 30), by the differential equations,

$$\phi_x = -\frac{\partial^2 u}{\partial x^2} \tag{21}$$

and $$\phi_y = -\frac{\partial^2 v}{\partial y^2} \tag{22}$$

The deflections u and v have also to satisfy conditions of external equilibrium, viz.

$$M_x = P(e_y + v) \tag{23}$$

and $$M_y = P(e_x + u) \tag{24}$$

where e_x and e_y are the net eccentricities of the applied force along the two bending planes with respect to the centroid of the section in its undeflected position. Thus, the equilibrium shape can be determined by the simultaneous solution of Equations (14-24) given above.

A simple solution for these equations can be obtained by asuming the deflected shape to be defined by

$$u = u_m \cos \frac{\pi z}{L} \tag{25}$$

and $$v = v_m \cos \frac{\pi z}{L} \tag{26}$$

A further refinement of results is obtained by assuming the deflected shape to be defined by a part-cosine wave instead of a cosine wave. This device was first suggested by Westergard and Osgood[12] for bare steel columns and works well for columns with symmetrical bending. Thus,

$$u + e_x = (u_m + e_x) \cos \{\frac{2z}{L} \cos^{-1} (\frac{e_x}{u_m + e_x})\} \tag{27}$$

and

$$v + e_y = (v_m + e_y) \cos \{\frac{2z}{L} \cos^{-1} (\frac{e_y}{v_m + e_y})\} \tag{28}$$

where u_m and v_m are the deflections at the mid-section, and e_x and e_y are the eccentricities along the two bending planes and are equal at both ends.

The expressions for curvatures thus become

$$\bar{\phi}_x = (\frac{2}{L} \cos^{-1} \frac{e_x}{u_m + e_x})^2 (u + e_x) \tag{29}$$

and

$$\bar{\phi}_y = (\frac{2}{L} \cos^{-1} \frac{e_y}{v_m + e_y})^2 (v + e_y) \tag{30}$$

To include the effect of lack of straightness of the unloaded column, the initial deflected shape is generally expressed in the form of a cosine wave, thus

$$n_x = n_{mx} \cos \frac{\pi z}{L} \tag{31}$$

and

$$n_y = n_{my} \cos \frac{\pi z}{L} \tag{32}$$

The initial curvatures then become

$$\phi_{ox} = \left(\frac{\pi}{L}\right)^2 n_x \tag{33}$$

and

$$\phi_{oy} = \left(\frac{\pi}{L}\right)^2 n_y \tag{34}$$

The expressions for net curvatures are then written as follows:

$$\phi_x = \bar{\phi}_x - \phi_{ox} \tag{35}$$

and

$$\phi_y = \bar{\phi}_y - \phi_{oy} \tag{36}$$

Thus, the differential Equations (21) and (22) are replaced by linear Equations (35) and (36). Since equilibrium is satisfied only at mid-point, the cosine terms implicit in Equations (29), (30), (33) and (34) may be conveniently dropped, retaining only the peak values.

4.3 COMPUTATION PROCEDURE

A systematic computation procedure for obtaining the load-lateral deflection characteristic is now outlined. The manner in which the material properties and the distribution of steel in the cross-section are used in computing the moment-thrust-curvature relationships has already been described in Section 3.5.

Step 1: Assume, or read in an initial load value P and its increment at which the deflections are desired.

Step 2: Compute initial curvatures (Equations (33) and (34)).

Step 3: Assume, or read in trial values for mid-height deflections.

Step 4: Compute curvatures using Equations (29), (30), (35) and (36).

Step 5: Compute principal curvature, and direction of neutral axis (Equations (19) and (20)).

Step 6: Compute Moment-Thrust-Curvature relations for given curvature and different positions of neutral axis.

Step 7: Interpolate, for given load P, the values of M_x and M_y.

Step 8: Compute u_x and v_y from Equations (23) and (24).

Step 9: Compare results obtained from Step 7 with those from Step 8.

Step 10: If the difference between the two results is within the specified degree of accuracy, the solution has been obtained. If not, repeat Steps 4 - 9 with modified values of trial deflections.

Step 11: Take a new value of load and repeat Steps 3 - 10. Failure load is defined as that value of the load for which no equilibrium shape is obtained after a specified number of iteration cycles between Steps 3 and 9.

In Step 11, the new value of load is obtained in the first instance in accordance with the load increment specified in Step 1. Subsequently this increment is reduced as the slope of the load-deflection curve falls. In this manner, a sufficient number of points can be obtained to define more closely the peak of the load-deflection curve.

In Step 10, the trial values of deflections are modified in the following manner. In the first instance, the assumed deflection is incremented by a specified value. Then the rate of change of trial

deflections is compared with the rate of change of computed values, and the new trial value is computed by a formula similar to Newton-Raphson iteration formula. Let u be the trial value of deflection and let U be the computed deflection. Let δU be the change in U when u is changed by δu. Then, a better trial value is given by

$$u' = \frac{U\delta u - u\delta U}{\delta u - \delta U} \tag{37}$$

This formula may be applied to the x and y deflections independently at only a slight loss in the rate of convergence.

CHAPTER 5

THEORY - FAILURE LOADS WITH ACTUAL DEFLECTED SHAPE

5.0 GENERAL

The method outlined in the last chapter is adequate for columns with loads that are applied symmetrically with respect to the column mid-point in each of the two bending planes. The part-cosine wave assumption should result in computed deflections that are sufficiently close to the exact values for design purposes. Where the column has an applied loading that results in a non-symmetrical deflected shape, it becomes imperative to assess the column deflections along the entire length. In what follows, a general procedure for computing deflections at a number of discrete points in the case of columns with biaxial bending is derived. For this purpose the assumptions listed in Sections 3.1 and 4.1 are retained. The technique used is essentially a second-order Newton-Raphson type iteration procedure.

5.1 DETERMINATION OF EQUILIBRIUM SHAPE

Let the column length be divided into n equal segments as shown in Fig. 31. End A is identified as station 1 and end B as station (n + 1). Let the x and y eccentricites at end A be e_{xa} and e_{ya} respectively, and those at end B be e_{xb} and e_{yb}. The deflections, stress-resultants and other quantities pertaining to station s will be identified by the suffix s. Let u_s, v_s be the x and y deflections at station s.

A solution to the problem may be obtained by solving Equations (14) - (24) as applied at all the (n + 1) stations along the length of

the column. In general the effect of Equations (14) - (24) may be summarised as follows:

$$w_i = W_i\ (w_1, w_2, \ldots\ldots\ldots, w_m) \tag{38}$$

where $m = 2(n + 1)$

and $w_i, i = 1, 2, \ldots\ldots m$ represent all the deflection components at the $(n + 1)$ stations. W_i represents some complex function incorporating the moment-thrust-curvature relations as well as various conditions of geometric compatibility for the station i. Equation (38) may be expressed in another form, viz.

$$Z_i = Z_i\ (w_1, w_2, \ldots w_m) = w_i - W_i\ (w_1, w_2, \ldots w_m) = 0 \tag{39}$$

The type of equations represented by Equation (39) lend themselves favourably to solution by the Newton-Raphson iteration technique. Essentially, the technique consists of assuming some trial values for the solution, say w_i^1, $i = 1, 2, \ldots m$, and obtaining a set of correction values δw_i, such that the new values for the solution given by

$$w_i^2 = w_i^1 + \delta w_i \tag{40}$$

are better than the trial values. A repeated application of this procedure, adopting the new values for the solution as the new trial values, can be carried out until the correction terms δw_i are all reduced to values smaller than a pre-specified error ε. It can be shown that for the necessary conditions of convergence, the correction terms may be calculated by the solution of the following equations:

$$\begin{bmatrix} \frac{\partial Z_1}{\partial w_1} & \frac{\partial Z_1}{\partial w_2} & \cdots\cdots & \frac{\partial Z_1}{\partial w_m} \\ \frac{\partial Z_2}{\partial w_1} & \frac{\partial Z_2}{\partial w_2} & \cdots\cdots & \frac{\partial Z_2}{\partial w_m} \\ \vdots & \vdots & & \vdots \\ \frac{\partial Z_m}{\partial w_1} & \frac{\partial Z_m}{\partial w_2} & \cdots\cdots & \frac{\partial Z_m}{\partial w_m} \end{bmatrix} \begin{bmatrix} \delta w_1 \\ \delta w_2 \\ \vdots \\ \delta w_m \end{bmatrix} = - \begin{bmatrix} Z_1 \\ Z_2 \\ \vdots \\ Z_m \end{bmatrix} \tag{41}$$

where the functions Z_i and their derivatives are calculated for the point $\{w_i^1\}$. The functions W_i may be regarded as the computed deflections for the assumed deflection w_i so that at convergence their differences vanish.

The expressions for curvatures as given in Equations (21) - (22) may be rewritten in the finite difference form as

$$\phi_{xs} = -\frac{1}{h^2}(u_{s-1} - 2u_s + u_{s+1}) \tag{42}$$

and $$\phi_{ys} = -\frac{1}{h^2}(v_{s-1} - 2v_s + v_{s+1}) \tag{43}$$

Letting,

$$u_s = w_{2s-1} \tag{44}$$

and $$v_s = w_{2s} \tag{45}$$

Equations (42) - (43) may be rewritten as

$$\phi_{xs} = -\frac{1}{h^2}(w_{2s-3} - 2w_{2s-1} + w_{2s+1}) \tag{46}$$

and $$\phi_{ys} = -\frac{1}{h^2}(w_{2s-2} - 2w_{2s} + w_{2s+2}) \qquad (47)$$

Since the function W_i, and hence Z_i, depends on the relevant ϕ_x and ϕ_y only, we have for each node s,

$$Z_{2s-1} = w_{2s-1} - W_{2s-1}(w_{2s-3}, w_{2s-2}, \ldots\ldots, w_{2s+2}) \qquad (48)$$

and $$Z_{2s} = w_{2s} - W_{2s}(w_{2s-3}, w_{2s-2}, \ldots\ldots, w_{2s+2}) \qquad (49)$$

Equations (48) - (49) yield simplified expressions for the derivatives in Equation (41). Thus,

$$\frac{\partial Z_{2s-1}}{\partial w_{2s-k}} = -\frac{\partial W_{2s-1}}{\partial w_{2s-k}} \qquad k = 3, 2, 0, -1, -2 \qquad (50)$$

$$\frac{\partial Z_{2s}}{\partial w_{2s-k}} = -\frac{\partial W_{2s}}{\partial w_{2s-k}} \qquad k = 3, 2, 1, -1, -2 \qquad (51)$$

$$\frac{\partial Z_{2s-1}}{\partial w_{2s-1}} = 1 - \frac{\partial W_{2s-1}}{\partial w_{2s-1}} \qquad (52)$$

and $$\frac{\partial Z_{2s}}{\partial w_{2s}} = 1 - \frac{\partial W_{2s}}{\partial w_{2s}} \qquad (53)$$

all other derivatives being zero.

Equations (46) - (53) are valid for $2 \leqslant s \leqslant n$. In general, the values of u_1, v_1 and u_{n+1}, v_{n+1} will be determined by the boundary conditions. For the case of a pin-ended column,

$$w_1 = w_2 = w_{2n+1} = w_{2n+2} = 0 \qquad (54)$$

and therefore the values of the derivatives with respect to any of these variables need not be computed. Thus Equations (41) when considered along with Equations (50) - (54) are sufficient to obtain the values of the correction terms $\{\delta w_i\}$.

When the column has an initial lack of straightness defined by the deflections $\{\delta w_i^o\}$, the net curvatures are given by

$$\phi_{xs} = \bar{\phi}_{xs} - \phi_{xs}^o \tag{55}$$

and

$$\phi_{ys} = \bar{\phi}_{ys} - \phi_{ys}^o \tag{56}$$

where ϕ_{xs}^o and ϕ_{ys}^o are the initial curvatures and $\bar{\phi}_{xs}$ and $\bar{\phi}_{ys}$ are the total curvatures at station s.

5.2 COMPUTATION PROCEDURE

A step-by-step procedure for obtaining the load-deflection response is now outlined.

Step 1: Assume, or read in an initial load value P and its increment at which the deflections are desired.

Step 2: Compute initial curvatures.

Step 3: Assume or read in trial values for column-deflections.

Step 4: Compute net curvatures using Equations (55) - (56).

Step 5: For each station s, compute principal curvature and direction of neutral axis (Equations (19) - (20)).

Step 6: For each station s, compute moment-thrust-curvature relations for given curvature and different positions of neutral axis.

Step 7: For each station s, interpolate for given load P the values of M_{xs} and M_{ys} and hence obtain e_{xs} and e_{ys}.

Step 8: Compute deflections

$$u_{ms} = e_{xs} - e_{xA} + (e_{xB} - e_{xA}) \frac{(s-1)}{n} \tag{57}$$

and

$$v_{ms} = e_{ys} - e_{yA} + (e_{yB} - e_{yA}) \frac{(s-1)}{n} \tag{58}$$

Step 9: Change the values of the x-curvatures computed in Step 4 by an amount $\frac{\Delta}{h^2}$ where Δ is a small fixed quantity, and repeat Steps 5 - 8, obtaining u'_{ms} and v'_{ms}.

This results in

$$\frac{\partial W_{2s-1}}{\partial w_{2s-3}} = -\frac{1}{2}\frac{\partial W_{2s-1}}{\partial w_{2s-1}} = \frac{\partial W_{2s-1}}{\partial w_{2s+1}} = \frac{u'_{ms} - u_{ms}}{\Delta} \tag{59}$$

and

$$\frac{\partial W_{2s}}{\partial w_{2s-3}} = -\frac{1}{2}\frac{\partial W_{2s}}{\partial w_{2s-1}} = \frac{\partial W_{2s}}{\partial w_{2s+1}} = \frac{v'_{ms} - v_{ms}}{\Delta} \tag{60}$$

Step 10: Now change the value of the y-curvature computed in Step 4 by an amount $\frac{\Delta}{h^2}$, and once again repeat Steps 5 - 8 obtaining u''_{ms} and v''_{ms}. We now obtain

$$\frac{\partial W_{2s-1}}{\partial w_{2s-2}} = -\frac{1}{2}\frac{\partial W_{2s-1}}{\partial w_{2s}} = \frac{\partial W_{2s-1}}{\partial w_{2s+2}} = \frac{u''_{ms} - u_{ms}}{\Delta} \tag{61}$$

and

$$\frac{\partial W_{2s}}{\partial w_{2s-2}} = -\frac{1}{2}\frac{\partial W_{2s}}{\partial w_{2s}} = \frac{\partial W_{2s}}{\partial w_{2s+2}} = \frac{v''_{ms} - v_{ms}}{\Delta} \qquad (62)$$

Step 11: The matrix Equation (41) may now be formed with the help of Equations (48) - (54) and Equations (59) - (62) and solved for the correction terms $\{\delta w_i\}$.

Step 12: If for all i, $|\delta w_i| \leqslant \varepsilon$, a deflected shape has been obtained and one may now proceed to Step 13. Otherwise obtain the corrected deflections $\{w_i^2\}$ by Equation (40) and repeat Steps 4 - 11 taking the corrected deflection values as the new trial values.

Step 13: Increase the load value P by the increment specified in Step 1 and repeat Steps 3 - 12.

Step 14: If no convergence is obtained in Step 12 within a pre-specified number of cycles, the increment in P may be reduced by a specified ratio (say half) and Steps 3 - 12 may be repeated till the value of the increments diminishes to a pre-specified small value.

Step 15: The highest load for which a deflected shape is obtained, is taken as the failure load of the column.

CHAPTER 6

APPLICATION TO COMPOSITE COLUMNS IN BIAXIAL BENDING

6.0 GENERAL

Based on the procedures outlined in the foregoing chapters, three computer programs were developed for use on the CDC 6600 computer. All three programs were written for composite columns in uniaxial or biaxial bending, but are equally applicable to reinforced concrete sections or bare metal sections. The first program - for the moment-thrust-curvature relations - is also incorporated in the other two programs in the form of a subroutine. The second program, called COLUMPC, traces the load-deflection response of a column in biaxial bending with symmetrically applied end eccentricities. The program assumes the deflected shape to be part of a cosine wave. The third program, called COLUMAS, also traces the load-deflection response of the column in biaxial bending, but calculates the actual deflected shape of the column and has no restriction on the values of end eccentricities. All three programs can account for the effects of residual stresses of any desired distribution over the column cross-section. Initial lack of straightness in the form of a cosine wave can be considered in Program COLUMPC, while Program COLUMAS allows for initial lack of straightness of any form.

The computer results presented first are aimed at demonstrating the accuracy of the programs. Comparisons are made with available results for moment-thrust-curvature relations for reinforced concrete sections and composite column sections. Results for the failure loads of concrete encased steel sections and concrete-filled rectangular tubes in uniaxial

bending are obtained as particular cases of biaxial bending and compared with existing results.

Having checked the validity of the computer programs for particular cases, computer results from these programs have been used to examine the accuracy of the design method proposed by Basu and Sommerville[28] as applied to composite columns in biaxial bending and compression. The design method has previously been shown to be sufficiently accurate for composite columns in uniaxial bending and compression, but its application to the case of biaxial bending and compression has so far not been checked for accuracy either experimentally or analytically. In the design method, the strength of composite columns in biaxial bending is obtained by means of an interaction formula that relates the biaxial strength to uniaxial strengths in two orthogonal directions. The accuracy of the interaction formula is examined in the light of computer results on the one hand, and test results on the other, for the nine composite columns with symmetrical end eccentricities described in Chapter 2. Finally, the design method is evaluated for more general cases of biaxial bending with various combinations of end eccentricities in the two bending planes.

6.1 EXAMPLES OF MOMENT-THRUST-CURVATURE RELATIONS

6.1.0 General

To check the validity of the moment-thrust-curvature calculations common to all the three computer programs described in this thesis, comparisons were made with moment-thrust-curvature relations as obtained by three investigators for various types of sections. Section 6.1.1 describes studies on a square reinforced concrete section in uniaxial and biaxial

bending as reported by Warner[81]. In Section 6.1.2, a square concrete-filled steel tube in uniaxial and biaxial bending is analysed and results compared with those obtained by Robertson[84]. Comparisons are made in Section 6.1.3 with Basu's[26] results on a rectangular concrete encased steel section in uniaxial bending. Having demonstrated the applicability and accuracy of the results obtained from the computer programs for these cases, the effect of residual stresses on the moment-thrust-curvature relations for a concrete encased steel section is described in Section 6.1.4.

6.1.1 Reinforced Concrete Section in Biaxial Bending

Moment-thrust-curvature relations for a square reinforced concrete section shown in Fig. 32 were obtained by Warner[81], adopting a procedure very similar to the one outlined above. Warner plotted the values of resultant eccentricity e_r against curvature for different values of axial load in non-dimensional form. Separate plots were obtained for different values of θ, the direction of the neutral axis.

The values of various parameters are given below:

$$\varepsilon_u = 2.0\ \varepsilon_y$$
$$\sigma_u = 0.055\ \sigma_y$$
$$A_s = 0.02\ A_g$$
$$\gamma_1 = 2.2$$
$$\gamma_2 = 4.0$$
$$k_1 = 0.85$$

The stress-strain curve for concrete was that corresponding to Equation (3). For steel, a bilinear stress-strain relationship was assumed.

The results obtained are given in Figs 33-36, corresponding to $\theta = 0^{o}$, 15^{o}, 30^{o}, and 45^{o}. In each case, curves are plotted for $P/P_u = 0.2$, 0.4, 0.6, and 0.8. The curvatures are expressed as ϕ/ϕ_o where $\phi_o = \varepsilon_u/a$. It may be seen that the two sets of results are identical.

6.1.2 Concrete-filled Steel Tube in Biaxial Bending

Robertson[84] obtained the moment-thrust interaction surface for a 10 in x 10 in x 1/4 in steel tube filled with concrete. In his calculations he adopted a slightly different technique of integrating stresses over the section, and a different numerical procedure.

The section is shown in Fig. 37. The concrete stress-strain curve used was that corresponding to Equation (1). A bilinear stress-strain curve was used for steel.

The parameters were:

C_1	= 2.410	C_2	= -1.865
C_3	= 0.500	C_4	= -0.045
ε_u	= 0.0025	σ_u	= 3360 lbf/sq.in
ε_y	= 0.0012	σ_y	= 3584 lbf/sq.in

The interaction surface is obtained as the envelope of all possible combinations of P, M_x and M_y, and may be described in the form of contours for different axial load values. Figures 38 and 39 show the comparative results obtained by Robertson and the computer program.

Contours for P/P_u = 0, 0.1 and 0.2 are plotted in Fig. 38, and for P/P_u = 0.3, 0.4, 0.5, 0.6, 0.7, 0.8, and 0.9 are plotted in Fig. 39. It may be observed that the biggest contour is obtained for P/P_u = 0.2. This implies that the moment of resistance is maximum at a finite axial load (around 0.2 P_u), and not at P = 0. Thus the moment of resistance first increases with axial load, until it reaches a value around 0.2 P_u, and then starts diminishing. This phenomenon has also been observed by previous investigators[26,53,84,85]. The results obtained show good agreement with those of Robertson.

6.1.3. Concrete-encased Steel Section in Uniaxial Bending

Basu[26] presented the moment-thrust-curvature relations for a steel I-section (12 in x 8 in at 65 lb) encased in concrete (16 in x 12 in outer dimensions). The section also has four 1/2 in ϕ bars as longitudinal reinforcement at 1 in cover (Fig. 40).

The stress-strain curve for concrete was in accordance with Equation (1). A bilinear-stress-strain relation for steel was adopted. Values of various parameters were:

C_1 = 2.4100 $\quad$ C_2 = -1.8650

C_3 = 0.5000 $\quad$ C_4 = -0.0450

ε_u = 0.0025 $\quad$ σ_u = 3000 lbf/sq.in

ε_y = 0.001116 $\quad$ σ_y = 32928 lbf/sq.in

k_1 = 1.0000

The results are plotted as moment versus curvature for increasing values of P/P_u = 0.0, 0.25, 0.50, and 0.75. Curves presented here are for minor axis bending. Figure 41 shows the excellent agreement between the results obtained by Basu and by the computer program described here.

6.1.4 Effect of Residual Stresses

Residual stresses can significantly effect the ultimate strength of axially loaded bare steel sections especially in the presence of geometrical imperfections. The encasement of a steel section by concrete is likely to reduce the effect of residual stresses on column strength. However, as the concrete contribution to the overall column strength reduces, the influence of these stresses may be expected to grow. This effect has not been investigated by previous researchers on composite columns. In this section, the effect of residual stresses on the moment-thrust-curvature relations for an encased section has been described. Both types of residual stress patterns mentioned in Section 3.3 were considered. The stress patterns used had the following values for the parameters:

PATTERN 1 (AISC)

$$\sigma_f = 75\ MN/m^2 \quad \sigma_{fw} = -50\ MN/m^2 \quad \sigma_w = -50\ MN/m^2$$

PATTERN 2 (Cambridge)

$$\sigma_f = 125\ MN/m^2 \quad \sigma_{fw} = -100\ MN/m^2 \quad \sigma_w = 175\ MN/m^2$$

Figures 42 and 43 show the results for $\theta = 0^o$ (major axis bending) and $\theta = 90^o$ (minor axis bending) respectively, and consist of moment-

curvature curves for different thrust levels (P/P_u = 0.0, 0.25, 0.50, and 0.75). The curvatures are expressed in terms of $\phi_o = \varepsilon_u/a$.

It may be seen that the residual stresses have only a slight influence on the moment-thrust-curvature relations. In the case of the AISC pattern, the moment resistance capacity is increased for zero axial load, but is reduced for axial loads greater than about 0.1 P_u. In the case of the Cambridge pattern, the effect on moment of resistance is almost opposite to that of AISC pattern. This is probably due to the fact that Cambridge pattern has predominantly compression in the web, while in the case of AISC pattern, the web is entirely in tension. However, it was anticipated that the altered moment-thrust-curvature relations could have a definite though small effect on the load bearing capacity of long columns. This is further discussed in Section 6.3.3.

6.2 EXAMPLES OF UNIAXIAL FAILURE LOADS

6.2.0 General

Results were compared with those obtained by Basu [26] for the case of concrete-encased sections in uniaxial bending. The columns studied here were the ones tested at the Building Research Establishment and reported previously [42]. Comparison is also made for the case of columns with a rectangular tubular section filled with concrete in minor axis bending.

6.2.1 Concrete-encased Steel Sections

Two series of test columns were chosen for the purpose. The section used for series 'AE' is shown in Fig. 44. Other data common to this series of columns is given below:

$C_1 = 2.410$ $C_2 = -1.865$

$C_3 = 0.500$ $C_4 = -0.045$

$\varepsilon_u = 0.0025$ $k_1 = 1.0000$

$\varepsilon_y = 0.00122$ $\sigma_y = 16.1$ tonf/in^2

The four columns in this series had different lengths and different concrete cube strengths. The results presented here were obtained using Program COLUMPC. The comparative results as obtained by Basu and as obtained by COLUMPC are listed in Table 8.

A second batch of columns analysed by Basu and designated as series FE in the Building Research Establishment tests had a cross-section shown in Fig. 40. Other pertinent data for this series is as follows:

$C_1 = 2.410$ $C_2 = -1.865$

$C_3 = 0.500$ $C_4 = -0.045$

$\varepsilon_u = 0.0025$ $k_1 = 1.000$

$\varepsilon_y = 0.00112$ $\sigma_y = 14.7$ tonf/in^2

Results for two of the columns in this series namely FE3 and FE4 are also included in Table 8. It is clear from the results presented that the theoretical failure loads obtained by COLUMPC agree very closely with those obtained by Basu. The slight variation in the two sets of results may be attributed to the different computational procedures.

6.2.2 Concrete-filled Rectangular Steel Tubes

Sen and Chapman[50] presented ultimate load tables for concrete-filled rectangular and circular tubular columns in a CIRIA publication. The tables given were for columns in uniaxial bending only. The ultimate loads quoted were obtained by a part-cosine wave assumption, and allowed

for the effects of long-term loading and initial imperfections. Long-term loading effects were allowed for by doubling the strain at various stress levels of the assumed instantaneous stress-strain curve for concrete. The initial imperfection was represented as an initial end eccentricity of 0.9 x 0.00006 L^2/D where L is the length of the column, and D is the size of the column in the plane of bending. For the purpose of comparison, a rectangular column section 5.0 x 3.0 x 0.250 in was randomly selected and analysed for three values of end eccentricities in minor axis bending using the part-cosine wave assumption computer program COLUMPC. Other pertinent data is as follows:

C_1	= 2.410	C_2	= -1.865
C_3	= 0.500	C_4	= -0.045
σ_y	= 16.0 tonf/sq.in	E_s	= 13000 tonf/sq.in
σ_u	= 2400 lbf/sq.in	ε_u	= 0.0050 (after doubling)
k_1	= 1.000		

The column length was taken as 10 ft, for which the initial end eccentricity was 0.2592 in. The eccentricity values chosen were such that e/D = 0, 0.1, and 0.2. Table 9 compares the results from Program COLUMPC with the ultimate load values given by Sen and Chapman. Since all the assumptions in the two sets of results are identical, the closeness of the results is not surprising.

It is thus clear that the present computer program for the determination of failure loads in biaxial bending gives results in close agreement with existing uniaxial bending computer programs due to Basu[26] and Sen[56] which have already been verified by tests. It is also clear that good agreement is obtained between the biaxial moment-thrust-curvature relations as predicted by this theory and others recently presented[81,84].

It remains to be shown that the prediction of ultimate loads for the case of biaxial bending by the present computer programs is valid. This is achieved by comparing, in the next section, the theoretical results with the experimental results reported in Chapter 2 on nine composite columns in biaxial bending.

6.3 COMPARISON WITH TEST RESULTS FOR COLUMNS IN BIAXIAL BENDING

6.3.0 General

Computer results were obtained by the nine test columns described in Chapter 2. Since all the columns tested had equal eccentricities at the two ends for each of the two principal bending planes resulting in symmetrical bending, all the computations were carried out using the part-cosine wave assumption for the deflected shape. The effects on column strength of two types of imperfections commonly occurring in columns, namely the residual stresses locked in the steel sections and the lack of initial straightness, were studied in various combinations.

6.3.1 Residual Stresses

The nature of residual stresses in rolled steel sections was discussed in Section 3.3. In the calculations described here, a residual stress pattern of the AISC type was adopted with $\sigma_f = 0.3\ \sigma_y$.

6.3.2 Initial Lack of Straightness

The initial lack of straightness of the centroidal axis in the composite column is assumed to be the same as that of the bare metal stanchion. This imperfection is expressed as an initial mid-height deflection. When other forms of imperfections, particularly residual stresses are being considered simultaneously, it is customary to take

the magnitude of the initial mid-height deflection as L/1000 where L is the length of the column. Alternatively, a Perry-Robertson imperfection factor, as incorporated in BS449[36], accounting for all types of imperfections may be considered assuming an initial mid-height deflection of $0.00006\ L^2/D$, where D is the size of the bare metal section in the plane of the bending. In the general case of columns with biaxial eccentricities, the plane of bending cannot be properly defined. One approach is to consider the initial mid-height deflection solely in the plane of minor axis, as is indicated by the results shown in Table 10. The column cross-section chosen for this study is that of the test columns of Chapter 2. The material properties selected were those of Column E. The results shown are for axially loaded columns with an initial lack of straightness in three different planes, along the major axis, along the minor axis, and along an axis at 45^{o} from both the major and minor axes. It may be seen that the greatest reduction in strength occurs when the initial imperfection is along the minor axis. Thus the minor axis orientation for the lack of initial straightness has therefore been adopted for all the subsequent computations.

6.3.3 Comparison Between Test and Computer Results

6.3.3.1 Failure Loads:

Computer results were obtained for the following combinations of column imperfections, and are listed in Table 11.

Case I : Results without any imperfections.

II : Results with residual stresses only.

III : Results with an initial mid-height deflection of L/1000 only.

IV : Results with a combination of Case II and Case III imperfections.

Case V : Results with an all-inclusive mid-height deflection of $0.00006\ L^2/D$.

Results for Case IV show good agreement with test results. The average value of P_{xy}/P_{test} for this case was 0.96 with a standard deviation of 0.10. The maximum error obtained was 25% for Column G (on the safe side), but this was an exceptional deviation. If the results for Column G are excluded, the average P_{xy}/P_{test} is improved to 0.99 with a standard deviation of 0.06. Considering that an error of up to 5% is only to be expected when using part-cosine wave assumption for the deflected shape of the column, the Case IV results indicate excellent correlation with the tests.

The effect of residual stresses on the failure loads was not consistent. This observation is in line with the findings of Sharma and Gaylord[22] for bare metal sections in biaxial bending and compression. However, in general, the failure loads were reduced or remained unaltered for columns with short lengths or with small eccentricities, while they were increased for longer columns with larger eccentricities. The variation was within ±3%. It would appear therefore that in certain cases the presence of residual stresses can enhance column strength.

The effect of initial lack of straightness is always to reduce the column strength. The Perry-Robertson/BS449 formula for initial lack of straightness gives smaller values than the L/1000 criterion for short columns, but results in larger values for medium and long columns. This is immediately reflected in the results obtained for Cases III and V.

Results obtained for Case V are close to those for Case IV, indicating that the effect of initial imperfection can be suitably con-

sidered by either of the two criteria used. The average value of P_{xy}/P_{test} for Case V was 0.94 with a standard deviation of 0.13.

The comparison between experimental and analytical results has also been given in Fig. 45.

6.3.3.2 Deflections:

It is interesting to compare the experimental load-deflection response of the nine test columns with the theoretically calculated values. In Fig. 46 the vertical and the horizontal deflections for three of the nine columns have been plotted. The particular columns chosen for this comparison were one each from the three specimens of the same length. In addition, for each of the three columns chosen, the difference between the experimental and theoretical (Case IV) failure loads was the least amongst specimens of the same length. This was intended to minimise the difference on the load-axis so that the comparison between deflections could be most appropriate. Thus, the results plotted are for Columns A, E, and H.

The values of comparable experimental and theoretical deflections may be seen to be generally close for each of the three columns. The experimental and theoretical values for deflections corresponding to the maximum loads are nearly equal in each case. Of particular note is the similar trend of divergence between horizontal and vertical deflections for about half the failure load and convergence around the failure load observed both in experimental and theoretical plots. Results for other columns showed similarly close agreement between the experimental and theoretical deflections. The good correlation found for deflections gives added confidence in the close agreement observed for failure loads as described in the previous section.

6.3.4 Accuracy of the Part-cosine Wave Assumption

The accuracy of the solutions obtained on the basis of the part-cosine wave assumption for deflections is now examined in the light of solutions based on more exact estimates of deflections. For this purpose results were obtained for the nine test columns using Program COLUMAS. Computations were carried out only for the Case IV imperfections as described in the last section. Each column was divided into eight equal divisions along the length. Results are presented in Table 12, which also lists the comparable results from the COLUMPC program. The maximum error is of the order of 5.43% while the average error is only 3.52%, all on the safe side. Basu and Hill[27] found that the part-cosine wave assumption for the computation of uniaxial failure loads of composite columns erred only by a maximum of 5% with respect to the computations based on true deflected shape. A similar value for the error was found by Sharma and Gaylord[22] in their studies on biaxial bending of bare metal sections. Thus there is sufficient evidence to conclude that in the case of columns loaded symmetrically about the column mid-height in each of the two bending planes, the part-cosine wave assumption for deflections is an acceptable approximation resulting in failure loads that are within 5-6% of the failure loads obtained by a more rigorous computation of the deflected shape. Where the biaxial moments applied at the two ends are not symmetrical about the column mid-height, it will not be possible to apply the simpler theory assuming the deflected shape in the form of a part-cosine wave. This stems from the difficulty in locating the cross-section with maximum principal curvature as the maximum curvatures in each of the two component planes occur at different locations along the column length. Recourse has to be had to the more

general analysis involving determination of the actual deflected shape as described in Chapter 5, and on which Program COLUMAS is based. The accuracy of the currently proposed design method in its application to columns loaded in this fashion has been examined by the application of the more rigorous theory as described in the next section.

6.4 INVESTIGATION OF CURRENTLY PROPOSED DESIGN METHOD IN ITS APPLICATION TO COLUMNS HAVING GENERAL BIAXIAL END ECCENTRICITIES

6.4.0 General

The empirical design method for composite columns proposed by Basu and Sommerville[28] was derived on the basis of numerical results for the uniaxial failure loads of several composite columns obtained using a part-cosine wave assumption for deflections. Their program was capable of treating cases where the two end eccentricities for the uniaxial bending of the column are unequal. As mentioned in the previous section a part-cosine wave assumption for columns with unequal end eccentricities in the same plane at the two ends becomes unworkable in the case of biaxial bending.

For computing the strength of composite columns in biaxial bending, Basu and Sommerville advanced an approximate interaction formula in terms of the uniaxial strengths of the column under the given loading. This formula is an extension of the Bresler[29] formula for the biaxial bending of short reinforced concrete columns. Bresler showed that the failure load for biaxially compressed short columns can be approximately given by

$$\frac{1}{P_{xy}} = \frac{1}{P_x} + \frac{1}{P_y} - \frac{1}{P_u} \qquad (63)$$

where P_x = Failure load of the short column under uniaxial bending about the y-axis with eccentricity e_x.

P_y = Failure load of the short column under uniaxial bending about the x-axis with eccentricity e_y.

P_u = Squash load.

P_{xy} = Failure load of the short column under biaxial bending with eccentricities e_x and e_y along x and y respectively.

The Bresler formula is based on the material interaction surface. The formula is exact for perfectly elastic materials and yields satisfactory results for short reinforced concrete columns. However, it is not applicable to long columns as instability effects are not included in deriving the formula.

Basu and Sommerville extended the Bresler formula for the case of long columns by suggesting that instead of uniaxial failure load values for short columns, the uniaxial failure load values for long columns be used, and that the value of the squash load be substituted by the failure load under axial loading with the column constrained to bend about its stronger axis. Thus

$$\frac{1}{P_{xy}} = \frac{1}{P_x} + \frac{1}{P_y} - \frac{1}{P_a} \qquad (64)$$

where P_a is the larger of P_{ax} and P_{ay},

P_{ax} = Failure load under axial loading with the column constrained to bend about y-axis,

P_{ay} = Failure load under axial loading with the column constrained to bend about x-axis,

P_x = Failure load under uniaxial bending about the y-axis with eccentricity e_x, and

P_y = Failure load under uniaxial bending about the x-axis with eccentricity e_y.

The same authors also proposed simple design formulae to evaluate P_x, P_y, P_{ax} and P_{ay}, and gave the basis on which these formulae were derived. No proof was given for the interaction formula of Eq. 64, although its relationship to the current elastic interaction formula contained in British design codes was pointed out. In what follows, the accuracy of the Basu and Sommerville design formulae, including Eq. 64, is examined in the light of numerical results obtained for several composite columns in biaxial bending using the methods described in Chapters 4 and 5. In Section 6.4.1 the validity of Eq. 64 is examined as applied to the nine test columns. Later, in Section 6.4.2, numerical results for a composite column with various combinations of end eccentricities are compared with values obtained from Basu and Sommerville's design formulae.

The accuracy of the method based on the actual deflected shape with respect to the number of subdivisions is examined in Section 6.4.3.

6.4.1 Symmetrical Bending

Failure loads for the nine test columns under biaxial bending were computed using the interaction formula. Uniaxial failure loads were computed (a) using the design formulae presented by Basu and Sommerville, and (b) by the analytical procedure of Chapter 4 using Program COLUMPC.

Table 13 gives the results obtained by the empirical formulae. It may be readily observed that the biaxial interaction formula is uniformly conservative. The margin is greater in the case of longer columns than for shorter columns. This may be attributed to the fact that for

shorter columns the actual failure surface is close to the simplified (planar) material failure surface implied in the interaction formula. The empirical and test results vary by as much as 48%. The average P_{xy}/P_{test} is 0.71 with a standard deviation of 0.10.

Table 14 shows the improvement in the results obtained when analytically computed uniaxially eccentric failure loads are used in the interaction formula. The agreement is very close indeed for short columns. The difference between theory and test results increases for medium and for long columns. The average P_{xy}/P_{test} for this case is 0.83 with a standard deviation of 0.16.

Comparing the ratios P_{xy}/P_{test} obtained from Table 13 and Table 14 it is clear that the biaxial-interaction formula gives close agreement for short columns, while it is conservative for long columns. The difference in results given in Tables 13 and 14 stems from the fact that uniaxial failure loads used in Table 13 are themselves conservative as compared with the analytical values. Application of the conservative-biaxial formula further increases the margin of safety.

The interaction formula studied here has been shown to be conservative for obtaining failure loads from uniaxial loads. The formula gives consistently conservative results when used in conjunction with the design formulae for uniaxial failure loads proposed by Basu and Sommerville. The margin of safety is greater for long columns than for short columns. Good agreement between calculated and experimental values is obtained for short columns when analytically computed uniaxial failure loads are used with the interaction formula. For long columns and for columns with increasing eccentricity, the formula becomes more conservative.

6.4.2 Asymmetrical Bending

In this section the relative differences between the theoretical failure loads and those obtained by Basu and Sommerville's design method for the case of asymmetrical biaxial bending are examined. Failure loads were obtained analytically using Program COLUMAS and by the empirical design formulae for a 12 ft long column with various combinations of end eccentricities. The cross-section and material properties were arbitrarily selected as those of test Column E, since this column represented the middle of the range for slenderness as well as end eccentricities.

Let $\bar{e}_x$ and $\bar{e}_y$ be defined as the larger of the two end eccentricities lying in the x- and y-planes respectively, and let β_x and β_y be defined as the ratios of the smaller to the larger of the two end eccentricities lying in the x and y bending planes respectively. The entire range of end eccentricity combinations can be covered by assigning values of 1.0, 0.5, 0.0, -0.5, and -1.0 to both β_x and β_y. This results in 25 cases when both $\bar{e}_x$ and $\bar{e}_y$ are on the same end, i.e. the larger of the two end eccentricities lying in one plane are at the same end for both x- and y-bending planes (Series S). Additional 9 cases result when $\bar{e}_x$ and $\bar{e}_y$ are located on opposite ends (Series T). Figure 47 shows the difference between the two types of loading. For the purpose of this study $\bar{e}_x$ and $\bar{e}_y$ were taken as 5.00 in and 2.90 in respectively, the same values as for test Column E. The column length was subdivided into 16 segments (compare Section 6.4.3).

The results have been presented in Table 15. Series T failure loads are always greater than those for Series S. The percentage differences between the design failure loads and the exact failure loads

for Series S have also been tabulated. Clearly the design method is uniformly conservative by 25-43%. It is even more conservative for Series D type loading with errors varying from 32-51%. This indicates that the Basu and Sommerville's design formulae may give over conservative results when applied to composite columns with asymmetrical biaxial bending. Figures 48 and 49 show the variation of failure loads corresponding to Series S loading with respect to β_x and β_y respectively. Also plotted are the design failure loads. The wide difference between the theoretical and design values is again observed, and clearly points to the need for an improvement in estimating the failure loads for composite columns with this type of loading.

In conclusion it may be stated that a computer program is now available which can be used to study the failure loads of composite columns under general biaxial bending with varying values for the crucial parameters such as length and end eccentricity combinations. In this way sufficient data can be collected to make it possible to derive simple formulae to predict the strength of such columns. Until such time as the new design formulae are derived and shown to be safe, the existing conservative design formulae can be used with confidence.

6.4.3 Accuracy of the Method Based on the Actual Deflected Shape

The method described in Chapter 5, in which the failure loads are calculated on the basis of the actual deflected shape, should give the exact failure load if the column length is subdivided into a large number of segments. However, the computation time increases rapidly with increase in the number of subdivisions. To determine the optimum number of segments that may be used with confidence in subdividing the

column, two extreme cases of loading were analysed for different numbers of column segments. The first case was that of a column with equal biaxial end eccentricities at both ends ($\beta_x = 1.0$, $\beta_y = 1.0$), resulting in a symmetrical deflected shape in single curvature in both the bending planes. The other case was that of a column with equal but opposite end eccentricities at both ends ($\beta_x = -1.0$, $\beta_y = -1.0$), resulting in an asymmetrical deflected shape having reverse curvatures in both the bending planes. These two cases correspond to the two extreme combinations of biaxial end eccentricities. The column cross-section, material properties, magnitudes of end eccentricities, and the column length chosen for the comparison given here are the same as those for the study described in the preceding section.

Table 16 presents the results obtained from Program COLUMAS for the number of subdivisions varying from 4 to 20 for both modes of bending mentioned above. It may be observed that for columns in symmetrical bending, the results for number of subdivisions equal to 16 and 20 are almost the same. Thus the exact failure load for this case may be taken as that obtained for 20 subdivisions. The error in estimating the failure load by taking 8 subdivisions is only 0.1 per cent on the safe-side. The variation of computed failure load with the number of column subdivision is shown in Fig. 50.

Interesting results are obtained for columns with anti-symmetrical end eccentricities (Fig. 51). It is found that to compute the exact failure load more than 20 subdivisions are required. More important, however, is the fact that for fewer number of subdivisions, the computed failure load is on the unsafe side. The error in the computed failure load with 16 segments on the basis of the failure load obtained with 24

segments is more than 3.5 per cent on the unsafe side. While this error may be acceptable in engineering calculations, the error obtained by having fewer segments than 16 may be quite serious.

The source of this error may be found by observing that in the case of symmetrical bending, the location of the critical section with maximum curvature is known, namely the mid-point. Even with 8 subdivisions there are sufficient number of points on either side of this section to obtain a satisfactory estimate of the critical curvature. This is clearly not the case when the column is subjected to anti-symmetrical eccentricities. The critical sections now are near the column ends. Because of the sharp change in curvature here, an accurate assessment of the curvature at these sections would not be possible, unless a large number of subdivisions is employed. Also as the number of subdivisions is decreased, the first station from the column end at which the equilibrium is satisfied moves farther from the critical section. As a result there is an effective reduction in the net eccentricity of the line of action of the applied force and consequently the failure load is over-estimated.

The curve shown in Fig. 50 approaches the exact failure load asymptotically. However, the curve for anti-symmetrical end eccentricities would not approach the exact failure load asymptotically from above as it appears from Fig. 51. The lowest point on the curve is obtained when sufficient albeit small number of stations are located on either side of the critical section. Subsequently, as the number of column subdivisions increases, the accuracy in the estimation of the maximum curvature also increases and the failure loads would then show a tendency to approach the exact failure load asymptotically from below.

This is shown in Fig. 52 with an exaggerated vertical scale. Thus the error with 17 subdivisions will be somewhat less than the 3.5% mentioned above.

For results presented in the preceding section, the column length was subdivided into 16 segments for all the cases. This number was chosen as it represented a compromise between economy of computer time on the one hand and accuracy of the computed results on the other. The error in the worst case, that is for anti-symmetrical end eccentricities, has been shown to be less than 3.5%. For other combinations of end eccentricities the error will be less than this value, thereby justifying the use of 16 subdivisions for all the calculations.

CHAPTER 7

APPLICATION TO STIFFENED PLATES IN COMPRESSION

7.0 GENERAL

Figure 53. shows the elevation of a typical box girder bridge continuous over intermediate supports. The cross-sectional views at a point near a support and another near the mid-span are also shown. In each case the distribution of normal stress across the section based on simple beam theory, i.e. ignoring shear lag, has been shown alongside. In practice, the stress distribution is of course influenced by the presence of shear, eccentric loading inducing torsion and other factors. The study described in this chapter nevertheless relates primarily to stiffened plates that are subjected to uniform compression such as the bottom flange in Fig. 53(b) and the top flange in Fig. 53(c). The particular purpose of the study is to investigate the effect of residual stresses and the lack of initial straightness on the strength of stiffened compression plates.

A compression panel of practical dimensions was arbitrarily chosen. The breadth to thickness (b/t) ratio of the plate panels between stiffeners was taken as 60. Although with this b/t ratio, the section chosen is more slender than would normally be used, it was selected so that the interaction of local and overall buckling could be included in this study. The dimensional details of the cross-section including the stiffener are given in Fig. 54.

The results are presented in non-dimensional form for two reasons. First, to facilitate comparisons with other studies and second, to provide a basis for the application of these results to other cross-sectional shapes. It is acknowledged that results for different shapes of the cross-section will not necessarily lie on the curves obtained for the particular cross-section chosen here. However, from previous experience of the behaviour of other axially loaded steel columns the scatter is likely to be within a narrow band. With this in view, the objectives of this study may be stated thus:

1. To assess the relative effect of various types of column imperfections on the strength of the stiffened compression panels.

2. To demonstrate how the necessary design curves for a rapid design of stiffened plates may be obtained.

Another factor influencing the stiffened plate strength is the local buckling strength of the plate spanning between the stiffeners. In Section 7.4 an approximate method which accounts for the interaction of the local and overall buckling has been described.

7.1 ASSUMPTIONS

It is assumed that the steel plating has evenly spaced longitudinal stiffeners spanning between cross-frames. The loading on the stiffened plates is assumed to be uniaxial in the direction of the stiffener span with equal end eccentricities. For the main part of the study, where the effects of residual stresses and initial lack of straightness are studied, the loading is assumed to be concentric with the geometrical centroid of the total stiffener-plate assembly.

The failure loads have been obtained using the method outlined in Chapter 4, in which the deflected shape of the column is assumed to be in the form of a part-cosine wave, reducing to a cosine wave for axial loads. Assumptions made in Chapters 3 and 4 about the material properties, strain distribution, and small deflections are all retained. Further assumptions regarding the distribution of residual stresses and the values of initial lack of straightness are discussed in Sections 7.3.1 and 7.3.2 below.

7.2 MOMENT-THRUST-CURVATURE RELATIONS

Moment-thrust-curvature relations for the cross-section of Fig. 54 were obtained according to the procedure laid out in Chapter 3. As the cross-section is asymmetrical about the horizontal axis the moment-thrust-curvature curves for bending with the plate in greater compression than the stiffener (mode A) are different from those for bending with the stiffener in greater compression than the plate (mode B). Mode A curves are shown in Fig. 55 and mode B curves in Fig. 56. When the plate is under a greater compression than the stiffener, the moment of resistance of the cross-section exceeds the plastic moment value for axial loads varying from 0 to 0.8 times the squash load value. The maximum moment of resistance, 1.36 times the plastic moment under zero axial load, is obtained for an axial load approximately equal to 0.6 times the squash load. Such an increase in the moment of resistance is not observed for the other mode of bending in which the stiffener is in greater compression than the plate. This is illustrated in Fig. 57, which shows the moment-thrust relations for a fixed value of curvature (0.0026 per in, corresponding to $\phi/\phi_o = 10.0$) for both modes of bending. The bulge noticed for mode A bending may be explained as follows.

The full plastic moment corresponds to infinite curvature with the compressive and tensile stresses on opposite sides of the neutral axis both being at the yield level (Fig. 58). The neutral axis does not coincide with the geometric centroidal axis and is located towards the heavier part of the cross-section, in this case towards the plate. When an axial load is present, the position of the neutral axis shifts. In mode B bending, this shift is away from the centroid as illustrated in Fig. 58. The strain and stress diagrams shown in Fig. 58 are for a fixed value of curvature and for increasing depths of the neutral axis. This is accompanied by an increase in the net axial force acting on the section. Also marked on the stress diagrams are the locations of the resultant compressive and resultant tensile forces. For increasing loads, the shift in neutral axis position is consistently away from the geometric centroid, with more and more of the stiffener area reaching yield in compression. Consequently the resultant of the compressive stresses moves towards the geometric centroid of the whole cross-section. There is little change, however, in the position of the resultant tensile force, which remains within the plate thickness. The resulting loss in the lever arm is reflected in the continuously diminishing moment of resistance. However, in mode A bending, for small axial loads the neutral axis shifts in the direction of the geometric centroid as shown in Fig. 56. Any tensile yield in the stiffener is reduced, causing the resultant of the tensile stresses to move away from the geometric centroid. The location of the resultant compressive force undergoes little change. There is thus an increase in the moment of resistance not only because of an increase in the net force on the cross-section but also due to an increase in the lever arm. This trend continues until the entire plate is in compressive yield and the stiffener area closest to the plate also begins to yield in compression. At this stage, the moment of resistance of the cross-section will be a maximum. This corresponds to an axial load of

approximately 0.6 times the squash load for the cross-section chosen. Beyond this value of the load, for increasing positions of neutral axis, the stiffener rapidly goes into compressive yield which is accompanied by a similarly rapid reduction in the lever arm, diminishing in the limit to zero when the load on the section reaches the squash load value. This explains the reasons behind different moment-thrust-curvature relations for the two modes of bending.

The moment-thrust-curvature curves shown in Figs 54-55 were obtained for the cross-section free of residual stresses. Similar curves can be obtained for the cross-section with residual stresses.

The divergence observed for the moment-thrust-curvature relations for the two modes of bending leads directly to differences in the inelastic failure loads of columns of similar cross-sections having finite length. The effects of residual stresses and of initial lack of straightness on the failure loads of stiffened plates of varying slenderness are studied in the next section.

7.3 RESULTS OF PARAMETRIC STUDY

7.3.0 General

Inelastic failure loads were obtained for axially loaded stiffened plate elements having the cross-section shown in Fig. 54 for slenderness ratios varying from 12.5-250. For the complete range of slenderness ratios, the effects of residual stresses and lack of initial straightness were systematically studied. These results were obtained for axial loading. Later, the effect of eccentricity of loading on the column strength is also investigated.

7.3.1 Residual Stress Distribution in Welded Stiffened Plates

The high temperatures involved in the welding process produce thermal strains several times larger than the steel yield strain in the

immediate vicinity of the weld. The material away from the weld has thermal strains of much lower order. The uneven rate of cooling in the areas near and away from the weld results in considerable residual stresses. The distribution of residual stresses across the section is, in general, very irregular. Dwight and Moxham[69] have investigated this problem in some depth. It is observed that the welds themselves, together with the metal in their immediate neighbourhood, are invariably stressed up to yield in tension. In order to maintain statical equilibrium, the rest of the section remains in a state of residual compression. Experiments reported by Dwight, Chin and Moxham[86] on welded box sections indicate a residual stress pattern of the type shown in Fig. 59. Similar patterns were also reported by Nishino, Ueda and Tall[67] working at Lehigh. Dwight and Moxham recommended an idealised residual stress pattern for use in calculations. This is shown in Fig. 60. The width of the tension block is thought to be largely independent of the total width of the plate. In addition, when two or more plates meet at a weld, the width of the tension block for each of these is assumed to be the same, and may be calculated by the following equation

$$\eta_1 t_1 = \eta_2 t_2 = \frac{C\,A}{\sigma_y\,\Sigma t}$$

where Σt is the sum of plate thicknesses, C is a constant whose value recommended by Dwight and Moxham is 400 tonf/in^2, and A is the cross-section of the added metal. For the cross-section shown in Fig. 54, the value of A is arbitrarily taken as 0.15 in^2.

Knowing the lengths of the tension blocks, the average stress arising in the compression zone (σ_r) is calculated by satisfying the equilibrium of normal forces on the section. The resulting stress-distribution is shown in Fig. 61. However, this residual stress distribution has an unbalanced moment about the centroidal axis x-x. To ensure complete

statical equilibrium, correcting stresses in the compression zone are calculated for a moment that is equal and opposite to the unbalanced moment. Figure 62 shows the distribution of correcting residual stresses and Fig. 63 shows the resulting residual stress distribution, used in the subsequent computations. The maximum compressive residual stress (σ_{rm}) may be seen to occur at the tip of stiffener and is approximately equal to 0.18 σ_y.

7.3.2 Initial Lack of Straightness

In stiffened plates two types of geometric imperfections may be commonly encountered. The first corresponds to the lack of straightness of the plate along its line of intersection with the stiffener. This overall out-of-plane deformation of the stiffener is denoted by Δ_o (Fig. 64). The second type of geometric imperfection, which may be called the ripple component of geometric imperfection, relates to the additional initial deformations (δ_o) in the plate elements measured with respect to a surface parallel to the surface defined by the stiffener out-of-plane deformations. Figure 64 shows the nature of these secondary deformations. In the present study only the stiffener out-of-plane deformations are considered. The ripple component of imperfection is usually small in magnitude compared with the stiffener out-of-plane deformations and mainly effects the local plate buckling strength. Thus the initial lack of straightness of the stiffener-plate combination is taken to be the same as the stiffener-out-of-plane deformation Δ_o.

In general, it is difficult to estimate the magnitude of the lack of initial straightness for practical cases. The Merrison Design Appraisal Rules[60], current at the time the calculations presented here were carried

cut, recommended two values for this out-of-plane deformation associated with the two directions in which the stiffened plate can bend. For bending with the plate in greater compression than the stiffener (i.e. mode A bending) a value of L/400 was recommended. L is taken as the length of the stiffened plate between cross-frames. For the other mode of bending (i.e. mode B), in which the stiffener has a greater compression than the plate, an initial lack of straightness of magnitude L/600 was recommended. Following the results of tests carried out by Dowling, Chatterjee, Frieze and Moolani[72], and Dorman and Dwight[87], the out-of-plane deformation for stiffeners as specified in the Merrison Design Appraisal Rules[60] have been halved for both modes of bending in the new Merrison Design Rules[88]. Thus the current values are L/800 and L/1200 for mode A and mode B bending respectively. These values are also supported by the measurements of imperfections on actual structures[89]. Since the calculations presented in this thesis are based on higher values of out-of-plane deformations, the failure loads obtained for axially loaded stiffened plates are on the conservative side compared with the failure loads that would be obtained using the currently recommended values for out-of-plane deformations.

7.3.3 Strength of Ideally Straight Columns

The failure load of an ideally straight column with ideal elastic perfectly plastic stress-strain properties may be obtained by the well-known Euler equation. For low slenderness values, the strength is li limited by the yield stress of the material. Figure 65 shows the variation of column strength with slenderness ratio for such a column. Although no such ideal column exists in practice, this hypothetical case is chosen as the basis for comparison when studying the effects of various imperfections. The failure loads for different slenderness

ratios are expressed as a fraction of the squash load. The slenderness ratio at which the failure curve shows a discontinuity is given by

$$\lambda_e = \pi\sqrt{\frac{E}{\sigma_y}} \qquad (66)$$

which represents the Euler load for which the stress over the section equals the yield stress of material. For the material of the plates chosen in this study, E = 13000 tonf/in^2 and σ_y = 22 tonf/in^2 resulting in λ_e = 76.4.

7.3.4 Effect of Residual Stresses

The effect of residual stresses on the strength of an ideally straight column may be obtained by the tangent modulus theory using an idealised elastic-plastic stress-strain curve for the material. This results from the observation that the presence of residual stresses causes a deviation from the linear elastic zone of the stress-strain curve at a stress well below the yield stress. The deviation begins as soon as the fibre under maximum compressive residual stress attains the yield stress of the material. The idealised elastic-plastic average stress-strain curve for the column cross-section of Fig. 54 having a residual stress distribution of Fig. 63 is depicted in Fig. 66. The curve is obtained on the following bases:

1. The stress-strain curve deviates from the linear elastic range at a stress that is equal to the difference between the yield stress of the material and the maximum compressive residual stress in the section.

2. The stress-strain curve approaches the flat plastic range at a point corresponding to a permanent off-set of 0.002%. This is done to retain the value of yield stress as defined in various codes.

3. The curve is assumed to be parabolic between the two linear zones. In addition the tangents at the two points of contact are assumed to coincide with the two linear segments.

The tangent modulus failure loads are plotted in Fig. 67. The maximum effect is noticed at a slenderness value where the elastic critical failure mode changes to the yield failure mode. Figure 68 shows the variation of percentage loss in strength due to residual stresses. The maximum loss in stiffened plate strength is about 14 per cent for a slenderness ratio of λ_e(= 76.4), falling sharply on either side of this value.

7.3.5 Effect of Initial Lack of Straightness

Figure 69 shows the variation of failure loads with slenderness when the columns are given an initial lack of straightness. The magnitudes of the initial lack of straightness are in accordance with Section 7.3.2. The failure loads for mode B bending, i.e. failure by compression in the stiffener outstand are less than those for mode A bending with failure by compression in the plate up to a slenderness ratio of about 150. For slenderness ratios greater than 150, mode B results are greater than those for mode A. Figure 70 depicts the percentage loss in strength on the basis of the failure loads for ideally straight elastic perfectly plastic columns. It may be observed that the loss in strength increases steadily until the slenderness ratio λ_e, and then tends to reduce. The maximum loss for mode A bending is around 27 per cent and for mode B bending, approximately 47 per cent. Clearly the section is weaker for failure with mode B bending for a slenderness range of 0 - 150 in spite of a smaller amount of initial lack of straightness. The trend is reversed for slenderness ratios greater than 150,

beyond which the difference in the failure loads for the two modes merely reflects the difference in the two levels of imperfection. For such large slenderness ratios, if the imperfections for mode A and mode B were the same, the failure loads obtained would also be the same, and would approach the Euler load for diminishing values of imperfections.

7.3.6 Combined Effect of Initial Lack of Straightness and Residual Stresses

Failure loads were obtained with the column cross-section having a residual stress pattern shown in Fig. 63 for the two modes of bending with the same imperfections as adopted in Section 7.3.5. The results are plotted in Fig. 71. Mode B results are found to be smaller than mode A results for a range even larger than in the case without residual stresses. An interesting feature of these curves is the cusp obtained for both the modes of bending. The cusp occurs due to the rectangular nature of the residual stress-pattern. For a residual stress-pattern with gradual transition from the compressive to the tensile zones, the cusp in both the curves would vanish resulting in a smooth curve. The stress at which the cusp occurs is about the same for the two modes of bending, but there seems to be no direct relation with the magnitude of maximum compressive residual stress. The percentage loss of strength for this case for both modes of bending is plotted in Fig. 72. For the sake of comparison, the curves obtained in Fig. 70 are also superimposed.

It is clear that the effect of combining residual stresses with an initial lack of straightness is to reduce the column strength for mode B bending over the entire range of slenderness ratios. For mode A bending also a reduction in strength is indicated except for a range of slenderness ratios from 85 to 210, for which there seems to be a small

increase in strength with a maximum value of about 5% of the ideal column strength. This may be explained on the following basis. The residual stress pattern of Fig. 63 shows a compressive stress of approximately $0.18\ \sigma_y$ at the tip of the stiffener. For mode B bending, this results in an earlier initiation of yielding, and eventual collapse, as compared with the case when residual stresses are not considered. For mode A bending, for low slenderness ratios where the failure is initiated by the yielding of the compressive zone of the flange, the presence of compressive residual stresses in the greater portion of the flange again causes an earlier collapse. However, in this mode of bending for slenderness ratios from 85 - 210 when the collapse is due to instability initiated by lack of equilibrium only, the presence of tensile stresses in part of the flange and of compressive stresses in the stiffener directly strengthens the column.

7.3.7 Comparison with Existing Design Rules

At this stage it will be pertinent to compare the results obtained by the theory developed here with those predicted by available design formulae. In the BS153[90] use is made of the Perry formula with a value of imperfection factor given by $\eta = 0.003(L/r)$. To correlate with the results obtained for the two modes of bending, the imperfection factor may be taken as

$$\eta = \frac{c_o\, a_1}{r^2} \qquad (67)$$

where c_o is the initial lack of straightness and a_1 is the distance of the most stressed compressive fibre from the centroid of the section. In the formula given above, the value of c_o is taken as L/400 for mode A bending and as L/600 for mode B bending.

Figure 73 shows the variation of failure load with slenderness as obtained by the Perry-Robertson formula ($\eta = 0.003L/r$). Results are also plotted for the two modes of bending with appropriate values of c_o and a_1 substituted in the Perry formula. The Perry-Robertson curve is the same for the two modes of bending and lies in between the Perry curves for mode A and mode B bending. The curves clearly show that the use of Perry-Robertson formula would imply a greater value for the initial lack of straightness for mode A bending and a smaller value for mode B bending, as compared with the original Merrison values[60] for the corresponding modes.

Figure 74 has all the results for mode A bending grouped together. The effect of adding various imperfections can clearly be seen to result in a successive loss of stiffened plate strength. The curve for residual stresses combined with initial lack of straightness gives the least strength for slenderness values ranging from zero to around 85. For more slender columns, the residual stresses seem to enhance the column strength by a small amount. For the practical range of slenderness ratios, therefore, there is a clear need for accounting for residual stresses as well as an initial lack of straightness. The Perry formula with $c_o = L/400$ seems to represent the inelastic failure load quite closely for slenderness values up to 80, beyond which it overestimates the strength increasingly. It is also shown that the effect of both types of imperfections can be adequately represented by the Perry-Robertson formula with an all-inclusive imperfection of $\eta = 0.003(L/r)$ although for slenderness values greater than about 100, the formula tends to overestimate the column strength by as much as 10%.

Figure 75 shows the results for mode B bending grouped together. The observations for this mode are substantially different from those for mode B. The loss in strength due to various imperfections is evident for the whole range of slenderness. The smallest column strength is obtained with residual stresses combined with an initial lack of straightness. The Perry-Robertson curve is seen to be comparatively non-conservative by up to 24%, while the Perry curve with c_o = L/600 still over-estimates the column strength by 15% in the worst case at a slenderness value of 23. The last two values of percentages are based on the column strength that includes the effects of residual stresses as well as a lack of initial straightness. This points to the inadequacy of the Perry-Robertson formula in predicting the strength of the stiffened plate cross-sections for bending with the stiffener outstand in greater compression than the plate. However, with $\eta = 0.009\ (L/r)$ a close approximation can be made to the mode B bending analytical results obtained by combining residual stresses and initial lack of straightness.

If the results for mode A and mode B bending as shown in Figs 73 and 74 were to be superimposed, it would be obvious that the more critical design case is the one with the stiffener outstand in greater compression than the plate (mode B). This seemingly contradicts the pattern of failure observed in the tests carried out at Imperial College by Dowling, Chatterjee, Frieze and Moolani[72], who reported that the majority of failures were in mode A, but is in agreement with those reported by Murray[91]. This is readily explained by the fact that the welding procedures adopted in the preparation of the models tested at Imperial College caused a predishing of the stiffened plate panels between cross-girders in sympathy with mode A deflections. In these tests the possibility of local instability of the stiffener outstand (flat plates) was also considerably reduced by limiting the b/t ratio of outstands to 8. However, in the tests reported by

Murray[91], the stiffener outstands (bulb flats) were relatively slender having b/t ratio of 20 in most cases and the failure was often precipitated by the local instability of stiffeners. Also, Murray's tests were conducted on isolated panels in which the load was applied at the centroid of the gross cross-section whereas in the Imperial College tests the flanges were tested as part of a box and this causes an inevitable eccentricity of loading in the flanges that would tend to make it bend towards the stiffener outstand (mode A). In cases where the initial deformations are likely to be in sympathy with mode B bending, the stiffened plate strength would be grossly over-estimated if only mode A bending were to be considered. This points to the need for considering both the modes of bending at the design stage. Curves 2 in Figs 74 and 75 may accordingly be used as basic design curves for a rapid design, allowing for the fact that the imperfections implicit in these curves are comparatively higher than the values recommended in the current Design Rules[88].

7.4 LOCAL FLANGE BUCKLING

7.4.0 General

When the spacing between the stiffeners is too large, the strength of the stiffened plate in compression is adversely influenced by the local buckling of the plate situated in between the stiffeners. The U.S.S. Steel Design Manual[92] allows the problem of local plate buckling to be circumvented by specifying limiting values for the spacing between the stiffeners. The effect of local flange buckling can, however, be accounted for in an approximate manner by substituting an appropriate average stress-strain curve instead of the material stress-strain curve while computing the failure load. This was first suggested

by Vojta and Ostapenko[68]. Later Mittleman[75] made a similar assumption using the author's computer programs while examining the results of a test on a $\frac{1}{4}$ scale box girder model. The artifice used is to employ plate load-end shortening curves obtained by theoretical or experimental means as average stress-strain curves for the plate. Vojta and Ostapenko used Koiter's equation which has the limitation that it is applicable to the elastic post-buckling range only. This excludes anything but the very slender stiffened plates. To include the inelastic effects, Mittleman used Moxham's experimentally obtained load-end shortening curves[70]. Moxham has also suggested a theoretical approach for obtaining such load-end shortening curves. Earlier, Ratcliffe[66] had obtained a few experimental load-end shortening curves. His results were given for four different values of width to thickness ratios and were obtained for a fixed length of the plate. Moxham's experimental results were all obtained for a length to width ratio of 4, except in a few cases, which had a length to width ratio of 0.875. All of Moxham's theoretical results are based on a length to width ratio of 0.875, a value which was arrived at based on the observation that the maximum load values of the load-deflection curves were a minimum for this value. Moxham also concluded that the least value of maximum load is not sensitive to the length to width ratio. However, Moxham has not compared his theoretical curves with the experimental results except for a small number of cases. The agreement shown cannot be considered close. In view of the difficulty in establishing a suitable stress-strain curve, or a family of curves for various length to width ratios, the results described in this section which are based on Ratcliffe's experimental load-end-shortening curves, must only be considered as representative and cannot be used for

design purposes. They are intended to show how local plate buckling could be included in developing design curves for stiffened plates and also to show the extent to which the local plate buckling can reduce the stiffened plate strength.

7.4.1 Load-end Shortening Curves

Ratcliffe's experimental results are available for width to thickness ratios of 44, 54, 66 and 81. To obtain a load-end shortening curve for the section shown in Fig. 54 which has a width to thickness ratio of 60, an interpolated curve was obtained using the experimental curves for width to thickness ratios of 54 and 66. Ratcliffe has given curves both for welded as well as for stress free plates. For the purpose of this study, the curves for welded plates were adopted. The interpolated curve and the two parent curves are all shown in Fig. 76. Since the effect of residual stresses is already implicit in the load-end shortening curve, no further residual stesses are considered.

7.4.2 Effect of Local Flange Buckling on Failure Loads

Figure 77 shows the variation of failure loads with slenderness when local flange buckling effects are included. In calculating the failure loads an initial lack of staightness of L/400 was also considered. Also plotted are the failure loads obtained without considering local plate buckling (compare Fig. 69). In Fig. 78 the percentage loss of strength on the basis of the strength of ideal elastic perfectly plastic straight columns for the two cases are also plotted. For slenderness ratios greater than about 115, the curve with local plate buckling merges with the curve without local plate buckling because the strains at the failure stage are within the linear elastic zone of the load-end shorten-

ing curve. In this zone the curve coincides with the material stress-strain curve. For smaller slenderness ratios, the difference continues to increase and the maximum loss of strength is obtained at a slenderness ratio of approximately 75 and is of the order of 51%. This is about twice the value obtained when local flange buckling is not considered. Clearly the effect of local flange buckling on the column strength is of considerable importance for slenderness ratios less than about 110 - 115.

At this stage the inadequacy of the average stress-strain curve used can be pointed out. The failure load at zero slenderness is shown at about 66% of the squash load (Fig. 77). However, the local buckling effects at very low slenderness values (near zero) would be expected to be negligible. This discrepancy points to the need for employing a more representative load-end shortening curve.

Despite the inaccuracy of the load-end shortening curves indicated at low slenderness values, the loss in strength observed for intermediate range of slenderness shown in Figs 77 and 78 indicates the necessity of including the effects of local buckling on the column strength where such effects are likely to occur, that is, when the spacing between the stiffeners is larger than that required to prevent local plate buckling.

7.4.3 Use of Effective Width Concept to Account for Local Plate Buckling

In this section an attempt will be made to correlate the stiffened plate strength obtained by including the effect of local plate buckling (shown in Fig. 77) with the strength obtained on the basis of an effective width criterion specified in BS153[90]. This code gives formulas to compute the effective cross-sectional area of a member in compression using the effective width of the plate in terms of its width in between adjacent

stiffeners. The strength of the effective cross-section so obtained is calculated by using the Perry-Robertson (BS153) formula and expressed as a fraction of the squash load of the gross section. The variation of the stiffened plate strength calculated in this manner, with respect to the slenderness ratio of the gross cross-section has been plotted in Fig. 77 along with the theoretically based curve using experimental average stress-strain curves. It may be observed that the correlation between the theoretical results and the results based on BS153 is good. This leads to an important conclusion. In section 7.3.2 it was shown that the Perry-Robertson curve agreed well with the failure curve obtained for axially loaded stiffened plates failing in mode A when no plate buckling was considered. It has now been shown that by using an effective width such as that given in BS153, a satisfactory correlation with the theoretical results can still be obtained by using the Perry-Robertson curve.

It should be noted however that the effective width that may be used to compute the collapse load (such as those given in BS153) are not necessarily the same as those required for rigidity, that is, for the calculation of deflections. It is also recognised that the correlation between the loads obtained from effective width calculations and the collapse loads obtained by a consideration of average stress-strain curves to include local plate buckling is itself subject to verification by further research to demonstrate that either approach would agree well with true results for a full range of b/t ratios.

7.5 ECCENTRICALLY LOADED STIFFENED PLATES

7.5.0 General

Depending upon the detailing of the junction between stiffened plate elements acting as flanges and those acting as webs, the compressive loading on the flange elements can be eccentric with respect to the geometric centroid of the stiffener-plate column element. In general, the effect of the end moments so introduced is to reduce the ultimate load of such stiffened plates. These effects can be considered by constructing load-moment interaction curves, which may subsequently be used for design purposes.

7.5.1 Load-moment Interaction Curves

It is customary to represent the load-moment interaction curves as relations between P/P_u and M/M_u where M is the applied end moment, P_u is the squash load, and M_u is the ultimate moment of resistance in the pure bending case. In general, the effect of end moments on the failure loads is to reduce it. Thus, in no case can the ultimate load obtained in the presence of end moments be greater than the corresponding axial failure load. However, the maximum moment capacity, in the case of unsymmetrical sections does not necessarily occur for the no axial load condition, especially for columns with low slenderness raiots, but may occur for some fraction of the squash load. For columns with medium to high slenderness ratios, there is usually a continuously steady reduction in the moment capacity with increasing loads.

To illustrate these remarks, load-moment interaction relations were obtained for the column cross-section shown in Fig. 54 for both mode A and mode B bending. The slenderness values chosen were 25, 75 and

150 representing the stocky, the medium and the slender stiffened plates. Figure 79 shows the load-moment interaction diagrams for both mode A and mode B bending. For very slender columns (slenderness ratio = 150), there exists a steady reduction in ultimate loads with increasing end moments for both mode A and mode B bending. The effects of end moments seem to be most drastic for columns with medium slenderness, particularly for mode B bending. For mode A bending, at first a sharp drop in strength is observed even for small end moments, but as the moments increase further the rate at which the loss of strength occurs with increasing moments is slowed down and there follows a steady loss in strength with increasing end moments. For stocky stiffened plates, there is a steady loss in strength with increasing moments for mode B bending. For mode A bending, the loss of strength is very gradual for end moments as high as M_u. For load values ranging between 0.25 P_u and 0.68 P_u the ultimate moment capacity in fact exceeds the value at zero load. For P/P_u ranging between 0 and 0.25, the moment capacity remains in excess of 95% of the value at zero load. Thus for short stiffened plates in mode A bending, the end moments appear to have only a small effect on the column failure load.

Results presented in this section once again illustrate the high sensitivity of stiffened plates with intermediate slenderness ratios to various types of imperfections, in this case the eccentricity of end-loading.

7.5.2 Strengthening Effect of Initial Lack of Straightness in Opposition with End Eccentricities

For design purposes it is essential to consider the effect of the worst possible combination of factors in estimating the strength of any structure, including stiffened plates. However, to correlate results from

laboratory tests it is often necessary to take into account the beneficial effects of certain actual circumstances. One such situation arises when the column initial lack of straightness is such that the failure ought to occur in mode B bending, but due to the over-riding effects of end eccentricities the failure actually may occur in mode A bending. Clearly, the failure loads obtained would be higher than the mode A results shown in the interaction curves of Fig. 79. To illustrate this, Fig. 80 shows the interaction curves for mode A and mode B bending, along with an additional curve for the case when the end eccentricities cause failure in mode A bending while the initial lack of straightness is in sympathy with mode B bending. An increase in strength is indicated for all values of end moments and is as high as 68% for end moments, equal to approximately one-half of the ultimate moment at zero load. This shows the significant amount of strengthening that may be provided by negative initial lack of straightness.

7.6 IMPLICATIONS FOR DESIGN

It has been shown that for isolated, axially loaded stiffened plates in compression, failure will always be governed by mode B bending, i.e. with the stiffener outstand in greater compression than the plate. However, when such plates form the compression flange of a box girder, three factors complicate the situation. In the first instance, the out-of-plane deformations caused by the welding of the stiffener to the plate cause the initial deformations to occur more often in mode A than in mode B. This is reflected in a greater occurrence of the failure of stiffened compression panels in mode A than in mode B as observed in tests on box girder models carried out at Imperial College[72]. The second com-

plication arises from the overall flexure of the box (Fig. 81). Since the plate is always further removed from the neutral axis of the box than the stiffener, the moments acting on the stiffened panel in compression are consistently in sympathy with mode A bending and in opposition to mode B bending. A third factor, which is of a secondary nature but nevertheless further exaggerates the moments acting on the column, originates from the initial eccentricity of loading favouring mode A bending due to the connection detail between the web and the flange (Fig. 82), although in practice the presence of cross-frames at regular intervals tends to reduce this effect. If for a column with L/r = 75, the eccentricity of loading is taken to be equal to the distance between the centroid of the plate and the centroid of the stiffener-plate combination, the failure load for mode A bending with mode A initial deformations may be seen to be less than the failure load for mode A bending with mode B initial deformations (Fig. 80). Clearly, in these circumstances, that is, when the initial lack of straightness in mode B does not exceed the magnitude of the eccentricity of loading (favouring mode A bending and opposing mode B bending), then the collapse will occur in mode A and not in mode B.

We thus have (a) an explanation as to why the majority of the compression flange failures in the series of tests on box girders carried out at Imperial College[72] occurred with the plate in failing in compression and the stiffener in tension, and (b) a possible simple design approach suggesting itself in outline.

However, before outlining the possible design method, it is necessary to deal with the local buckling effects that limit the strength of stiffened panels. Local buckling of the plate in between the stiffener influences only mode A collapse loads, and can be accounted for in the way

outlined in Section 7.4. The local buckling of the stiffener, on the other hand, would invalidate some of the arguments set out above, and could lower the stiffened panel strength considerably below that predicted for mode A bending even in the presence of restraining moments. The post-buckling reserve of a stiffener, supported along its line of intersection with the plate would be negligible compared with any such reserve possessed by the plate panel in between the stiffeners. It would, therefore, appear to be highly undesirable to have the strength of the stiffened panel to be curtailed by such a premature failure due to relatively less stable stiffeners. Conversely, it would be highly desirable to proportion stiffeners in such a way as to prevent their local buckling. In the Imperial College boxes, where flats were used as stiffeners, such failures were prevented by limiting the depth to thickness ratio to 8. In the one case where a mode B failure did occur at an end panel with mode B type initial deformations, the flats failed by compressive yielding and did not buckle locally before the collapse load of the box was attained. Thus to prevent local buckling of the stiffeners, it should be possible by further research to specify limits for the cross-sectional dimensions of the stiffener. These limits would of course depend upon the material strength and width to thickness ratios of the plate panels in between the stiffeners. In the absence of such information, the current rules in Ref. 88 could be used to check the design of stiffeners.

If the local buckling of the stiffener could be eliminated by a suitable design, only mode A or mode B failures as treated in this study would need to be considered. It has already been shown that the use of Perry-Robertson formula gives good agreement with the predicted collapse loads for mode A failure in which the effects of residual stresses and

initial lack of straightness of L/400 (based on Merrison Design Appraisal Rules[60]) were included. Therefore, the application of this formula might be expected to give good agreement with test results. This is indeed the case, as illustrated by the findings from tests carried out at Imperial College[72] and Cambridge University[87]. It has also been shown that local buckling of the plate in between the stiffeners can be accounted for with sufficient accuracy by the effective width approach already incorporated in BS153. Therefore, use of the Perry-Robertson formula in conjunction with the effective widths incorporated in BS153 can be safely recommended for design where mode A failures are indicated, particularly as the new values of initial lack of straightness specified in the current Merrison Design Rules[88] are only half of those used in this study.

Where mode B failures are indicated, use of the Perry-Robertson formula has been shown to be inadequate. However, using a higher imperfection factor $\eta = 0.009\ (L/r)$, the Perry formula has been shown to give good agreement with mode B curves.

The suggested simple design procedure may now be outlined as follows:

(1) Proportion stiffener outstands so as to prevent local buckling. Pending further research, Merrison Design Rules[88] clauses may be applied to check whether local buckling is likely to limit stiffened panel strength and if so the stiffener outstand should be redesigned to prevent this occurring.

(2) Check initial eccentricity of loading, e, by considering bending moment gradient over the column cross-section derived by a consideration

of the flexure of the box (cf. Fig. 81).

If $e >$ mode B initial deformation (L/1200), the plate-stiffener combination column cross-section fails in mode A, otherwise in mode B.

(3) For mode A failure, if $e \leqslant L/800$ (the new value of initial deformation), the cross-section may be designed as an axially loaded column using the Perry-Robertson formula and effective widths in accordance with BS153 to account for local plate buckling.

It is important to remember that the Perry-Robertson curves imply a consideration of residual stresses and initial lack of straightness of L/400 as shown above, which may be considered to be equivalent to a consideration of residual stresses, an initial lack of straightness of L/800 and an implied end eccentricity of approximately L/800.

(4) For mode B failure, if $e \leqslant L/1200$, the cross-section may be designed as an axially loaded column using an imperfection factor $\eta = 0.009\ (L/r)$ in the Perry formula (Curve 5 in Fig. 75).

In this case the imperfections considered are residual stresses, initial lack of straightness of L/1200 and an implied end eccentricity of approximately L/1200.

(5) Where eccentricities are outside the limits mentioned in steps (3) and (4) above, an appropriate reduction in strength can be considered using load-moment-interaction curves such as those given in Fig. 79.

(6) No separate allowance needs to be made for residual stresses, as they are already included in the design formulas/curves mentioned in earlier steps. The presence of residual stresses only modifies the strength but has no influence on the preferred mode of bending.

CHAPTER 8

CONCLUSIONS

8.0 GENERAL CONCLUSIONS

(1) Experimental results on the ultimate load behaviour of short, medium and long composite columns in biaxial bending have been made available.

(2) Two analytical methods for the determination of the strength of such columns have been developed within this thesis. The first method, an approximate one based on an assumed deflected shape in the form of a part of a cosine wave, is applicable to columns in symmetrical bending in each of the two bending planes. The other method, based on the determination of the actual deflected shape, is more exact and general, and is applicable to columns with any combination of end eccentricities.

(3) Comparisons between experimental and theoretical results for composite columns show good agreement for both methods of analysis.

(4) The analyses developed here are not limited in their application to composite columns alone. They have also been used to study the influence of imperfections on the strength of stiffened plates in compression.

(5) It has been shown that the presence of residual stresses and initial lack of straightness may reduce the strength of stiffened plates in compression by up to 50% (for $L/r \approx 75$) based on the ideal elastic perfectly plastic column strength (40% on the tangent-modulus strength).

(6) A simple design procedure has been outlined which is based (a) on the elimination of local buckling of the stiffener outstand by suitable design, and (b) on the use of the Perry formula to closely represent the inelastic failure loads of stiffened plates in compression.

8.1 PARTICULAR CONCLUSIONS RELATING TO COMPOSITE COLUMNS IN BIAXIAL BENDING

8.1.1 Composite Action

The test results fully substantiate the validity of two of the fundamental assumptions made in the theoretical analysis of composite columns. These relate to the continuity of strains between steel and concrete interfaces and the planar distribution of strains over the cross-section. The distribution of strains deduced from strain measurements at the four tips of the H-section and at several points on the concrete surface were found to be essentially linear for all columns even for loads very close to the respective failure loads. The variation of strain away from the planar distribution was found to be within a maximum of 10% just before collapse. From the planar nature of the strain distribution it was also evident that the strains remain continuous between steel and concrete, thereby endorsing the assumption of composite action. It should be noted however that these composite columns, like all others tested to-date, were tested in symmetrical bending, and no primary shear loading likely to break the bond between steel and concrete was introduced.

8.1.2 Failure Strain of Concrete

The crushing strain of concrete observed in almost all the tests was approximately 0.00400. This corresponds to the strain just before concrete begins to spall.

8.1.3 Failure Mechanism of the Test Columns

In each case the first indications of distress were recorded when the tip of the flange stressed most in compression reached yield. This was followed by tension yield in the diagonally opposite tip and finally by the crushing of the concrete in compression. It was also observed that the first yield in steel occurred well below the collapse load of the column except for long columns where the difference was small and hence no simple failure criterion could be established.

8.1.4 Accuracy of the Method Based on the Actual Deflected Shape

In principle, by taking a large number of column subdivisions, the calculated failure loads can be made to approximate to the exact failure load with only a negligible error. In practice, the number of subdivisions that may be employed is limited by the available computer time and storage. It has been shown that for symmetrical bending, failure loads that are within 0.1 per cent of the exact value may be obtained by using as few as 8 subdivisions. However, for columns with antisymmetrical end eccentricities about both the bending planes, the number of subdivisions required for a similar accuracy is more than 24. More important, in such cases the results obtained by using a smaller number of segments are found to be on the unsafe side. As a compromise between the accuracy of results and the required computer time, it was shown that by using 16 segments speedy results could be obtained with an error of only ± 3.5 %.

8.1.5 Accuracy of the Method Based on the Part-cosine Wave Assumption for the Deflected Shape

The part-cosine wave assumption can be conveniently applied to columns having symmetrical end eccentricities in each of the two bending

planes. It has been shown that the maximum error introduced by using this assumption is of the order of 5.5% and the average error is only 3.5% when applied to the nine test columns. The percentages are based on the theoretically exact failure loads, and are on the safe side.

8.1.6 Effect of Residual Stresses on the Strength of Composite Columns

It was found that the consideration of residual stresses in the steel core of the nine composite columns tested resulted in a variation of ± 3% in the failure loads. The computed failure loads were found to reduce or remain unaltered for columns with short length or with small eccentricities, while the strength of long columns or columns with larger eccentricities was found to be enhanced by the presence of residual stresses. This originates from the nature of the residual stress distribution which, although initiating larger deflections, causes a delayed collapse due to the presence of strains opposite in sign to the imposed strains having a major flexural component. For short columns, or columns with small eccentricities, the flexural strains are less important compared with direct compressive strains, and the residual strain distribution has little or no effect on the failure load.

8.1.7 Effect of an Initial Lack of Straightness on the Strength of Composite Columns

The presence of an initial lack of straightness in a column results, as is well known, in a reduction in its strength. It was shown that for columns in symmetrical biaxial bending, the maximum reduction in strength occurs when the initial lack of straightness is oriented along the minor axis. Since the exact orientation of initial imperfection in columns with arbitrary end eccentricities resulting in the least failure

loads is difficult to locate, it is recommended that the minor axis orientation be adopted in all cases for simplicity.

8.1.8 Comparison of Test Results with the Two Analytical Methods

Both methods have been shown to give good agreement with the observed failure loads. When residual stresses together with an initial lack of straightness of L/1000 are included, the computer results based on the approximate method have been shown to give failure loads having a standard deviation of 10% with the average value of P_{xy}/P_{test} within an error of -5%. The method based on the actual deflected shape gives results that are 1.5% to 5.5% higher than the approximate method. This results in an even closer approximation of test results. The standard deviation remains at about 10% but the average P_{xy}/P_{test} has an error of less than 0.5%.

The theoretical and experimental deflections for the nine test columns also showed a correspondingly good agreement.

8.1.9 Validity of the Design Method as Applied to Composite Columns in Biaxial Bending

Basu and Sommerville's design method has been shown to be always conservative when applied to composite columns in biaxial bending. The interaction formula relating uniaxial strengths to the biaxial strength has been shown to be adequate for short columns but significant errors are obtained for long columns. Errors varying from 25 - 43% were also observed for columns having asymmetrical end eccentricities. The errors were least for columns with symmetrical end eccentricities in both the bending planes and were maximum for columns with equal and opposite end eccentricities in each of the two bending planes. Intermediate values

were obtained for other combinations of end eccentricities. This large difference between actual failure loads and those predicted by the design method points to the need for an improved design method. It is suggested that the use of the analytical procedures developed in this thesis can lead to the derivation of a more exact design method in future.

8.2 PARTICULAR CONCLUSIONS RELATING TO STIFFENED PLATES IN COMPRESSION

8.2.1 Effect of Residual Stresses

In most cases residual stresses as predicted by currently available theory have been shown to have a detrimental effect on the strength of stiffened plates in compression. The effect has been noted both for straight columns (up to 13%) and for columns having an initial lack of straightness (up to 16%), although for columns in the range of slenderness ratios 85 - 210 the residual stress patterns used provide a small increase in strength (up to 5%) for bending with the plate in a greater compression than the stiffener.

8.2.2 Effect of Initial Lack of Straightness

An initial lack of straightness also has a detrimental effect on the stiffened plate strength of the same order of magnitude as the residual stresses. Initial imperfections of the same magnitude have a greater effect with the stiffener in a greater compression than the plate (mode B), as compared with the plate in a greater compression than the stiffener (mode A). It was shown that the values of imperfections recommended in an earlier version of the Merrison Design Rules[60], namely L/400 for mode A bending and L/600 for mode B bending, resulted in the mode B bending being the more critical case for design. With the new

values of imperfection[88], respectively L/800 and L/1200 for the two modes of bending, the same would still be true.

8.2.3 Effect of Local Plate Buckling

An approximate method for considering local plate buckling was described in Section 7.4 above. The method is based on the use of load-end-shortening curves for the plates in place of material stress-strain curves. Using Ratcliffe's experimental curves, it has been found that maximum loss in strength due to the interaction of local and overall buckling could be as high as 25% for slenderness ratios around 75. Local buckling effects depend, of course, on the width to thickness ratio of the plate. With more adequate load-end-shortening curves, it should be possible to obtain a more accurate estimate of the effect of local plate buckling on the stiffened plate strength.

It was also shown that the use of effective widths such as those specified in BS153 leads to a satisfactory correlation with strength curves obtained from the inelastic column failure criterion combined with average load-end shortening curves.

8.2.4 Sensitive Range of Slenderness Ratios for Stiffened Plates with Imperfections

It has been shown that stiffened plates in the range of slenderness ratios 20 - 100 are the most sensitive to various types of imperfections. Residual stresses (when considered in conjunction with an initial lack of straightness) appear to have a maximum effect in the range 20 - 60 for both modes of bending. The loss in strength is as high as 25%. Initial imperfections appear to have a maximum effect around a slenderness of 75. The effects of residual stresses as well as of initial lack of

straightness are more pronounced for mode B bending than for mode A bending. Local buckling effects have been shown to be important for all slenderness values less than about 100, although the magnitude of loss in strength depends on the width to thickness ratio of the plate.

8.2.5 Effect of End Eccentricities

The presence of end eccentricity of loading has a pronounced effect for plates with slenderness ratios in the range 30 - 100. Small eccentricities can result in a sharp loss of strength for this range of slenderness ratios. For plates outside this range, the loss in strength is more gradual. The presence of end eccentricities can also over-ride any tendency of the stiffened plate panels in actual box girders to bend in mode B due to initial lack of straightness being in that mode, and cause failure to occur in mode A.

8.2.6 Simple Design Approach for Stiffened Compression Panels in Box Girders

Provided that the stiffeners are detailed so as to preclude their failure by local buckling, the stiffened plate panels can be designed on the basis of the Perry-Robertson curve and a suitable effective width criterion such as that specified in BS153 to include local plate buckling for mode A bending, or on the basis of the Perry formula with modified η (= 0.009 L/r) for mode B bending. The panels may be treated as axially loaded as long as the applied end eccentricities do not exceed a value equal to the magnitude of the initial lack of straightness for the relevant mode. For other cases, suitable modification in strength can be made by the use of load-moment interaction curves.

8.3 FUTURE WORK

The way now appears to be clear to the derivation of improved design formulas by a direct application of the computer programs developed to predict the strength of composite columns in biaxial bending. A corollary of such a study would be to identify those cases in which the minor axis instability has a negligible effect on columns with applied major axis bending moments, thereby eliminating the need to consider the more tedious biaxial bending failures in the design.

An immediate extention of the present work can be made to columns with end-restraints. Further, the same procedures can be applied to frames without sidesway. This can be achieved by applying necessary conditions of compatibility at the junction of beam and column elements, each of which is treated in the same manner as the isolated column. It is envisaged that a consideration of the change in geometry due to the relative deflections between adjacent nodes can lead to the study of the collapse load of space-frames including sidesway. It has been shown that such a procedure can be made to be equally applicable to frames comprising bare metal sections and reinforced concrete sections as well as composite sections. A consideration of torsion of the elements would be necessary.

In its application to the design of stiffened plates, the existing method can be applied to other cross-sectional shapes and other width-to-thickness ratios of the plate in order to cover most practical cases. By applying more adequate load-end-shortening curves, the effect of local plate buckling on the strength of stiffened plates can be studied more accurately. Similarly, by considering load-end-shortening curves for the stiffener outstand, the effect of local buckling of stiffeners can be studied. The method can also be conveniently extended to include the restraining effects of cross-frames on the strength of multiple span stiffened plate panels.

REFERENCES

1. Euler, L. De curvis elastis. Lausanne and Geneva, 1744.
2. Beer, H., and Schulz, G. Bases théoriques des courbes Européennes de flambement. Const. Metallique, no. 3, 1970.
3. Euler, L. Sur la force de colonnes. Memoires de l'Académie de Berlin, 1759.
4. Lagrange, J.L. Sur la figure des colonnes. Mélanges de Philosophie et de Math. de la Soc. Roy. de Turin. Turin, 1770, p. 123.
5. Lamarle, E. Mémoire sur la flexion du bois. Ann. des travaux publics de Belgique, vol. 4, 1846, pp. 1-36.
6. Considére, A. Resistance des pieces comprimées. Congrès International de Procedés de Construction, 1889.
7. Engesser, F. Zeitschrift fur Architektur und Ingenieurwesen, 1889, p. 455.
8. Shanley, F.R. Inelastic Column Theory. J. Aeronaut. Sci., 1947, p. 261.
9. Ostenfeld, A. Exzentrische und zentrische Knickfestigkeit. Zeitschrift des Vereines deutscher Ingenieure, vol. 94, 1898, p. 1462.
10. von Kármán, T. Die Knickfestigkeit gerader Stäbe. Physikalische Zeitschrift, vol. 9, 1908, p. 136. and Untersuchungen über Knickfestigkeit. Mitteilungen über Forschungs arbeiten auf dem Gebiete des Ingenieurwesens, no. 81, Berlin, 1910.
11. Ros, M. Die Bemessung Zentrisch und exzentrisch gedruckter Stäbe auf Knickung. Rept 2d. Internat. Cong. Bridge and Structural Eng., Vienna, 1928.

12. Westergaard, H.M., and Osgood, W.R. Strength of Steel Columns. Trans. ASME. vols. 49-50, APM-50-9, 1928, p. 65.

13. Jezek, K. Die Tragfähigkeit des exzentrisch beanspruchten und des querbelasteten Druckstabes aus einem ideal plastischen Material. Sitzungsberichte der Akademie der Wissenschaften in Wien, Abt. IIa, vol. 143, 1934.

14. Timoshenko, S. Sur la stabilité des systèmes élastiques. Annales des ponts et chaussées, Parts III, IV and V, 1913.

15. Bleich, F. Stahlhochbauten, Vol. II, Julius Springer Berlin, 1933, p. 925.

16. Winter, G. Lateral Stability of Unsymmetrical I-Beams and Trusses in Bending. Trans. ASCE, 1943, p. 247.

17. Goodier, J.N. Flexural-Torsional Buckling of Bars of Open Sections, under Bending, Eccentric Thrust or Torsional Loads. Cornell Univ. Eng. Exp. Sta. Bull. 28. Ithaca, N.Y., 1942.

18. Klöppel, K., and Winkelmann, E. Experimentelle und Theoretische Untersuchungen über die Traglast von Zweiachsig Aussermittig Gedrückten Stahlstäben. Der Stahlbau, vol. 31, no. 2, February, 1962, p. 33.

19. Birnstiel, C., and Michalos, J. Ultimate Load of H-columns under Biaxial Bending. Journal of the Structural Division, Proc. ASCE, vol. 89, no. ST2, April, 1963.

20. Harstead, G.A., Birnstiel, C., and Leu, K-C. Inelastic H-columns under Biaxial Bending. Journal of the Structural Division, Proc. ASCE, vol. 94, no. ST10, October, 1968, pp. 2371-98.

21. Harstead, G.A. Elasto-Plastic Behaviour of Columns Subjected to Biaxial Bending. Ph.D. Thesis, New York University, New York, June, 1966.

22. Sharma, S.S., and Gaylord, E.H. Strength of Steel Columns with Biaxially Eccentric Load. Journal of the Structural Division, Proc. ASCE, vol. 95, no. ST12, December, 1968, pp. 2797-2812.

23. Milner, H.R. The elastic-plastic stability of stanchions bent about two axes. Ph.D. Thesis, University of London, 1965.

24. Baker, J.F., Horne, M.R., and Heyman, J. The Steel Skeleton, vol. II, Cambridge University Press, London, 1956.

25. Wood, R.H. Column Design: a New Approach. Building Research Station Note 263/71, September, 1971.

26. Basu, A.K. Computation of failure loads of composite columns. Proc. Instn. civ. Engrs., vol. 36, March, 1967, pp. 557-578. also, Proc. Instn. civ. Engrs., vol. 38, October, 1967, pp. 305-312. (Discussion).

27. Basu, A.K., and Hill, W.F. A more exact computation of failure loads of composite columns. Proc. Instn. civ. Engrs., vol. 40, May, 1968, pp. 37-60.

28. Basu, A.K., and Sommerville, W. Derivation of formulae for the design of rectangular composite columns. Paper 72065, Proc. Instn. civ. Engrs., 1969, Supp., pp. 233-280.

29. Bresler, B. Design Criteria for reinforced concrete columns under axial load and biaxial bending. J. Am. Concr. Inst., vol. 57, November, 1960, pp. 481-490.

30. Yam, L.C.P. Ultimate-load behaviour of composite T-beams having inelastic shear connection. Ph.D. Thesis, University of London, 1966.

31. Burr, W.H. Composite Columns of Concrete and Steel. Proc. Instn. civ. Engrs., vol. 188, 1912, pp. 114-126.

32. Talbot, A.N., and Lord, A.R. Tests of Columns: An Investigation of the Value of Concrete as Reinforcement for Structural Steel Columns. Univ. of Illinois Eng. Exp. Sta. Bull., no. 56, March, 1912, p. 44.

33. Mensch, L.J. Composite Columns. J. Am. Concr. Inst., vol. 2, no. 3, November, 1930, pp. 263-280.

34. Emperger, F. Discussion on Mensch's Paper[33]. Proc. Am. Concr. Inst., vol. 27, 1930-31, pp. 1311-18.

35. Saliger, R. Discussion on Mensch's Paper[33]. Proc. Am. Concr. Inst., vol. 27, 1930-31, pp. 1318-21.

36. British Standard Specification for Structural Steel in Buildings, BS449, 1959. (Reset and reprinted 1965).

37. Faber, O. Savings to be Effected by the More Rational Design of Cased Stanchions as a Result of Recent Full-size Tests. The Structural Engineer, vol. 34, no. 3, March, 1956, pp. 88-109.

38. -- , Discussion on Faber's Paper[37]. The Structural Engineer, vol. 35, no. 4, April, 1957, pp. 148-155.

39. ACI Committee 318. Building Code Requirements for Reinforced Concrete (ACI 318-56). Am. Concr. Inst., 1956.

40. Rizk, A.A. The Effect of Concrete Encasement on the Behaviour of Steel Framed Buildings. Ph.D. Thesis, University of Leeds, September, 1957.

41. Jones, R. Composite Action in Steel-framed, Concrete Encased, Multi-storey Buildings. The Instn. struct. Engrs. - 50th. Anniversary Conference, October, 1958.

42. Stevens, R.F. Encased Steel Stanchions and BS449. Engineering, vol. 188, no. 4879, October, 1959, pp. 376-377.

43. Bondale, D.S. The Effect of Concrete Encasement on Eccentrically Loaded Columns. Ph.D. Thesis, University of London, 1962.

44. Roderick, J.W., and Rogers, D.F. Load Carrying Capacity of Simple Composite Columns. Journal of the Structural Division, Proc. ASCE, vol. 95, no. ST2, February, 1969, pp. 209-228.

45. Furlong, R.W. Strength of Steel-Encased Concrete Beam-Columns. Journal of the Structural Division. Proc. ASCE, vol. 93, no. ST5, October, 1967, pp. 113-124.

46. Furlong, R.W. Design of Steel-Encased Concrete Beam-Columns. Journal of the Structural Division, Proc. ASCE, vol. 94, no. ST1, January, 1968, pp. 267-281.

47. Klöppel, K., and Goder, W. Collapse Load Tests on Concrete-Filled Steel Tubes and Derivation of a Design Formula (in German). Der Stahlbau, vol. 26, January and February, 1957, p. 1 and p. 44.

48. Chapman, J.C., and Neogi, P.K. Almondsbury Interchange: Experiments on Concrete-Filled Tubular Columns. Engineering Structures Laboratory Report, Civil Engineering Department, Imperial College, March, 1965.

49. Neogi, P.K., Sen, H.K., and Chapman, J.C. Concrete-Filled Tubular Steel Columns under Eccentric Loading. The Structural Engineer, vol. 47, no. 5, May, 1969, pp. 187-195.

50. Sen, H.K., and Chapman, J.C. Ultimate Load Tables for Concrete-Filled Tubular Steel Columns (Circular, Square and Rectangular Columns). Technical Note 9, CIRIA, 1970.

51. Neogi, P.K. Concrete-Filled Tubular Columns. Ph.D. Thesis, University of London, 1967.

52. Richart, F.E., Brandtzaeg, A., and Brown, R.I. The Failure of Plain and Spirally Reinforced Concrete in Compression. Univ. of Illinois Eng. Exp. Sta. Bull., no. 190, April, 1929.

53. Sen, H.K. Triaxial Effects in Concrete-Filled Tubular Steel Columns. Ph.D. Thesis, University of London, 1969.

54. Knowles, R.B., and Park. R. Axial load design for concrete filled steel tubes. Journal of the Structural Division, Proc. ASCE, vol. 96, no. ST10, October, 1970, pp. 2125-2153.

55. Guiax, P., and Janss, J. Buckling Behaviour of Columns made with Steel Tubes and Filled with Concrete. Report issued by Centre de Recherches Scientifiques et Techniques de L'Industrie des Fabrications Metallique, CIDET Issue 70/421E, November, 1970. (In French).

56. Gesund, H. Stress and moment distributions in three-dimensional frames composed of non-prismatic members made of non-linear materials. Chapter 13. Space Structures, Blackwell, Oxford and Edinburgh, 1967, pp. 145-153.

57. Brettle, H.J., and Taylor, J.M. Comparison of Experimental Results with Ultimate Strength Theory for Reinforced Concrete Columns in Biaxial Bending. Civil Engineering Transactions, Instn. civ. Engrs., Australia, vol. CE11, no. 1, April, 1969, pp. 63-74.

58. Sharples, B.P.M. The Structural Behaviour of Composite Columns. Ph.D. Thesis, Cambridge University, 1970.

59. Roderick, J.W. Further Studies of Composite Steel and Concrete Structures, International Association for Bridge and Structural Engineering. IX Congress, Amsterdam, May 8-13, 1972, pp. 157-164.

60. Committee of Investigation into the Design and Erection of Steel Box Girder Bridges. Appendix A - Interim Design Appraisal Rules, Department of the Environment, September, 1971.

61. Timoshenko, S. Uber die Stabilität versteifter Platten, Der Eiesenbau, 1921, p. 147.

62. Loshkin, A.S. On the calculation of Plates with Ribs. Jour. Applied Math. and Mechanics, vol. 2, Moscow, 1935, p. 225. (In Russian).

63. Barbré, R. Stabilität gleichmässig gedrückter Rechteckplatten mit Längs Quersteifen, Ingenieur - Archiv, vol. 8, 1937, p. 117.

64. Bleich, F. Buckling Strength of Metal Structures, McGraw-Hill Book Company, 1952, p. 359.

65. Dwight, J.B., Chin, T.K., and Ratcliffe, A.T. Local buckling of thin-walled columns, effect of locked-in welding stresses. CIRIA Res. Rep. No. 12, (Pt. 2), May, 1968.

66. Ratcliffe, A. T. The strength of plates in compression. Ph.D. Thesis, Cambridge University, October, 1968.

67. Nishino, F., Ueda, Y., and Tall, L. Experimental Investigation of the Buckling of Plates with Residual Stresses. Test methods for compression members, ASTM STP419, Am. Soc. Testing Mats., 1967, p. 12.

68. Vojta, J.F., and Ostapenko, A. Ultimate Strength Design of Longitudinally Stiffened Plate Panels of Large b/t. Lehigh University Fritz. Eng. Lab. Report, no. 248.18, August, 1967.

69. Dwight, J.B., and Moxham, K.E. Welded Steel plates in compression. The Structural Engineer, vol. 47, no. 2, February, 1969, pp. 49-66.

70. Moxham, K.E. Buckling tests on individual welded steel plates in compression. Cambridge University Report No. CUED/C - Struct/TR3 (1971)

71. Moxham, K.E. Theoretical prediction of the strength of welded steel plates in compression. Cambridge University Report No. CUED/C - Struct/TR2 (1971).

72. Dowling, P.J., Chatterjee, S., Frieze, P.A., and Moolani, F.M. The experimental and predicted behaviour of rectangular stiffened steel box girders. Paper No. 6. International Conference on Steel Box Girder Bridges, Institution of Civil Engineers, London, 13-14 February, 1973.

73. Lundquist, E.E. Comparison of three methods for calculating the compressive strength of flat and slightly curved sheets and stiffener combination. NACA Tech. Note 455.

74. von Kármán, T., Sechler, E.E., and Donnell, L.H. The strength of thin plates in compression. Trans ASME, Applied Mechanics, vol. 54, no. 2, January, 1932.

75. Mittleman, M.L. A theoretical and experimental investigation in connection with steel box girders. M.Sc. Thesis, Imperial College, University of London, 1971.

76. Dwight, J.B., Little, G.H., and Rogers, N.A. An approach to stiffened steel compression panels. Cambridge University Report No. CUED/C - Struct/TR 32 (1973).

77. Column Research Council. Guide to Design Criteria for Metal Compression Members. Edited by Bruce G. Johnston. John Wiley & Sons, Inc., New York, 1966, pp. 191-200.

78. Horne, M.R. The Plastic Design of Columns, British Constructional Steelwork Association, London, p. 6.

79. Barnard, P.R., and Johnson, R.P. Ultimate strength of composite beams. Proc. Instn. civ. Engrs., vol. 32, Oct. 1965, pp. 161-179.

80. Desayi, P., and Krishnan, S. Equation for the stress-strain curve for concrete. J. Am. Concr. Inst., Proceedings, vol. 61, no. 3, March, 1964.

81. Warner, R.F. Moment curvature relation for reinforced concrete columns in biaxial bending. UNICIV Report No. R-28, University of New South Wales, Kensington, N.S.W., Australia, 1968.

82. Huber, A.W., and Beedle, L.S. Residual Stress and the Compressive Strength of Steel. The Welding Journal, vol. 33, no. 12, December, 1954, pp. 589s-614s.

83. Young, B.W. Residual Stresses in Hot-rolled Sections. Cambridge University Report No. CUED/C - Struct/TR.9 (1971), p. 12.

84. Robertson, J.N. The strength of short rectangular composite columns under biaxially eccentric loading. M.Sc. Thesis, Imperial College, University of London, 1968.

85. Ramamurthy, L.N. Investigation of the ultimate strength of square and rectangular columns under biaxially eccentric loads. Symposium on Reinforced Concrete Columns, Publication SP-13, American Concrete Institute, 1966.

86. Dwight, J.B., Chin, T.K., and Ratcliffe, A.T. Local buckling of thin-walled columns, effect of locked-in welding stresses. CIRIA Res. Rep. No. 12 (Pt. 1), May, 1968.

87. Dorman, A.P., and Dwight, J.B. Tests on stiffened compression panels and plate panels. Paper No. 5, International Conference on Steel Box Girder Bridges, Institution of Civil Engineers, London, 13-14 February, 1973.

88. Inquiry into the Basis of Design and Method of Erection of Steel Box Girder Bridges. Report of Committee - Appendix 1. Interim Design and Workmanship Rules, Part II - Design Rules, London, HMSO, 1973.

89. Measured Imperfections. Unpublished. Quoted in the following paper: Flint, A.R., and Horne, M.R. Conclusions of Research Programme and Summary of Parametric Study. Paper No. 10. International Conference

on Steel Box Girder Bridges, Institution of Civil Engineers, London, 13-14 February, 1973.

90. British Standard Specification for Steel Girder Bridges. Part 3B. Stresses BS153 : Parts 3B and 4 : 1958. British Standards Institution.

91. Murray, N.W. Buckling of Stiffened Panels Loaded Axially and in Bending. The Structural Engineer, Vol. 51, No. 8, August, 1973, pp. 285-301.

92. Brockenbrough, R.L., and Johnston, B.G. USS Steel Design Manual, 1968.

TABLE 1

COLUMN DESIGNATION

No.	Column Designation	Length in	1/d	Eccentricity along X in	Eccentricity along Y in
1	A	72	7.2	2.50	1.45
2	B	72	7.2	5.00	2.90
3	C	72	7.2	7.50	4.35
4	D	144	14.4	2.50	1.45
5	E	144	14.4	5.00	2.90
6	F	144	14.4	7.50	4.35
7	G	288	28.8	2.50	1.45
8	H	288	28.8	5.00	2.90
9	I	288	28.8	7.50	4.35

TABLE 2

RESULTS OF TESTS ON CUBE SPECIMENS

No.	CRUSHING LOAD FOR CUBES (tonf)							Cube Strength lbf/in^2	Column Designation
	1	2	3	4	5	6	Average		
1	131.0	142.0	136.0	147.0	140.0	131.0	137.83	8576	B
2	122.5	147.0	151.0	152.5	147.0	144.0	143.95	8957	A,C,E
3	151.0	152.0	155.0	158.0	151.0	148.0	152.50	9489	D,F
4	124.0	132.0	131.0	130.0	142.0	135.0	132.33	8234	G
5	135.0	149.0	148.0	145.5	140.0	148.0	144.25	8975	H
6	151.0	153.0	161.0	166.5	149.5	159.5	156.83	9758	I

TABLE 3

RESULTS OF TESTS ON COUPONS FROM H-SECTION

No.	Coupon Size in x in	Coupon From -	Yield Load lb	Ultimate Load lb	Young's Modulus 10^6 x lbf/in^2	Yield Stress lbf/in^2
1	1.000 x 0.250	Flange	11800	18000	30.14	47200
2	1.000 x 0.250	Flange	11850	18050	30.22	47400
3	1.000 x 0.250	Flange	11550	17750	30.04	46200
4	1.000 x 0.250	Flange	11750	18050	30.14	47000
5	1.000 x 0.250	Flange	11100	17250	29.84	44400
6	1.000 x 0.250	Flange	11000	17350	29.93	44000
7	1.000 x 0.235	Web	10150	15750	28.00	43190
8	1.000 x 0.235	Web	10200	16200	28.24	43400
9	1.000 x 0.250	Flange	11450	-	29.75	45800
10	1.000 x 0.235	Web	11200	16350	29.78	47660
11	1.000 x 0.235	Web	11000	16400	29.16	46810
12	1.000 x 0.250	Flange	11400	17600	28.28	45600
13	0.738 x 0.252	Flange	8400	13100	29.79	45170
14	0.738 x 0.252	Flange	8400	13100	29.01	45170
				AVERAGE	29.45	45642

AVERAGE STRAIN = 0.00155

TABLE 4

RESULTS OF TESTS ON REINFORCEMENT BARS

No.	Specimen Diameter in	Yield Load lb	Ultimate Load lb	Yield Stress lbf/in^2	Young's Modulus lbf/in^2
1	0.4946	8350	11900	43460	28.76×10^6
2	0.5020	8650	12250	43700	29.78×10^6
3	0.4883	8800	12050	46990	29.81×10^6
4	0.4905	8350	12250	44190	30.60×10^6
5	0.5010	8550	12200	43370	31.00×10^6
6	0.4924	8850	12250	46470	29.80×10^6
7	0.4279	8240	12100	44070	28.91×10^6
8	0.5010	9050	12700	45900	31.05×10^6
			AVERAGE	44770	29.96×10^6

AVERAGE STRAIN = 0.00149

TABLE 5

RESULTS FROM STUB COLUMN TESTS ON H-SECTION

No.	Area of Cross-Section sq. in	Failure Load tonf	Maximum Strength lbf/in^2	Mode of Failure
1	4.62	85.0	41212.2	Buckling of Flanges
2	4.62	83.0	40242.4	Buckling of Flanges
3	4.62	85.0	41212.2	Buckling of Flanges
4	4.62	83.0	40242.4	Buckling of Flanges
5	4.62	82.0	39757.5	Buckling of Flanges
6	3.524	68.5	43541.4	Overall Yielding, including Strain Hardening

TABLE 6

RESULTS FROM TESTS ON SHORT AXIALLY LOADED COMPOSITE SECTIONS

No.	Column Designation	Column Strength Tons	Steel Contribution Tons	Concrete Contribution Tons	Concrete Strength lbf/in^2	Cube Strength lbf/in^2	Ratio K_1
1	G	375.0	109.822	265.178	6279.4	8234	0.7626
2	D	390.0	109.822	280.178	6634.6	9489	0.6992
3	H	335.0	109.822	225.178	5332.2	8975	0.5941
4	I	256.5	109.822	146.678	3473.3	9758	0.3559
5	I	320.0	109.822	210.178	4977.0	9758	0.5100
						AVERAGE	0.6415

NOTES:

(1) Steel contribution is calculated for a steel area of 4.62 in^2 and a reinforcement area of 0.76 in^2.

(2) Ratio K_1 is defined as concrete strength/cube strength.

(3) In calculating average, result 4 is ignored since the specimen exhibited slipping between concrete and steel - this may have been due to differential loading of steel and concrete.

TABLE 7

SUMMARY OF RESULTS FOR TESTS ON BIAXIALLY LOADED COMPOSITE COLUMNS

No.	Column Designation	Cube Strength lbf/in^2	Failure Load Tons
1	A	8957	126.0
2	B	8576	65.0
3	C	8957	47.5
4	D	9489	93.0
5	E	8957	57.5
6	F	9489	42.0
7	G	8234	67.5
8	H	8975	35.5
9	I	9758	29.5

TABLE 8

UNIAXIAL FAILURE LOADS FOR ENCASED SECTIONS

Column No.	L_{eff} in	e_y in	U_w lbf/in^2	$\sigma_u = \frac{2}{3}U_w$ lbf/in^2	$\bar{P}$ theory (Basu) tonf	$\bar{P}$ theory (Program COLUMPC) tonf
AE1	28	1.0	3100	2167	74.3	75.1
AE2	46	1.0	3950	2633	75.4	76.2
AE3	82	1.0	3800	2533	60.1	60.2
AE4	118	1.0	4250	2833	49.1	48.3
FE3	180	1.0	3150	2100	242.9	241.3
FE4	180	2.0	2950	1967	172.2	171.0

TABLE 9

UNIAXIAL FAILURE LOADS FOR RECTANGULAR FILLED TUBES

Length	e/D	Ultimate Load (Sen and Chapman)	Ultimate Load (COLUMPC)
120	0.0	33.2	33.1
120	0.1	26.8	26.7
120	0.2	23.0	22.9
Column Squash Load		71.6	71.6

TABLE 10

EFFECT OF THE ORIENTATION OF THE LACK OF INITIAL STRAIGHTNESS

Orientation of Initial Imperfection	Failure Load P/P_u (Program COLUMAS)
1. Along Major Axis	0.83525
2. Along 45° Axis	0.81610
3. Along Minor Axis	0.80219

TABLE 11

BIAXIAL FAILURE LOADS OBTAINED FROM THE COMPUTER PROGRAM COLUMPC

Column	Case I Without imperfect-ions tonf	Case II Residual stresses only tonf	Case III Lack of straightness of L/1000 tonf	Case IV Residual stresses with lack of straightness of L/1000		Case V All inclusive lack of straightness of $0.0006\ l^2/D$		Test failure load tonf
				tonf	P_{xy}/P_{test}	tonf	P_{xy}/P_{test}	
A	135.3	133.7	132.5	131.0	1.0397	133.3	1.0579	126
B	68.5	68.5	67.8	67.7	1.0415	68.0	1.0462	65
C	45.8	45.7	45.5	45.4	0.9558	45.5	0.9579	47.5
D	107.6	105.7	103.1	102.0	1.0968	101.6	1.0925	93
E	56.6	57.6	55.3	56.0	0.9739	54.8	0.9530	57.5
F	40.0	40.2	39.4	39.6	0.9429	39.2	0.9333	42
G	53.3	53.3	50.2	50.2	0.7493	44.8	0.6687	67
H	35.5	35.9	34.3	34.8	0.9803	32.1	0.9042	35.5
I	27.4	28.3	26.8	27.6	0.9356	24.3	0.8237	29.5

TABLE 12

EFFECT OF PART-COSINE WAVE ASSUMPTION

Column	Test Load	P_{xy} Part Cosine Wave	P^*_{xy} Exact	% Error $(1 - \frac{P_{xy}}{P^*_{xy}}) \times 100$
A	126	131.0	133.1	1.58
B	65	67.7	69.3	2.31
C	47.5	45.4	45.9	1.09
D	93	102.0	107.3	4.94
E	57.5	56.0	58.2	3.78
F	42	39.6	41.0	3.42
G	67.5	50.2	53.0	5.28
H	35.5	34.8	36.8	5.43
I	29.5	27.6	28.7	3.83
			Average error	3.52

TABLE 13

BIAXIAL FAILURE LOADS USING UNIAXIAL LOADS COMPUTED BY APPROXIMATE EXPRESSIONS IN THE INTERACTION FORMULA

Column designation	Uniaxial failure load P_x tonf	Uniaxial failure load P_y tonf	Major axis bending axial failure load P_{ax} tonf	Biaxial failure load P_{xy} tonf	Test failure load P_{test} tonf	Ratio P_{xy}/P_{test}
A	149.46	180.91	327.81	109.08	126.0	0.8657
B	75.93	119.90	322.43	54.32	65.0	0.8357
C	50.78	81.15	327.81	34.52	47.5	0.7267
D	99.72	122.48	284.61	68.13	93.0	0.7326
E	59.62	79.32	274.36	38.86	57.5	0.6758
F	43.37	61.02	284.61	27.83	42.0	0.6626
G	61.83	45.33	104.81	34.85	67.0	0.5201
H	44.83	35.72	108.88	24.32	35.5	0.6850
I	35.34	30.17	113.27	19.00	29.5	0.6441

TABLE 14

BIAXIAL FAILURE LOADS USING UNIAXIAL FAILURE LOADS OBTAINED FROM COMPUTER PROGRAM IN THE INTERACTION FORMULA

Column designation	Major axis uniaxially eccentric failure load P_x, tonf	Minor axis uniaxially eccentric failure load P_y, tonf	Major axis bending axial failure load P_{ax}, tonf	Biaxial failure load from formula P_{xy}, tonf	Ratio P_{xy}/P_{test}
A	165.42	202.96	337.50	124.85	0.9909
B	100.52	123.35	331.87	66.48	1.0228
C	65.30	86.18	337.50	41.75	0.8789
D	133.86	150.59	298.18	92.96	0.9996
E	80.19	89.62	286.76	49.65	0.8635
F	53.54	66.49	298.18	32.93	0.7840
G	60.77	53.59	122.45	37.11	0.5498
H	44.16	41.06	129.33	25.47	0.7175
I	34.14	34.96	136.86	19.77	0.6702

TABLE 15

COMPARISON OF EXACT FAILURE LOADS WITH BASU AND SOMMERVILLE'S DESIGN FAILURE LOADS FOR COLUMNS IN BIAXIAL BENDING

β_x	β_y	COLUMAS Failure load P/P_u		Design Failure load P/P_u	Percentage error in design failure load on the basis of	
		S	T		S	T
	1.0	0.16537	-	0.11025	33.33	-
	0.5	0.18075	-	0.12141	32.83	-
1.0	0.0	0.19533	-	0.13293	31.95	-
	-0.5	0.20801	-	0.13293	36.09	-
	-1.0	0.21611	-	0.13293	38.49	-
	1.0	0.18700	-	0.12844	31.32	-
	0.5	0.20270	0.21275	0.14384	29.04	32.39
0.5	0.0	0.21391	0.23985	0.16031	25.06	33.16
	-0.5	0.21889	0.26751	0.16031	26.76	40.07
	-1.0	0.22322	-	0.16031	29.14	-
	1.0	0.20644	-	0.12844	37.78	-
	0.5	0.21644	0.24525	0.14384	33.54	41.35
0.0	0.0	0.22128	0.28973	0.16031	27.55	44.67
	-0.5	0.22564	0.28818	0.16031	28.95	44.37
	-1.0	0.22987	-	0.16031	30.26	-
	1.0	0.21733	-	0.12844	40.90	-
	0.5	0.22311	0.26996	0.14384	35.53	46.72
-0.5	0.0	0.22772	0.32583	0.16031	29.60	50.80
	-0.5	0.23204	0.29913	0.16031	30.91	46.41
	-1.0	0.23643	-	0.16031	32.19	-
	1.0	0.22385	-	0.12844	42.62	-
	0.5	0.22927	-	0.14384	37.26	-
-1.0	0.6	0.23404	-	0.16031	31.50	-
	-0.5	0.23860	-	0.16031	32.81	-
	-1.0	0.24334	-	0.16031	34.12	-

TABLE 16

INFLUENCE OF NUMBER OF SEGMENTS ON THE ACCURACY OF THE COMPUTED FAILURE LOADS

Number of Segments	P/P_u from Program COLUMAS	
	Symmetrical End Eccentricities	Antisymmetrical End Eccentricities
4	0.16444	0.36271
8	0.16521	0.27641
12	0.16533	0.25366
16	0.16537	0.24334
20	0.16538	0.23746

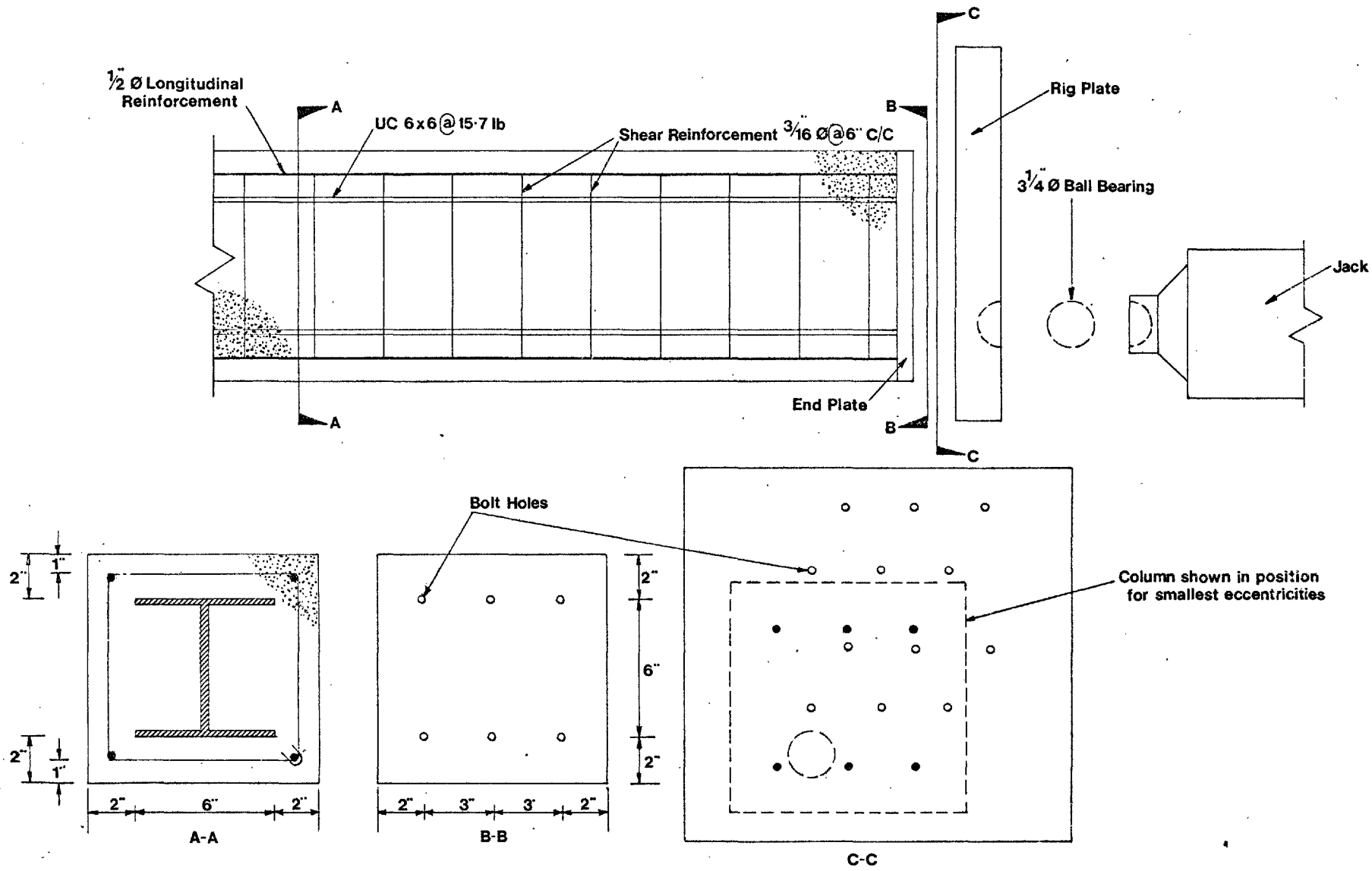

Fig.1 Details of composite column section and loading rig

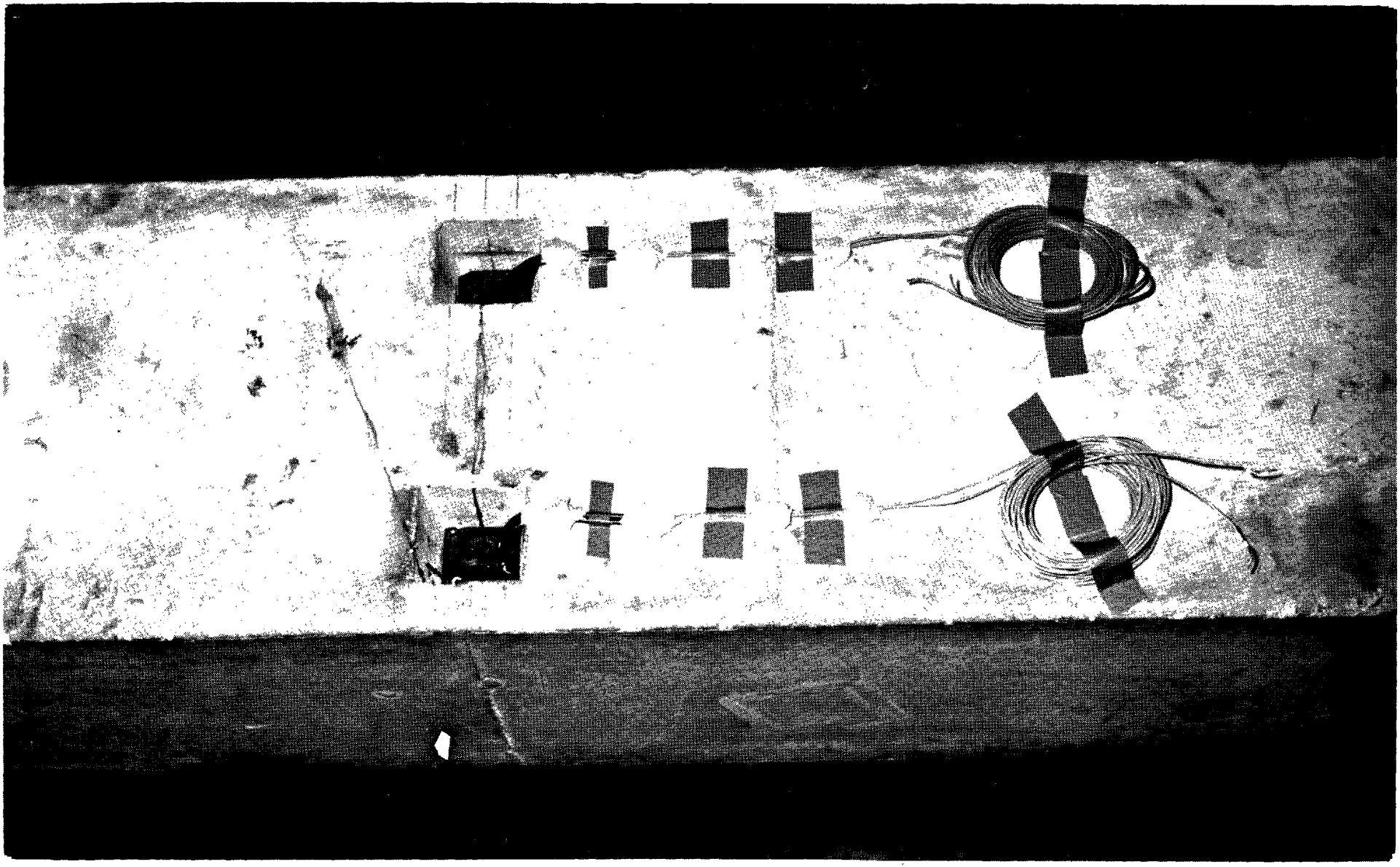

FIG.2.

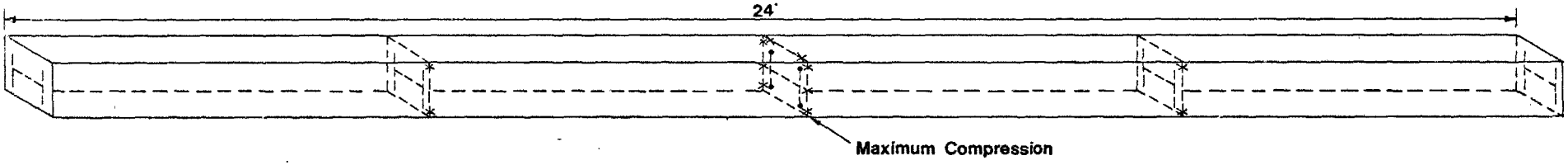

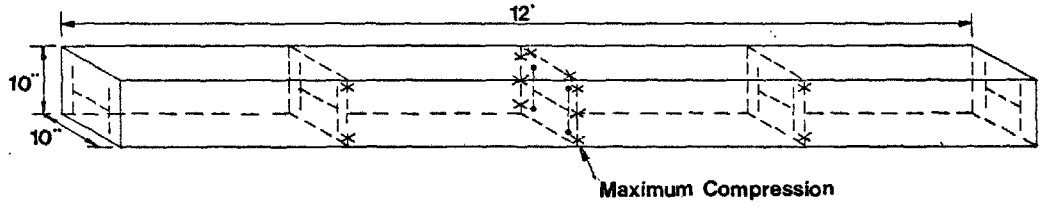

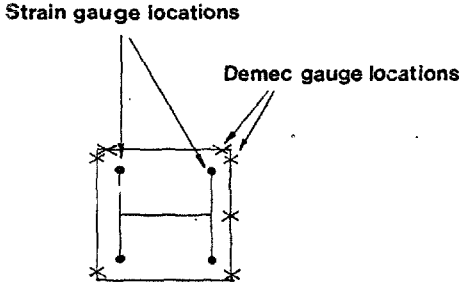

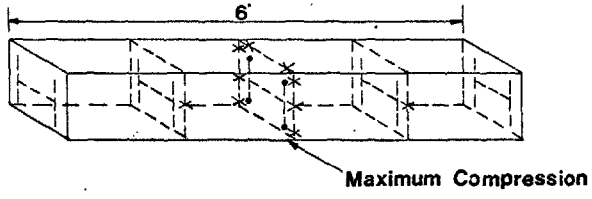

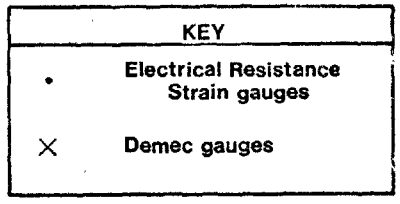

Fig.3 Positioning of gauges for strain measurements

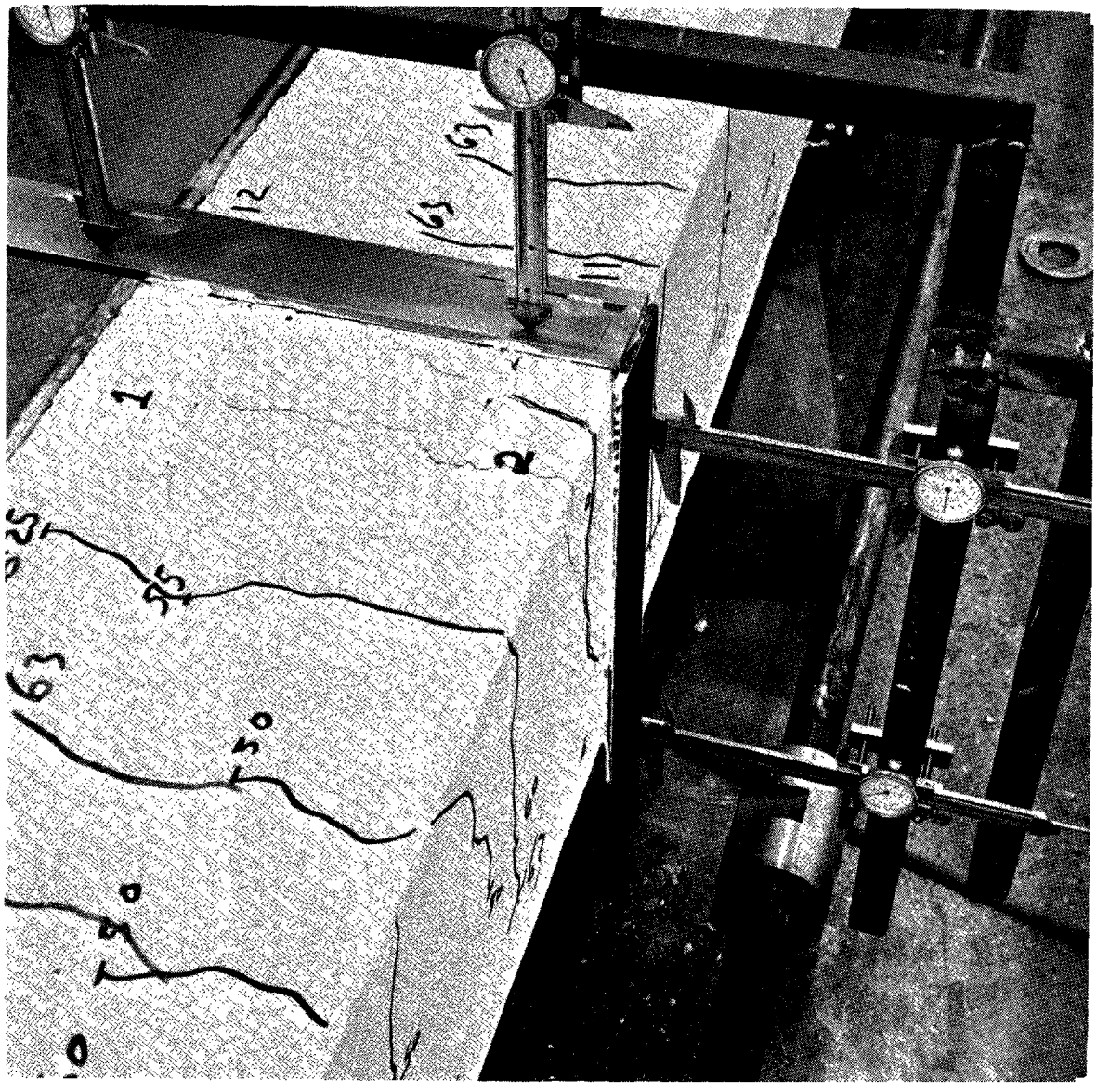

FIG.4.

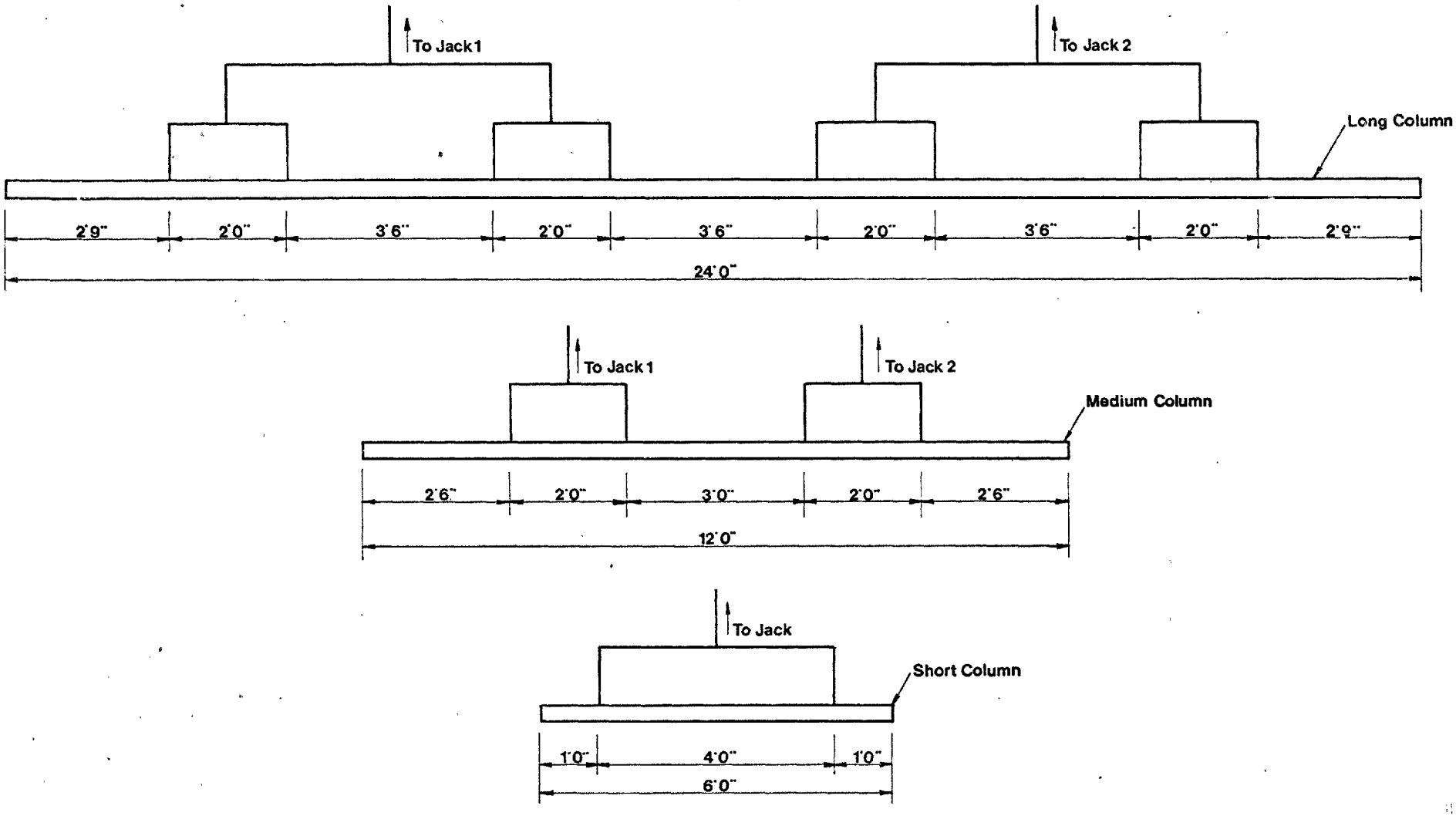

Fig.5 Arrangement of the rig for counterbalancing the column self weight

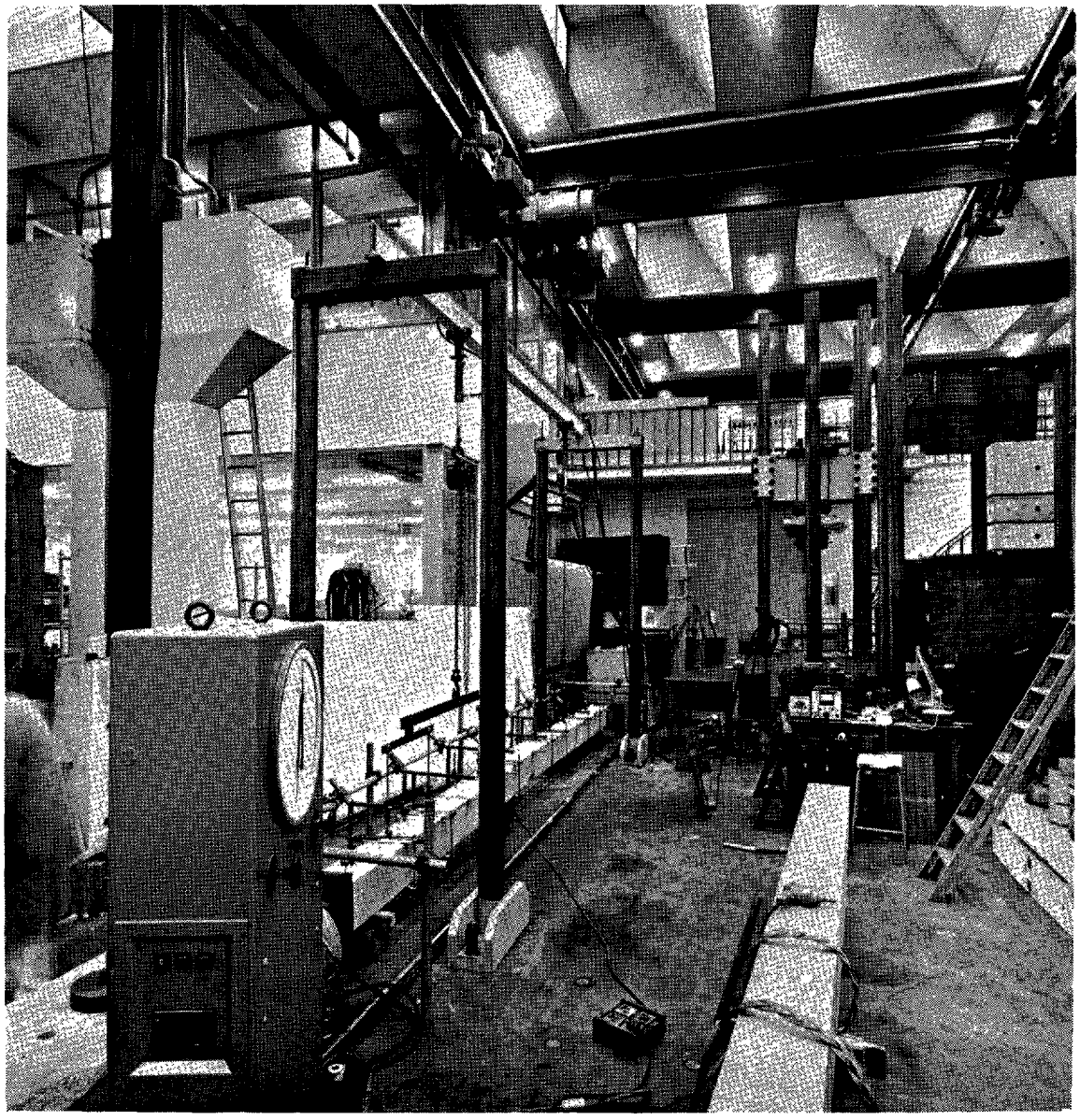

FIG. 6.

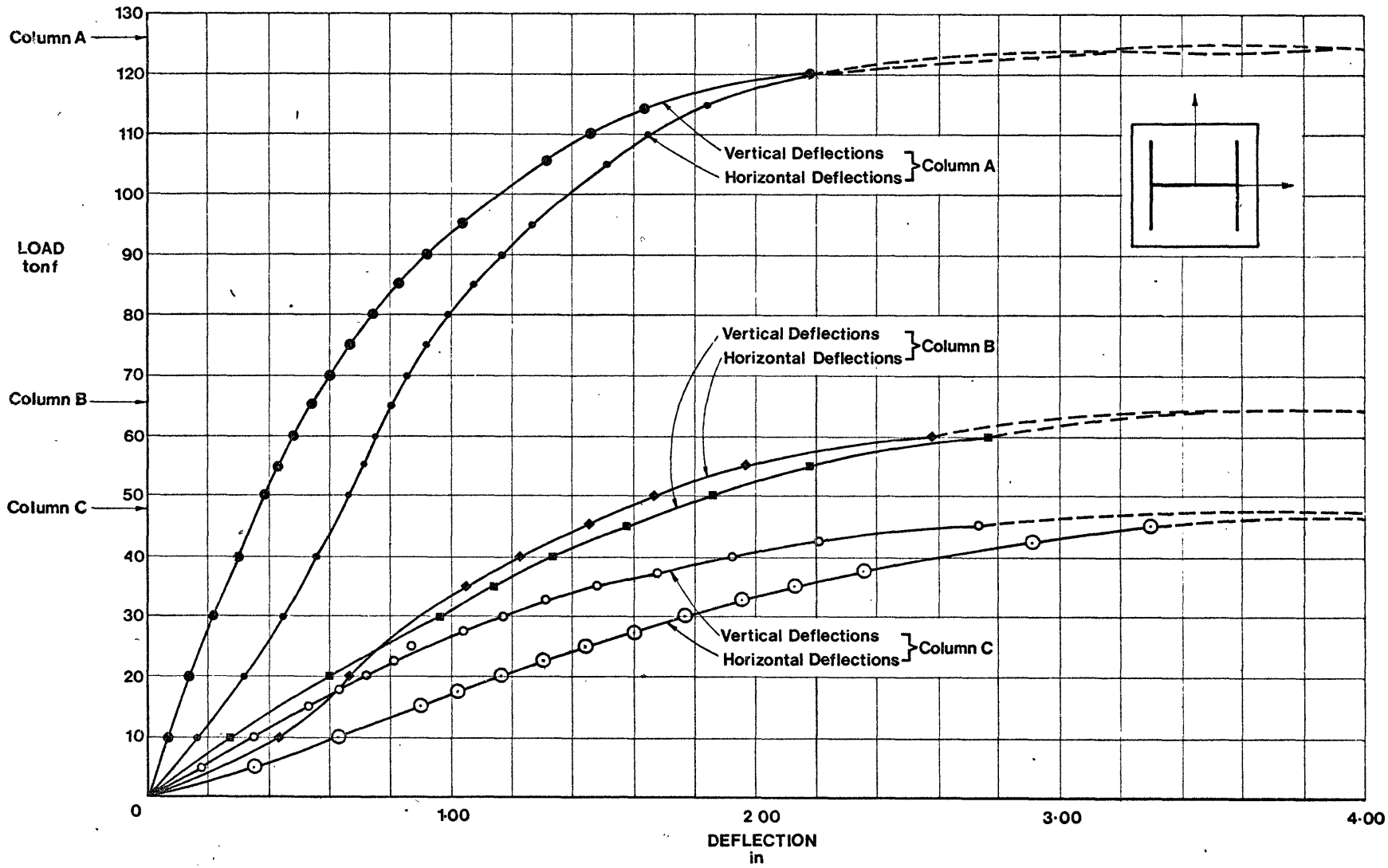

Fig.7 Load-deflection response for the 6 ft long columns

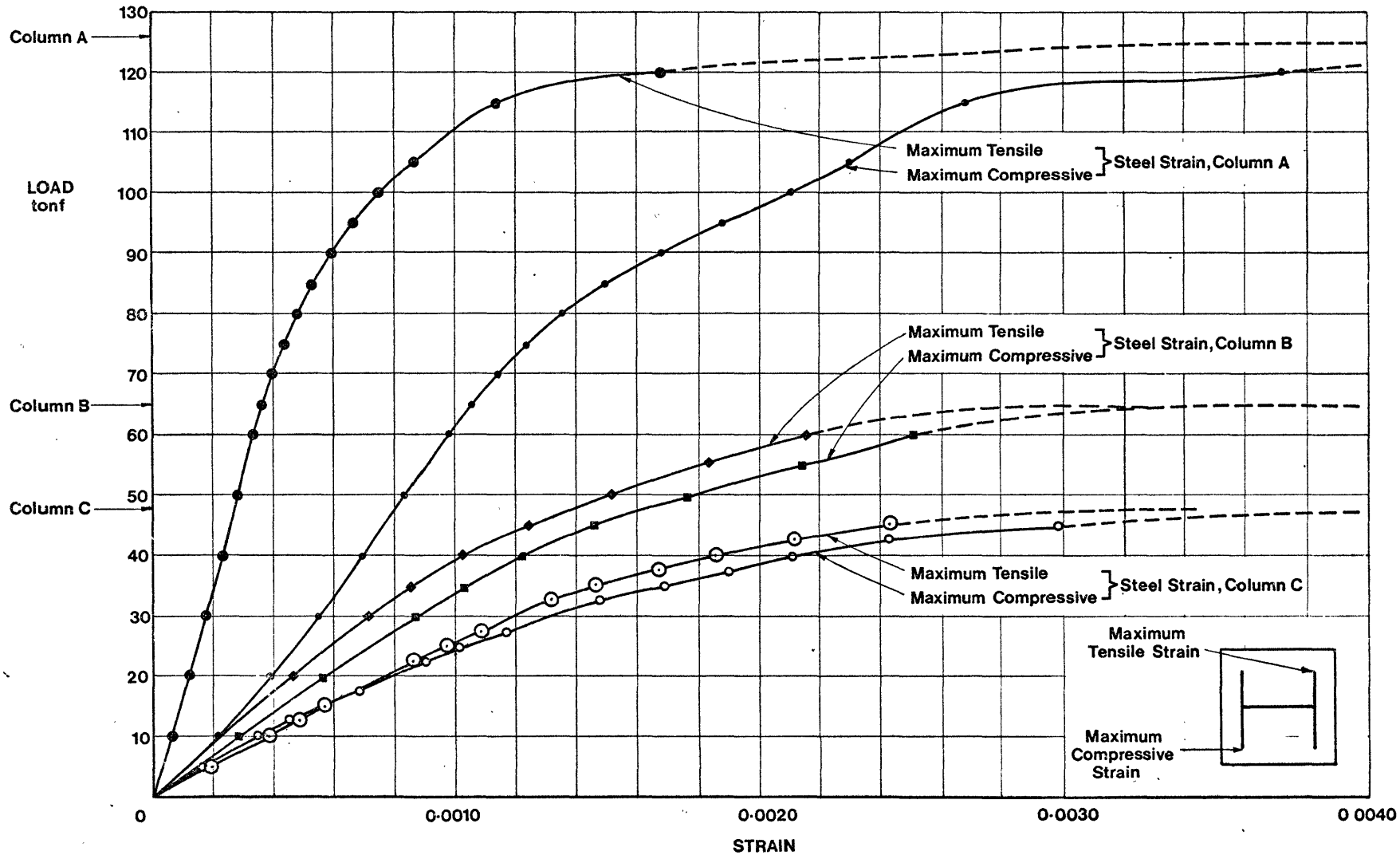

Fig.8 Load-strain response for the 6ft long columns

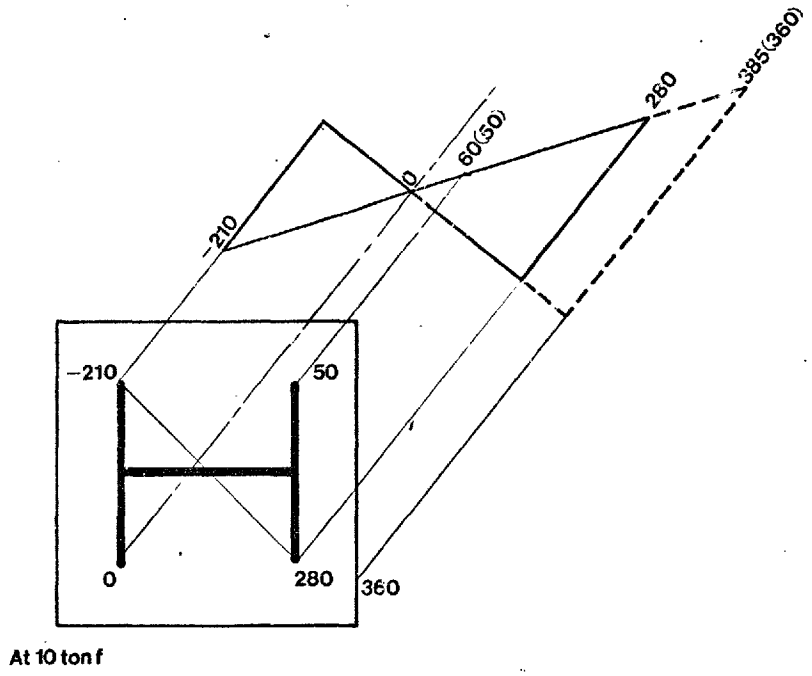

At 10 tonf

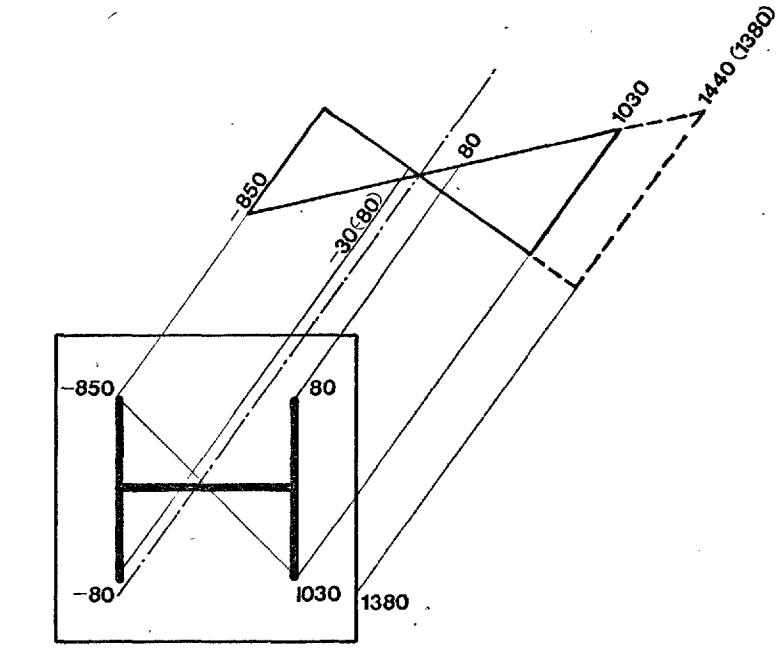

At 35 tonf

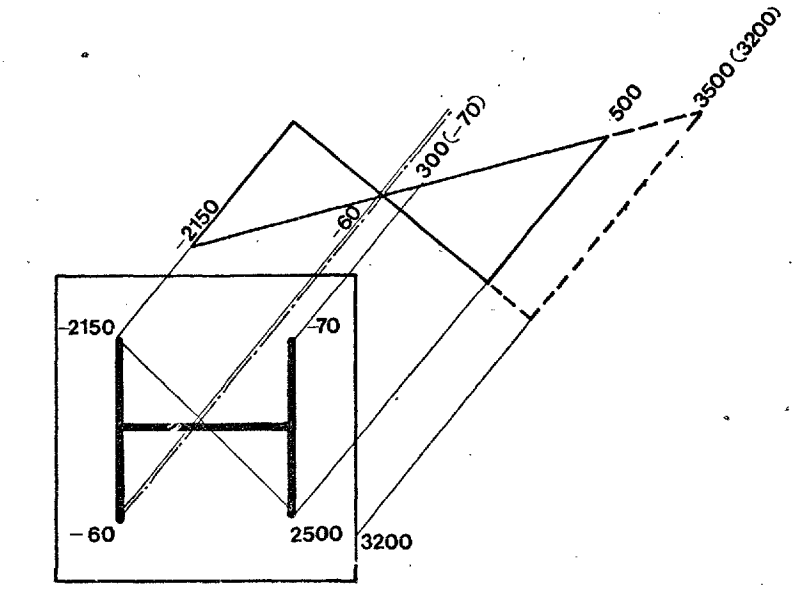

At 60 tonf

Fig.9 Strain distributions across the section for Column B

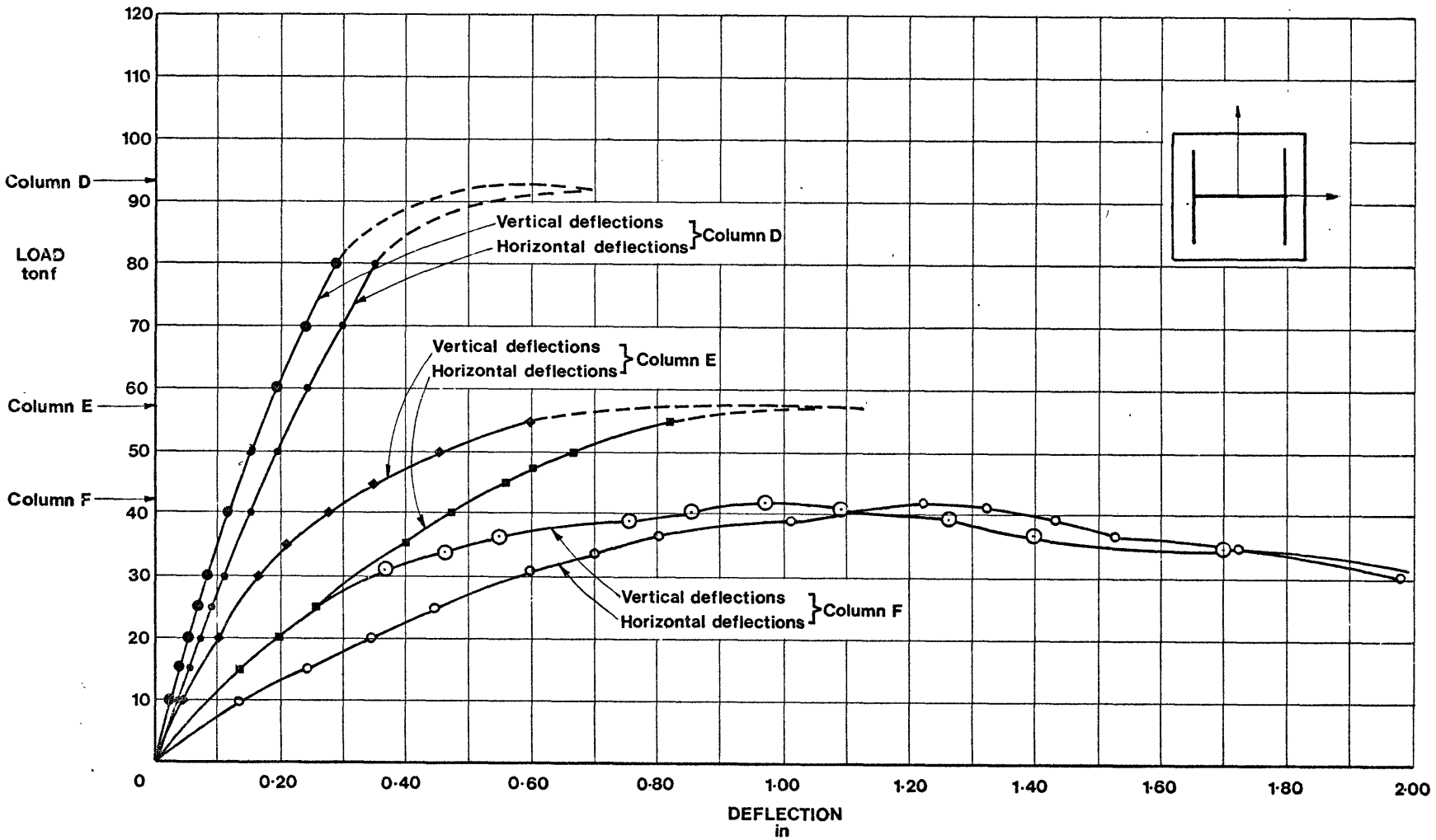

Fig.10 Load-deflection response for the 12 ft long columns

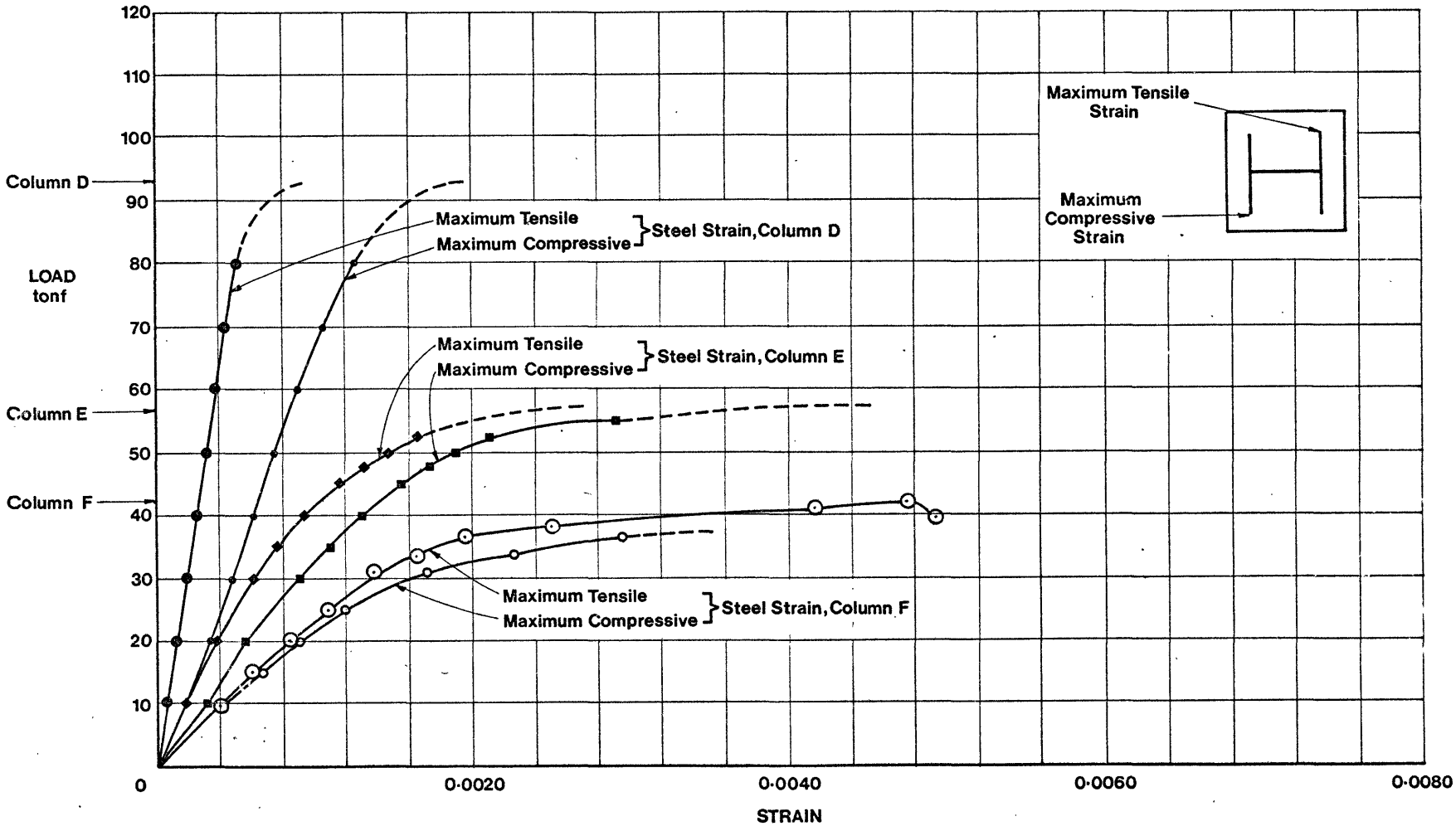

Fig.11 Load - strain response for the 12 ft long columns

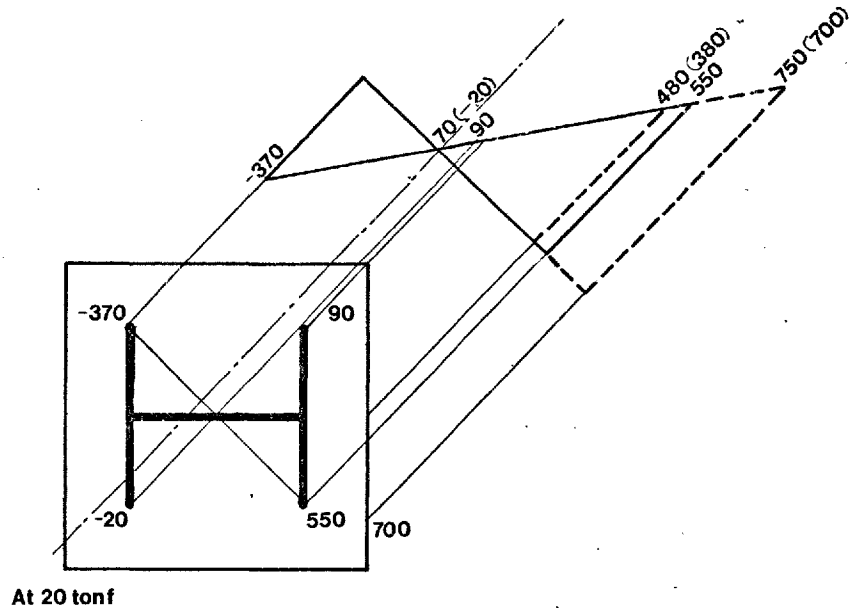

At 20 tonf

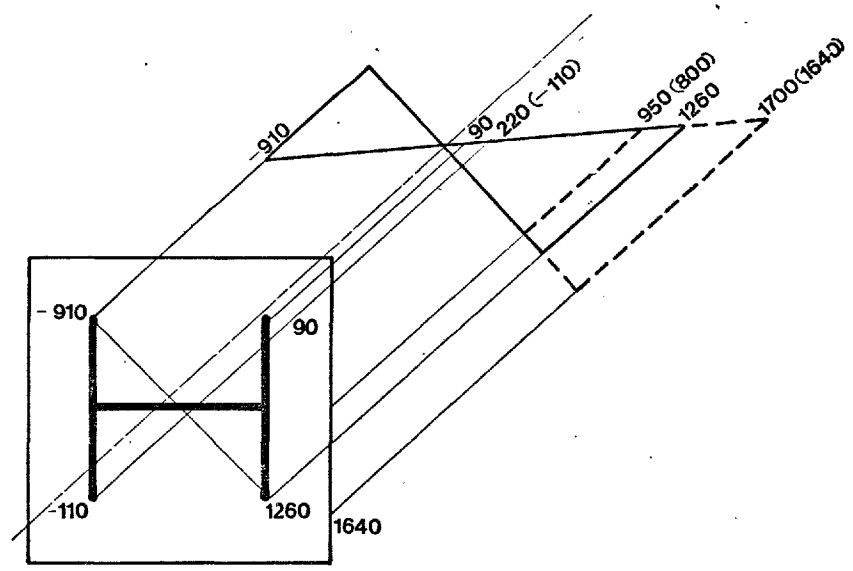

At 40 tonf

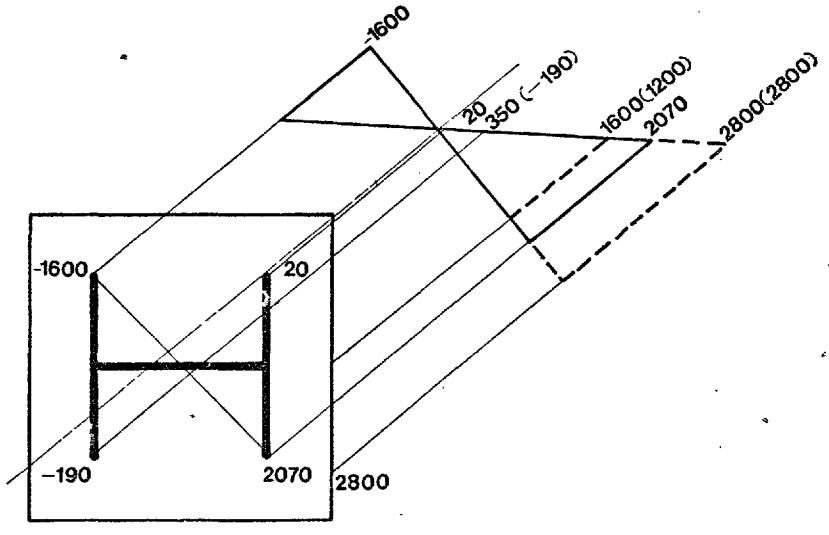

At 52·5 tonf

Fig.12 Strain distributions across the section for Column E

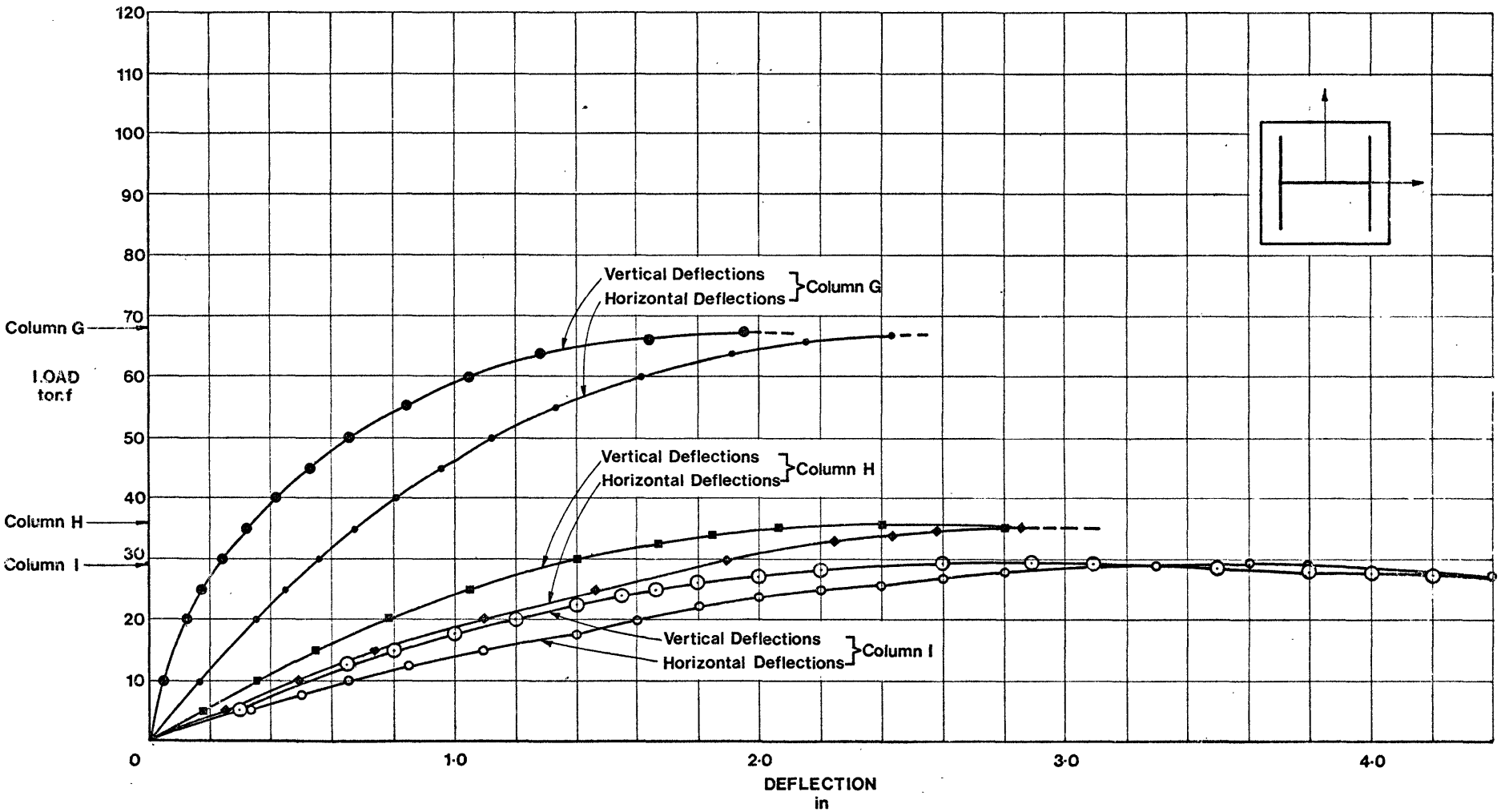

Fig.13 Load-deflection response for the 24 ft long columns

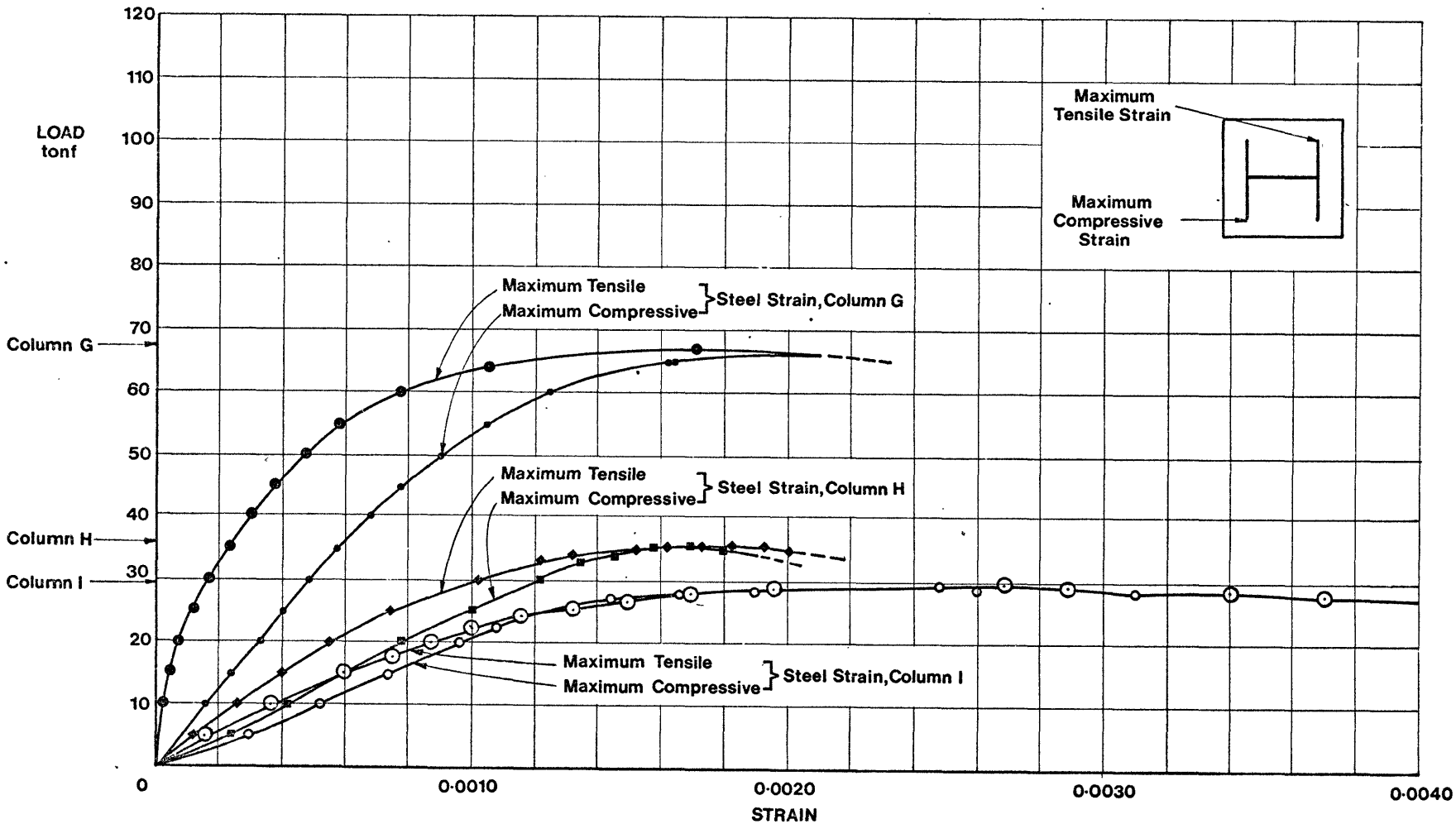

Fig.14 Load - strain response for the 24 ft long columns

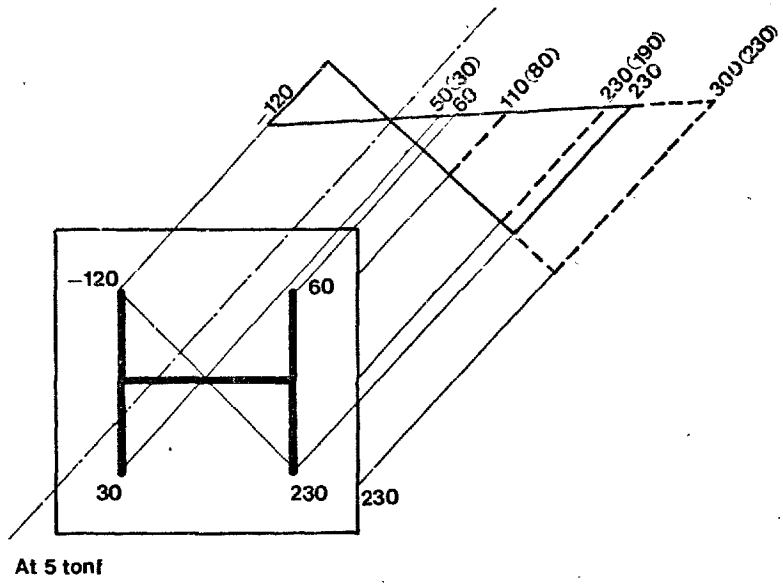

At 5 tonf

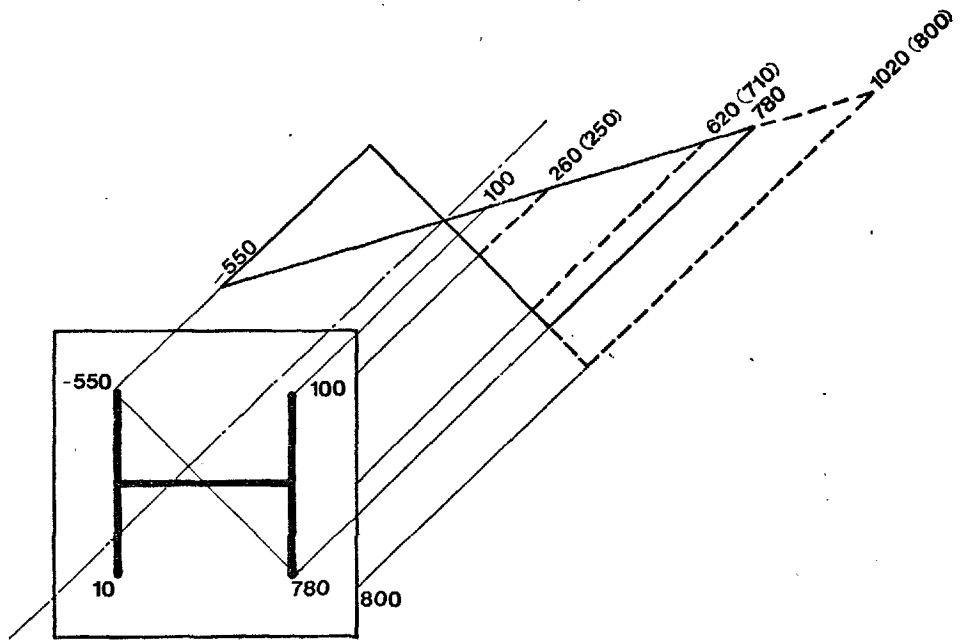

At 20 tonf

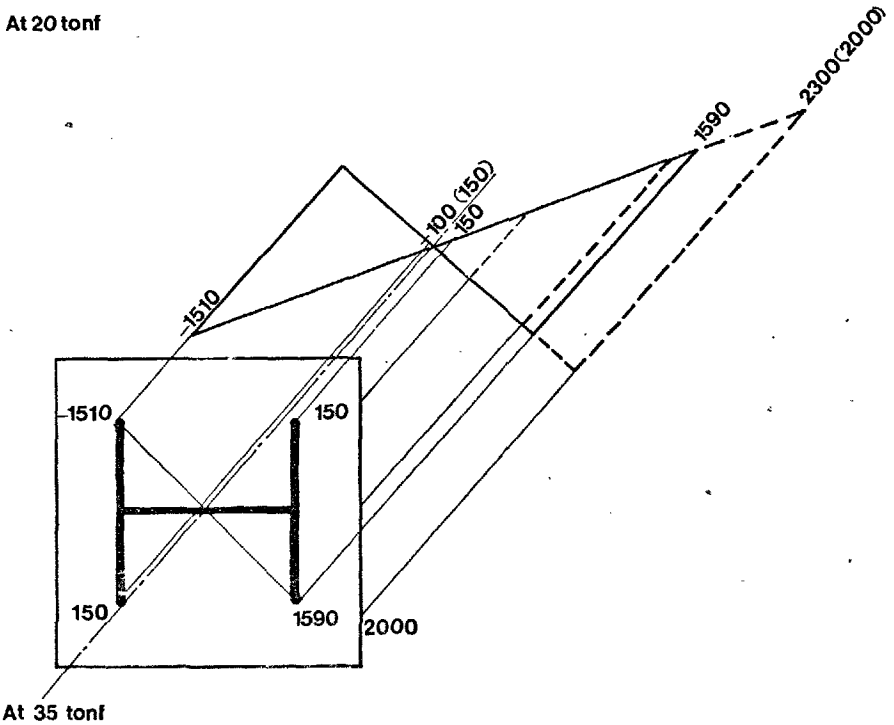

At 35 tonf

Fig.15 Strain distributions across the section for Column H

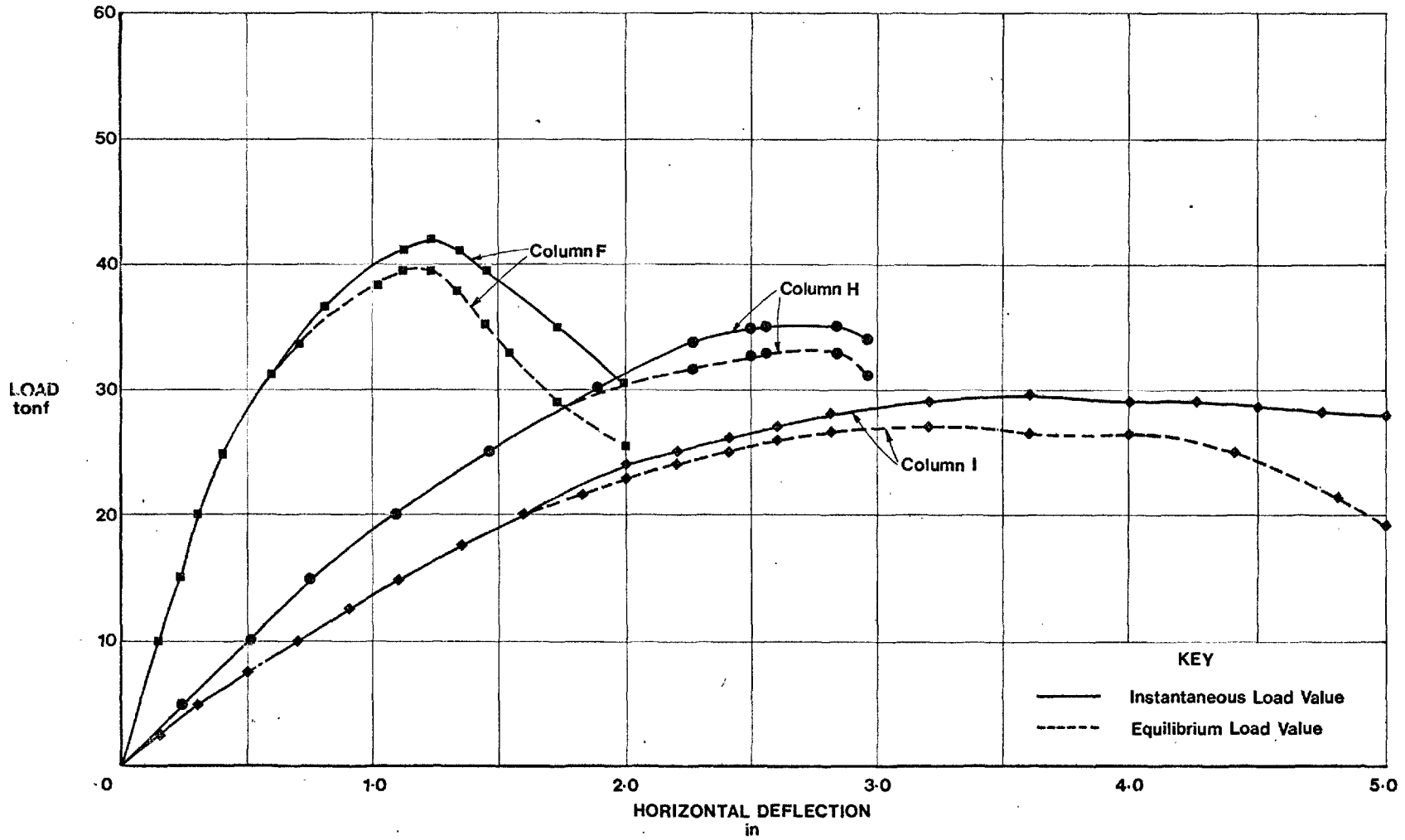

Fig.16 Comparison between instantaneous and equilibrium loads recorded in the loading machine

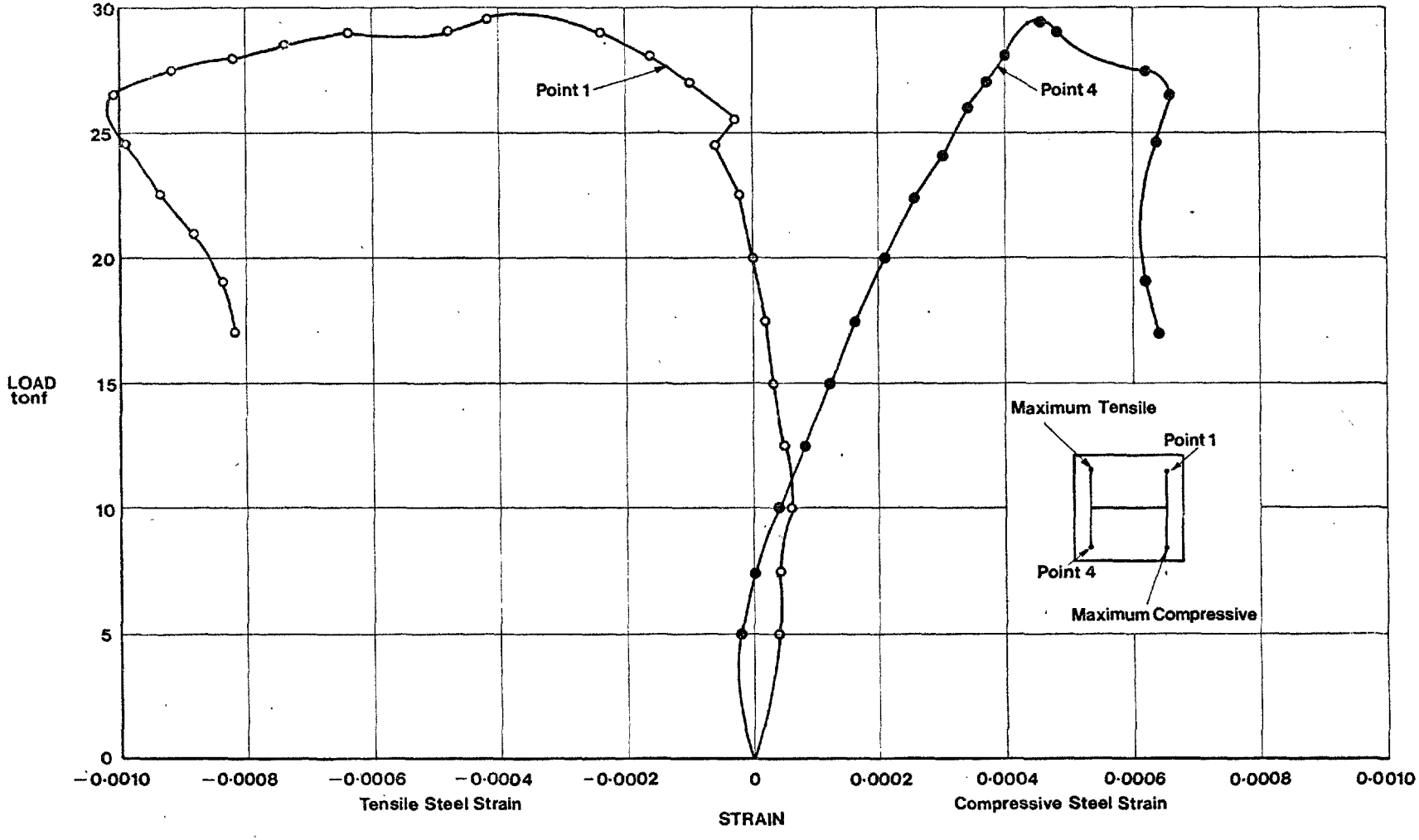

Fig.17 Response of strains near the neutral axis for Column I

FIG. 18.

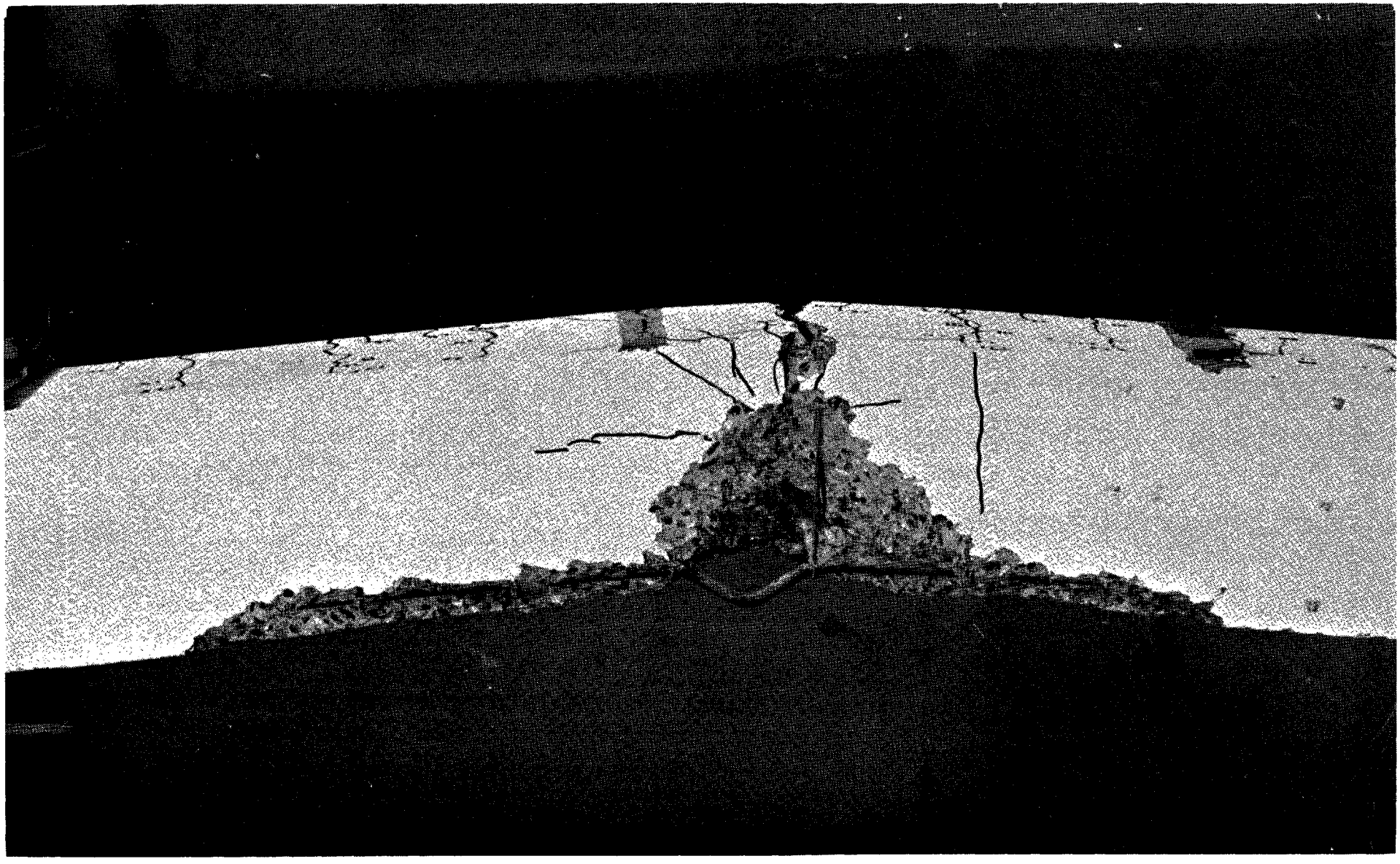

FIG.19.

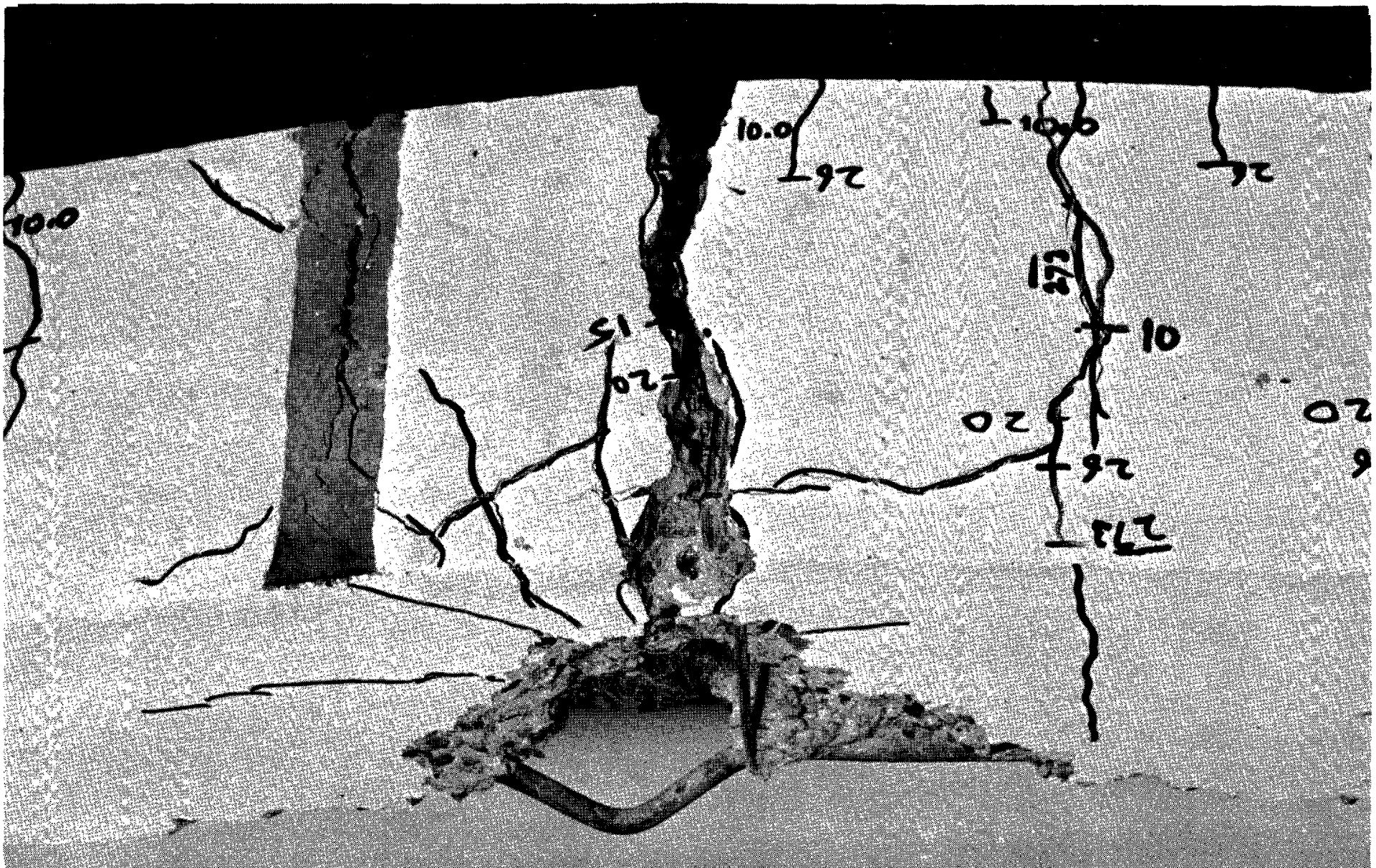

FIG. 20.

FIG. 21.

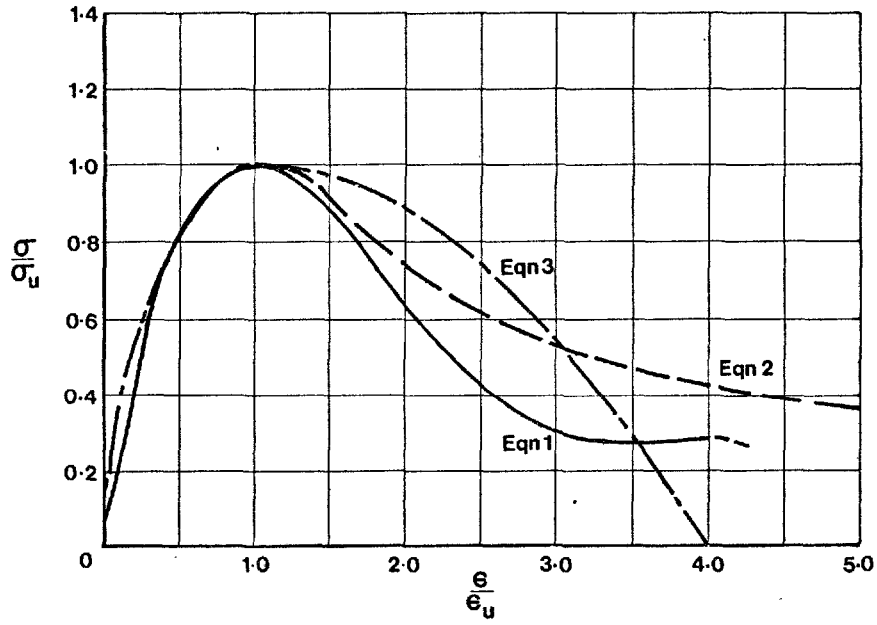

Fig.22 Concrete stress-strain curves

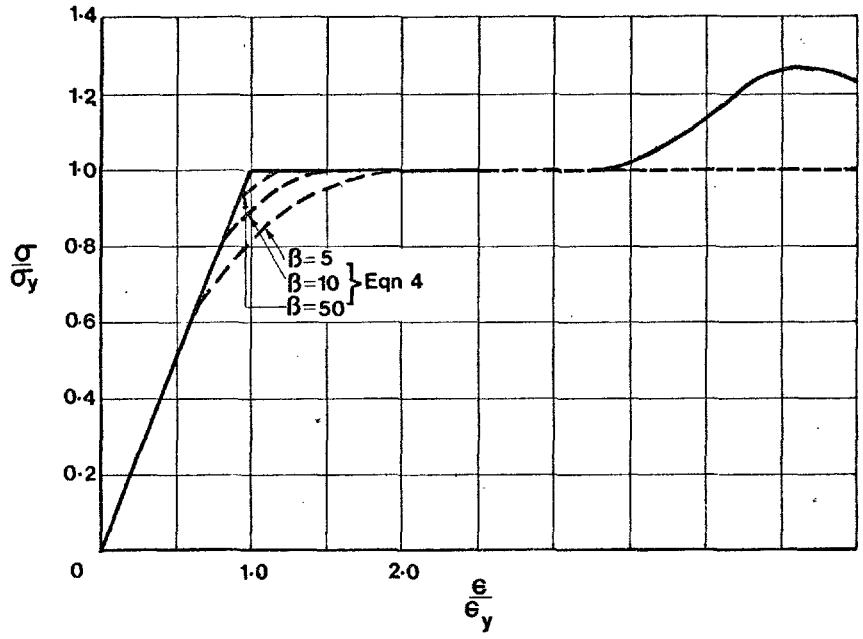

Fig.23 Steel stress-strain curves

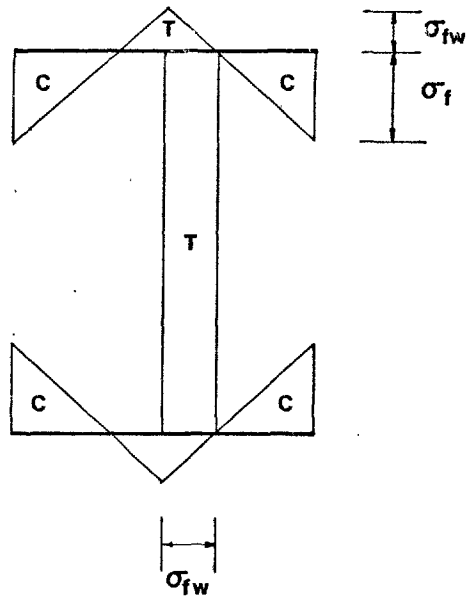

Fig.24 Linear residual stress distribution pattern (Ref.82)

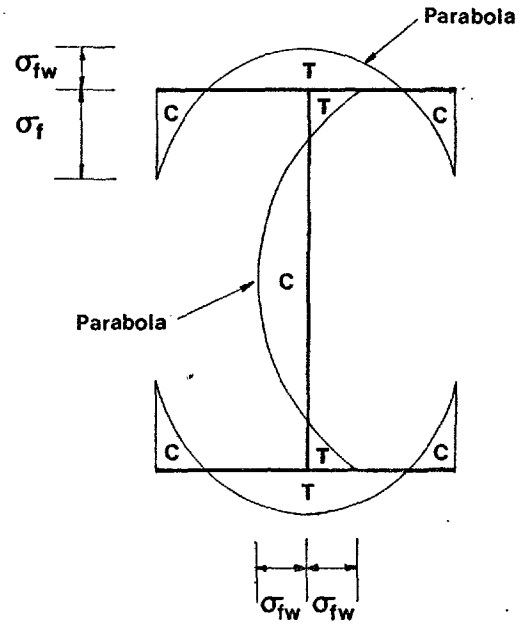

Fig.25 Parabolic residual stress distribution pattern (Ref.83)

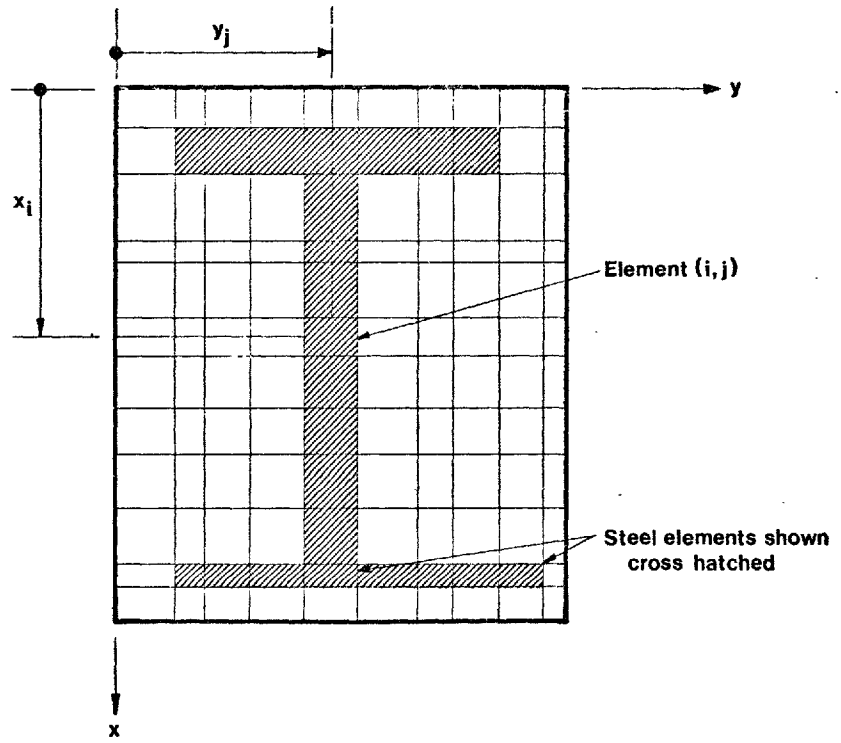

Fig.26 Discretization of the column cross-section

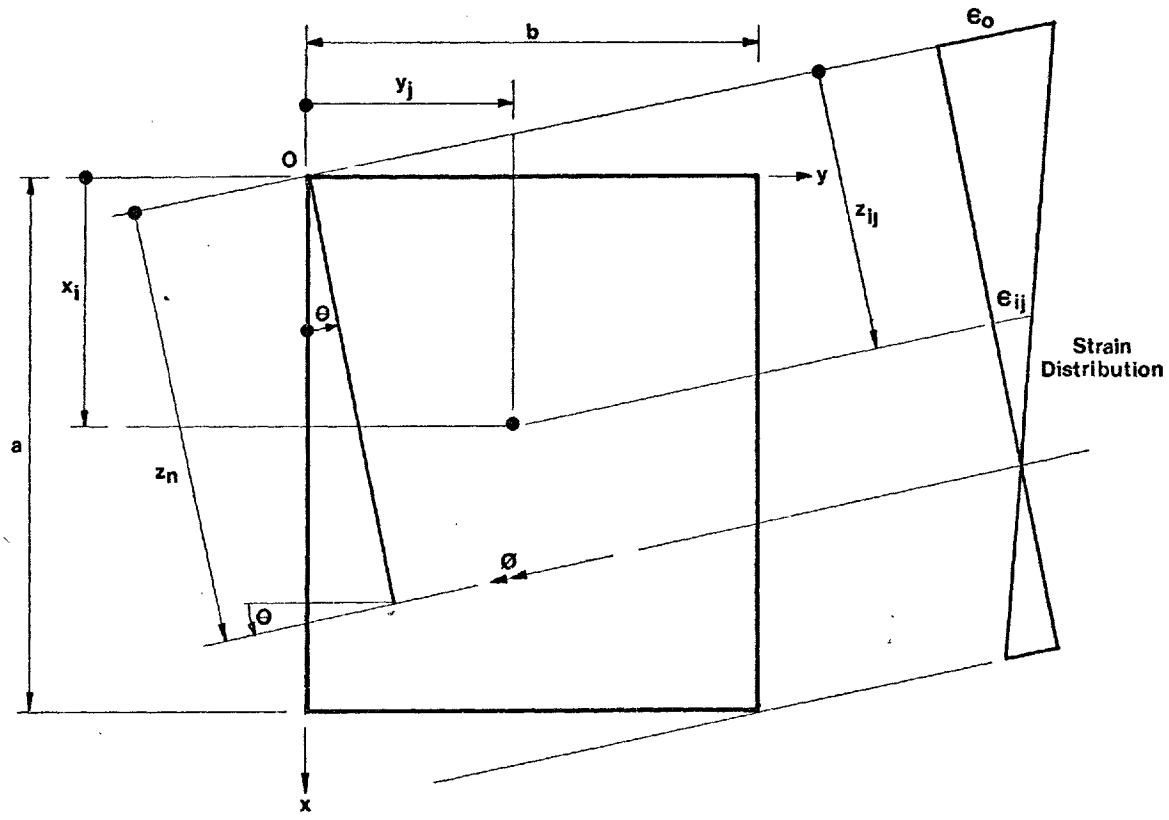

Fig.27 Sign-convention used in the analysis

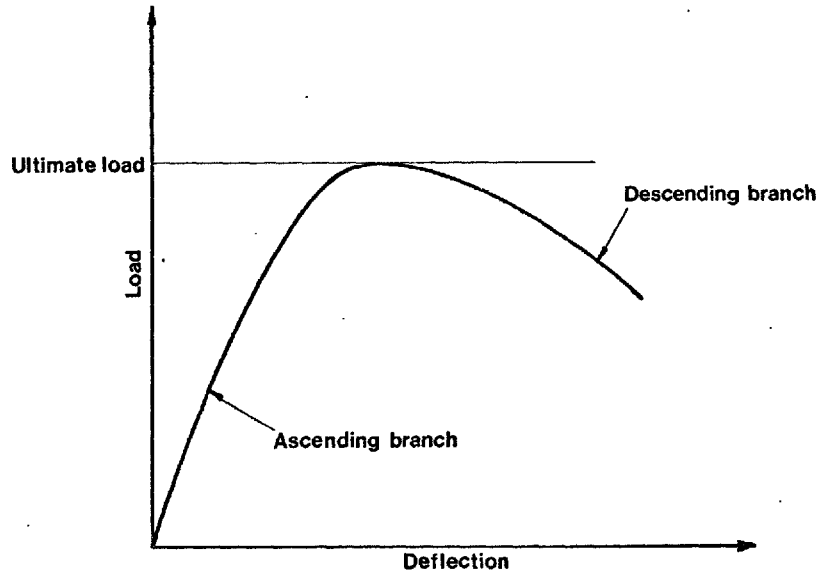

Fig.28 Typical load deflection plot for column in uniaxial bending

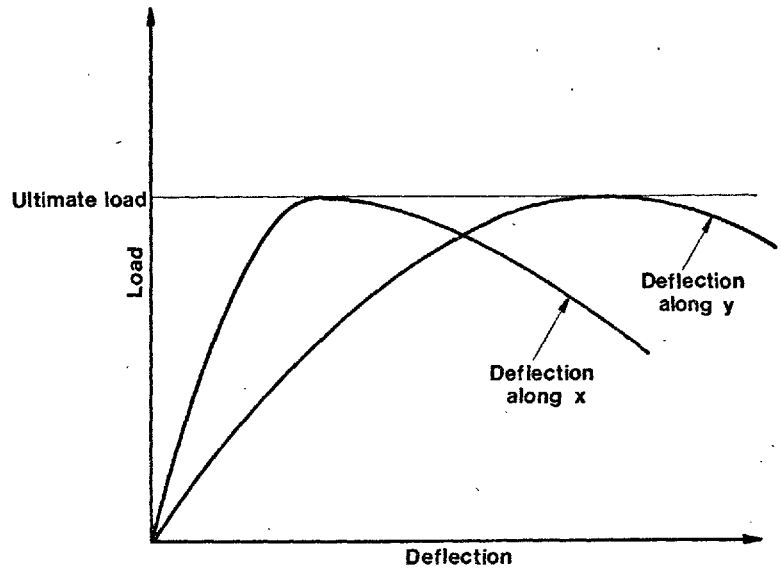

Fig.29 Typical load deflection plots for column in biaxial bending

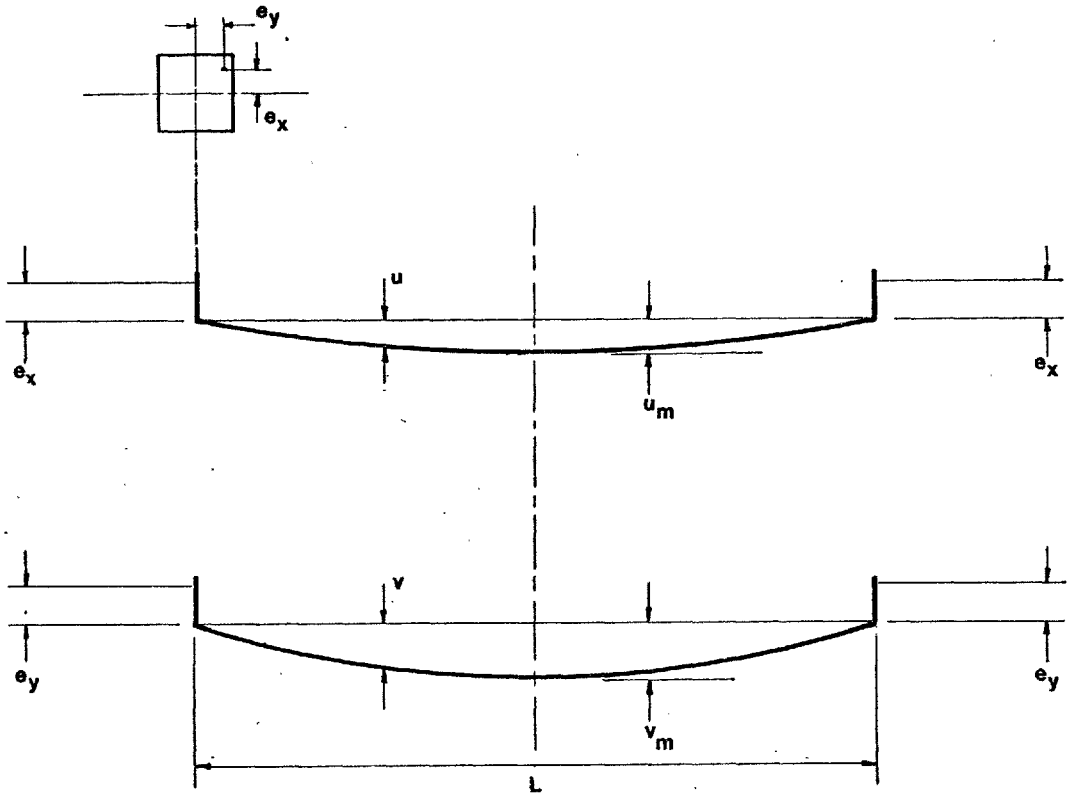

Fig.30 Column deflections under biaxial bending

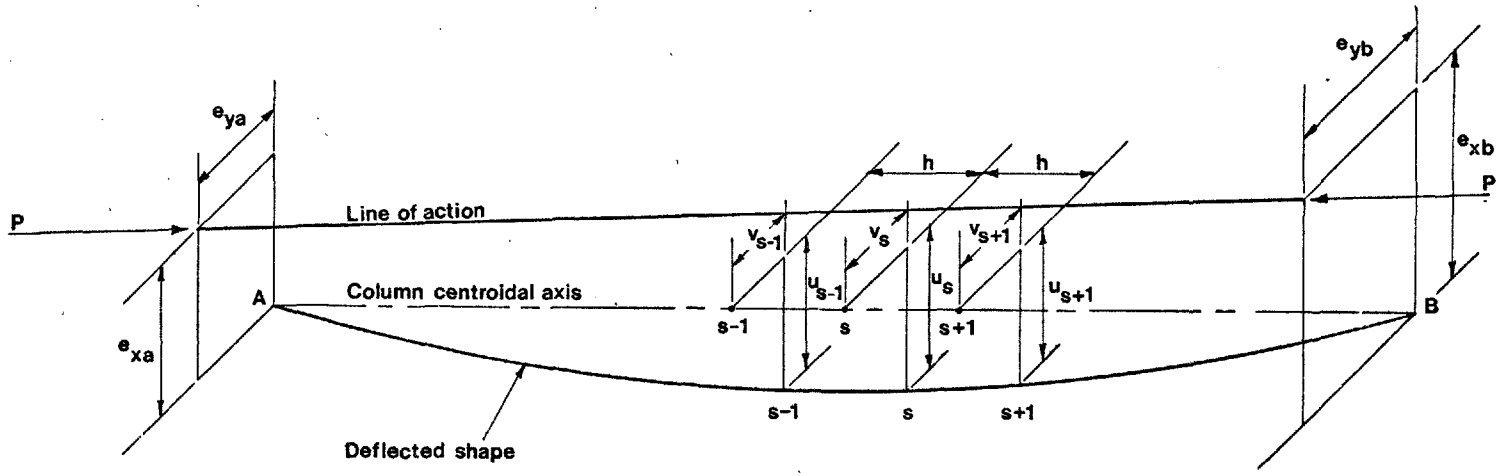

Fig.31 Column deflections under generalised biaxial eccentricities

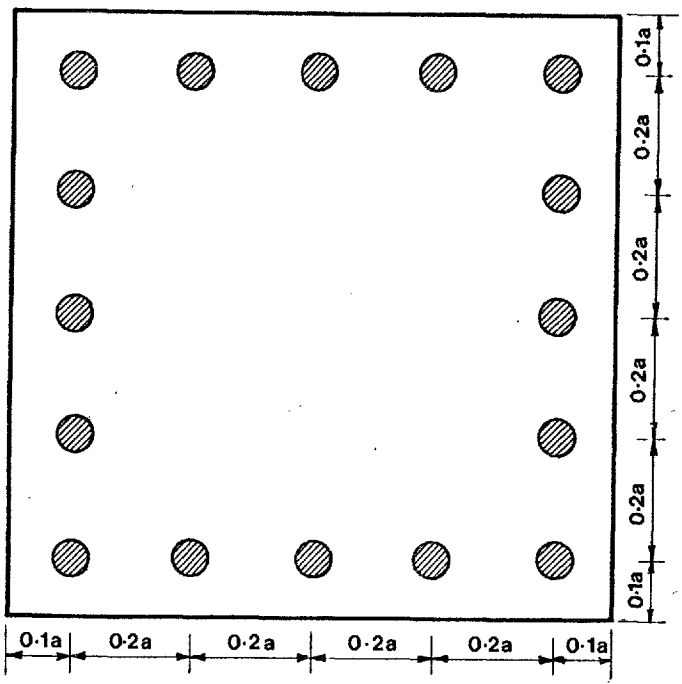

Fig.32 Reinforced concrete section for moment-thrust-curvature example

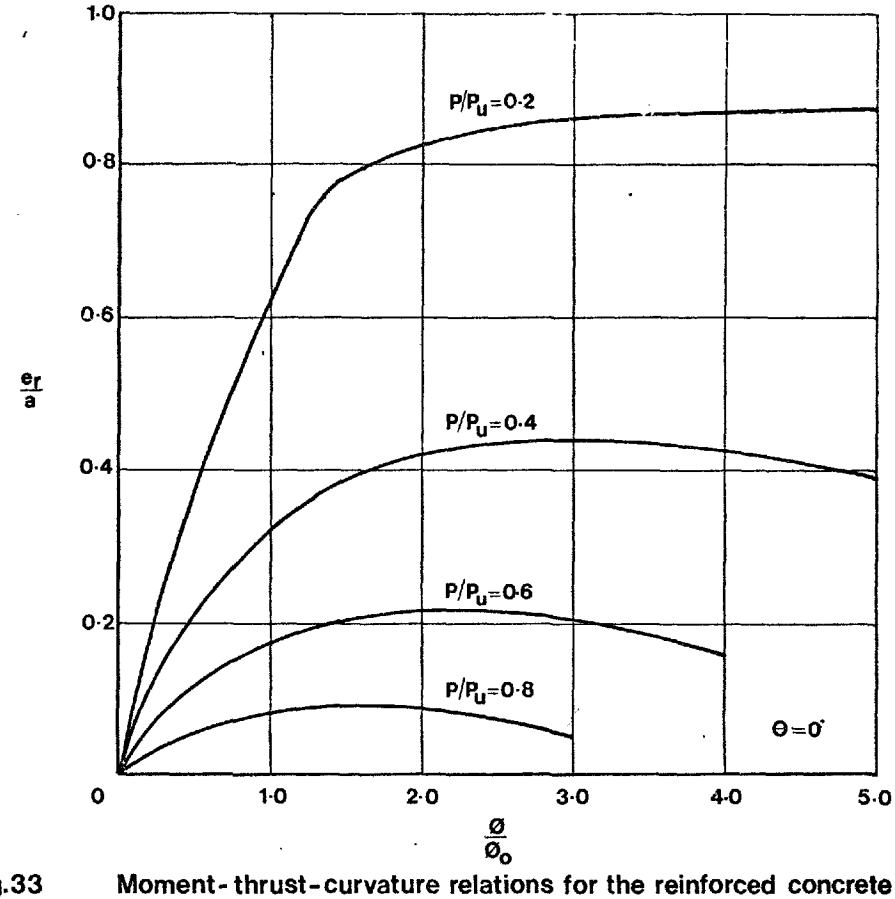

Fig.33 Moment-thrust-curvature relations for the reinforced concrete section of Fig.32 with Θ=0°

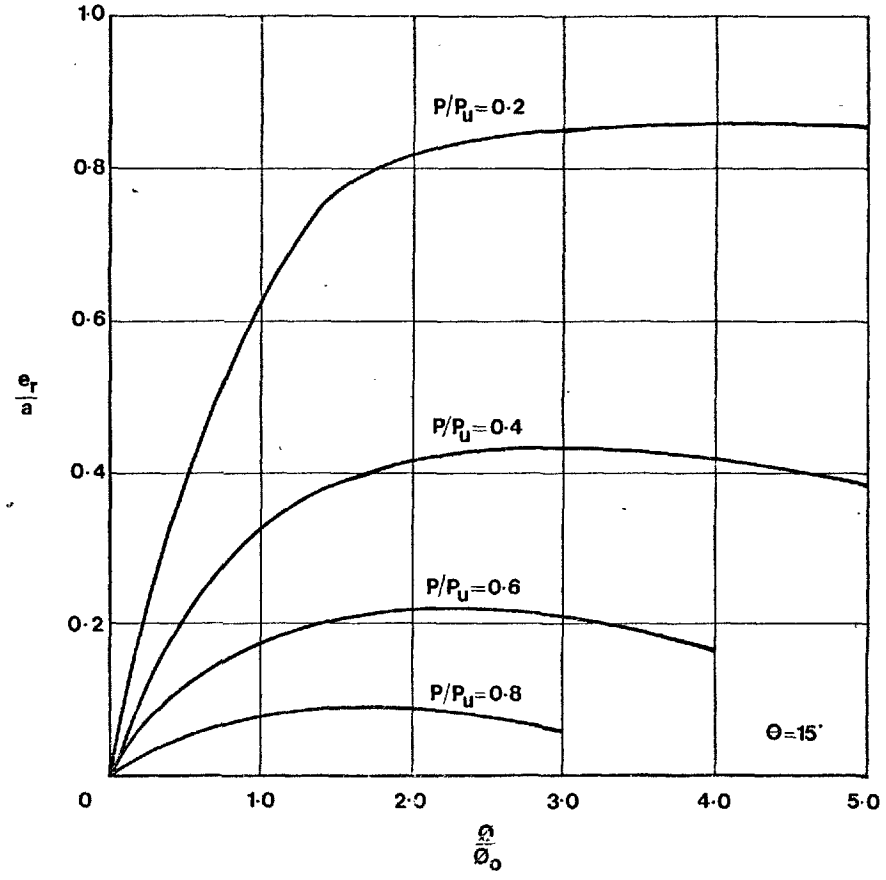

Fig.34 Moment-thrust-curvature relations for the reinforced concrete section of Fig.32 with Θ=15°

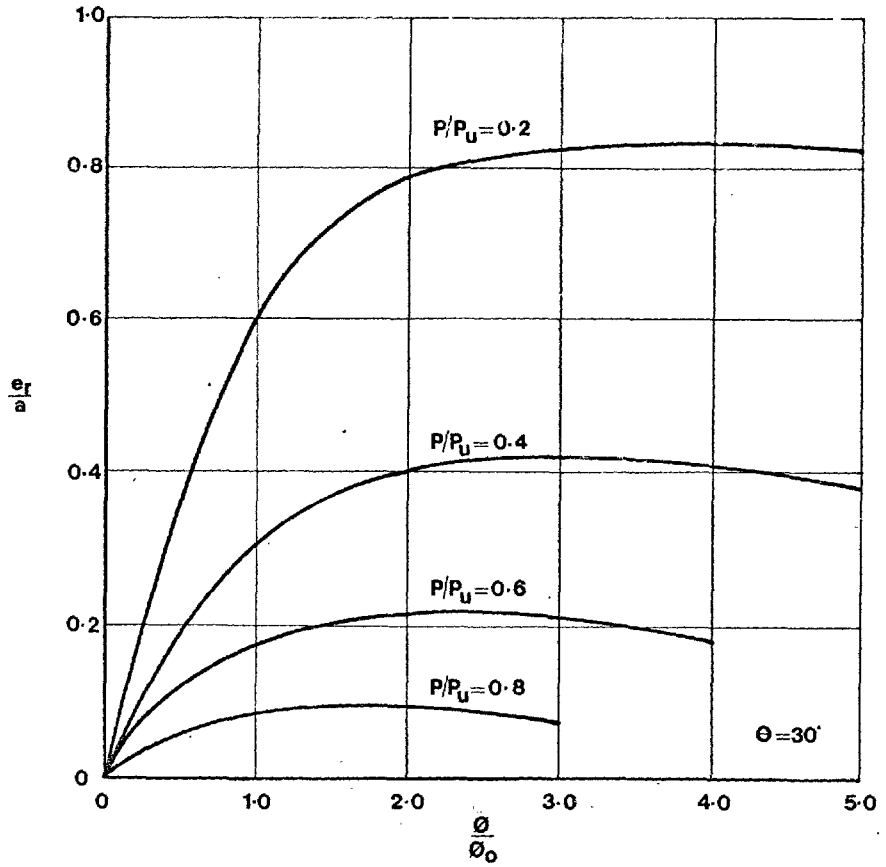

Fig.35 Moment-thrust-curvature relations for the reinforced concrete section of Fig.32 with Θ=30°

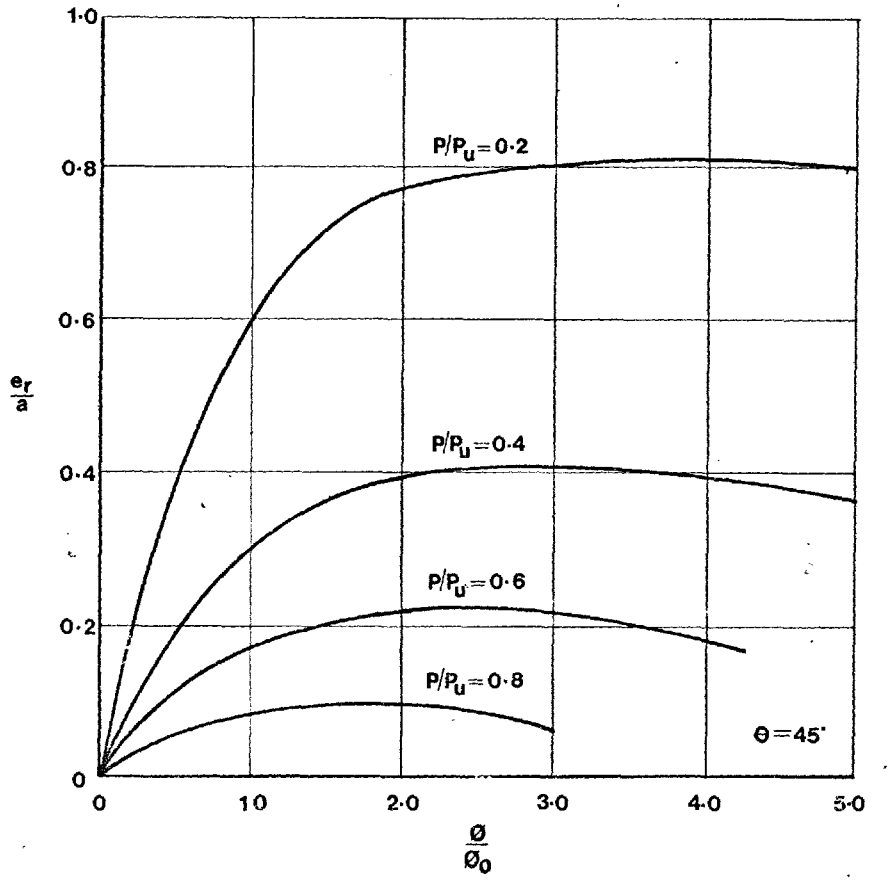

Fig.36 Moment-thrust-curvature relations for the reinforced concrete section of Fig.32 with Θ=45°

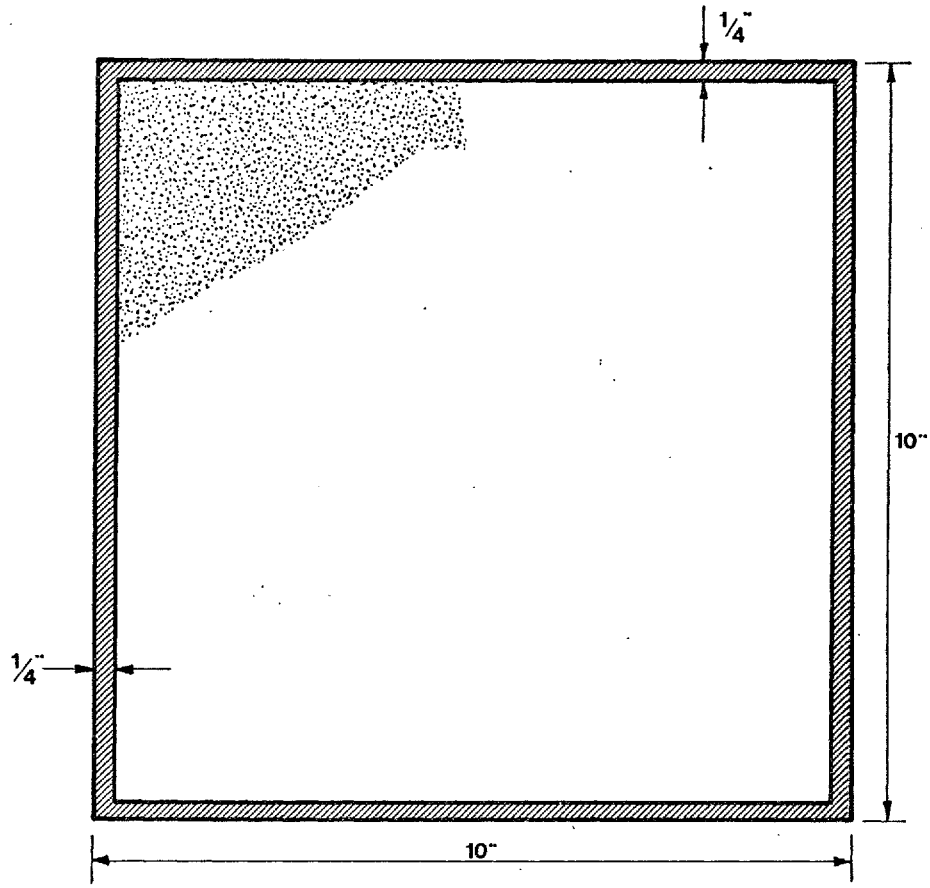

Fig.37 Concrete-filled steel tube section for moment-thrust-curvature example

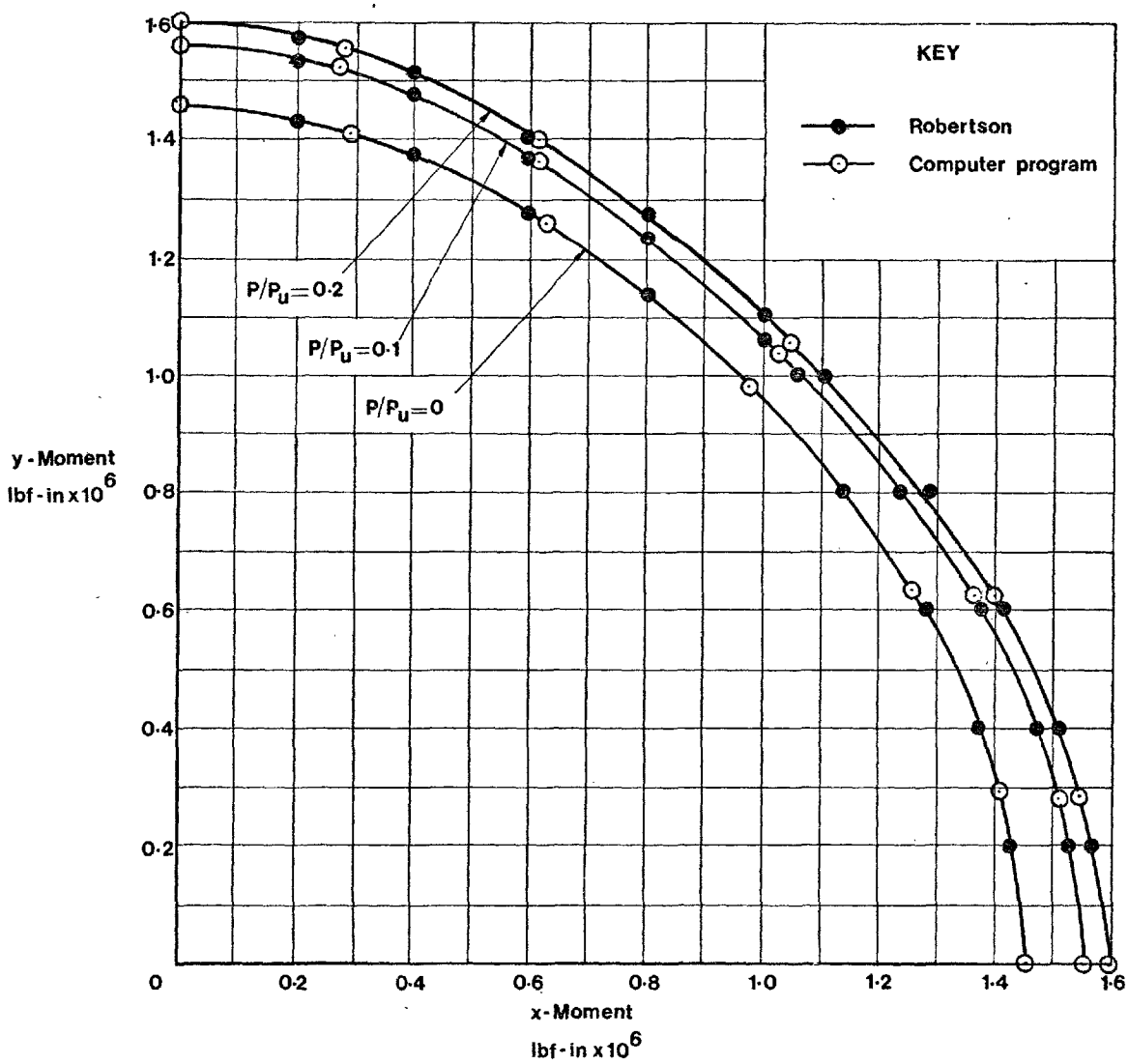

Fig.38 Moment - thrust interaction curves for concrete - filled tube of Fig.37, for P/P_u values 0, 0·1 and 0·2

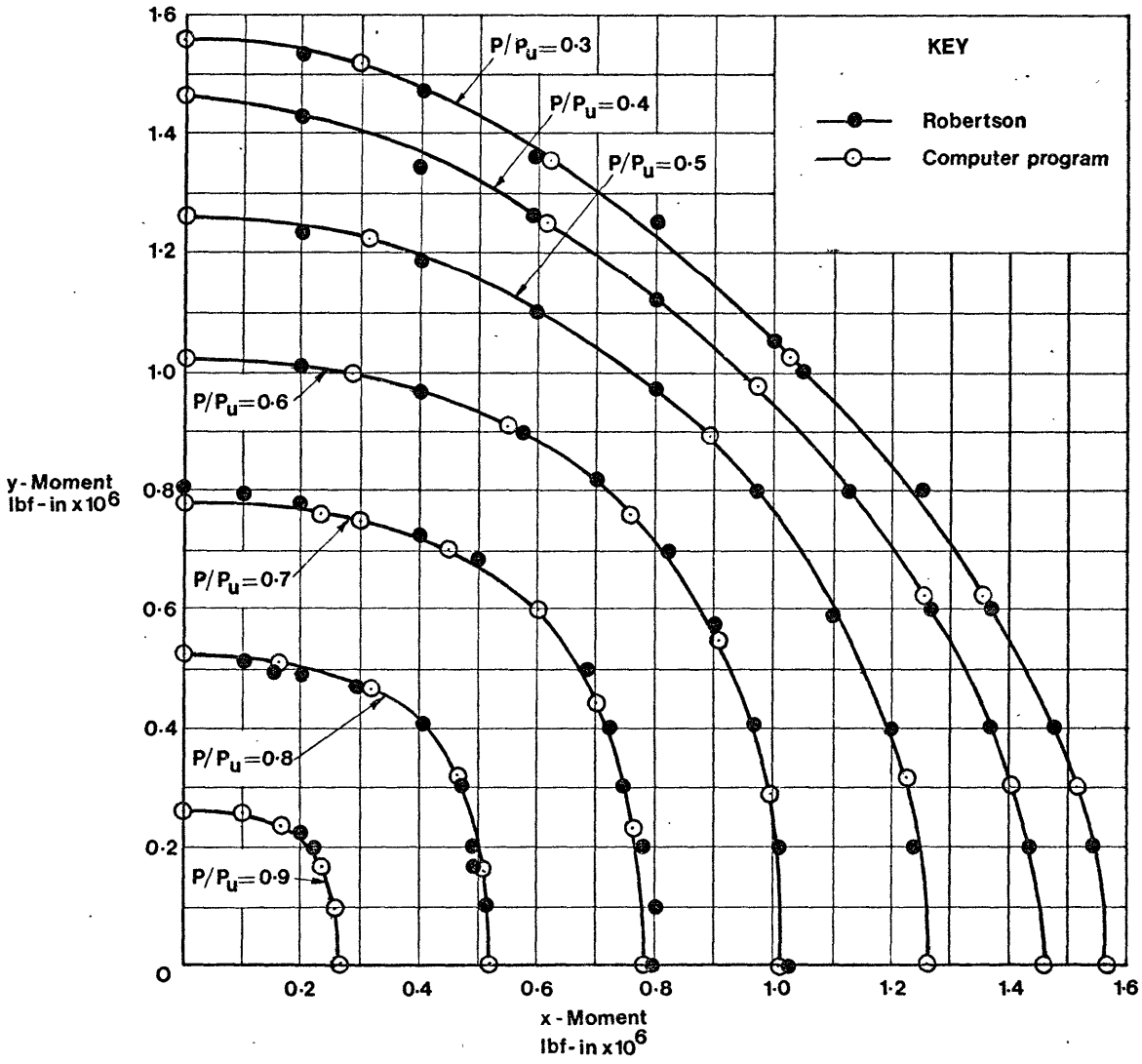

Fig.39 Moment - thrust interaction curves for P/P_u values greater than 0·2

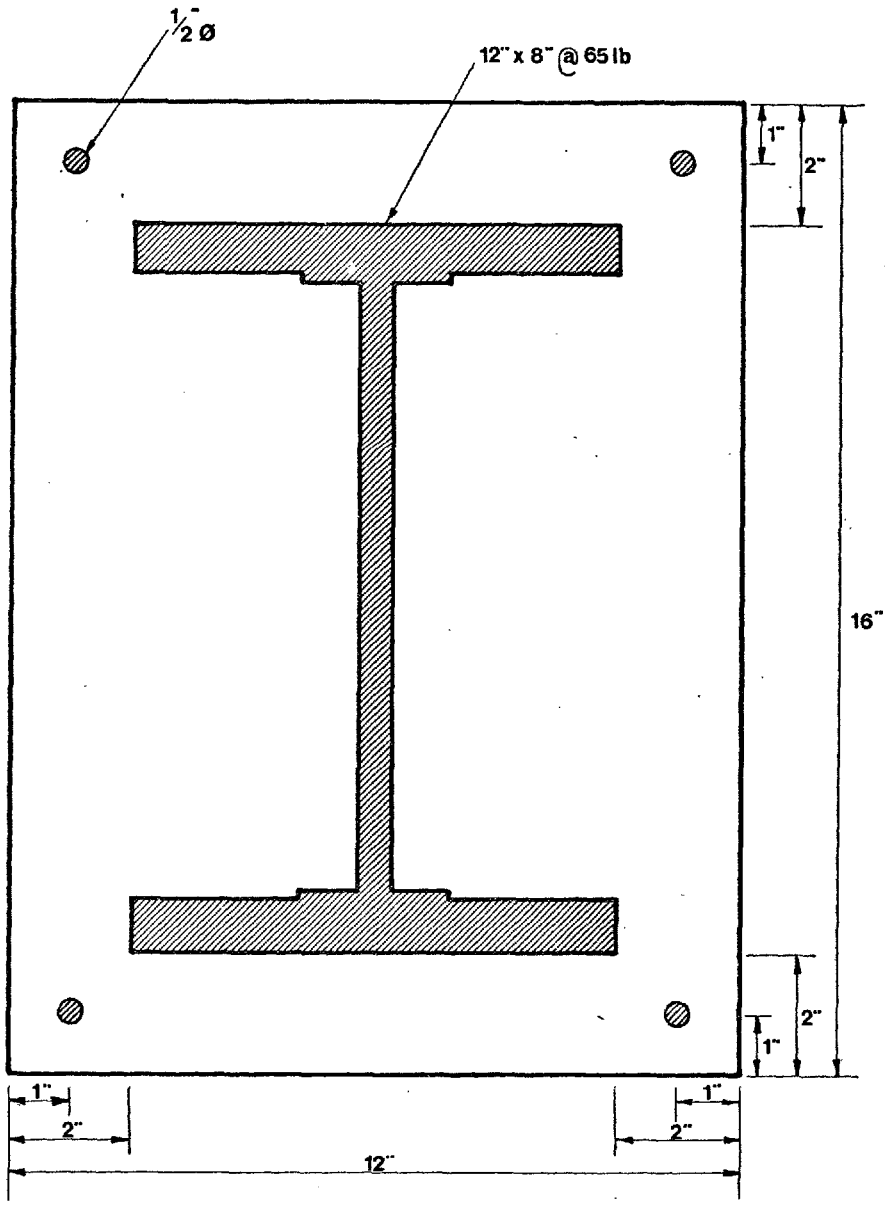

Fig.40 Steel section encased in concrete for moment-thrust-curvature and uniaxial bending failure load examples

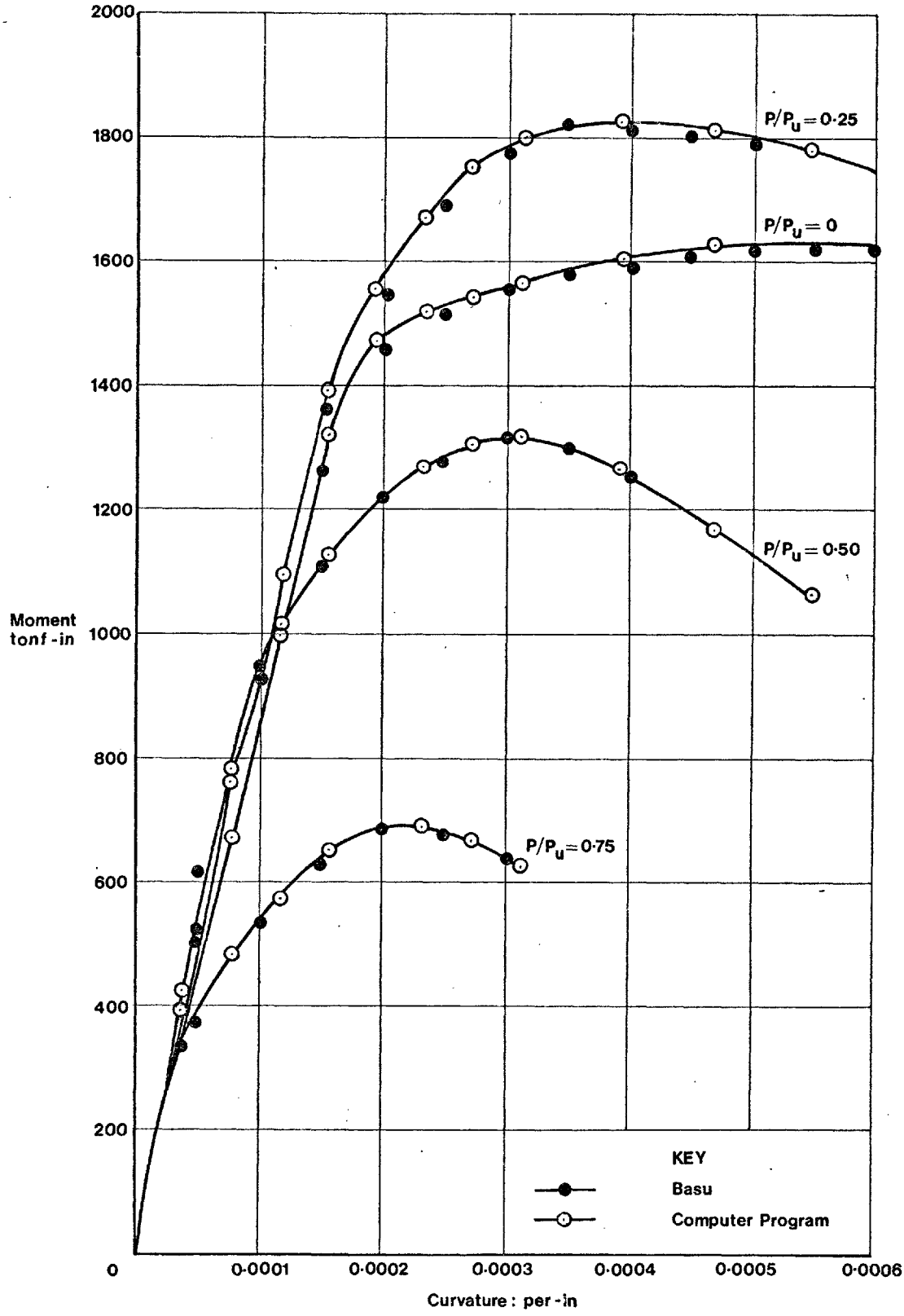

Fig.41 Minor axis bending moment-thrust-curvature relations for the concrete encased steel section of Fig.40

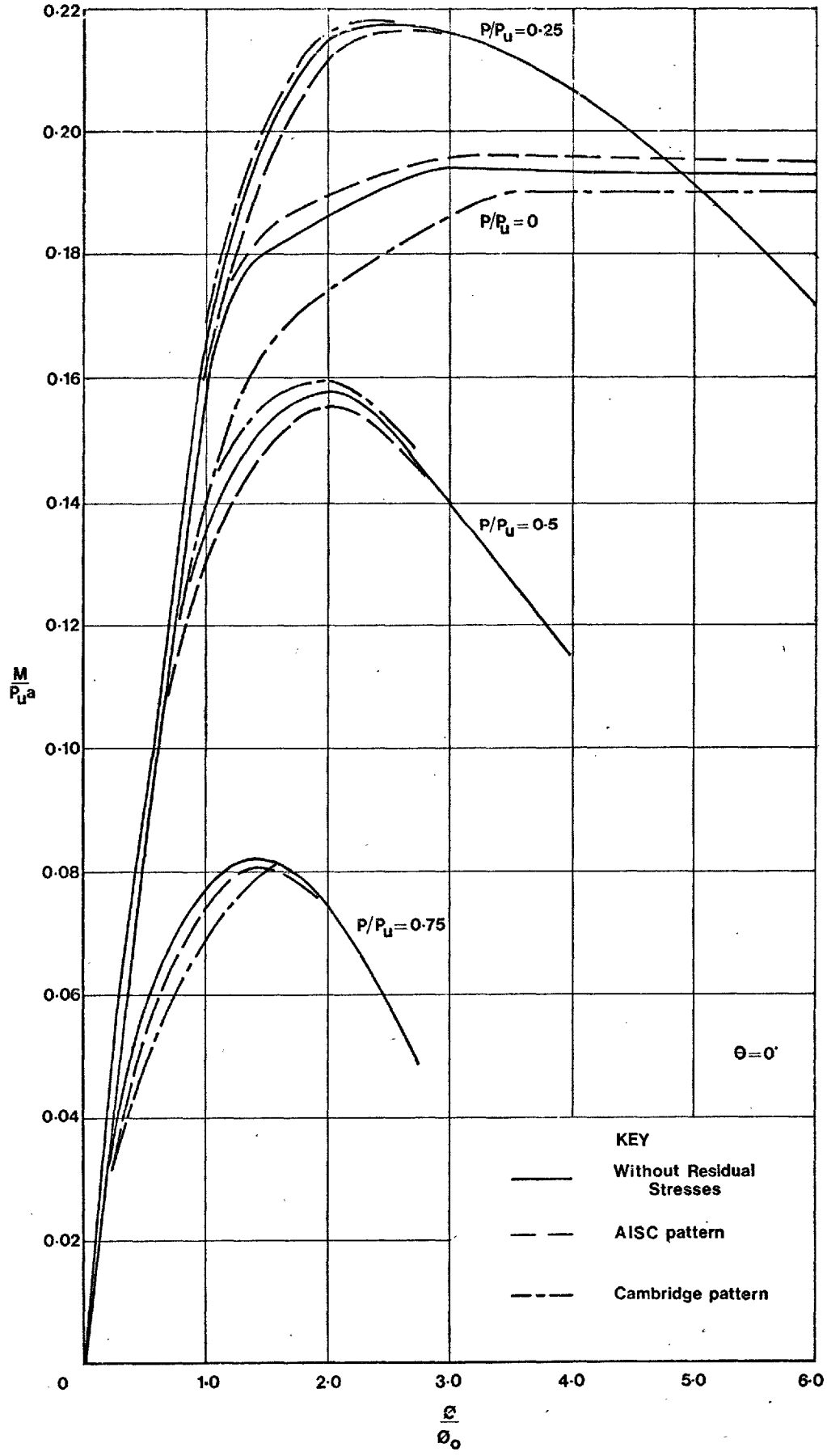

Fig.42 Effect of residual stresses on the moment-thrust-curvature relations for the concrete encased steel section of Fig.40 in major axis bending

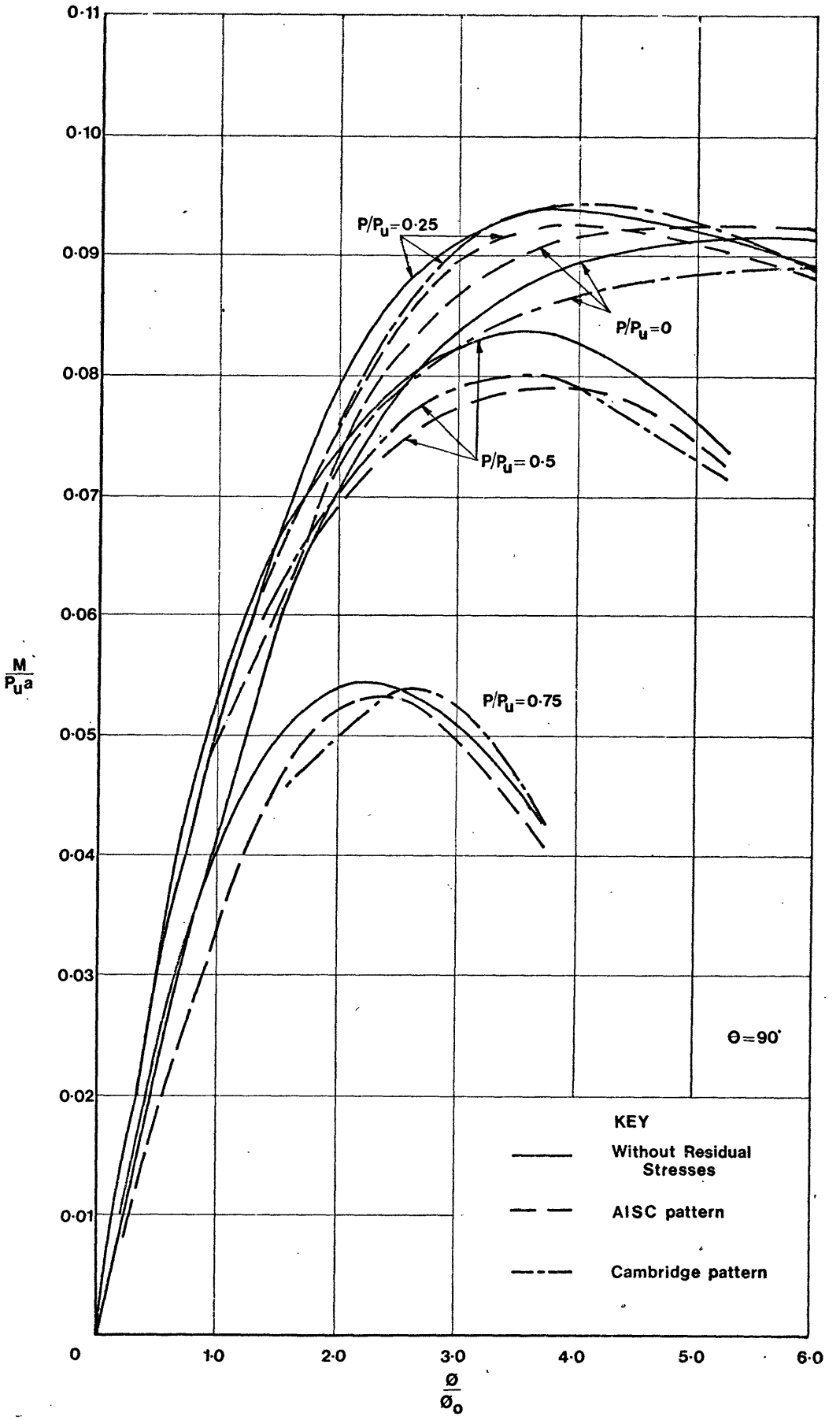

Fig.43 Effect of residual stresses on the moment-thrust-curvature relations for the concrete encased steel section of Fig.40

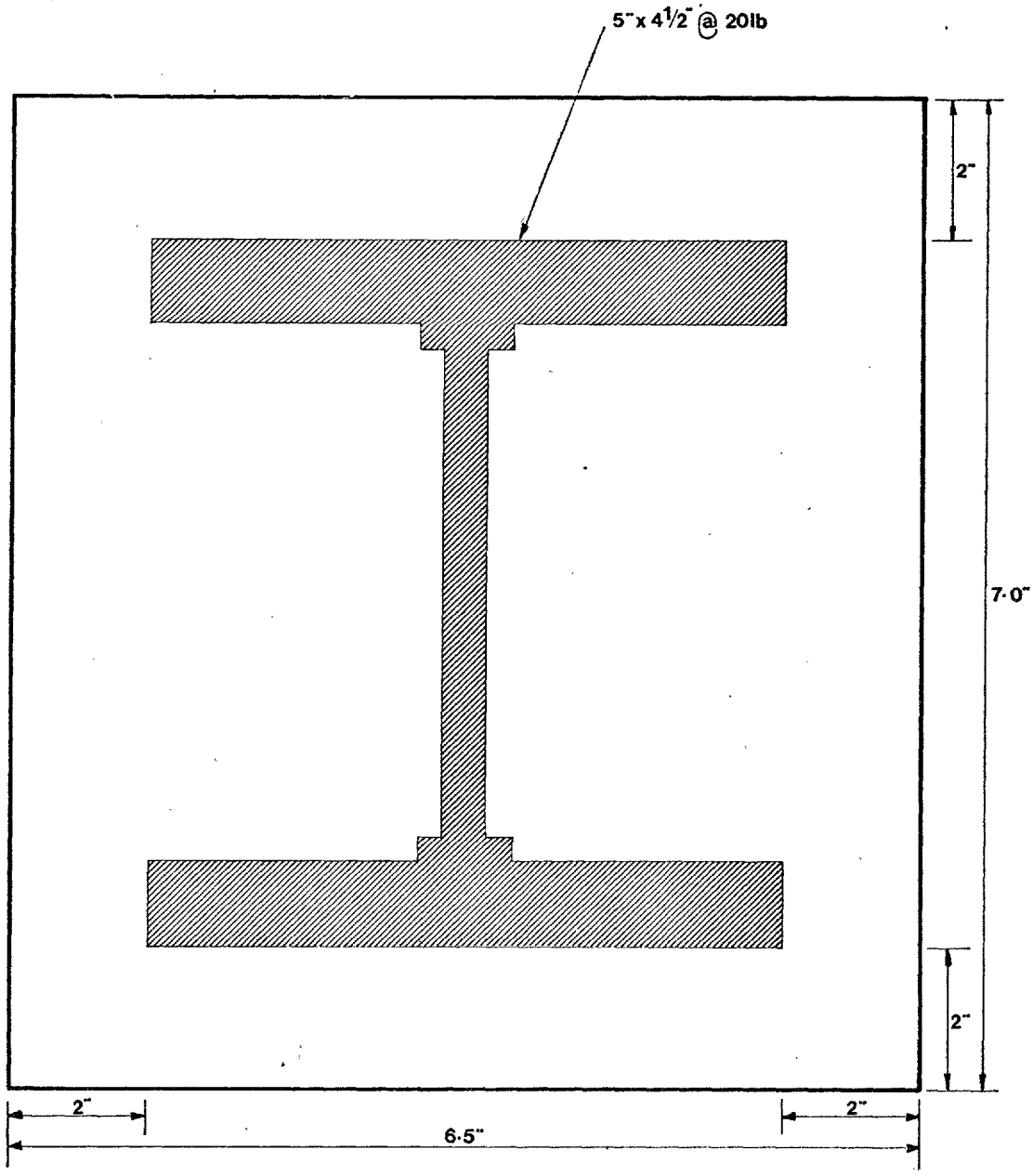

Fig.44 Concrete encased steel section (Series AE) for the uniaxial failure load example

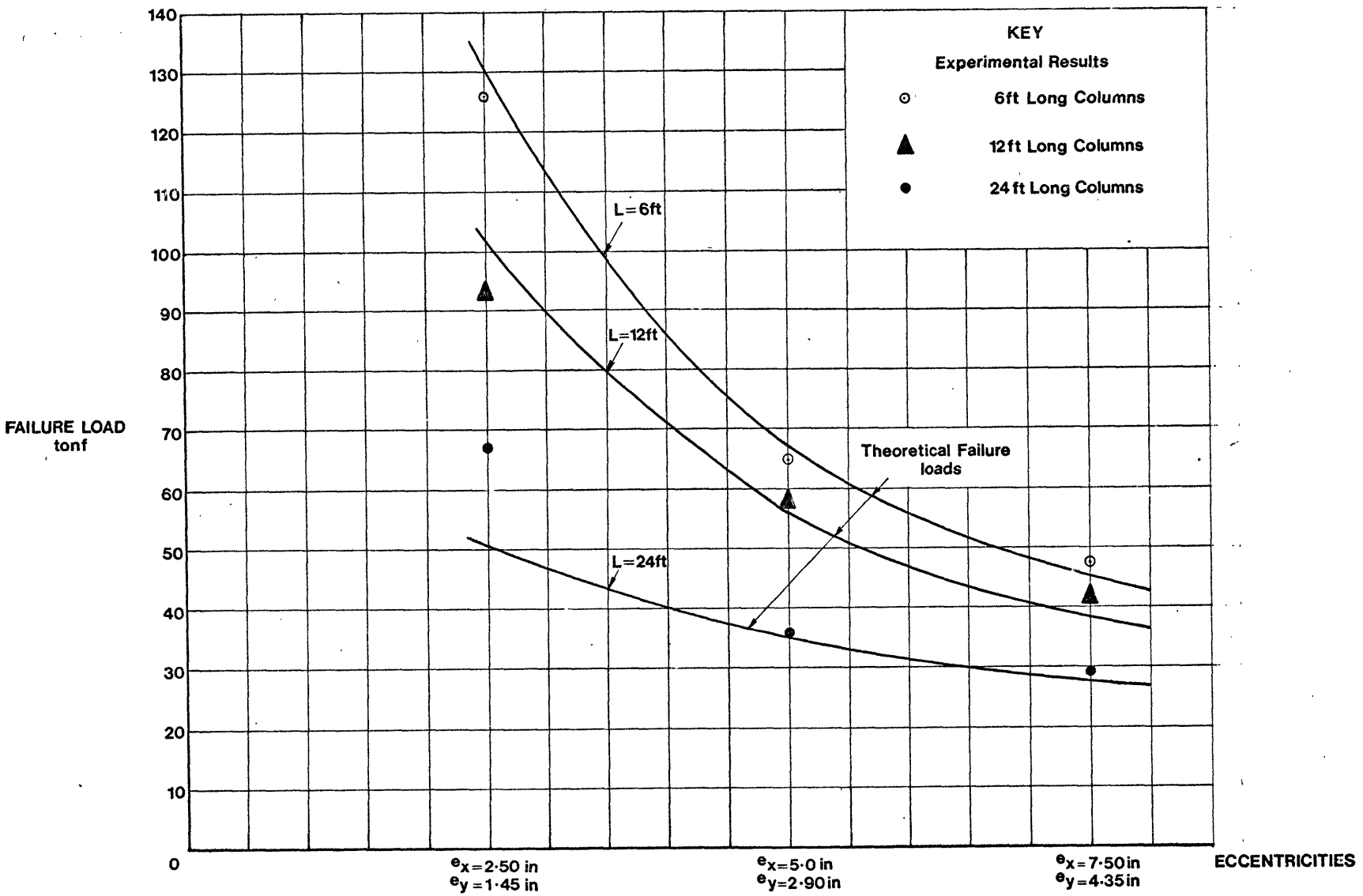

Fig.45 Comparison between experimental and analytical failure loads for the nine test columns

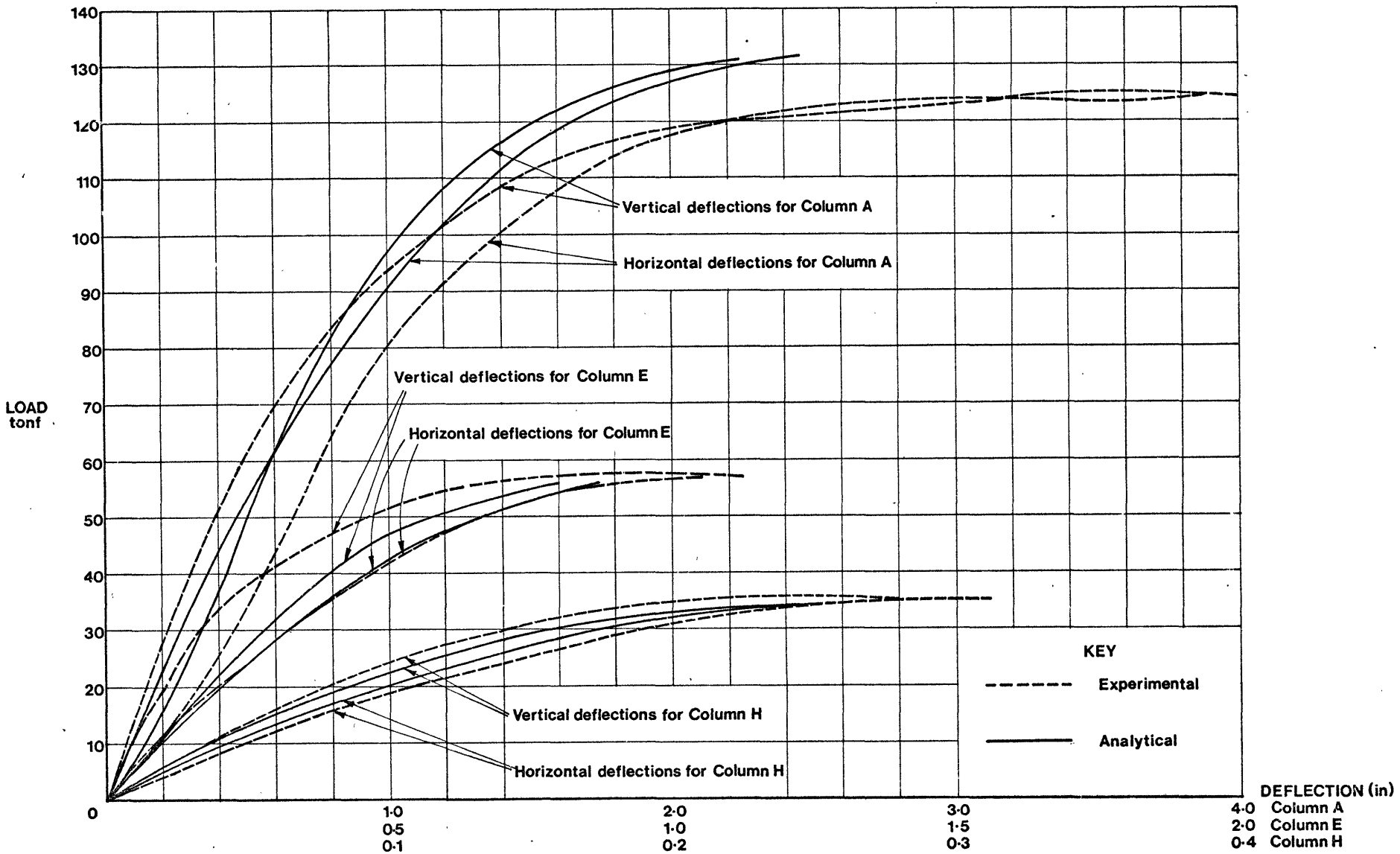

Fig.46 Comparison between experimental and analytical deflections for Columns A, E and H

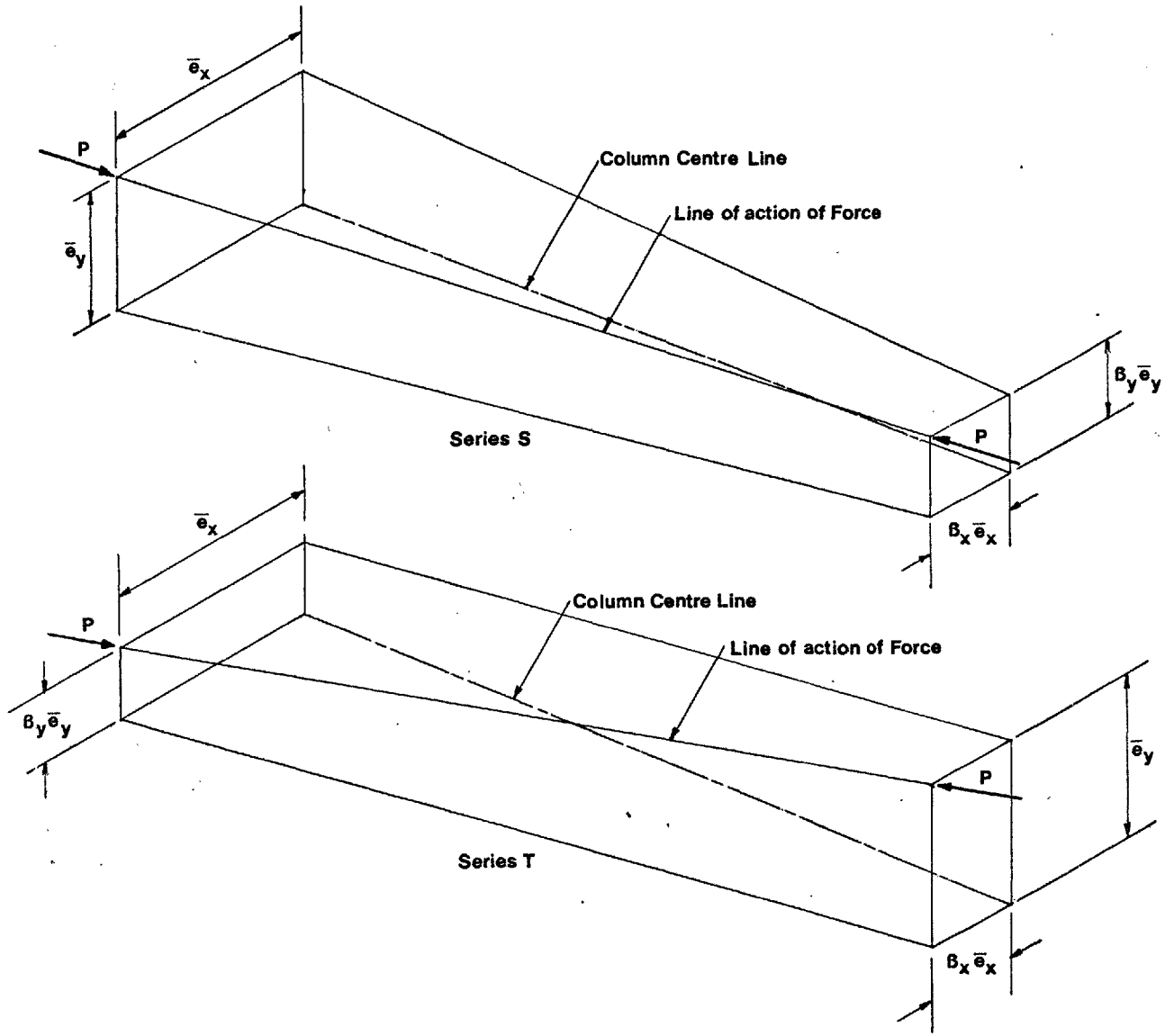

Fig.47 End-eccentricity combinations for Series S and Series T columns

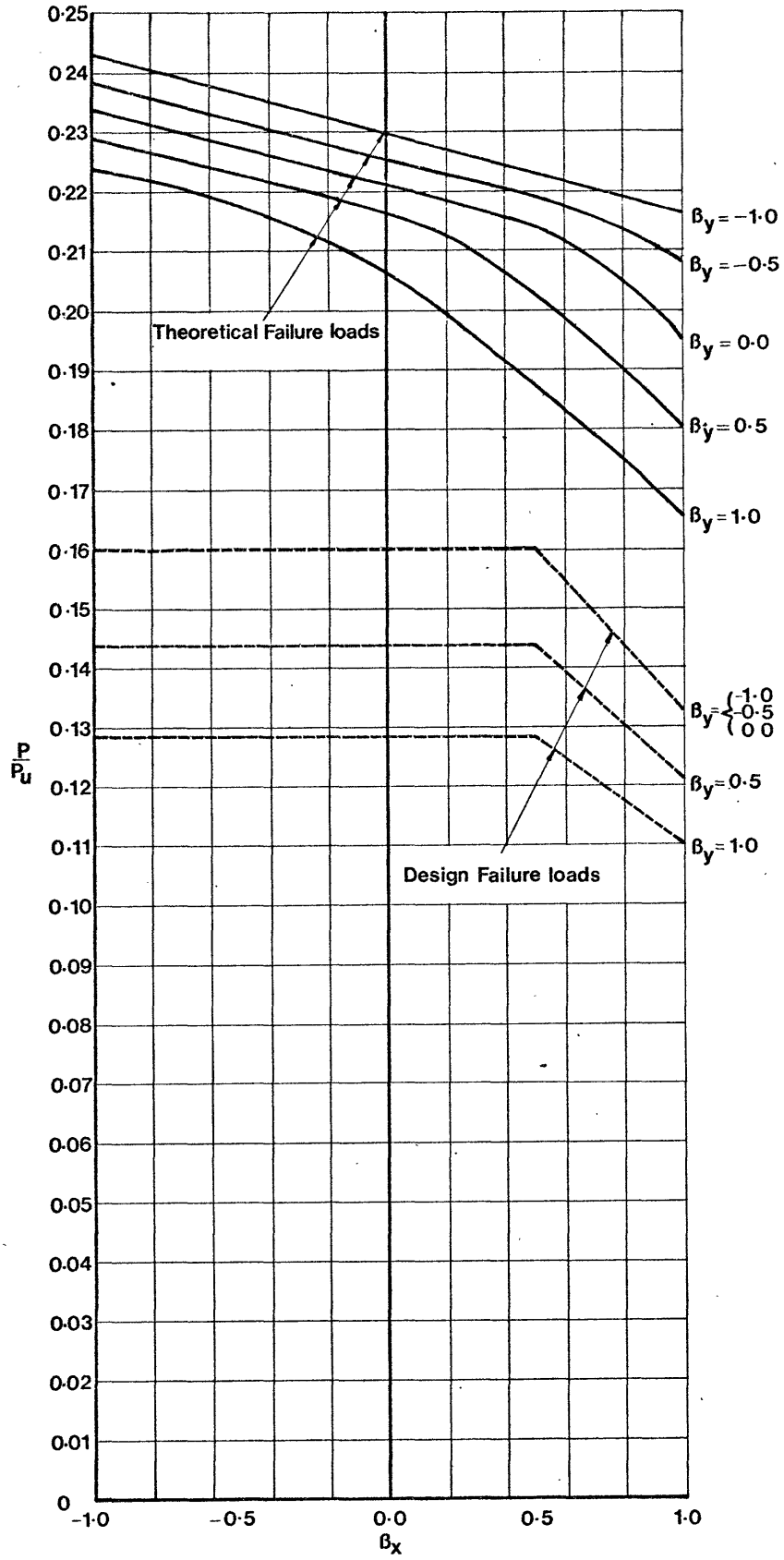

Fig.48 Variation of failure loads for columns in general biaxial bending (Series S) with respect to β_x

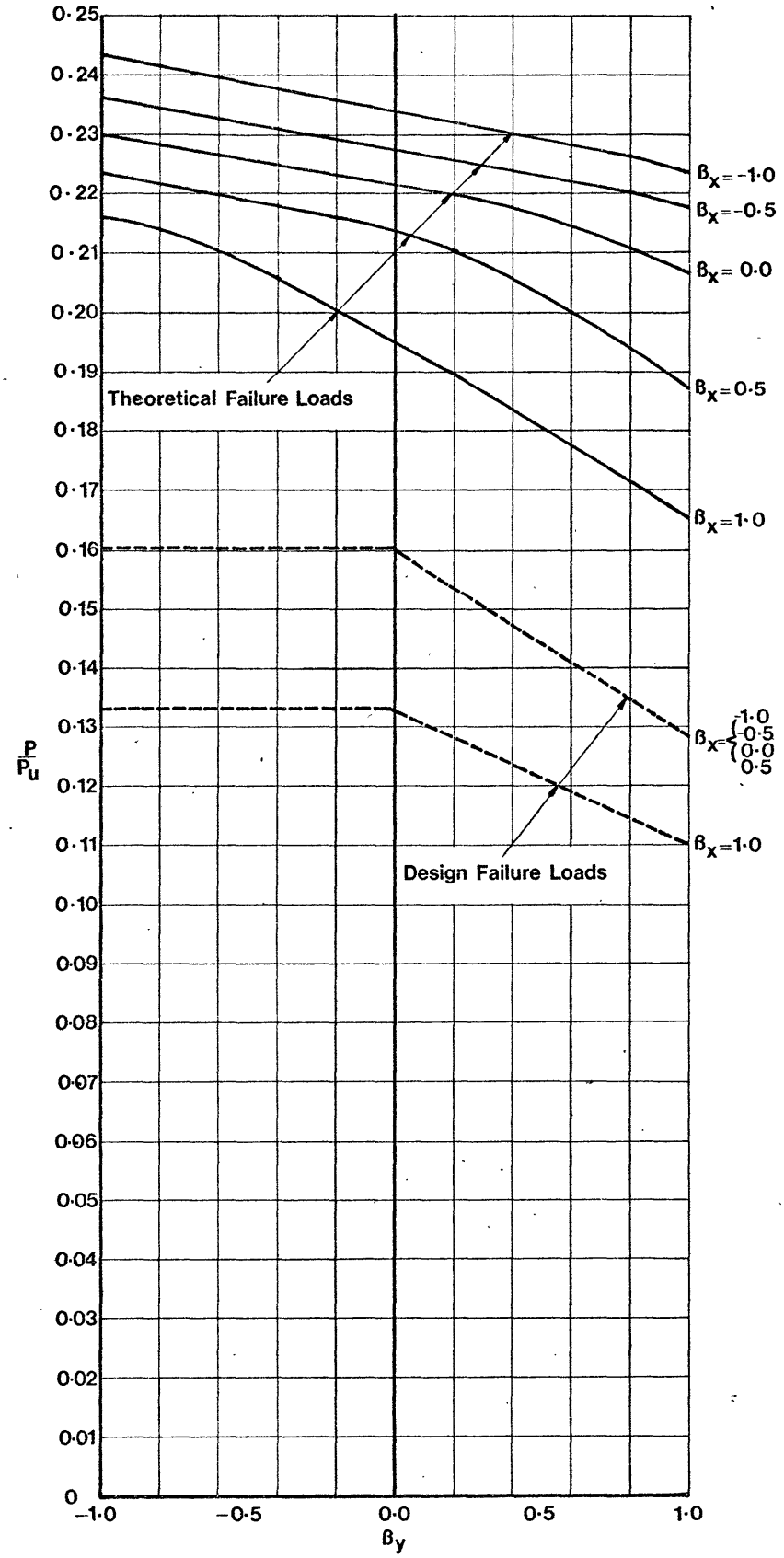

Fig.49 Variation of failure loads for columns in general biaxial bending (Series S) with respect to β_y

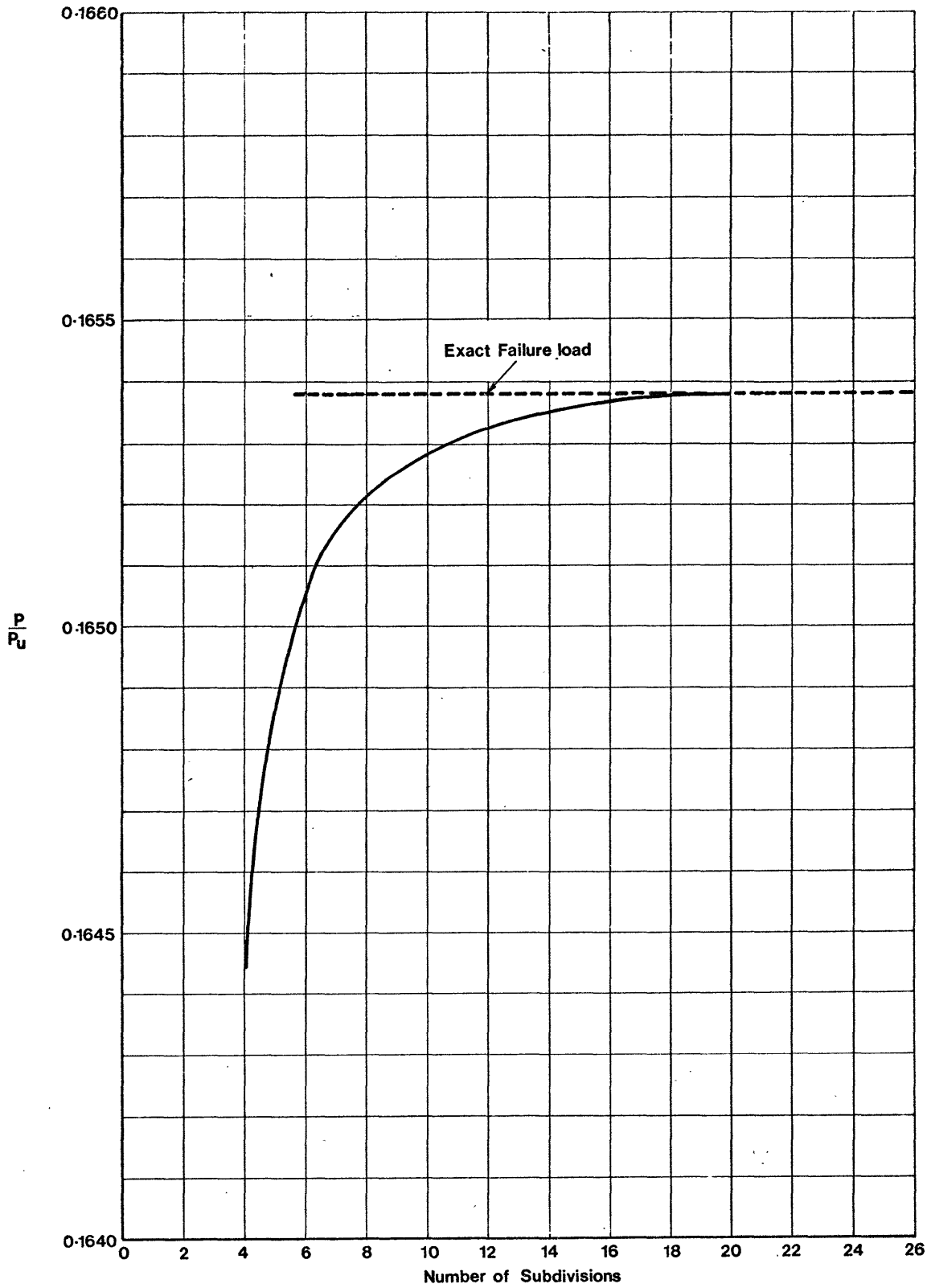

Fig.50 Variation of computed failure load with the number of column subdivisions for symmetrical end-eccentricities

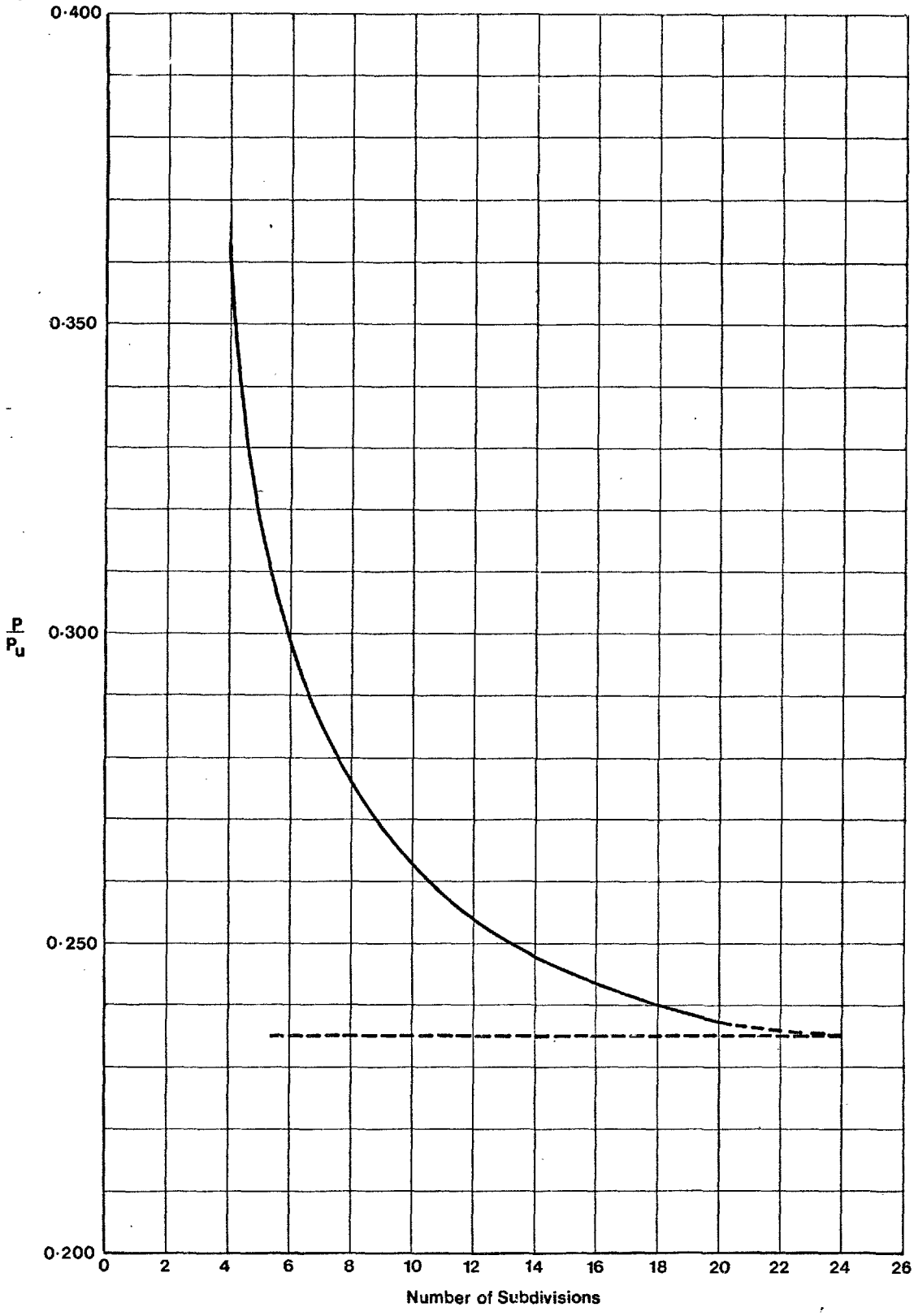

Fig.51 Variation of computed failure load with the number of column subdivisions for antisymmetrical end-eccentricities

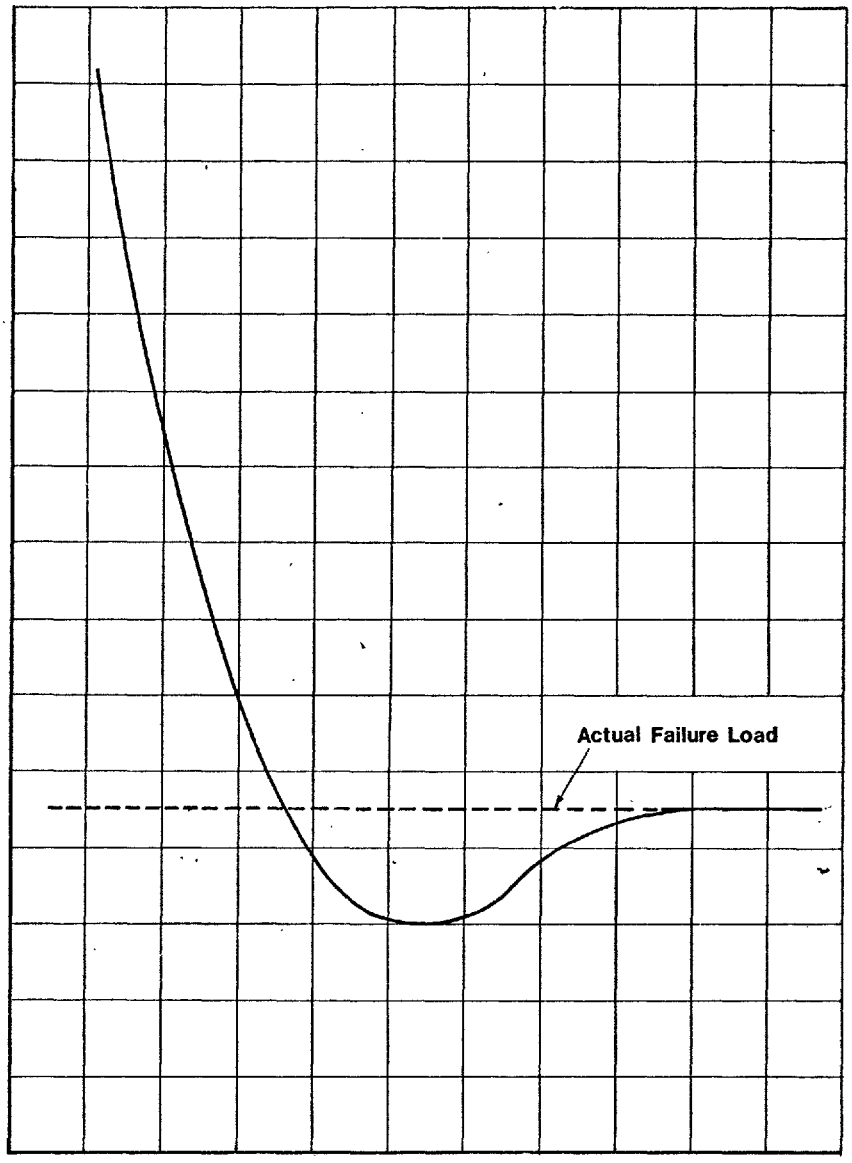

Fig.52 Variation of failure load with number of subdivisions in the case of asymmetrical bending shown to an exaggerated scale

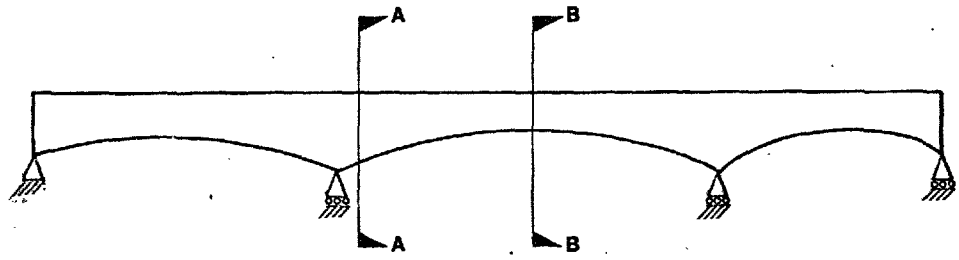

(a)

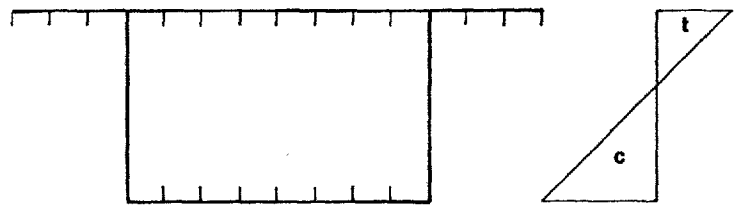

A-A
(b)

Stress distribution

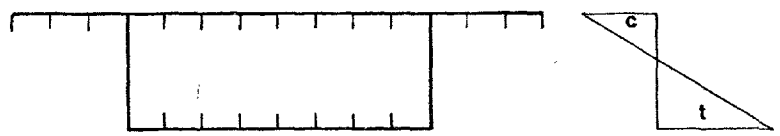

B-B
(c)

Stress distribution

Fig.53 Typical box girder bridge elevation and cross-sections

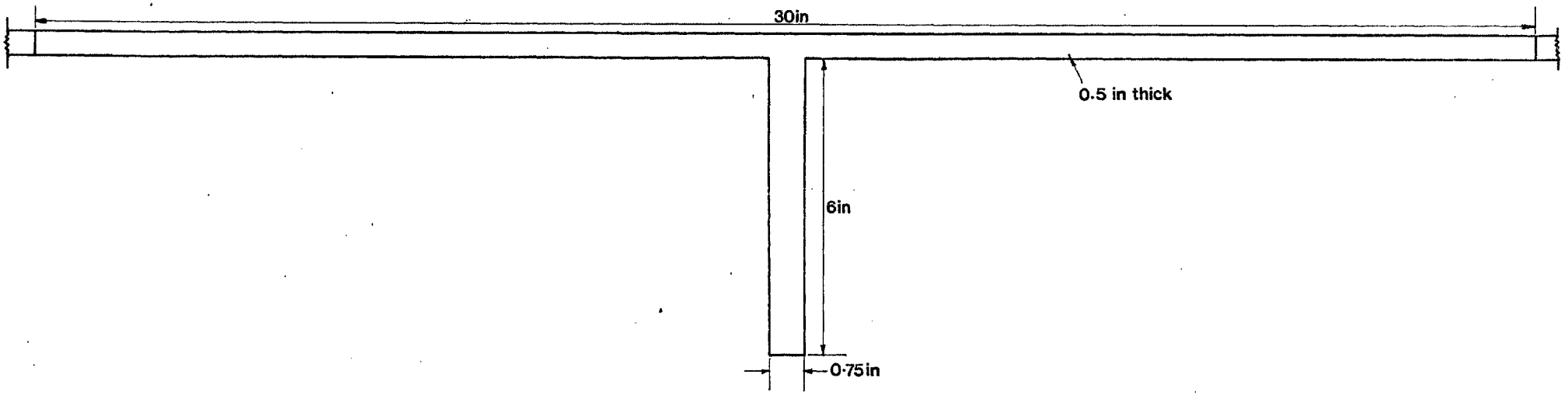

Fig.54 Dimensions of the stiffened plate cross-section

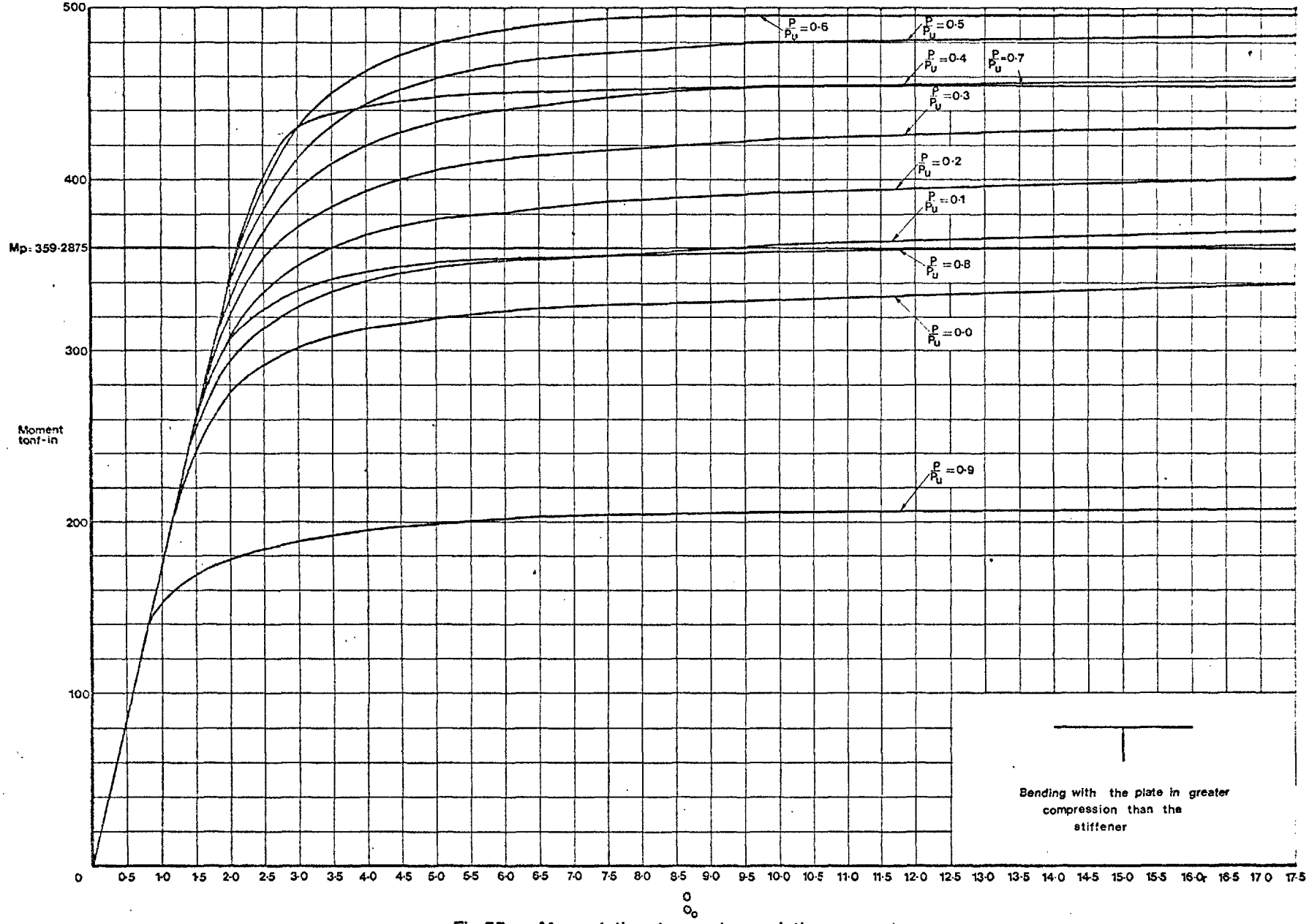

Fig.55 Moment-thrust-curvature relations

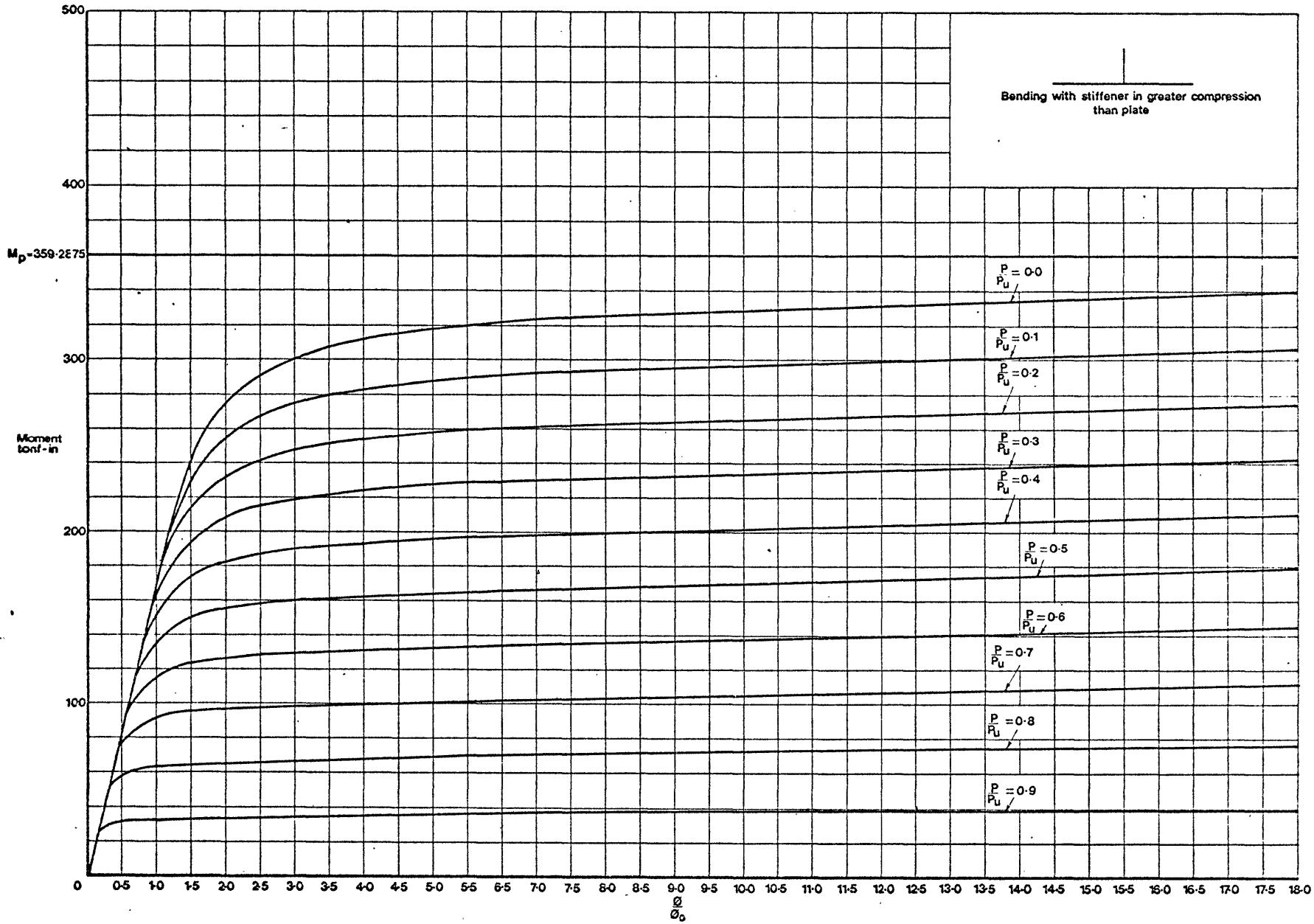

Fig.56 Moment-thrust-curvature relations

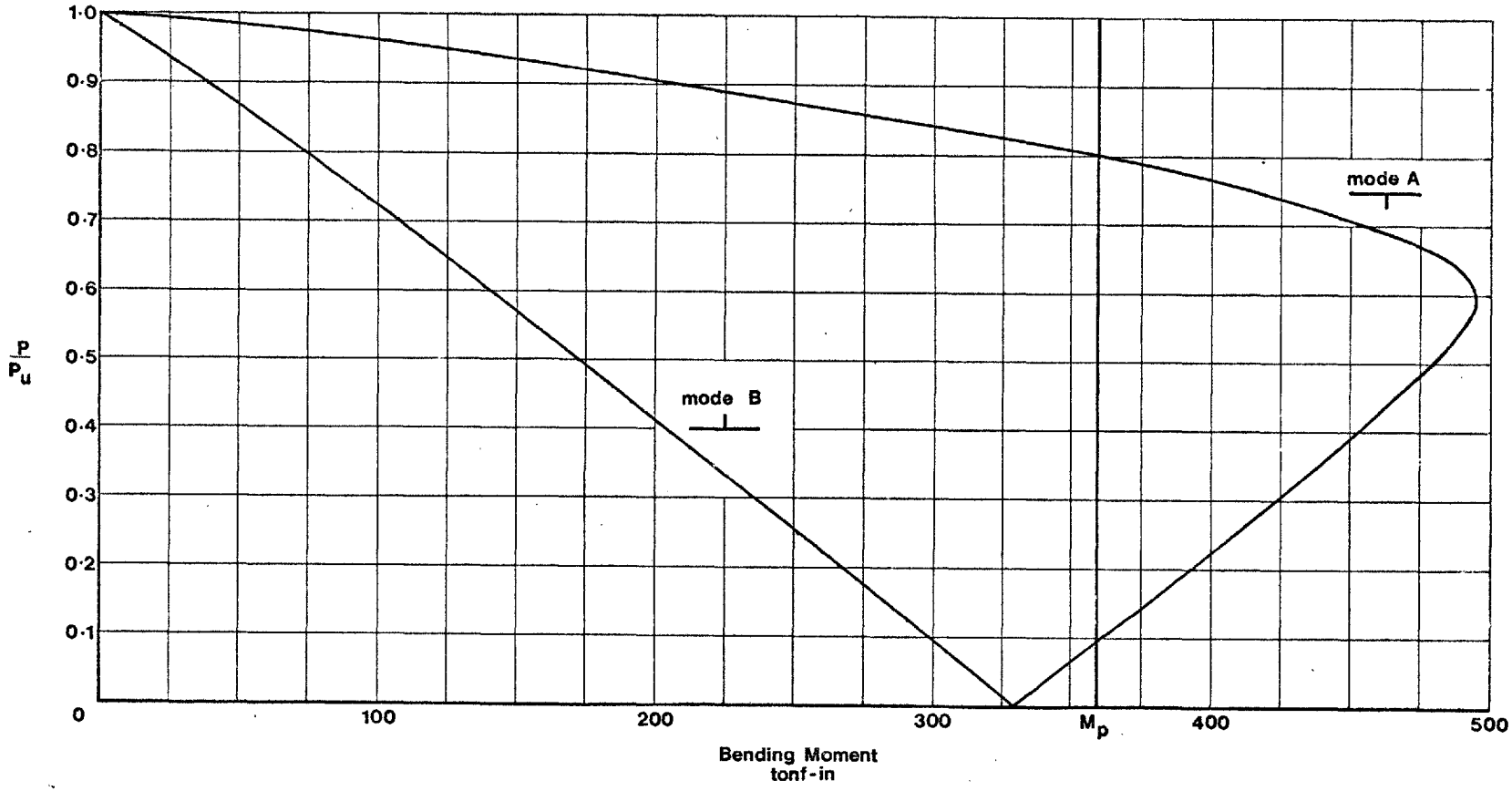

Fig.57 Load moment curves for fixed curvature (0·0026 per in)

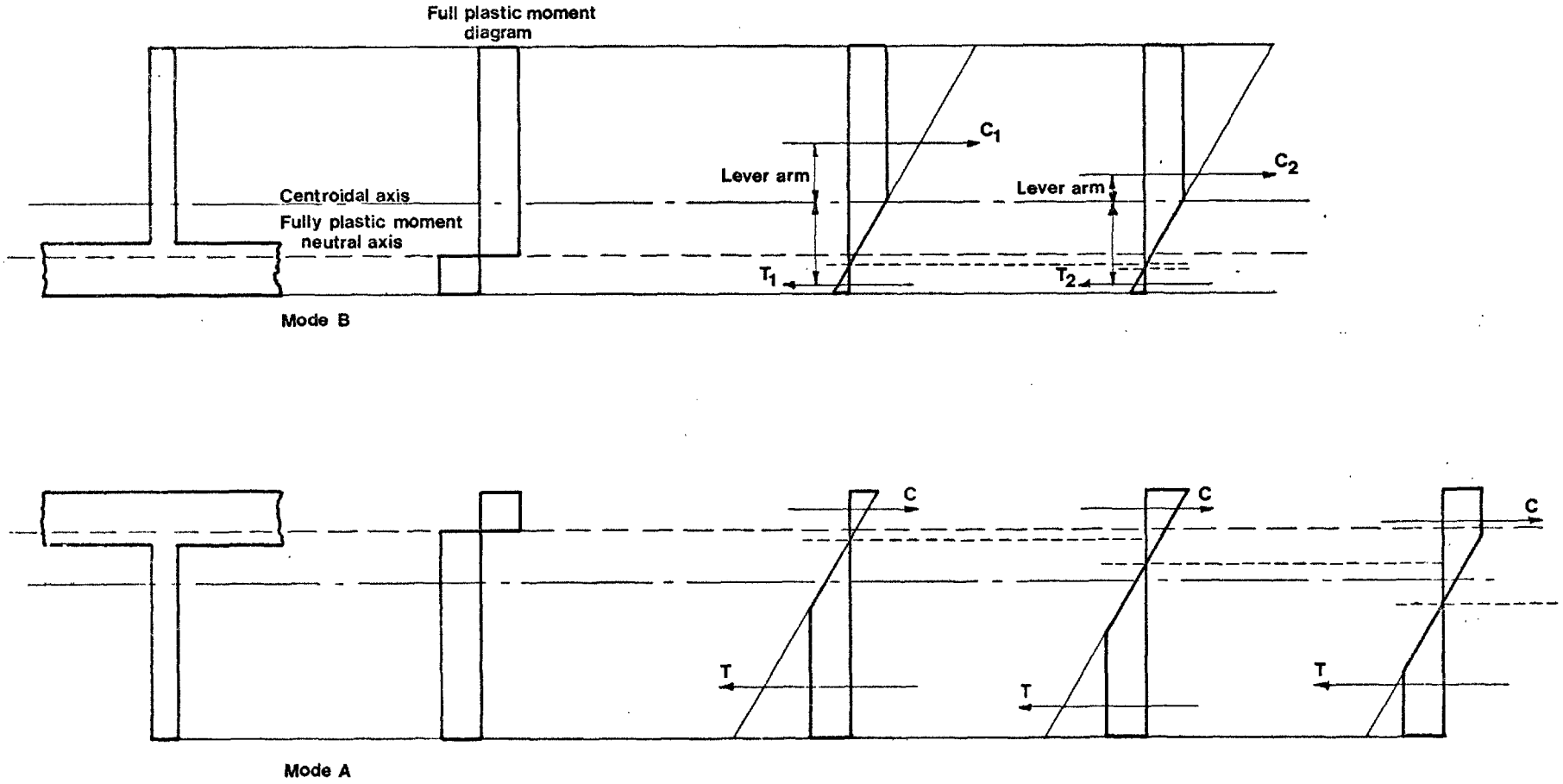

Fig.58 Stress and Strain distributions across the section for constant curvature and increasing axial loads

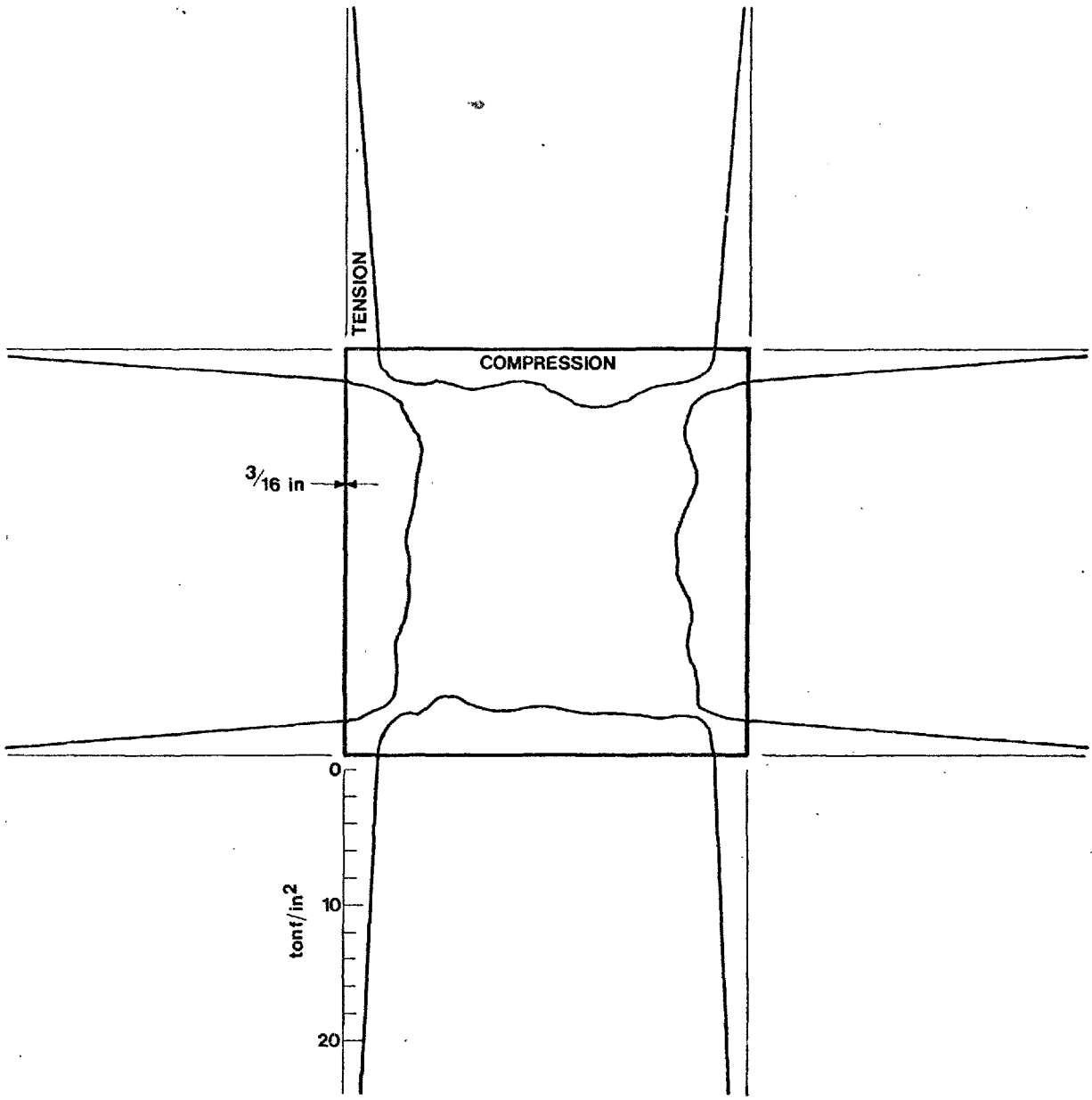

Fig.59 Typical residual stress pattern in a welded box member with $b/t = 80, \sigma_y = 26$ tonf/in^2

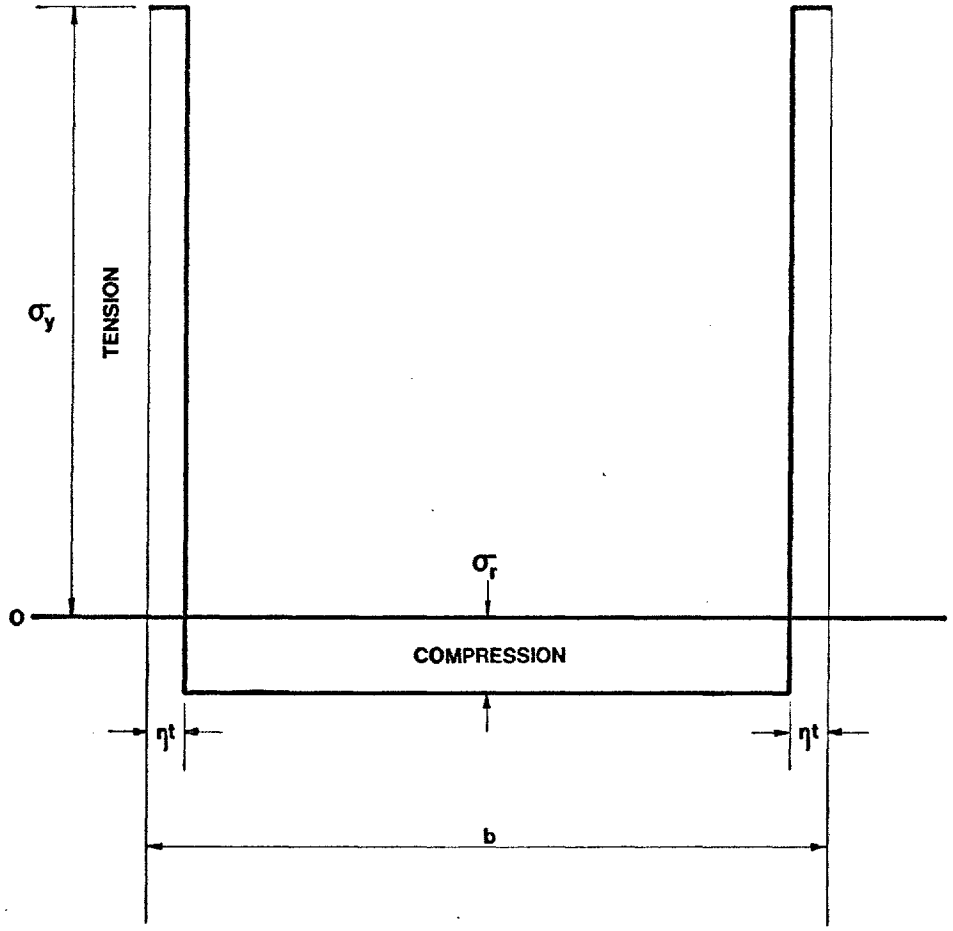

Fig.60 Idealised residual stress distribution in a plate with edge welds

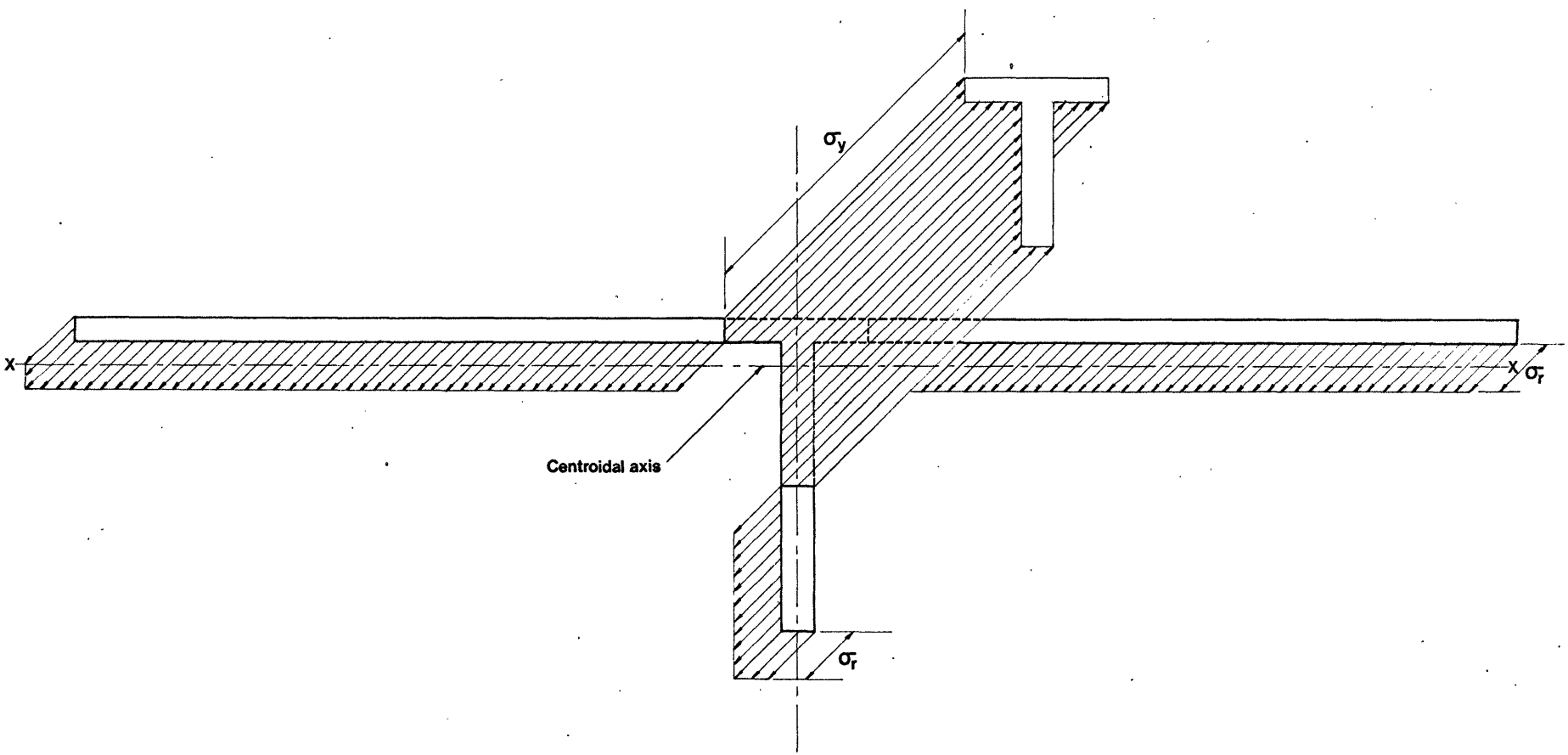

Fig.61 Idealised residual stress distribution based on Equation (65). The stress distribution has normal force equilibrium but lacks bending moment equilibrium about the centroidal axis

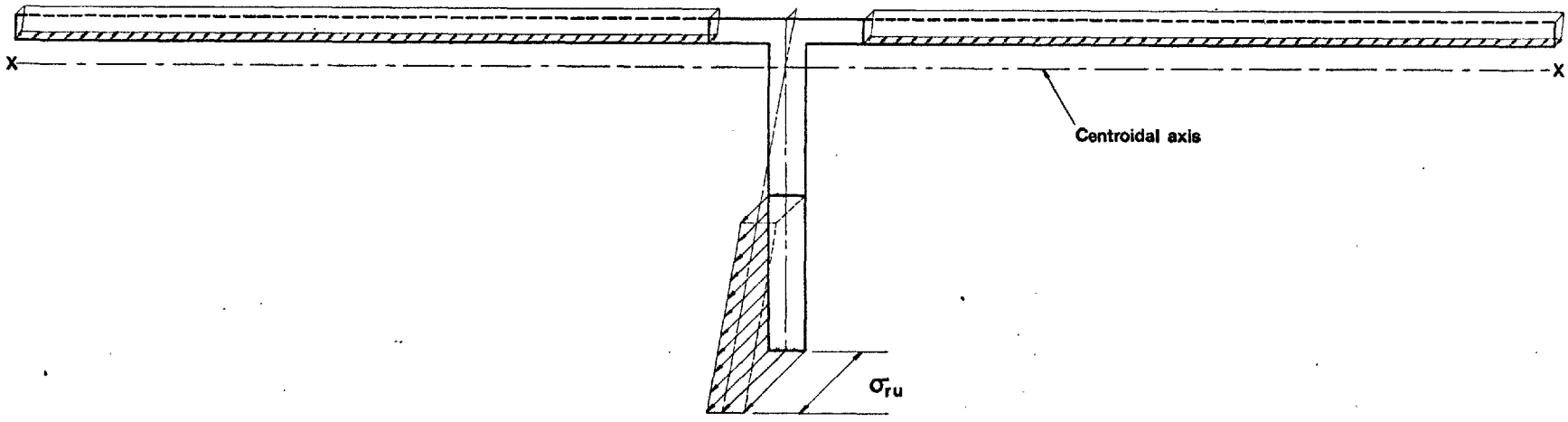

Fig.62 Residual stress distribution due to the unbalanced moment in Fig.61

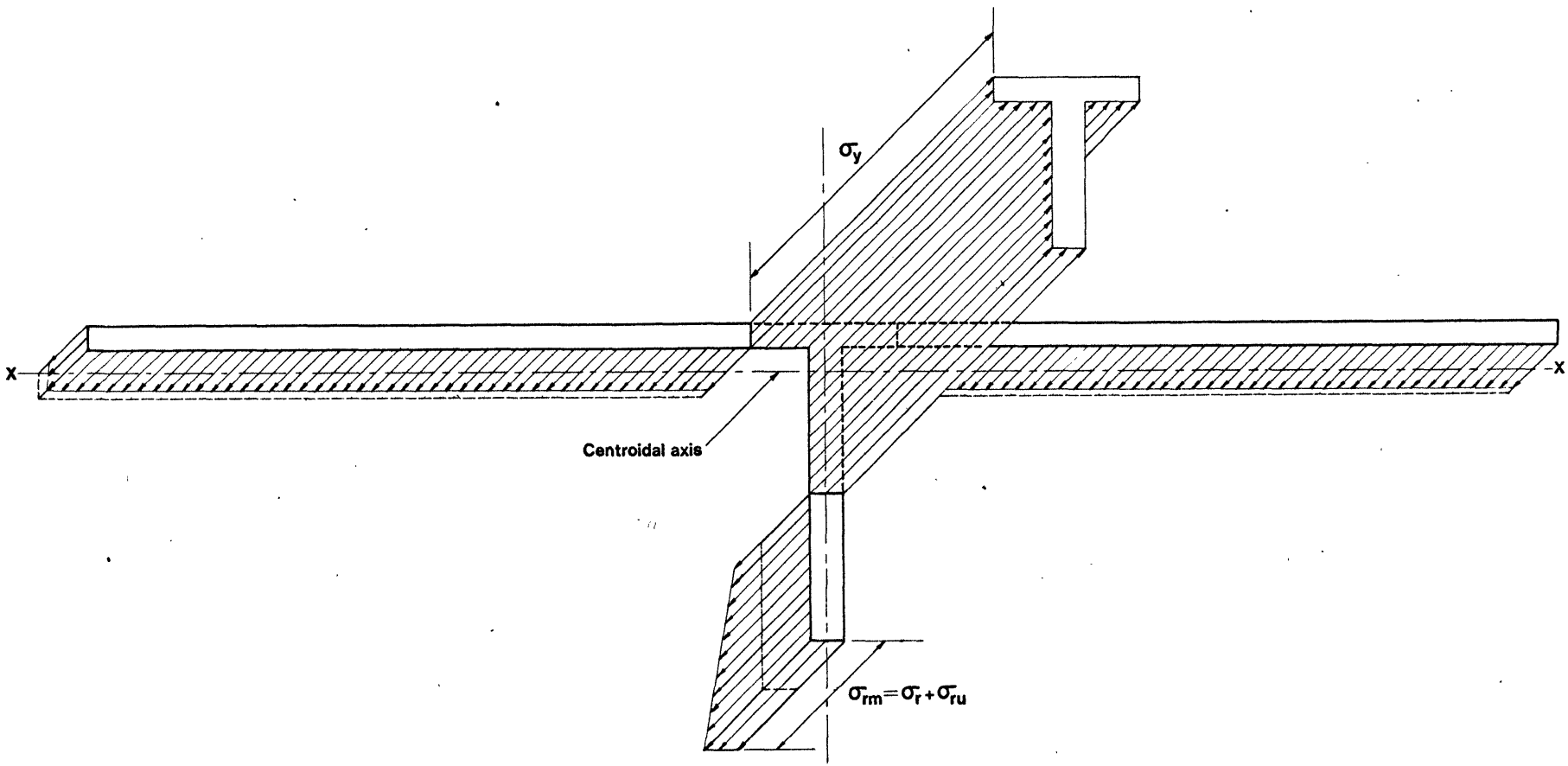

Fig.63 Corrected residual stress distribution diagram used in the calculations

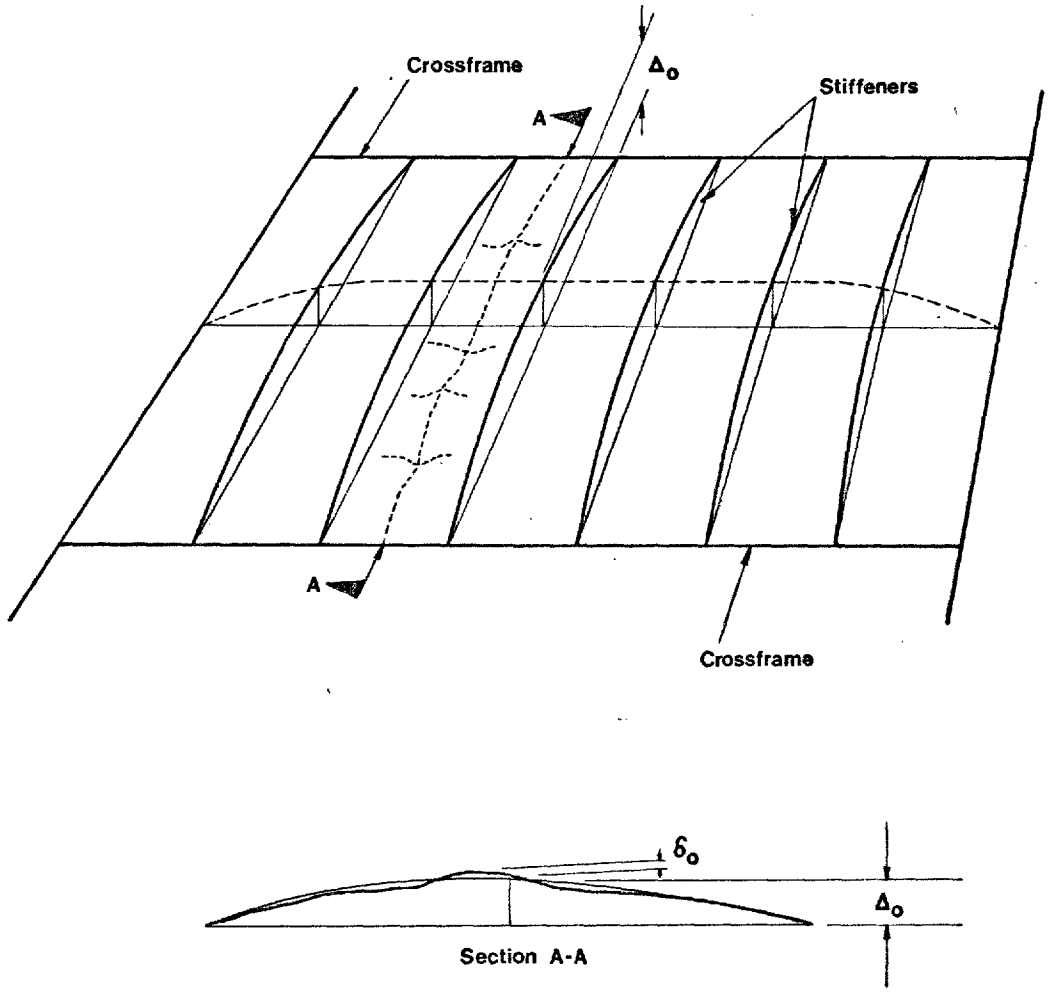

Fig.64 Stiffener out-of-plane deformation and the ripple component of out-of-plane deformation

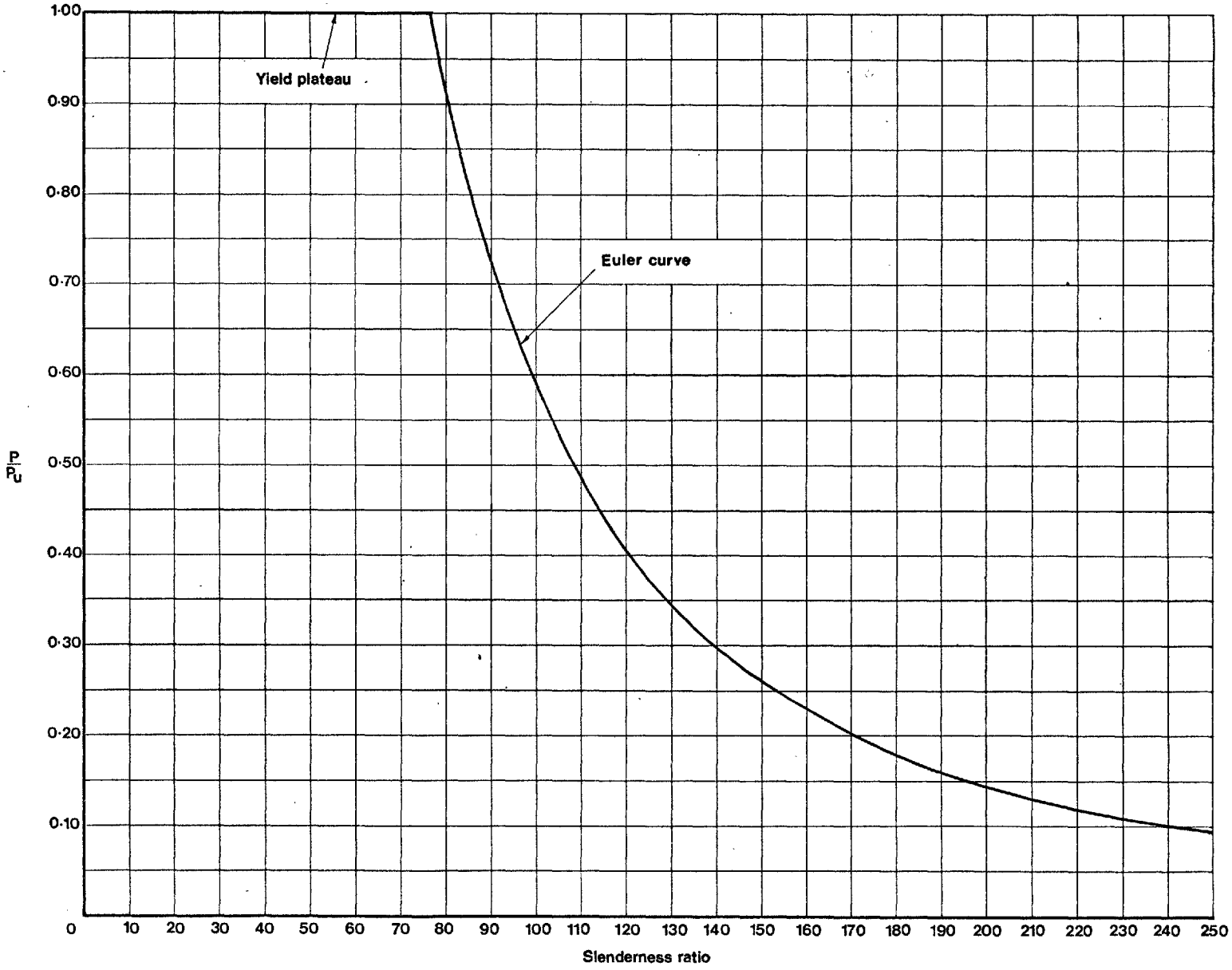

Fig.65 Strength of an ideally straight column having ideal elastic perfectly plastic material properties

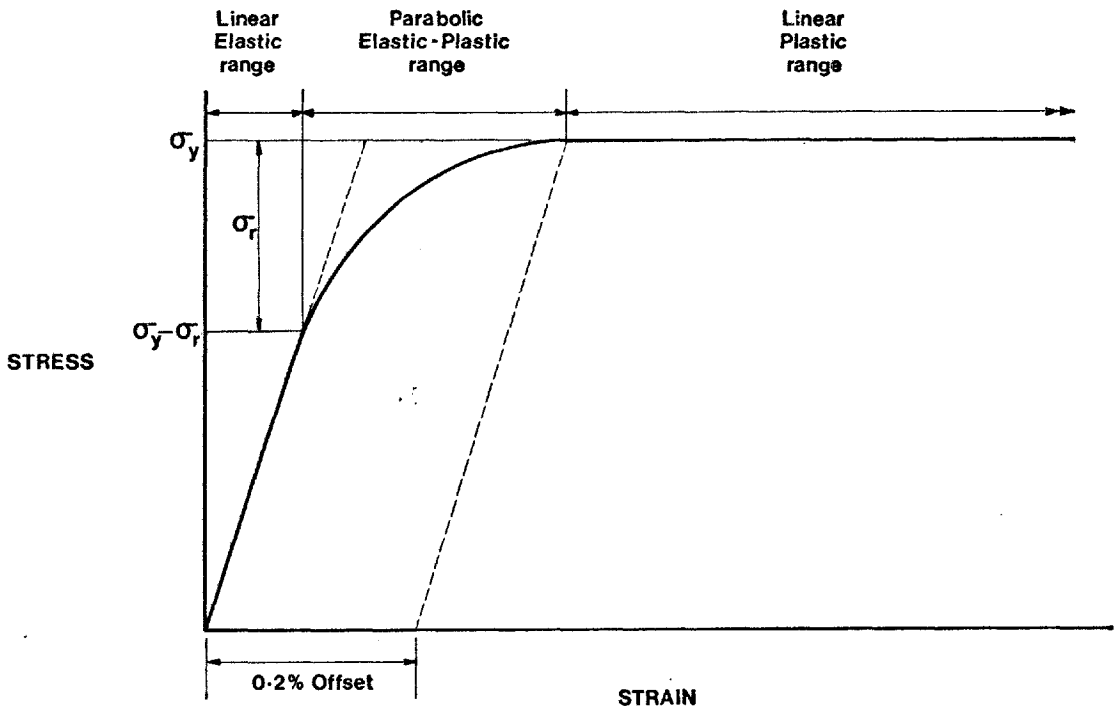

Fig.66 Idealized elastic-plastic average stress strain curve including the effect of residual stresses

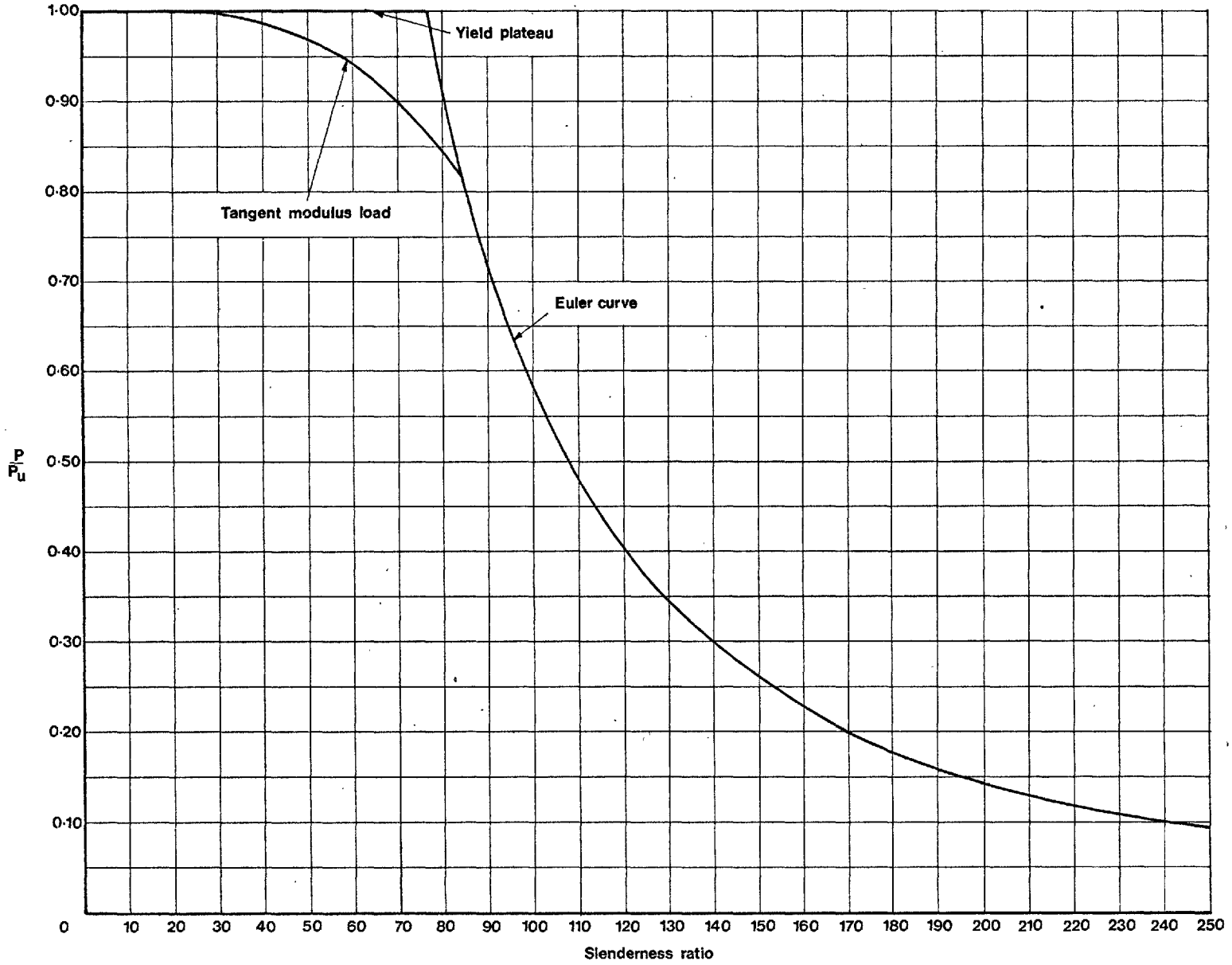

Fig.67 Strength of ideally straight columns with residual stresses

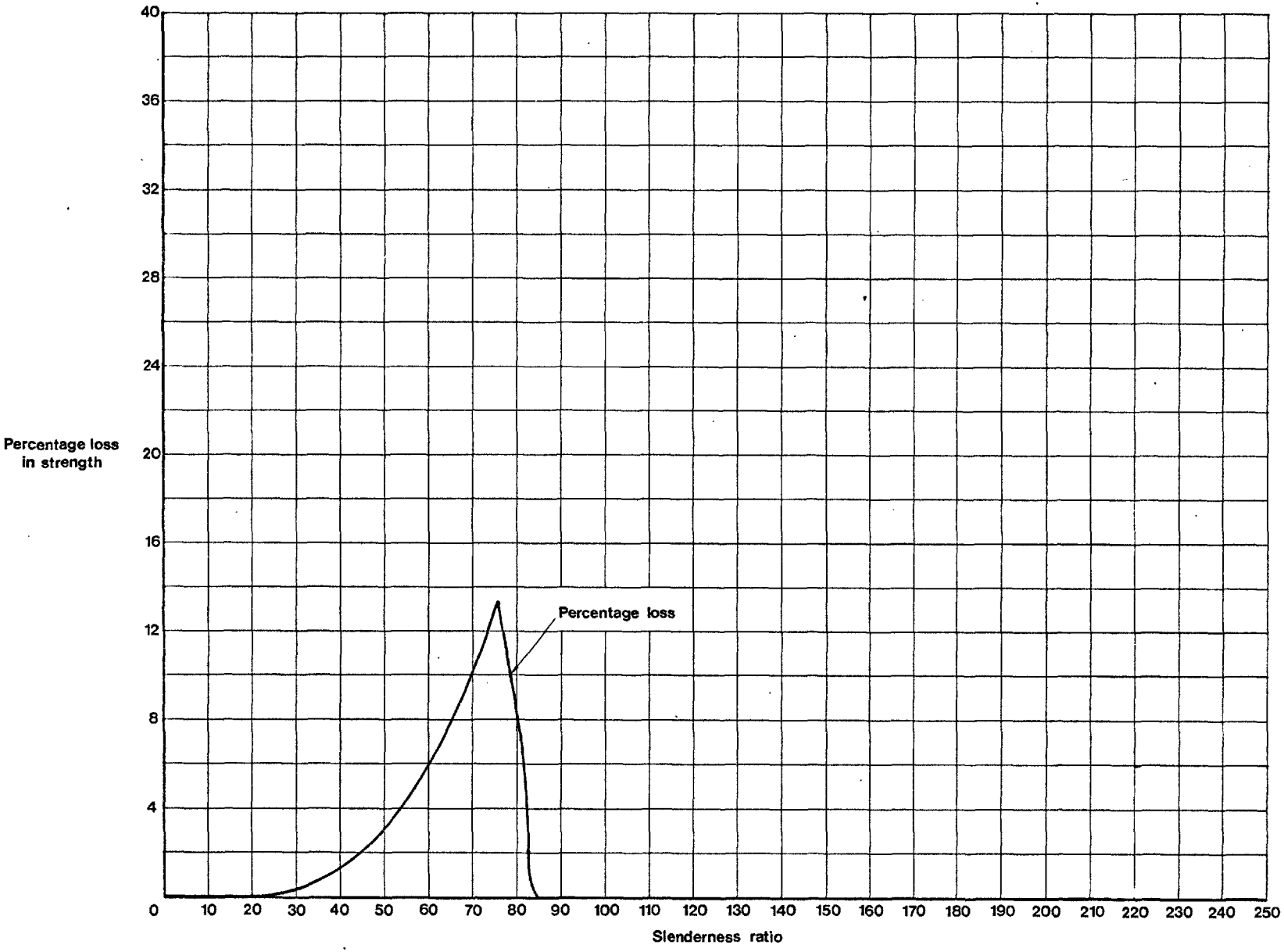

Fig.68 Loss in strength due to residual stresses on the basis of idealised elastic-plastic average stress strain curve

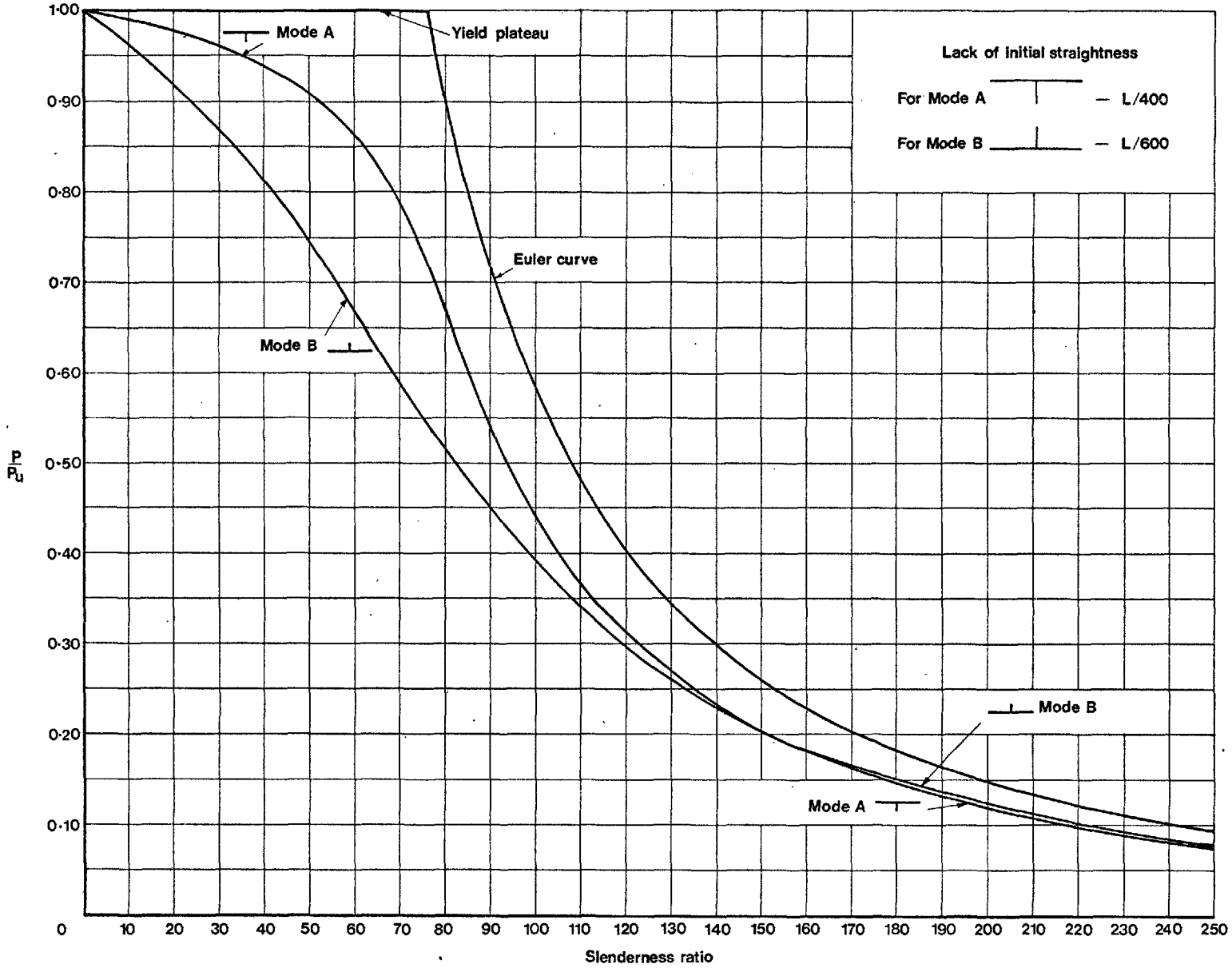

Fig.69 Strength of columns with initial lack of straightness

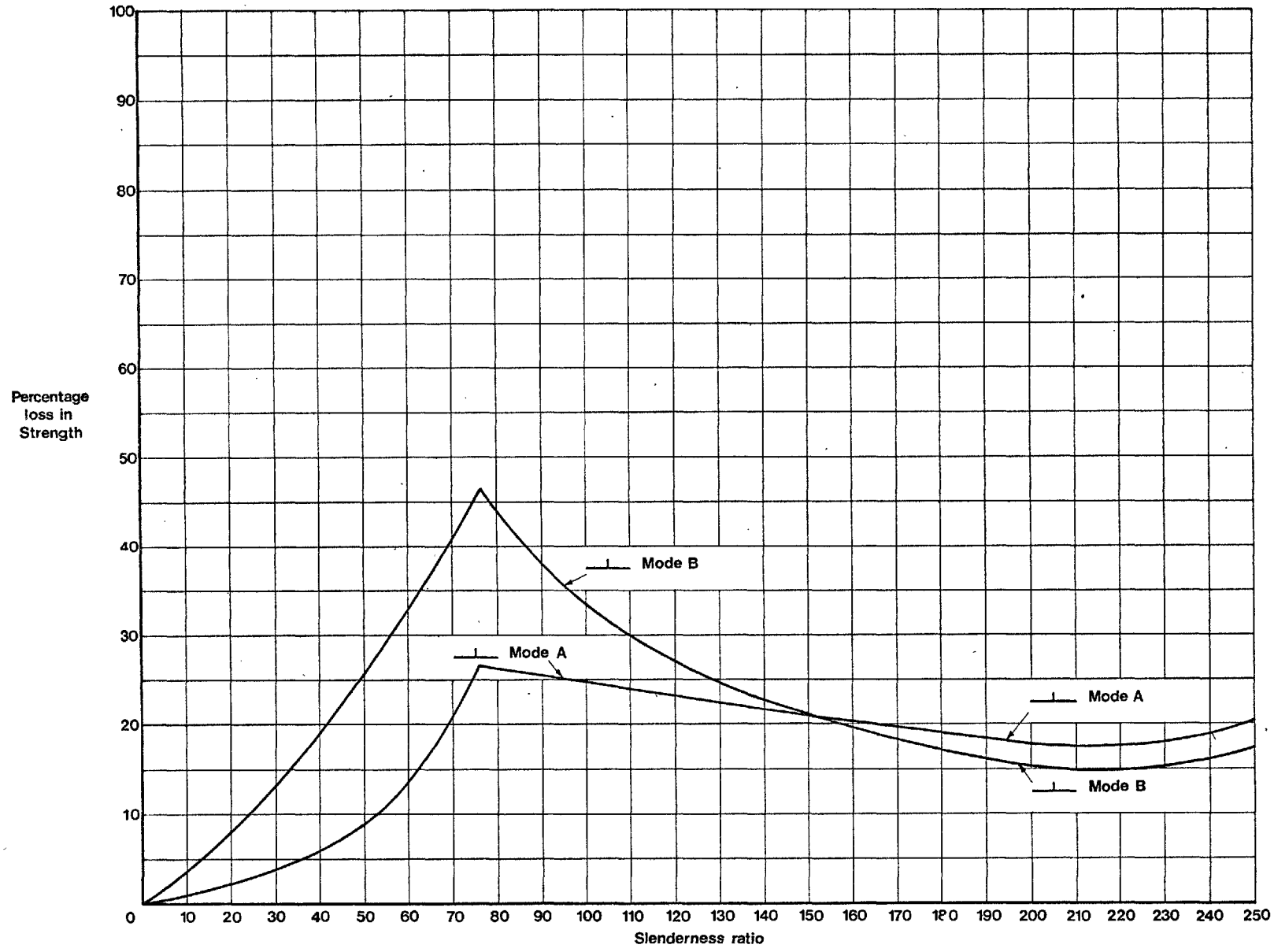

Fig.70 Loss in strength due to initial lack of straightness

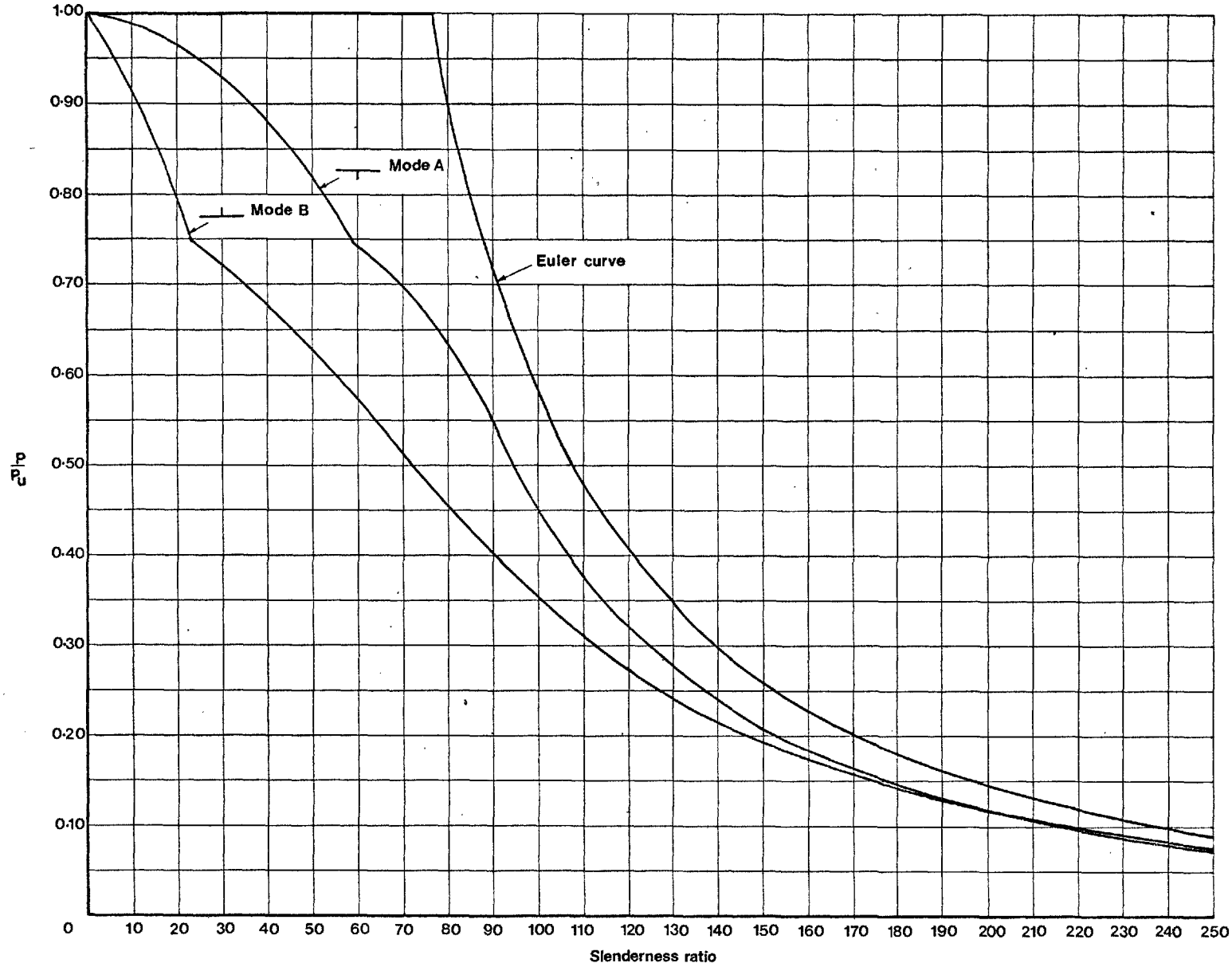

Fig.71 Failure loads including the effect of residual stresses and lack of initial straightness

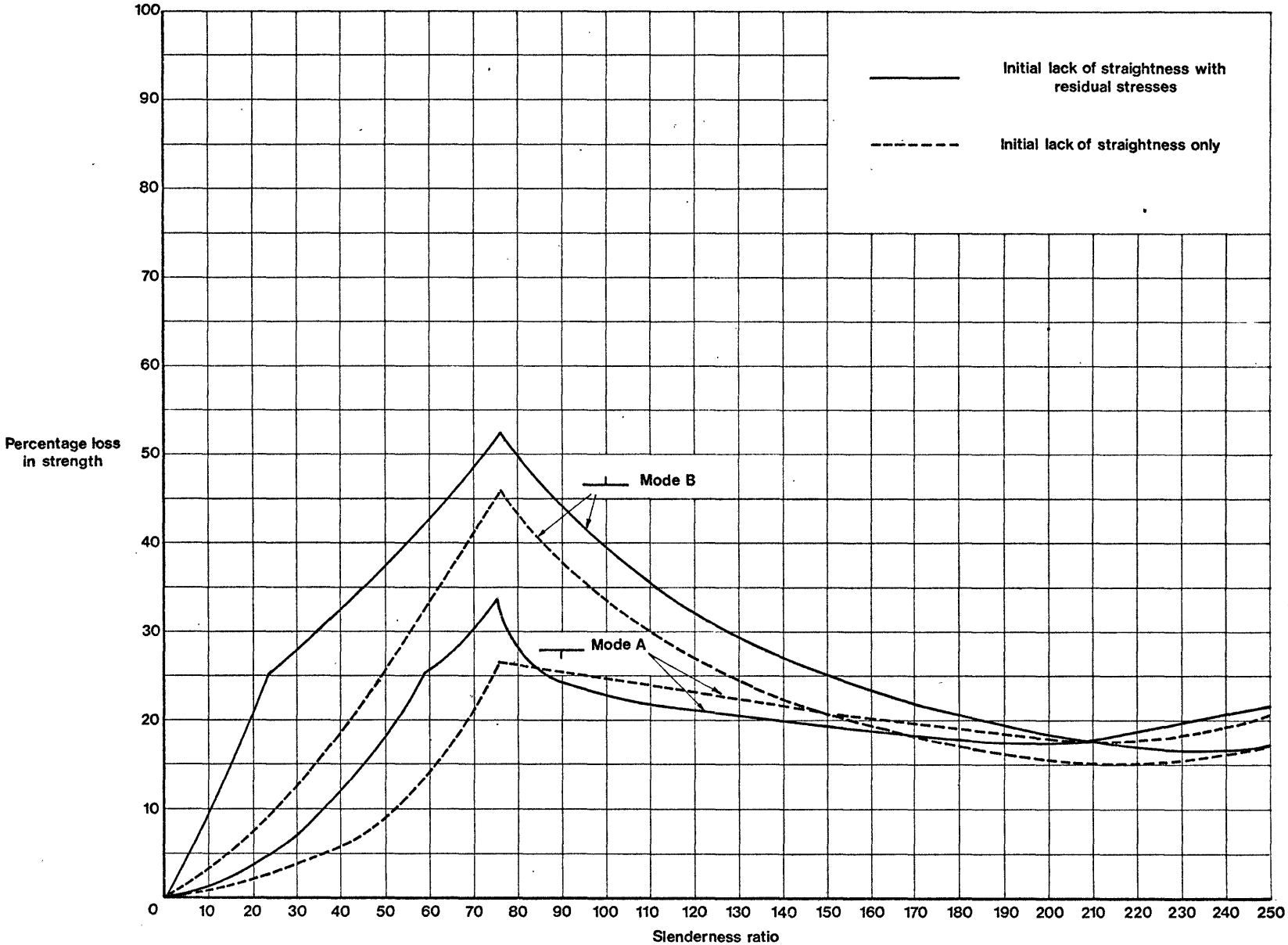

Fig.72 Loss in strength due to combined effects of residual stresses and lack of initial straightness

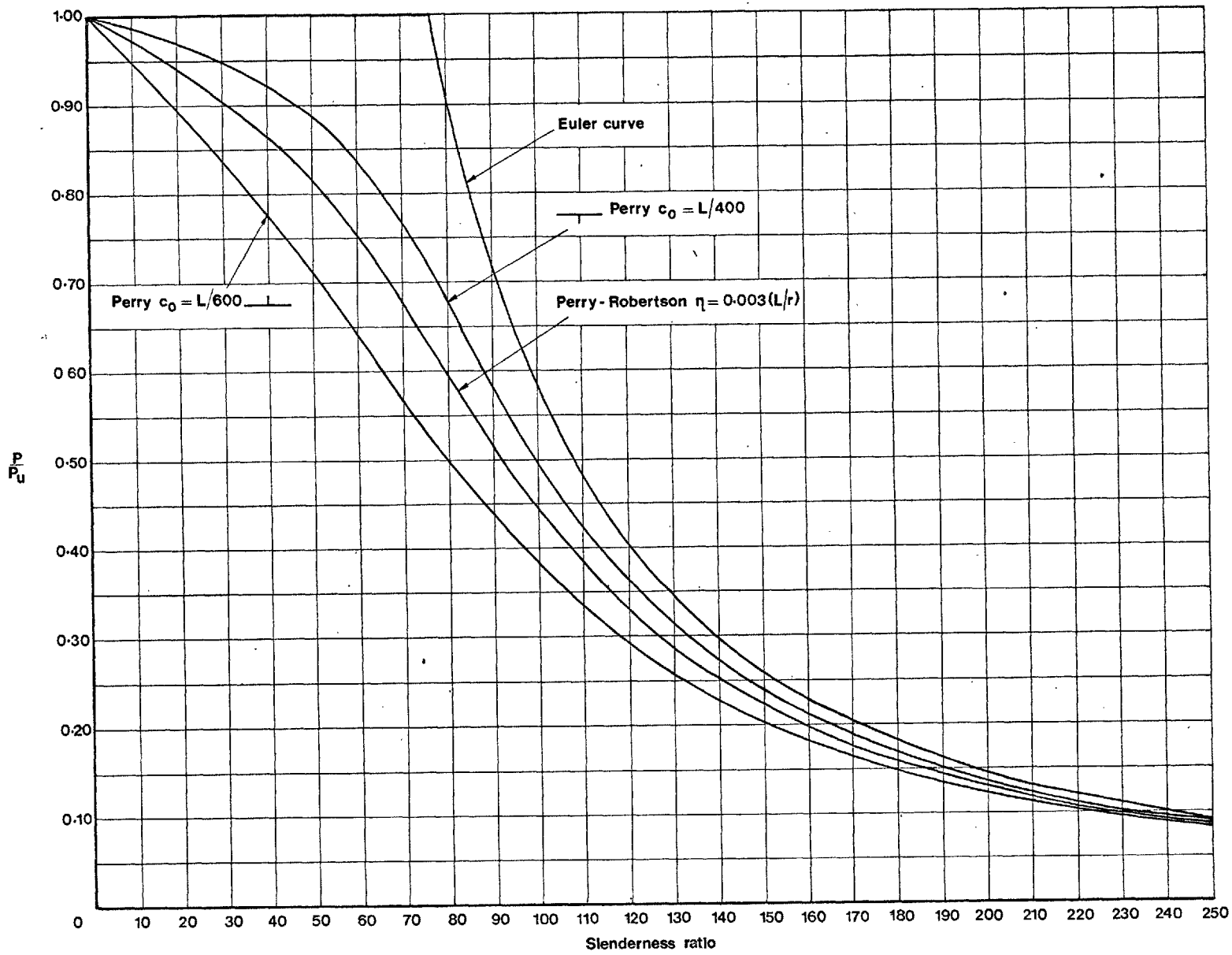

Fig.73 Failure loads from empirical formulae

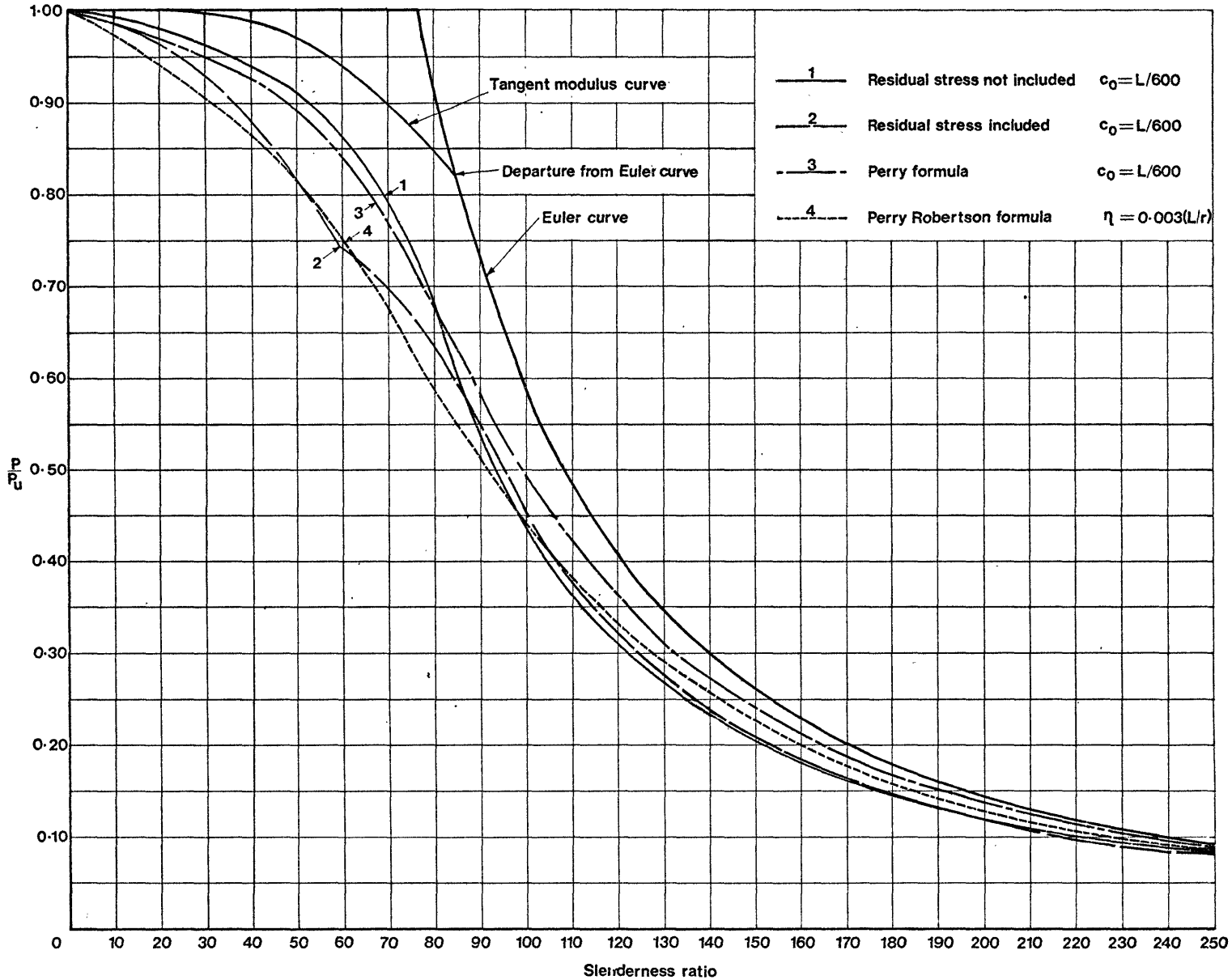

Fig.74 Comparitive failure load curves for Mode A bending

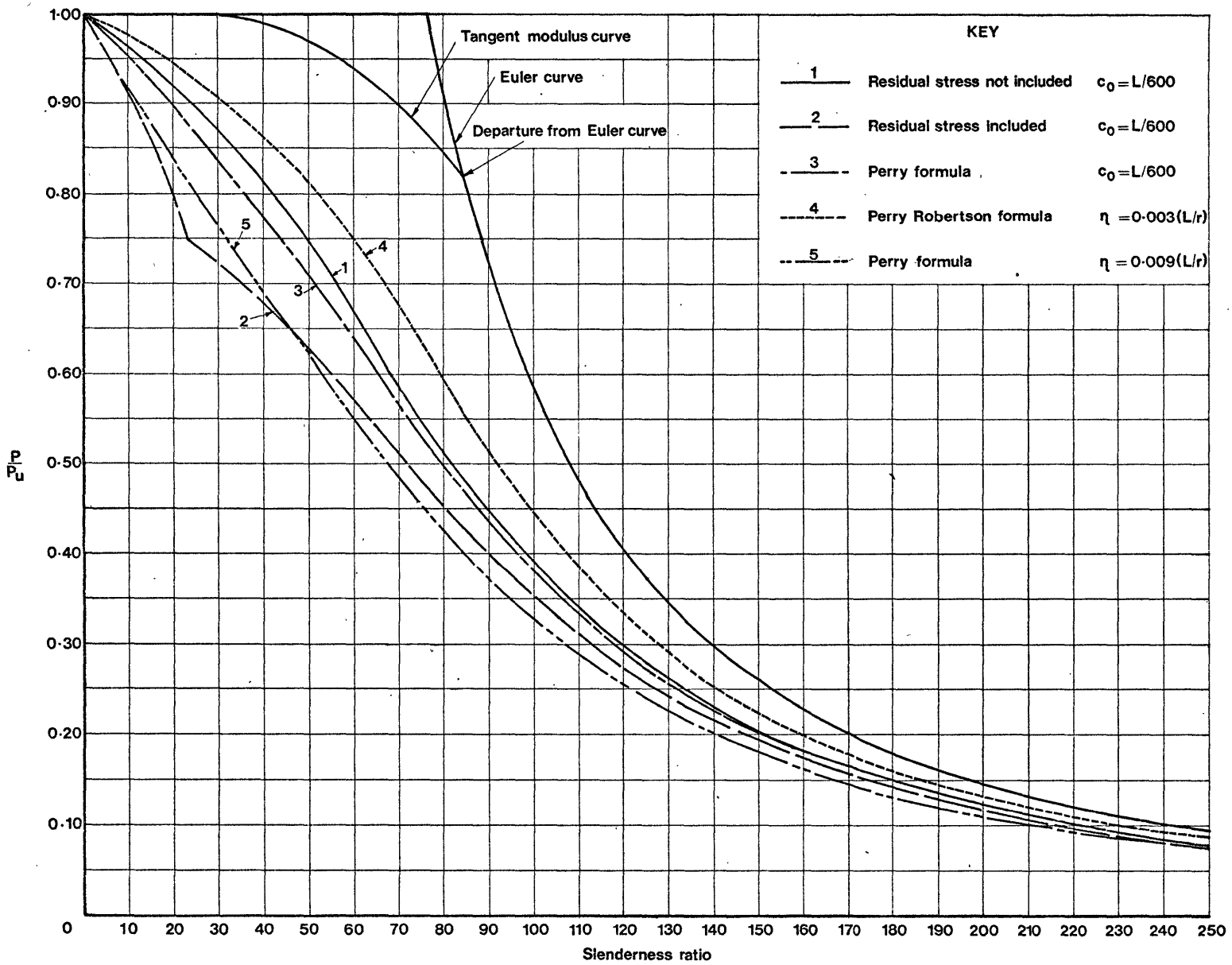

Fig.75 Comparitive failure load curves for Mode B bending

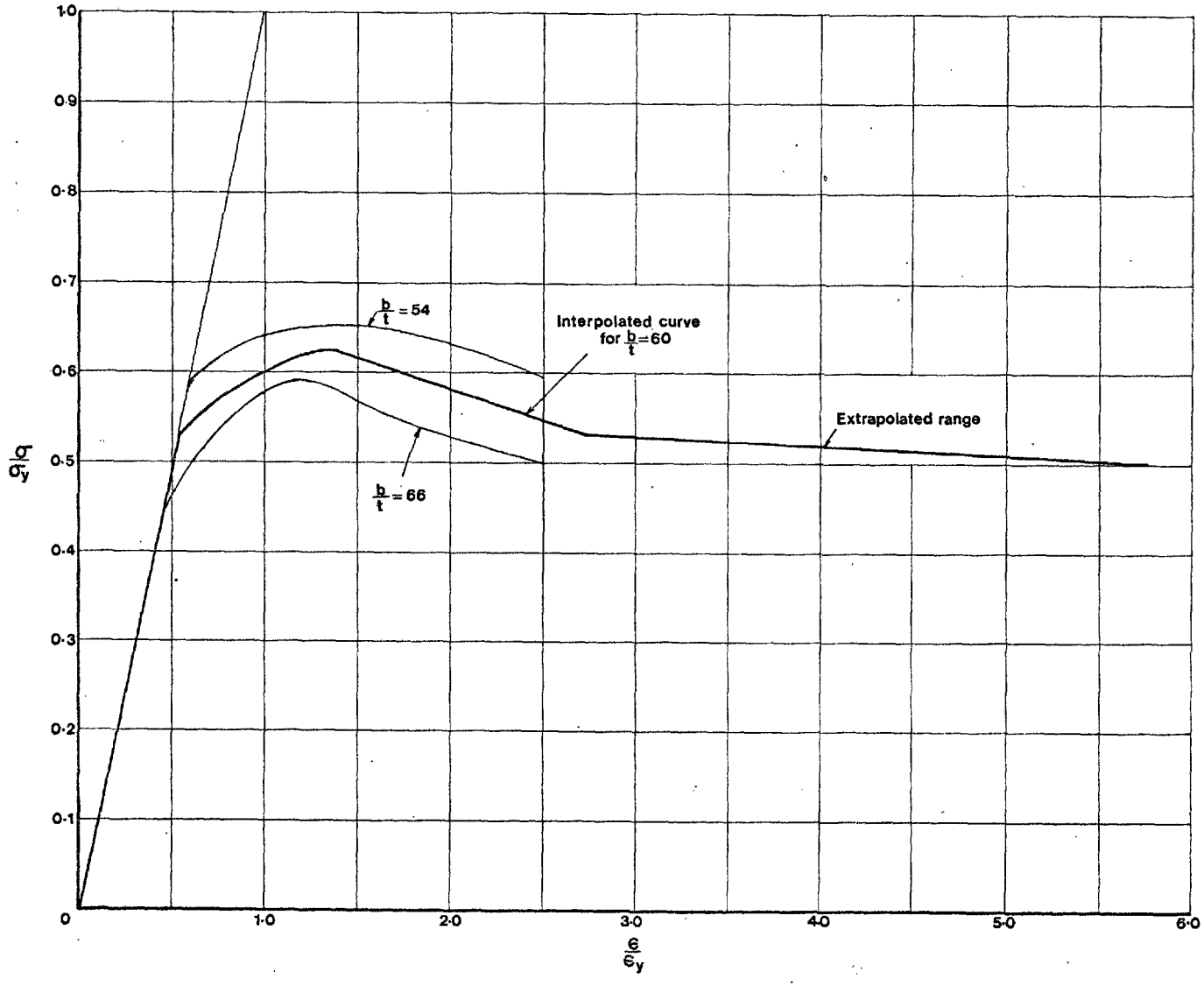

Fig.76 Load-end shortening curve for the cross-section chosen

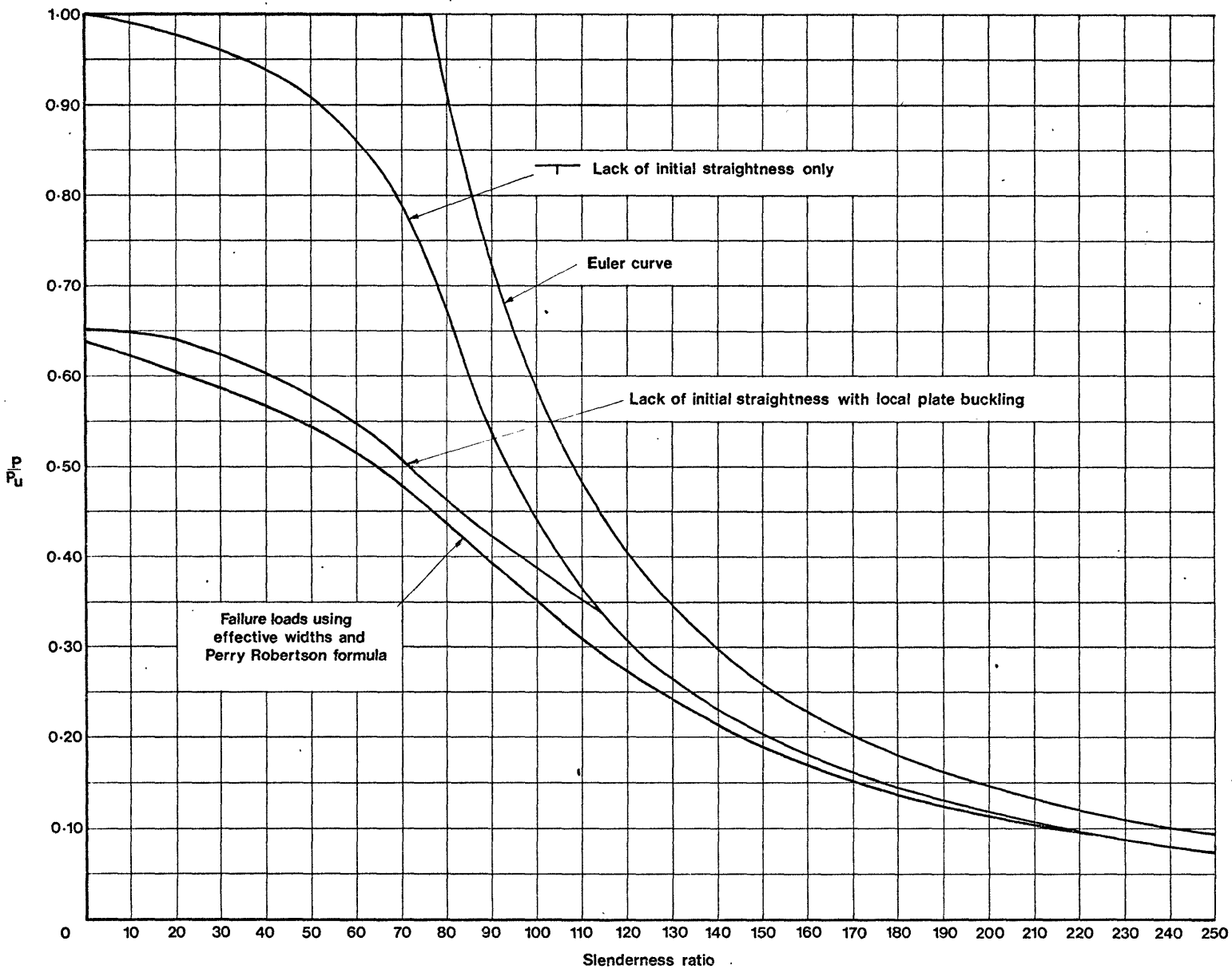

Fig.77 Failure loads including the effect of local plate buckling

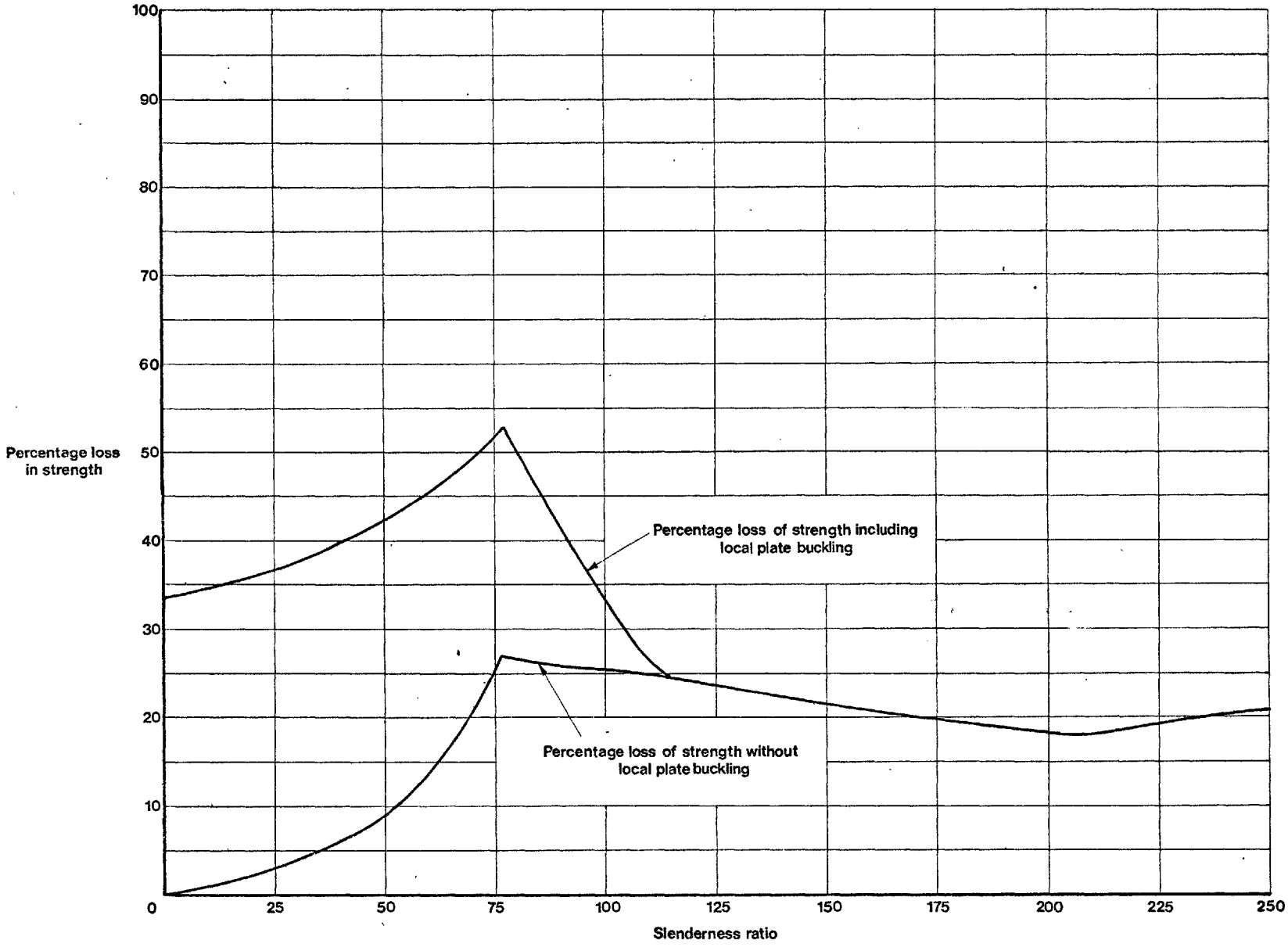

Fig.78 Loss in strength due to local plate buckling and initial lack of straightness

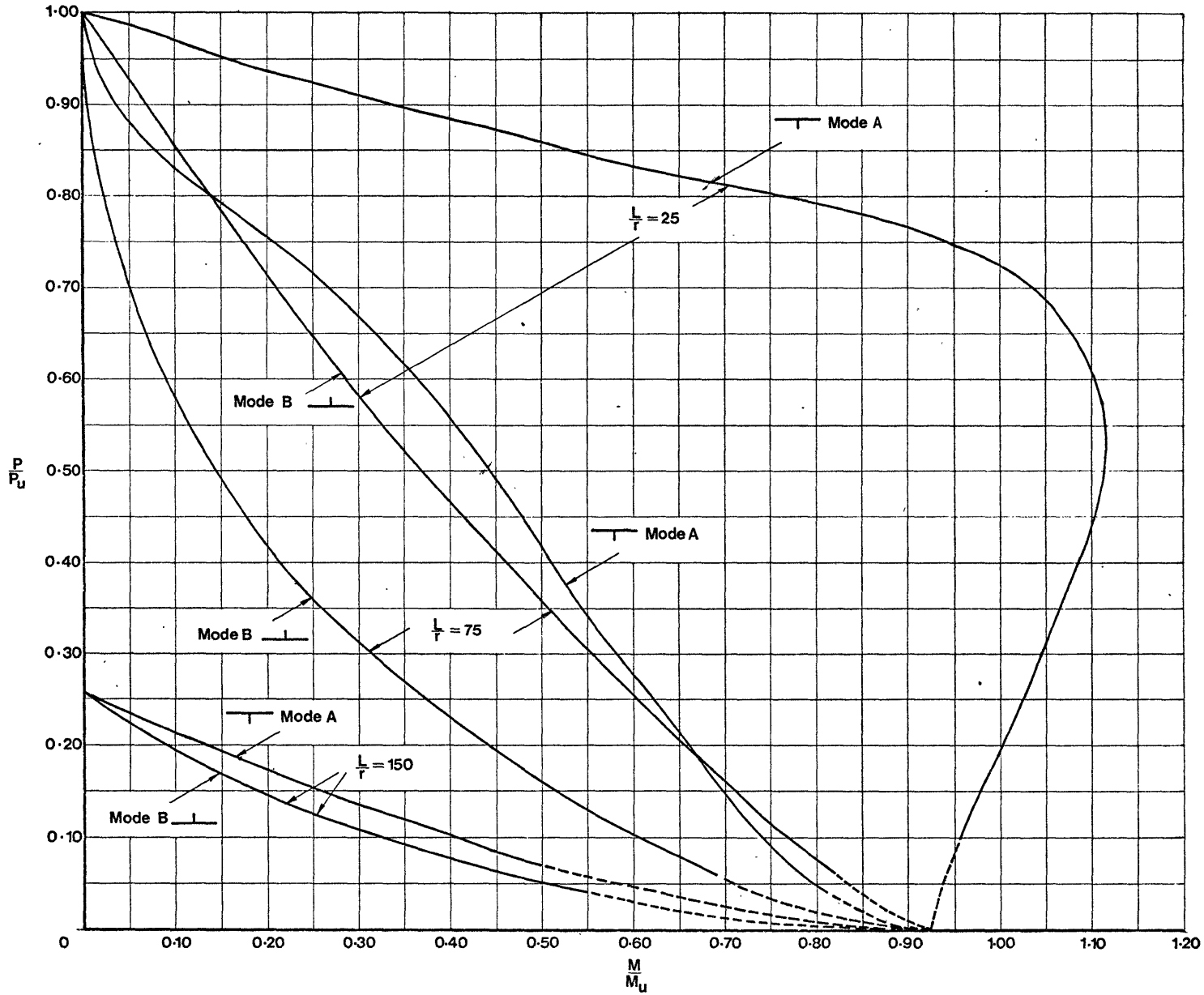

Fig.79 Load-Moment interaction curves for different slenderness ratios

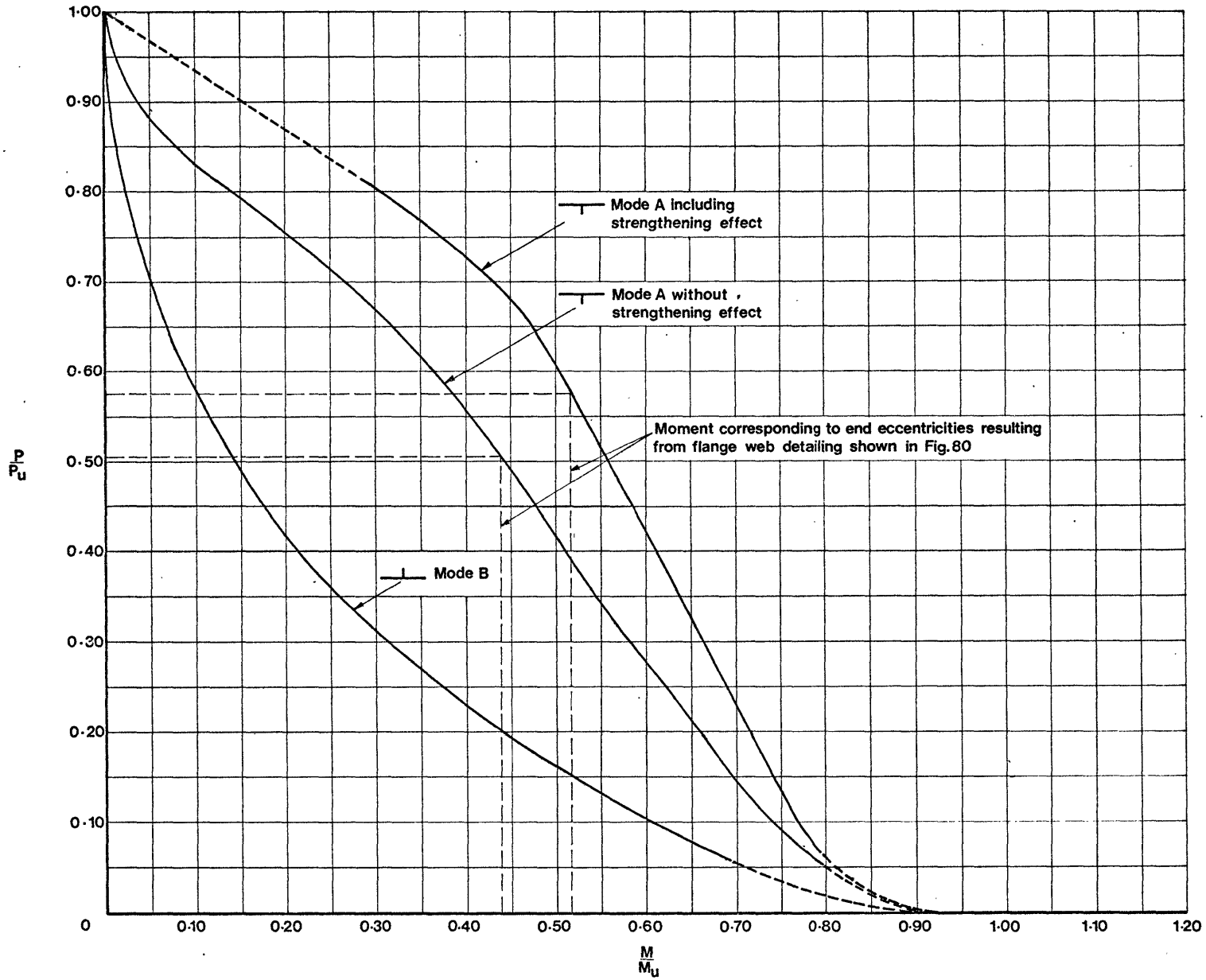

Fig.80 Load-Moment interaction curve for $\frac{L}{r}$=75 showing the strengthening effect of initial lack of straightness in opposition to applied moments

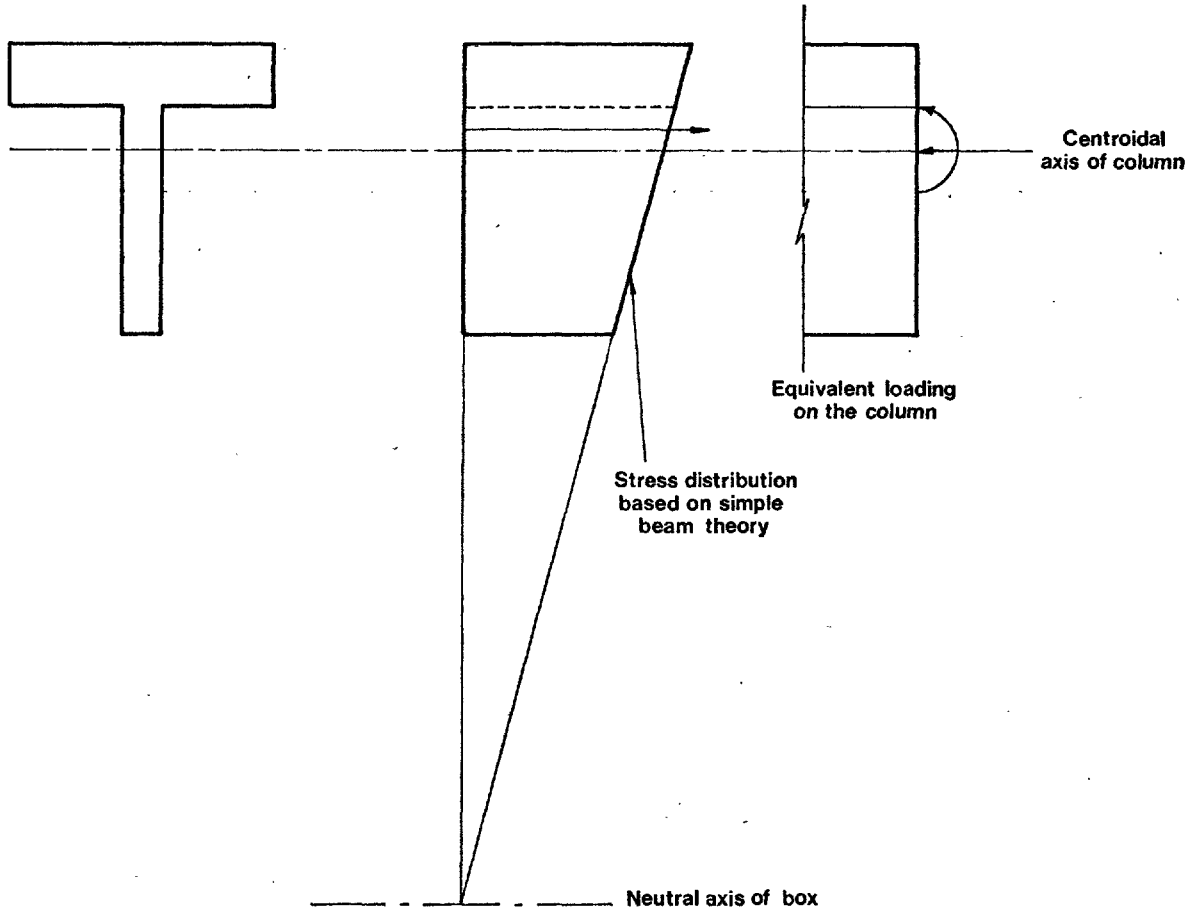

Fig.81 Stress distribution over the whole cross section

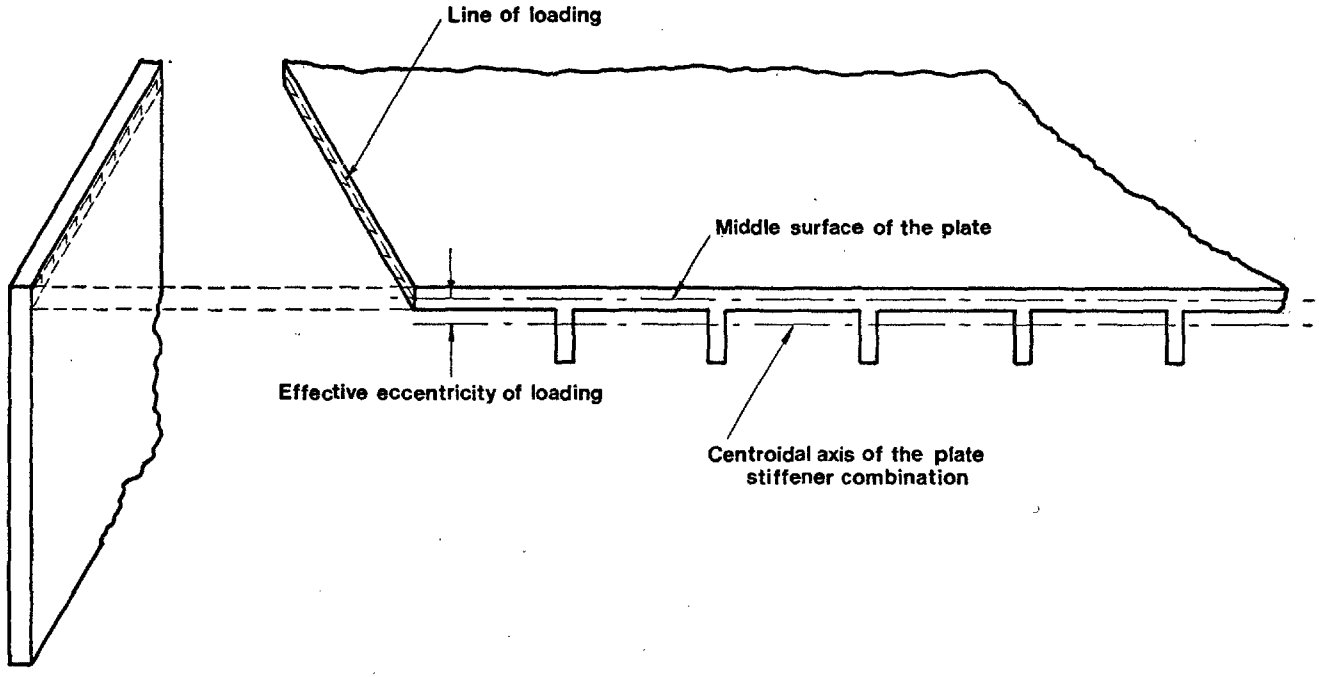

Fig.82 Typical web to flange junction in a box girder

NOTATION

A	-	Area of added metal in the welding process
A_c	-	Area of concrete in a composite section
A_g	-	Gross area of a composite section
A_s	-	Area of steel in a composite section
a	-	Side of a rectangular cross-section
a_1	-	Distance of top fibre from neutral axis in bare metal sections
b	-	Side of a rectangular cross-section
C	-	Constant used in residual stress calculations
C_1, C_2, C_3, C_4	-	Coefficients of the polynomial expression for concrete stress-strain curve
c_o	-	Initial out-of-plane deformation
D	-	Depth of bare metal section in the plane of bending
E, E_s	-	Modulus of elasticity for steel
E_o	-	Modulus of elasticity for concrete at origin
e	-	Eccentricity of applied force with respect to the geometric centroid
e_x, e_y	-	Eccentricity of applied force with respect to the geometric centroid in the x and y directions
$\bar{e}_x, \bar{e}_y$	-	Larger of the eccentricities of the applied force at the two ends in the xz and yz planes respectively
e_{xA}, e_{yA} e_{xB}, e_{yB}	-	Eccentricities of applied force with respect to the geometric centroid in the x and y directions at ends A and B respectively

e_{xs}, e_{ys} - Eccentricities of the line of action of the applied force at station s in the x and y directions respectively

h - Distance between stations along the length

k_1 - Factor relating the strength of concrete in a compression member to the concrete cube strength

L - Length of the column

M_x, M_y - Biaxial bending moments in the x and y directions respectively

M_{xs}, M_{ys} - Biaxial bending moments at station s in the x and y directions respectively

M_u - Ultimate moment of resistance under zero axial load (Plastic Moment)

n_a, n_b - Number of subdivisions of the column cross-section in the x and y directions respectively

n_x, n_y - Initial out-of-plane deformations along x and y directions respectively

n_{mx}, n_{my} - Mid-point (maximum) values of initial out-of-plane deformations along x and y directions respectively

P - Axial force in a column

P_a - Larger of P_{ax} and P_{ay}

P_{ax}, P_{ay} - Uniaxial bending axial failure loads of a column for bending in the xz and yz planes respectively

P_{test} - Test failure load of a column

P_x, P_y - Uniaxial bending failure loads with applied eccentricities in the x and y directions respectively

P_{xy} - Biaxial bending failure load

P_u - Squash load of a column

r	-	Radius of gyration
s	-	Station s along the length of a column
t	-	Thickness of flange
t_1, t_2	-	Thickness of plates welded together
u, v	-	Deflections along x and y directions respectively
u', u''	-	Calculated deflections along x and y directions respectively
v', v''		in consecutive cycles
u_m, v_m	-	Mid-point (maximum) deflections of a column under load
u_{ms}, v_{ms}	-	Calculated deflections at station s in the x and y directions respectively due to assumed deflections
u'_{ms}, v'_{ms}	-	Calculated deflections at station s in the x and y directions respectively due to an incremental deflection in the x-direction ('prime) and in the y-direction ("primes)
u''_{ms}, v''_{ms}		
u_s, v_s	-	Deflections at station s in the x and y directions respectively
w_i	-	Trial deflection component
w_i^1, w_i^2	-	Successive computed values of (i)th deflection component
W_i	-	Computed deflection component (function of w_i)
x, y	-	Co-ordinate axes in the plane of a cross-section
x_i, y_i	-	Co-ordinates of the centroid of the (i,j)th element
Z_i	-	Error function showing difference between w_i and W_i
z	-	Co-ordinate axis along the length of the straight column
z_{ij}	-	Distance of a point (x_i, y_j) from an axis passing through the origin and parallel to the neutral axis
z_n	-	Depth of neutral axis from the origin
α_{ij}	-	Yield stress of the material of (i,j)th element
β	-	Coefficient used to describe steel stress-strain curve

β_x, β_y - Ratio of smaller end eccentricity to the larger end eccentricity for x and y directions respectively

γ, γ_1 - Coefficients used to define concrete stress-strain curve

γ_2 - $\varepsilon_f/\varepsilon_u$

Δ - Incremental deflection used to compute rate of change of calculated deflection with respect to assumed deflections

Δ_o - Stiffener out-of-plane deformation

Δa_{ij} - Area of (ij)th element

ΔP_{ij} - Force in the (i,j)th element

δ_o - Ripple component of plate out-of-plane deformation

δw_i - Error correction in the (i)th component of assumed deflections

ε - Strain on arbitrary small constant

ε_o - Strain at the point O (origin)

ε_f - Limiting strain at which stress reduces to zero after collapse

ε_{ij} - Strain in the (i,j)th element

ε_u - Strain corresponding to maximum stress in concrete

η - Perry imperfection factor = $c_o a_1/r^2$

$\eta_1 t_1, \eta_2 t_2$ - Widths of plates 1 and 2 respective under tensile yield after welding

θ - Direction of the neutral axis, measured with respect to y-axis

λ_e - Critical slenderness ratio, for which the Euler load equals the squash load

σ - Stress

σ_c - Maximum compressive concrete cube strength

σ_f - Maximum compressive residual stress in the flange of an I- or H-section

σ_{fw} - Tensile residual stress at the junction of flange and web in an I- or H-section

σ_{ij} - Stress in the (i,j)th element

σ_r - Average compressive residual stress in welded cross-sections

σ_{rm} - Maximum compressive residual stress

σ_u - Maximum compressive concrete strength in the member

σ_w - Maximum residual stress in the web of an I- or H-section

σ_y - Yield stress of steel

ϕ - Curvature

ϕ_o - ε_u/a

ϕ_{ox}, ϕ_{oy} - Components of initial curvature in the x and y directions

ϕ_x, ϕ_y - Components of curvature in the x and y directions

$\bar{\phi}_x, \bar{\phi}_y$ - Components of total curvature in the x and y directions

ϕ_{xs}, ϕ_{ys} - Components of curvature at station s in the x and y directions

$\bar{\phi}_{xs}, \bar{\phi}_{ys}$ - Components of total curvature at station s in the x and y directions

ϕ^o_{xs}, ϕ^o_{ys} - Components of initial curvature at station s in the x and y directions